Fe(II) and Co(II) Spin Crossover Complexes using 1,3,4-Thiadiazole Bridging Ligands

Dissertation

zur Erlangung des wissenschaftlichen Grades
„Doktor der Naturwissenschaften – Dr. rer. Nat.“
im Promotionsfach Chemie

am Fachbereich Chemie, Pharmazie, Geographie und Geowissenschaften
der Johannes Gutenberg-Universität Mainz

vorgelegt von

Fabian Fürmeyer

geboren am 04. Dezember 1991 in Mainz

Mainz, September 2020

JOHANNES GUTENBERG UNIVERSITÄT MAINZ

Die vorliegende Arbeit wurde
in der Zeit von Mai 2017 bis September 2020
am Institut für Anorganische Chemie und Analytische Chemie/
Department Chemie
der Johannes Gutenberg-Universität Mainz
unter der Betreuung von Prof. Dr. Eva Rentschler angefertigt.

Ich, Fabian Fürmeyer, bestätige hiermit, dass ich diese Arbeit selbstständig verfasst habe und keine weiteren als die angegebenen Quellen und Hilfsmittel verwendet habe. Alle Ausführungen, die anderen sinngemäß oder wörtlich entnommen wurden, habe ich kenntlich markiert.

_____ _____

(Ort, Datum) (Unterschrift)

Dekan: Prof. Dr. Tobias Reich
Erste Berichterstatterin: Prof. Dr. Eva Rentschler
Zweite Berichterstatterin: [redacted]
Prüfer: [redacted]

Tag der mündlichen Prüfung: 27. Oktober 2020

"*Imagination is the only weapon in the war against reality.*"

~The Cheshire Cat~

L. C.

Für meine Familie

Kurzzusammenfassung

Die Fähigkeit einer metallorganischen Koordinationsverbindung zwischen zwei elektronischen Zuständen zu schalten, wird als Spin-Crossover (SCO) bezeichnet. 3d-Übergangsmetallionen können aufgrund der Aufspaltung der d-Orbitale in oktaedrischer Koordinationsumgebung abhängig von der Stärke des Ligandenfelds im low-spin (LS) oder im high-spin (HS) Zustand vorliegen. Der Wechsel zwischen diesen beiden Zuständen kann durch externe Stimuli wie Temperatur, Druck oder Licht herbeigeführt werden. Die mit dem Spinübergang einhergehenden Änderungen der strukturellen, magnetischen und spektroskopischen Eigenschaften ermöglichen eine potenzielle Anwendung als zentrale Bauteile in Speichermedien, Sensoren oder Displays. Für die genannten Anwendungen ist insbesondere ein abrupter SCO mit thermischer Hysterese von großer Bedeutung, um die benötigte Bistabilität zu gewährleisten. Dieses Verhalten hängt stark von den intra- sowie intermolekularen Wechselwirkungen der spintragenden Übergangsmetallionen ab. Hierbei sind zweikernige SCO-Verbindungen von besonderem Interesse, da sie einerseits die kleinesten und synthetisch einfachsten Einheiten darstellen, welche die Möglichkeit bieten sowohl intra- als auch intermolekulare Wechselwirkungen zu studieren, und andererseits zwischen den drei potentiellen Zuständen [HS-HS], [HS-LS] und [LS-LS] schalten können.

In der vorliegenden Arbeit wird das SCO-Phänomen anhand neuer, zweikerniger Fe(II)-Komplexen basierend auf symmetrischen 1,3,4-Thiadiazolbrückenliganden untersucht. Ein in der Literatur bekannter 1,3,4-Thiadiazolbrückenligand wurde hierzu gezielt modifiziert und vier neue Liganden konnten synthetisiert und charakterisiert werden. Die Liganden wurden zur Darstellung potenziell dinuklearer Fe(II)-Komplexe genutzt und die magnetischen und strukturellen Eigenschaften dieser Verbindungen mittels temperaturabhängiger, magnetischer Suszeptibilitätsmessung, Einkristall-Röntgenstrukturanalyse und Mößbauer-Spektroskopie untersucht. Insgesamt wurden neun symmetrische, bimetallische Fe(II)-Komplexe synthetisiert und charakterisiert. Die Verbindungen zeigen unterschiedliche Eigenschaften in Abhängigkeit der verwendeten Liganden, der nicht-koordinierenden Gegenionen und der Packung im Festkörper, wodurch vier zweikernige Fe(II)-SCO-Komplexe erhalten wurden. Des Weiteren konnte jeweils eine einkernige Fe(II)- und Co(II)-Verbindung dargestellt werden. Während der Fe(II)-Komplex keinen Spinübergang aufweist, zeigt der Co(II)-Komplex SCO-Eigenschaften. Die in der vorliegenden Arbeit vorgestellten Komplexe dienen als hervorragende Beispiele, um die komplexen und vielfältigen Einflüsse auf das empfindliche SCO-Verhalten zu verdeutlichen und zeigen das große Potenzial von 1,3,4-Thiadiazolliganden zur Darstellung und Untersuchung von SCO-Verbindungen.

Abstract

The ability of an organometallic coordination compound to switch between two electronic states is called Spin-Crossover (SCO). 3d transition metal ions can either be in the low-spin (LS) or high-spin (HS) state due to the splitting of the d-orbitals in an octahedral coordination environment. The change between these two states can be induced by external stimuli such as temperature, pressure or light. The changes in the structural, magnetic and spectroscopic properties associated with the spin transition enable potential applications as central components in storage media, sensors or displays. For the mentioned applications, an abrupt SCO with a thermal hysteresis is of utmost importance, as it provides the required bistability. This behavior strongly depends on the intra- and intermolecular interactions of the spin-bearing transition metal ions. In this context, dinuclear SCO compounds are of particular interest, since they are the smallest and synthetically simplest units, which offer the possibility to study intra- as well as intermolecular interactions, and can switch between three potential states, namely [HS-HS], [HS-LS] and [LS-LS].

In the present work the SCO phenomenon is investigated using new dinuclear Fe(II) complexes based on symmetric 1,3,4-thiadiazole bridging ligands. A 1,3,4-thiadiazole bridging ligand known in the literature was specifically modified and four new ligands were synthesized and characterized. The ligands were used to generate potential dinuclear Fe(II) complexes and the magnetic and structural properties of these compounds were investigated by temperature-dependent magnetic susceptibility measurement, single-crystal X-ray structure analysis and Mössbauer spectroscopy. A total of nine symmetrical, bimetallic Fe(II) complexes were synthesized and characterized. The compounds show different properties depending on the ligands used, the non-coordinating counter ions and the crystal packing in the solid state, resulting in four bimetallic Fe(II) SCO complexes. Furthermore, a mononuclear Fe(II) and a mononuclear Co(II) compound could be obtained. While the iron(II) complex shows no spin transition, the Co(II) complex shows SCO behavior. The complexes presented in this work serve as excellent examples to illustrate the complex and diverse intra- and intermolecular influences on the sensitive SCO behavior and show the great potential of 1,3,4-thiadiazole ligands to form SCO compounds.

Table of contents

Abbreviations and Units

Å	Ångstrom
abs.	absolute
Av., ave	average
B	Racah parameter
bpp	2,6-di(pyrazol-2-yl)pyridine
bpym	2,2'-bipyrimidine
bt	2,2'-bis-1,3-thiazole
btr	4,4'-bis-1,2,4-triazole
bzp	bromazepan
C	Celsius
c	centi
χ	magnetic susceptibility
calc.	calculated
conc.	concentrated
C_P	heat capacity
D	dimensional
d	doublet
DMF	N,N'-dimethylformamide
DMSO	dimethylsulfoxide
Δ	difference
δ	isomer shift
Δ_C	critical ligand field strength
ΔE_{HL}	energy difference between the high spin and the low spin ground state
ΔE_Q	quadrupole splitting
Δ_O, 10 Dq	octahedral ligand field strength
Δr_{HL}	difference between the equilibrium iron-donor atom distance of the high spin and the low spin state
Δ_T	tetrahedral ligand field strength
depe	1,2-bis(diethylphosphino)ethane
DSC	differential scanning calorimetry
E	energy
el	electronic
E_P	mean spin pairing energy
Σ	octahedral distortion parameter
EPR	electron paramagnetic resonance
equiv.	equivalents
ESI	electrospray ionization, electronic supporting information
et al.	et alii (and corworkers)
f	vibrational force constant

FD	field desorption
FT	fourier transformation
G	free Gibbs energy
g, g	gyromagnetic factor, gramm
γ_{HS}	mole fraction of the high spin state
H	enthalpy
h	hour
$h\nu$	light irradiation
HS	high spin
Hz	Hertz
I^2MOD	2,5-bis[(1*H*-imidazol-2-ylmethyl]amino)methyl-1,3,4-oxadiazole
I^2MTD	2,5-bis[(1*H*-imidazol-2-ylmethyl]amino)methyl-1,3,4-thiadiazole
I^4MTD	2,5-bis[(1*H*-imidazol-4-ylmethyl]amino)methyl-1,3,4-thiadiazole
Imz	imidazole
IR	infrared
J, J	coupling constant, joule
K	Kelvin
k	kilo
k_B	Boltzmann constant: $1.380649*10^{-23}$ JK^{-1}
L, L	total orbit momentum, ligand, liter
λ	wavelength
LIESST	light induced excited spin state trapping
LS	low spin
M	metal, mega, mass peak
m, m	mass, meter, mili, multiplet
MeCN	acetonitrile
MeOH	methanol
min	minute(s)
MLCT	metal to ligand charge transfer
MOF	metal organic framework
MS	mass spectrometry
μ, µ	dipole moment, micro
μ_B	Bohr magneton: $9.27401007823*10^{-24}$ JT^{-1}
μ_{eff}	effective magnetic moment
µSR	muon spin relaxation
n	nano
N_A	Avogadro constant: $6.022*10^{23}$ mol^{-1}
NIL	non-innocent ligand
NIR	near infrared
NMR	nuclear magnetic resonance
NSR	nuclear resonance scattering
ν	frequency
ODA	1,3,4-oxadiazole

Oe	Oersted
p	pressure
p.a.	pro analysi
PAS	positron annihilation spectroscopy
PBPMTD	2-(2-pyridyl)-5-[*N*,*N'*-bis(2-pyridylmethyl)amino]methyl-1,3,4-thiadiazole
PdAdH	bis-(2,6-pyridinecarboxaldehyde)
phen	1,10-phenanthroline
φ_i	*cis*-angles inside an octahedron
pic	picolylamine
PMAT	4-amino-3,5-bis{[(2-pyridylmethyl)amino]methyl}-4*H*-1,2,4-triazole
PMOD	2,5-bis[(2-pyridylmethyl]amino)methyl-1,3,4-oxadiazole
PMTD	2,5-bis[(2-pyridylmethyl]amino)methyl-1,3,4-thiadiazole
ppm	parts per million
PSRT	4-R-3,5- bis{[(2-pyridylmethyl)thio]methyl}-4*H*-1,2,4-triazole
PSTD	2,5-bis[(2-pyridylmethyl]thio)methyl-1,3,4-thiadiazole
ptz	1-propyltetrazole
py	pyridine
$(pyrrol)_3tren$	trianionic Schiff base resulting from the condensation of pyrrole-2-carboxaldehyde with 2,2′,2″-tris(ethylamino)amine
quant.	quantitative
r	distance
R	gas constant: 8.3144598 $JK^{-1}mol^{-1}$
r.t.	room temperature
Rtrz	4*R*-1,2,4-triazole
ρ	density
S	total spin, entropy
s, s	electron spin, second, singlet
SCO	spin crossover
SMM	single molecule magnet
SQUID	superconducting quantum interference device
T, T	temperature, tesla
t	tons, triplet
Ta	thiazole
TDA	1,3,4-thiadiazole
TDPT	4-Tolyl-3,5-di(2-pyridyl)-4*H*-1,2,4-triazole
TDTT	4-Tolyl-3,5-di(2-thiazolyl)-4*H*-1,2,4-triazole
terpy	2,2':6',2''-terpyridine
THF	tetrahydrofurane
TIESST	thermally induced excited spin state trapping
TLC	thin layer chromatography
TMDT	2,5-bis[(thiazol-2-ylmethyl]amino)methyl-1,3,4-thiadiazole
TOF	time of flight
tz	1,2,4-triazole

UV	ultra violet
V	volume
vib	vibrational
Vis	visible
XAS	X-ray absorption spectroscopy
X-ray	electromagnetic radiation with a wavelength ranging from 0.01 – 10 nm and a corresponding energy of 0.1 – 100 keV
Z	cell formula units
z	charge

1. Introduction

Magnetism is a phenomenon that has occupied human history for thousands of years. However, it must be mentioned that the most important findings for the understanding of magnetic behavior were only achieved in the last century. Moving electric charges and the intrinsic angular momentum of elementary particles have been found to be the cause of magnetism. Nowadays, materials, which show magnetic properties, are indispensable in everyday life. They are used, for example, in acoustic (loudspeakers, microphones) or magneto-mechanical components (frictionless bearings, magnetic separators), in medical diagnostics (magnetic resonance imaging), in data processing and telecommunications technology (switches, memories, sensors), as well as in chemical-analytical and spectroscopic techniques (NMR, EPR, MS, SQUID).[1–3] Due to the wide range of applications, it is obvious that even today's research is still intensively dealing with magnetic materials. The focus lies on the development of novel materials on a molecular scale as well as on the combination of magnetic properties with other technologically interesting properties.[2,3] Molecular systems are of great interest since the feasibility of chemical fine-tuning of the molecules and thus controlling the magnetic properties allows for tailor-made applications. Furthermore, chemical creativity can possibly lead to materials with previously unknown physical properties.[4] The main focus in the field of research towards molecular switches is on molecular magnetism and on electronically bistable molecules.

In the field of molecular magnetism, research is dealing, among others, with the maximization of storage capacity by reducing the size of magnetically controlled switches. In the early 1990s magnetic bistability in a single molecule was reported for the first time by *Sessoli et al*.[5] Molecules that show slow relaxation of their magnetization even in the absence of an external magnetic field and retain their magnetization as long as they are kept below a certain temperature are known as single molecule magnets (SMMs). These compounds are discussed for future applications as key building blocks in high density data storages, spintronic devices and quantum computation.[6–8]

Electronically bistable molecules on the other hand show electronic structures that are very sensitive to external stimuli such as changes in temperature or pressure, light irradiation or chemical triggers.[9] The research herein focuses on molecules that exhibit mixed-valence, valence tautomerism or spin crossover. Regardless of the final applications, these molecular materials must show molecular bistability, meaning the possibility to switch between two distinguishable states when exposed to an external stimulation. Furthermore, the molecular switching must be associated with a response function such as changes in optical, magnetic or structural properties for the use in applications as sensors, information storage devices or in the field of molecular electronics.[10–14]

Mixed-valence complexes contain two or more metal ions in different oxidation states. These metal ions are bridged by organic linkers, which mediate an intramolecular electron transfer between the redox-active centers.[15–17] Depending on the communication between the metal centers via the bridging ligand, these molecules are divided into three classes, classified after Robin-Day.[18] Class I represents complexes with no interaction of the redox-active centers, e.g. for long metal-metal distances or aliphatic ligands. Mixed-valence compounds of Class II exhibit weak electronic interactions and a particular valence state can be trapped and localized, if the thermal energy is not sufficient to overcome the energy barrier between the different states. For Class III complexes, the interaction between the metal ions is so strong, that the electron is completely delocalized over the whole molecule.
Molecules exhibiting valence tautomerism show external stimulus induced switching of their electronic ground states by transferring electrons from a donor to an acceptor, which results in changes of their chemical, spectroscopic, electronic or magnetic properties.[17,19,20] In order to observe the electron's transfer, thus valence tautomerism, the involved orbitals of the donor and the acceptor need to be energetically similar and the intramolecular electronic coupling needs to be in a specific range. If the coupling is too weak, the valence tautomeric transition will not take place. If the coupling is too strong, the electron will be delocalized and the discrete electronic structures are lost. This field of research emerged in the 1950s, with the first example of an solely organic molecule, showing valence tautomerism.[21–23] However, in the 1980s the transition metal complexes which exhibit valence tautomerism came into the focus of research. Generally, the complex-based valence tautomerism can be more precisely described by an electron transition from a redox active ligand or so-called "non-innocent ligand" (NIL) to a redox active metal ion such as cobalt, manganese or copper or vice versa (Equation 1.1).[24–32]

$$(\mathrm{NIL})^{x+1}\mathrm{M}^{y-1}\mathrm{L}_n \leftrightharpoons (\mathrm{NIL})^{x}\mathrm{M}^{y}\mathrm{L}_n \rightleftharpoons (\mathrm{NIL})^{x-1}\mathrm{M}^{y+1}\mathrm{L}_n \qquad (1.1)$$

The present work focusses on the third reason for electronic lability in metal complexes, namely spin crossover. Thus, the field of spin crossover research will be described in more detail in the following chapters.

1.1 The spin crossover phenomenon

Spin crossover (SCO) describes the transition between two electronic states of first row transition metal ions with an electron configuration of d^4–d^7 in an octahedral coordination environment induced by external stimuli such as temperature, pressure or light irradiation (Figure 1). This possibility to switch between two different states, thus exhibiting molecular bistability, and the changes for instance in color or magnetic moment renders these compounds highly promising candidates as key building blocks in data storage devices, displays, actuators or sensors.[13,33–38]

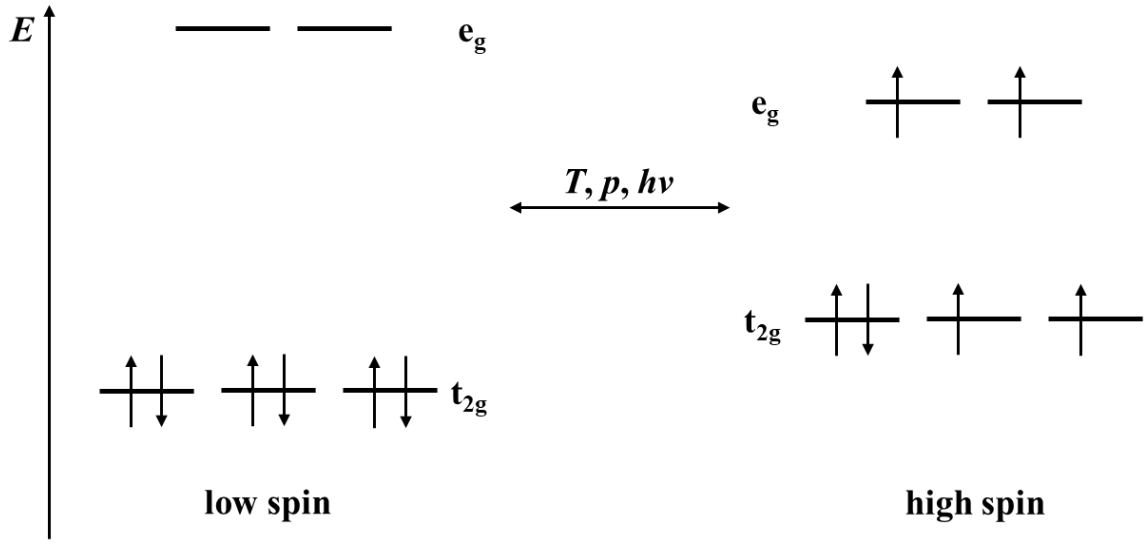

Figure 1. Schematic representation of the SCO between two electronic states by means of a Fe(II) $3d^6$ ion in an octahedral ligand field.

In an ideal octahedral coordination environment, the d-orbitals are split into the t_{2g} and the e_g set and the energy difference between these two sets is called ligand field strength Δ_O. For transition metals with d^4–d^7 electron configuration, the two different electronic ground states result from the two possible occupations of the electrons into these orbital subsets. Depending on the ratio between ligand field strength Δ_O and the spin pairing energy E_P, either the so-called high spin (HS) state with maximum spin multiplicity is stabilized ($\Delta_O<E_P$) or the low spin (LS) state with minimum spin multiplicity is preferred ($\Delta_O>E_P$). When the octahedral ligand field strength Δ_O and the spin pairing energy are in the same order of magnitude, a SCO can occur through small changes of external parameters.

Even though the spin crossover can be formulated for all transition metal ions with an electron configuration of d^4–d^7, there are some useful rules, resulting from ligand field considerations, whether a SCO can occur or not. Considering the fact that the ligand field strength Δ_O is increasing while the spin pairing energy E_P stays almost the same in higher homologue of first row transition metal complexes, it is expected that 4d and 5d transition metal complexes show a strong tendency to be in the LS state and that there are basically no SCO complexes found. Furthermore, oxidation of the metal center ion, while retaining the initial ligand sphere leads, to an increase of Δ_O whereas the E_P is not increasing that much. Thus, it is unlikely that the former SCO complex will retain its behavior upon oxidation. In addition, tetrahedral complexes will not show any SCO because the ligand field strength Δ_T is less than a half compared to Δ_O, resulting exclusively in complexes in the HS state. Finally, considering the stability of certain spin configurations with respect to the metal ion's nuclear charge, it is not surprising that Fe(II) (d^6) complexes are by far the most reported SCO compounds, followed by Fe(III) (d^5) and Co(II) (d^7).[39,40] In addition there are also some examples of spin transitions in complexes with Co(III) (d^6), Mn(II) (d^5), Mn(III) (d^4) and Cr(II) (d^4).[41] However consequently, the ligand environment must be specific and well-chosen for every different metal ion in order to observe SCO.

The SCO phenomenon was first observed in the 1930s when *Cambi et al.* reported a temperature-dependent change in the magnetic properties of Fe(III) tris-*N,N*-dialkyldithiocarbamates (**R_2NCS_2**). However, they wrongly interpreted the origin of the interesting magnetic properties not as thermally induced SCO, but as the presence of different magnetic isomers.[42–44] In principle, this discovery can be regarded as the birth of SCO, but nothing more happened for the next thirty years, at least as far as publications are concerned. This can certainly be explained by the fact that the spectroscopic possibilities and the knowledge of electronic structures were not yet well understood and established. In the 1960s *White, Ewald* and coworkers again studied the [Fe^{III}(**R_2NCS_2**)$_3$] family described by *Cambi* and clarified the correct underlying physical principles of the interesting magnetic properties.[45–47] They also observed that changing the pressure may lead to SCO behavior and carried out the first pressure-dependent study.[48] Almost simultaneously the first octahedral Fe(II) SCO complex with a six nitrogen donor coordination environment was published by *König* und *Madeja*. They systematically varied the anionic ligands in the [Fe^{II}(**phen**)$_2$(X)$_2$] system (with **phen** = 1,10-phenanthroline and X = Br^-, Cl^-, NCS^-, N_3^-, OCN^-, $HCOO^-$ and CN^-), which led to the preparation of the *cis*-[Fe^{II}(**phen**)$_2$(NCS)$_2$] complex with thermal SCO behavior.[49–51] Also the first publications on SCO behavior of Co(II) compounds appeared in this decade. *Stoufer*, *Busch* and *Hadley*[52] reported in 1961 on two electronic isomers of bis-(2,6-pyridinedicarboxaldehyde)-cobalt(II) iodide [Co^{II}(**PdAdH**)$_2$]I_2 and shortly afterwards in 1962 *Hogg* and *Wilkins*[53] investigated the [Co^{II}(**terpy**)$_2$]$(Br)_2 \cdot H_2O$ complex (with **terpy** = 2,2':6',2''-terpyridine), which exhibits values for the magnetic moment depending on the measuring temperature. The next twenty to thirty years were shaped by the intensive research for further novel SCO compounds. Most of these complexes contained an octahedral coordinated Fe(II) as central ion featuring a $\{N_6\}$ coordination environment, which were summarized in the first review article by *König* 1968[54], followed by reviews of *Goodwin* 1976[55] and *Gütlich* 1981.[56] The first example for spin state switching upon light irradiation in solid state was given in 1984 by *Decurtins et al.* They reported the compound [Fe^{II}(**ptz**)$_6$]$(BF_4)_2$ (with **ptz** = 1-propyltetrazole) being in the LS state at low temperatures and that the complex can be switched to the HS state when irradiated with monochromatic light (λ = 514.5 nm) below 50 K. This effect was introduced as "Light Induced Excited Spin State Trapping" (LIESST).[57,58] Furthermore, also the first examples of Mn(II), Co(III), Mn(III), Cr(II) and SCO compounds originate from this period. The first $3d^5$ Mn(II) SCO complexes (manganocene and 1,1'-dimethylmanganocene) were synthesized by *Ammeter et al.* and by *Switzer et al.* in 1974.[59,60] SCO on the basis of $3d^6$ Co(III) SCO complexes were first realized by *Kläui* in 1979 with [Co^{III}**L**$_2$]PF_6, where the central Co(III) is coordinated by two tripodal ligands with **L** = {$(C_5H_5)Co^{III}[P(O)(OEt)_2]_2$}.[61] *Sim* and *Sinn*[62] reported in 1981 the first $3d^4$ Mn(III) complex [Mn^{III}**(pyrrol)$_3$tren**] (where **(pyrol)$_3$tren** is the trianionic Schiff base resulting from the condensation of pyrrole-2-carboxaldehyde with 2,2′,2″-tris(ethylamino)amine) and finally *Halepoto et al.*[63,64] in 1989 the first $3d^4$ Cr(II) complex [$Cr^{II}I_2$(**depe**)$_2$] (with **depe** = 1,2-bis(diethylphosphino)ethane), showing SCO behavior.

Further examples of SCO compounds of the aforementioned ions are relatively rare even until today. In contrast to that, an enormous number of examples for Co(II), Fe(III) and especially Fe(II) were prepared with a variety of ligand combinations and certain sets of donor

functionalities, enabling the syntheses of not only mononuclear complexes but also of polynuclear compounds. In fact, the first dinuclear Fe(II) SCO complex was synthesized by *Kahn, Real et al.*[65] in the 1980s as well as the first trinuclear compound by *Reedjik*,[66] followed by the first tetranuclear Fe(II) complex in 2000 reported by *Lehn* and *Gütlich*.[67] Even higher nuclearities for SCO systems with Fe(II) are achievable as shown by *Dunbar* (pentanuclear)[68] and *Batten* (hexanuclear)[69] as well as polymeric 1D, 2D or 3D Fe(II) SCO networks[70] based on triazole-, tetrazole- and pyridine-type ligands, inspired by the pioneering work of *Haasnoot*.[71] The ideal coordination environment proven to be particularly favorable for observing SCO behavior in octahedral Fe(III) complexes are especially chalcogen donor ligands with $\{S_6\}$, $\{S_3O_3\}$, $\{Se_3S_3\}$ and $\{Se_6\}$ donor sets as well as Schiff-base ligands with $\{N_4O_2\}$, $\{N_3O_3\}$ and $\{N_2S_2O_2\}$ reviewed by *Nihei*[72] in 2007 and *Harding* in 2016.[73] The best known donor sets for Cobalt(II) SCO complexes are $\{N_6\}$ and $\{N_4O_2\}$ provided mainly by terimine systems or Schiff-bases with pyridine, pyridazine and phenol core units of the ligand which has been reviewed by *Hauser et al*., *Hayami et al*. and *Brooker et al*.[74–76] As already mentioned before, the $\{N_6\}$[77] coordination environment, commonly provided by five- and six-membered heteroaromatic ligands such as pyridines and azoles or a combination of these with pseudohalides (i.e. NCS^-, $NCSe^-$, $NCBH_3^-$ or $NCN(CN)_2^-$), is also most suitable for Fe(II) SCO complexes, although there are also examples with $\{N_4O_2\}$,[78] $\{N_4S_2\}$[79] and $\{N_4C_2\}$,[80] but significantly fewer. The milestones and important examples found until 2004 were summarized in a comprehensive book series, called "Spin Crossover in Transition Metal Compounds", edited by *Gütlich* and *Goodwin*,[81–83] which was followed by the book "Spin Crossover Materials" edited by *Halcrow*,[84] summarizing the achievements within the SCO phenomenon research field until 2013. Today, several decades after the beginning of the SCO research area, the properties of SCO materials are still not easy to predict. Although the dependence of SCO behavior on electronic as well as structural intra- and intermolecular interactions is well understood, the large influence of solid state interactions on the SCO cannot be easily controlled. Investigations are ongoing not only on mononuclear compounds, which maintained their attractiveness for fundamental studies, but also on polynuclear materials either compounds with discrete nuclearity reviewed by *Brooker et al*. in 2013[85] and 2018[86] or coordination polymers reviewed in 2013 by *Muñoz* and *Real*[87] and in 2017 by *Tong et al.*[88] Furthermore, several different interesting research areas have emerged, especially focus on rendering multifunctionality to the SCO systems. The addition of second functionalities to SCO compounds, whose response to external perturbations is synergistically dependent on the electronic spin state of SCO molecules, render these materials highly promising candidates for building optoelectronic, molecular electronic or spintronic devices. A review article recently published by *Kumar* and *Ruben* in 2017 covers the newest emerging trends, hence the combination of SCO and luminescence, photomagnetism or chirality of SCO materials, hybrid SCO materials, SCO-based micro and nanoarchitectures, SCO compounds as solvent sensors as well as the newest advances in SCO active grid complexes and in electrical and spin transportation of SCO materials.[89] Additionally, in 2019 the same authors published a review article targeting sublimable SCO complexes to prepare spin-switchable layers and their use to design molecular and thin-film devices.[90]

The greater research interest in Fe(II) SCO complexes is not only due to the variety of possible ligands systems, but even more to the pronounced change in the properties of these complexes when switched between HS and LS state. Namely, the greatest difference in the magnetic moment is observed for Fe(II) switching between the diamagnetic LS state with a total spin of $S = 0$, in which the electrons are all antiparallelly oriented in the t_{2g} orbitals ($t_{2g}^6e_g^0$), and the paramagnetic HS state with four unpaired electrons and a total spin of $S = 2$ ($t_{2g}^4e_g^2$). In addition, during the SCO the metal-donor atom bond lengths change drastically (≈0.2 Å), due to the occupation of antibonding e_g orbitals in the HS state, whereas in the LS state these orbitals are empty, and Fe(II) SCO complexes often show strong thermochromism. Thus, the analytical methods such as temperature-dependent magnetic susceptibility measurements, UV/Vis, NIR and Raman spectroscopy as well as X-ray crystallography show the best resolution for Fe(II) SCO compounds, which was especially important in the early years in this research field. The discovery of the Mössbauer effect (recoilless nuclear resonance absorption) by *Mössbauer* in 1958[91,92] opened the possibility to track the SCO behavior by Mössbauer studies, which was another contribution to the dominant investigations especially of Fe(II) complexes where the resolution is better compared to Fe(III) compounds.

The following chapters will provide a deeper insight in SCO behavior of Fe(II) complexes, by explaining in more detail the most important concepts and underlying physical relations.

1.2 Occurrence of SCO in octahedral Fe(II) complexes

1.2.1 Ligand field considerations

As already mentioned in the previous chapter, the five degenerated d-orbitals of a free metal ion split up in an ideal octahedral coordination environment into three orbitals with t_{2g} and two orbitals with e_g symmetry. This splitting is due to purely electrostatic interaction between the orbitals and the ligands, which are considered as negative point charges and thus form a "perturbation field" around the central ion. Compared to the five degenerated d-orbitals in spherically symmetric coordination surroundings, the e_g orbitals (x^2-y^2 and z^2), which are pointing directly to the ligand point charges in octahedral coordination, are energetically raised. The t_{2g} orbitals (xy, xz and yz) located between the metal-ligand binding axes are energetically lowered. The splitting of the formerly degenerated orbitals is achieved only with total energy conservation. Thus, the two e_g orbitals are destabilized by 3/5 Δ_O, resulting in an antibonding character, whereas the three t_{2g} orbitals are stabilized by 2/5 Δ_O (Figure 2), which results in a non-bonding character. The octahedral ligand field strength Δ_O is generally considered equal to 10 Dq and depends on the coordinating ligands as well as on the metal ion.[33,93,94]

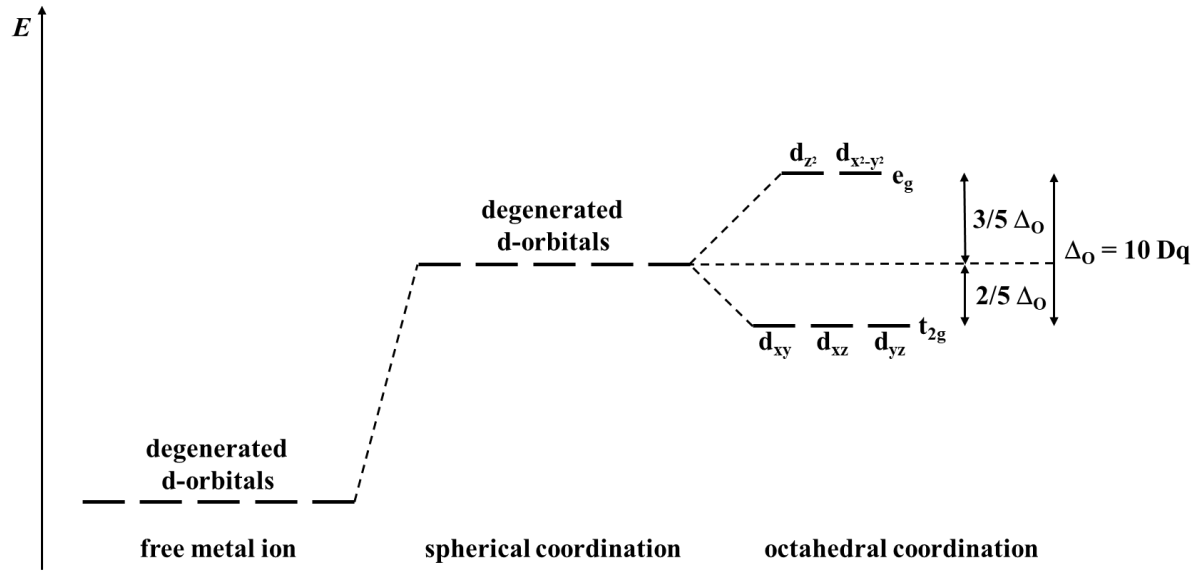

Figure 2. Schematic representation of d-orbitals splitting in an ideal octahedral coordination environment.

Occupation of the d-orbtials with electrons of an octahedral coordinated Fe(II) ($3d^6$) ion results either in the LS or in the HS state, depending on the relation between the ligand field strength Δ_O and the spin pairing energy E_P, which is basically referable to the electron-electron repulsion. In the LS state, where the octahedral ligand field strength Δ_OLS is large compared to the spin pairing energy E_P, all three t_{2g} orbital will be doubly occupied ($t_{2g}^6e_g^0$) and the electrons are antiparallely oriented. This results in in a diamagnetic ground state and a total spin of $S = 0$ (sum of the electron spins s, with $s = \pm 1/2$, depending on whether an electron is pointing upwards or downwards). In the HS state, where Δ_OHS is small compared to E_P the occupation of the d-orbitals follows the first Hund's rule.[95] Thus, each d-orbital is at first occupied with one electron before spin pairing occurs in the t_{2g} orbitals ($t_{2g}^4e_g^2$), resulting in a paramagnetic ground state with a total spin of $S = 2$ (Figure 3).[33,93,96]

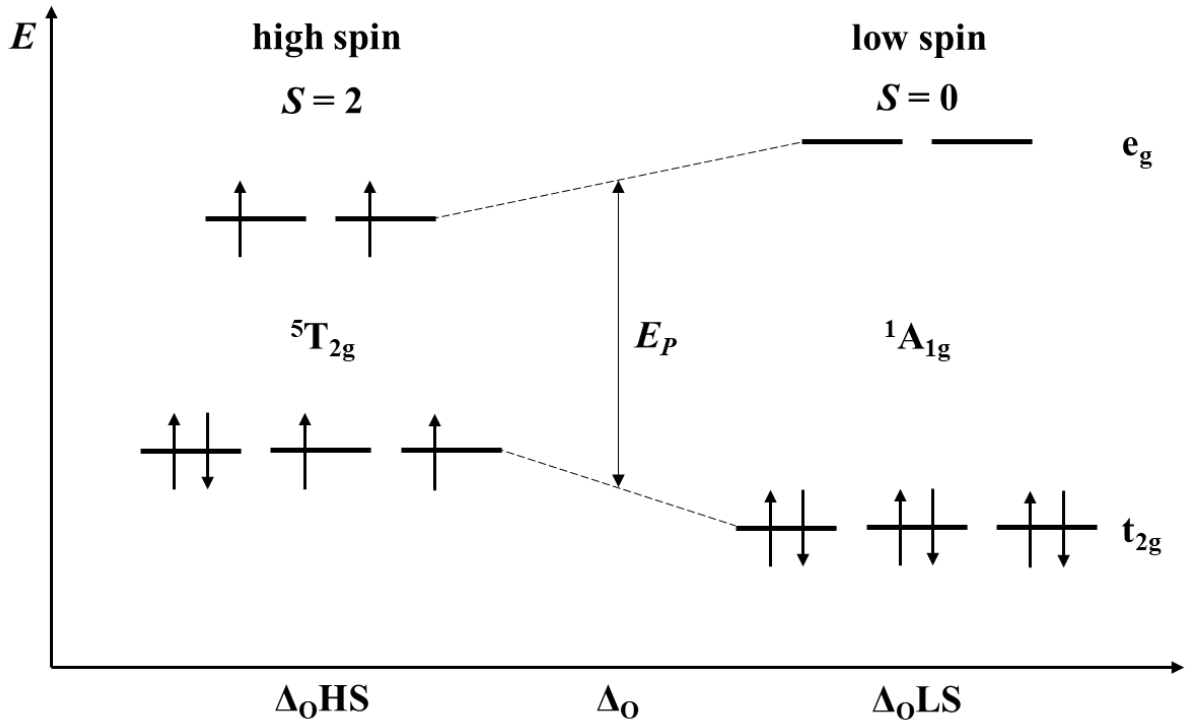

Figure 3. Schematic representation of ligand field splittings in a octahedral coordinated $3d^6$ Fe(II) ion and the resulting two possible electronic configurations by increasing the ligand field strength Δ_O. For the HS state ($^5T_{2g}$) applies $\Delta_O HS < E_P$ (left) while for the LS ($^1A_{1g}$) $\Delta_O HS > E_P$ is true (right).

The effect of the ligand field strength Δ_O on the spin state of the metal ion is clarified even more precisely using the Tanabe-Sugano diagram[97] for octahedral d^6 complexes (see Figure 4). In a Tanabe-Sugano diagram the influence of the ligand field strength Δ_O on the energies of the excited electronic states of a transition metal ion relative to the ground state is plotted in units of the Racah parameter *B*.[98] According to the Russel-Saunders coupling scheme, different states result due to the electron-electron repulsion of a free transition metal ion, which are described by the term symbolism ^{2S+1}L, where $2S+1$ stands for the spin multiplicity and *L* for the orbital momentum. The energies of the electronic states for the free d^6 metal ion are given on the y-axis, where the ligand field strength Δ_O equals zero. The ground state term is ^5D with the lowest electron-electron repulsion and thus the highest spin multiplicity (HS). In weak ligand fields this term is split into the $^5T_2$ ground term and the excited ^5E term. If Δ_O is rising, the $^1A_1$ term (LS) originating from ^1I of the free metal ion drops drastically and replaces the $^5T_2$ as ground state at the critical ligand field strength Δ_C. At this point, the critical ligand field strength Δ_C equals the spin pairing energy E_P. When Δ_O of the HS and the LS state are in vicinity to Δ_C, a spin transition from one to the other state can take place by an outer perturbation.[33,93,96]

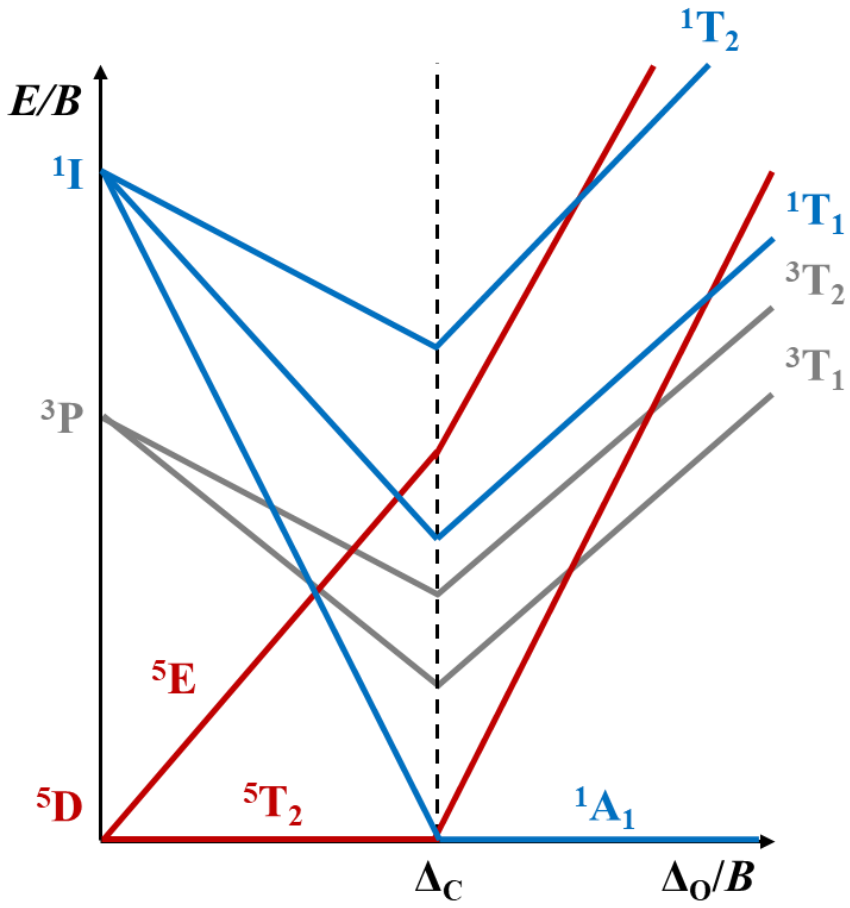

Figure 4. Simplified schematic representation of a Tanabe-Sugano diagram for a d^6 ion in an octahedral coordination environment. The crystal field terms for the HS state are colored in red while the terms for the LS state are blue. A more detailed diagram is given in the work of *Gütlich* or *Hauser*.[33,93]

In addition, in the Tanabe-Sugano diagram the maxima of absorption bands of d-d transitions correspond to the vertical transitions from the ground state to the respective excited states. This is true because according to the Franck-Condon principle the geometry of the complex and thus the ligand field strength Δ_O do not change within the time required for an absorption process (10^{-15} s). Hence, absorption spectra can be used to directly get the value of the ligand field strength Δ_O (10 Dq).[93] Typical values for HS, LS and SCO $3d^6$ Fe(II) complexes are given in Table 1.

Table 1. Typical values for Δ_O in cm^{-1} for HS, LS, and SCO complexes.[33]

		spin crossover complexes		
	HS	HS	LS	LS
Δ_O (10 Dq)/cm^{-1}	<11000	11500–12500	19000–21000	>21500

The octahedral ligand field strength Δ_O does not solely depend on the properties of the ligand and the central metal ion, but is also a function of the metal-ligand donor atom distance *r*(M-L). For neutral ligands the following equation applies, where μ stands for the dipole moment of the ligand.[33]

$$\Delta_O \approx \frac{\mu}{r(\mathrm{M-L})^6} \tag{1.2}$$

This relation results in two harmonic potential wells for the HS and the LS state of a Fe(II) SCO complex along the iron-donor atom distance (*r*(Fe-L)) reaction coordinate (Figure 5). In this schematic diagram, the $^5T_2$ potential well is shifted by the value Δr_{HL} to a higher metal-donor atom distance. This results from the occupation of the antibonding e_g orbitals in the HS state ($t_{2g}^4e_g^2$) leading to a stronger coulomb repulsion between the metal ion and the donor atom of the ligand, because the orbital lobes of these orbitals are pointing directly towards the ligand. In the LS state ($t_{2g}^6e_g^0$) only the non-bonding t_{2g} orbitals are occupied, thus resulting in significantly smaller iron-donor atom bond lengths. For Fe(II) in a $\{N_6\}$ coordination environment the average Fe-N bond length is *r*(LS) = 2.00 Å for the LS state and *r*(HS) = 2.20 Å, resulting in Δr_{HL} = 0.2 Å (10%). As a consequence of the increased bond lengths in the $^5T_2$ state, the bond strength is lowered as well as the vibrational force constant *f*. Therefore, the HS state has a higher vibrational state density compared to the LS ($^1A_1$) state. The vibratory energy levels for the HS and the LS state are depicted as horizontal lines in the harmonic potential well, respectively (Figure 5). The vertical displacement and consequently the energetic difference ΔE_{HL} of the HS and LS vibrational ground states strongly depends on the specific properties of the ligand such as donor strength and strain. It has to be mentioned that the intersection point of the two potential wells corresponds to the critical ligand field strength Δ_C in the Tanabe-Sugano diagram. However, in a correct physical meaning this intersection can never be the ground state of the system. Thus, for SCO systems the values for Δ_OHS and Δ_OLS are only close but never equal to Δ_C.[33,93,96]

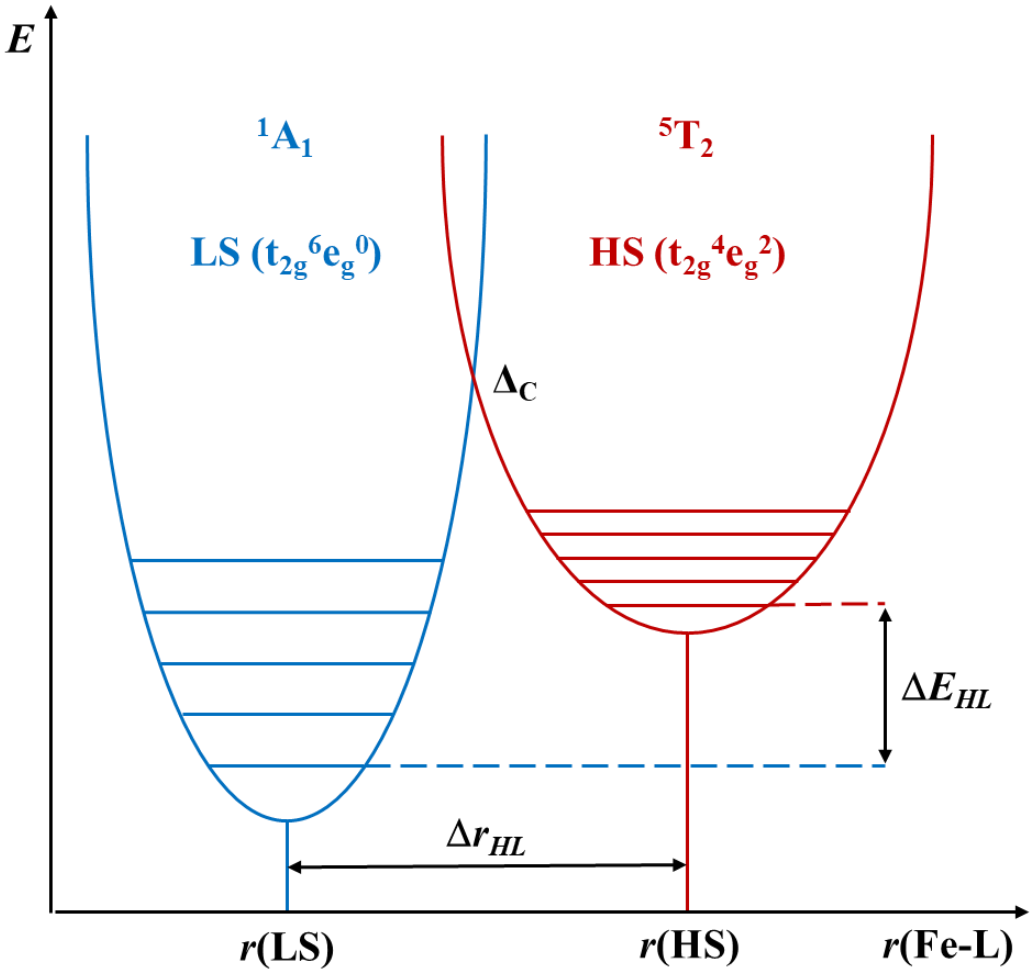

Figure 5. Simplified harmonic potential wells of the iron-donor atom symmetrical stretching vibration for a $3d^6$ Fe(II) ion octahedral coordination sphere in respective to the LS (blue) and the HS (red) state as a function of the iron-ligand donor atom distance *r*(Fe-L). ΔE_{HL} represents the difference between LS and HS vibrational ground states and *r*(LS) as well as *r*(HS) are the equilibrium iron-donor atom distance for the LS and the HS state, which are displaced by the distance Δr_{HL}.

1.2.2 Thermally induced SCO

If ΔE_{HL} is in the vicinity to the thermal energy (k_BT = 200 cm^{-1}) a temperature induced spin transition can occur which can be described by the Gibbs-Helmholtz equation, with ΔG as the difference in the Gibbs free energy, ΔH as the difference in the enthalpy and ΔS as the difference in the entropy (Equation 1.3).

$$\Delta G = \Delta H - T\Delta S \tag{1.3}$$

During the spin transition, the difference in the Gibbs free energy ΔG is equal to zero at the transition temperature $T_{1/2}$, thus depending only on the enthalpy difference ΔH and the entropy difference ΔS. Typical values for the enthalpy change ΔH are ranging from 10–20 kJ/mol, while

the values for the entropy change ΔS ranging from 50–80 J/mol for Fe(II) complexes. Since, the harmonic potential well of the LS state is lower in energy, it is thermodynamically favored at low temperatures. Increasing the temperature will cause an occupation of the higher vibrational states of the $^1A_1$ electronic state until the intersection between the two potential wells is exceeded. Afterwards, an entropy-driven, almost quantitative transition to the HS state takes place. The entropy difference between the two spin states is a consequence of electronic ΔS_{el} and vibrational ΔS_{vib} entropy changes. The electronic contribution ΔS_{el} arises from the 15-fold degeneration of the HS state ($^5T_2$), while the LS state ($^1A_1$) in an octahedral Fe(II) ion is not degenerate, and is a result of a spin as well as an orbit contribution. However, the orbital contribution is often quenched by symmetry lowering in the HS state and can be neglected. Hence, ΔS_{el} can be estimated by just taking into account the spin multiplicities of the HS ($S = 2$) and the LS ($S = 0$) state of a $3d^6$ Fe(II) ion. (Equation 1.4).[33,99,100]

$$\Delta S_{el} \approx \Delta S_{spin} = R\ln\frac{(2S+1)_{\mathrm{HS}}}{(2S+1)_{\mathrm{LS}}} = R\ln\left(\frac{5}{1}\right) = 13.4\ \mathrm{J mol^{-1} K^{-1}} \qquad (1.4)$$

Anyhow, ΔS_{el} is just the minor contribution to the total entropy difference ΔS and amounts to approximately 30%. The remaining 70% arise from ΔS_{vib} and thus from intramolecular stretching and deformation modes, due to the elongated metal-ligand donor atom distance and consequently the higher density of the vibrational states in the HS compared to the LS state.

1.2.3 SCO induced by pressure and light irradiation

As mentioned earlier, another example of external perturbation that can result in a spin transition is the use of pressure. This is known since the early 1960s[48] and can be understood by considering the contributions to the enthalpy change ΔH (Equation 1.5).

$$\Delta H = \Delta E_{el} + \Delta E_{vib} + p\Delta V + V\Delta p \qquad (1.5)$$

A change in pressure will have an influence on the position of the two HS and LS harmonic potential wells relative to each other. If pressure is applied, the distance between the ligand and the metal center will be reduced. Consequently, the HS state will be destabilized because of its longer coordination bond lengths and thus larger volume.[101] Hence, increasing the pressure in SCO systems favors the LS state, thus shifting the transition temperature $T_{1/2}$ to higher values due to the resulting larger energy difference between the HS and the LS state.[38,102–105] Additionally, the SCO behavior can also be inhibited by applying pressure, if a stable high pressure phase is formed.[104]

Spin state switching can also be induced by light irradiation, known as LIESST (Light Induced Excited Spin State Trapping) since 1984.[57,106–110] At a sufficiently low temperature (<50 K) it is possible to switch Fe(II) SCO complexes upon light excitation from the thermodynamically favored LS to the metastable HS state, which has an almost infinite lifetime at these temperatures. Shortly afterwards *Hauser* observed the reverse process by irradiating the HS

complex (reverse-LIESST effect).[111] These findings further established the great research interest in Fe(II) SCO complexes because these exciting photo-physical properties are unique in Fe(II) and cannot be observed in other transition metal ions. Further, it enables the rapid switching of individual molecules between two metastable states which is the basic idea of information processing and storage.[112–114]

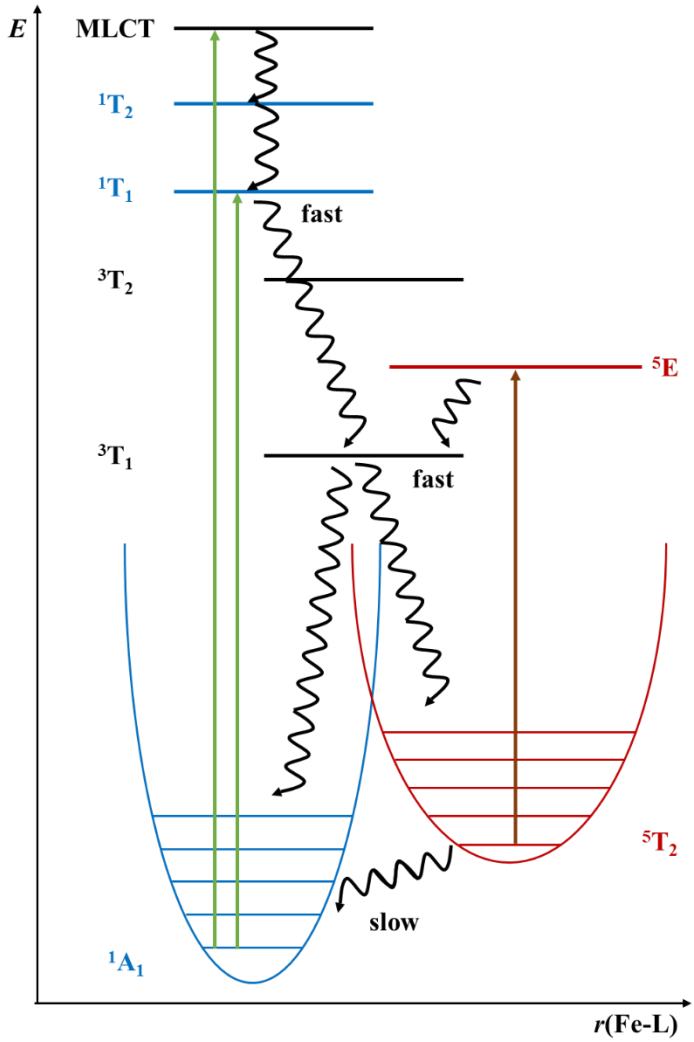

Figure 6. Simplified energy diagram of the different electronic ground and excited states of an octahedral $3d^6$ Fe(II) SCO complex as a function of the metal-ligand donor atom distance *r*(Fe-L). The LS and HS states are represented as harmonic potential wells, whereas the excited singlet, triplet, quintet states and the MLCT state are depicted as horizontal lines. In addition, straight arrows indicate excitations and curly arrows combine non-radiative and radiative relaxation pathways.

Figure 6 shows the essential electronic states of a Fe(II) SCO complex versus the metal-donor atom distance, which are necessary to explain the LIESST effect. Exciting the thermodynamically LS ($^1A_1$) ground state with green light (usually with λ = 514.5 nm, green arrows in Figure 6) at low temperatures, results either in a spin allowed transition in the excited

$^1T_1$ state or in a transition to a low-lying metal to ligand charge transfer (MLCT) state, which can be possibly observed for ligands with extended π-systems. Afterwards, the system can either relax directly back to the thermodynamically favored LS ground state ($^1A_1$) via non-radiative or radiative pathways, or through fast intersystem crossing and internal conversion processes via the excited $^3T_1$ also to the LS ($^1A_1$) or to the metastable HS ($^5T_2$) state. Consequently, all molecules can be converted to the HS state after a sufficient irradiation time and are basically trapped in this metastable state with a very long lifetime because the energy barrier between the HS and the LS state cannot be thermally overcome at low temperatures and the forbidden radiative relaxation to the LS state is very slow ($^5T_2 \rightarrow {}^1A_1$). The reverse-LIESST effect occurs when the SCO complexes in the metastable HS states are excited to the ^5E state by the use of red light (λ = 820 nm, dark red arrow in Figure 6) and relax again via a subsequent cascade of internal conversions as well as inter system crossing decays into the LS state.[112–114] The main problem of the LIESST effect is the occurrence at low temperatures, which is highly unpractical for future applications. *Létard* tackled this problem in 2006 by screening about 60 compounds and relating their photomagnetic properties to the inner coordination sphere of the ligand with the ultimate goal to find a light-inducible SCO complex operating at room temperature.[115]

1.2.4 Characterization of SCO behavior

In Chapter 1.2.2 the fundamental understanding of a thermally induced spin transition in a single Fe(II) complex was described. Consequently, it is expected that the transition will always be abrupt because the transition takes place between two electronic states and the molecule can only be in either the LS or the HS state. However, if there are several switchable spin centers, the thermal spin transition in solid state can vary clearly, as it is accompanied by drastic structural distortions and volume changes, propagating through the solid. In this regard, the level of intermolecular cooperativity (Chapter 1.3.2) plays an important role, which is basically a measure for this propagation and is determined by the crystal lattice properties.[33,96] Figure 7 shows the different spin transition curves for the HS mole fraction versus the temperature, observable for SCO behavior of multiple switchable metal centers. If the intermolecular cooperative interactions are weak, a gradual SCO behavior is observed. Thus, the spin transition takes place over a wide temperature range (Figure 7 a), which is mostly true for SCO complexes in solution. The molecules can be interpreted as independent spin centers and therefore the thermal population of the HS state follows the Boltzmann statistics.[116,117] A higher level of cooperativity results in an abrupt spin transition, which takes place simultaneously for all molecules in a narrow range of a few kelvins (Figure 7 b). Furthermore, it can possibly lead to a thermal hysteresis (Figure 7 c), which is often a result of structural phase changes. The hysteresis grants the system bistability, referring to the ability of a system to be present in two different electronic states in a certain range of external perturbation (usually temperature) and thus showing a “memory-effect”. Consequently, a SCO with a wide thermal hysteresis and preferably with the two transition temperatures $T_{1/2}{}^{\downarrow}$ below and $T_{1/2}{}^{\uparrow}$ above room temperature is the most desirable since it is necessary for possible applications in storage or memory devices.[13,116,118] A review article provided by *Brooker* in 2015 highlights the relation between scan rate and hysteresis width.[34] Stepwise spin transition can be observed in mononuclear as

well as in polynuclear SCO compounds which is also a result of high cooperativity.[33,119–122] As a consequence, short-range and long-range interactions of different strength lead to ordered HS-LS phases during the spin transition, firstly described by *Sasaki* and *Kambara*.[123] Especially in dinuclear SCO complexes, the additional intermediate [HS-LS] state can either be a 1:1 mixture of [HS-HS] and [LS-LS] molecules or discrete [HS-LS] complexes, however this will be explained in more detail in Chapter 1.4.2. An incomplete spin transition usually occurs when gaps and defects are present in the crystal lattice (Figure 7 e). Thus, a significant fraction of molecules will stay in the HS state even at low temperatures. Sometimes it may be a kinetic effect, because as mentioned earlier the HS to LS transition rate becomes extremely small at sufficiently low temperatures. Consequently, rapid cooling or quenching of the sample can lead to a freezing of the metastable HS state at very low temperatures. This effect is known as "Thermally Induced Excited Spin State Trapping" (TIESST).[124–127] The retention of LS complexes at elevated temperatures is usually not observed, because of the higher entropy in the HS state and because kinetic factors are negligible.[116]

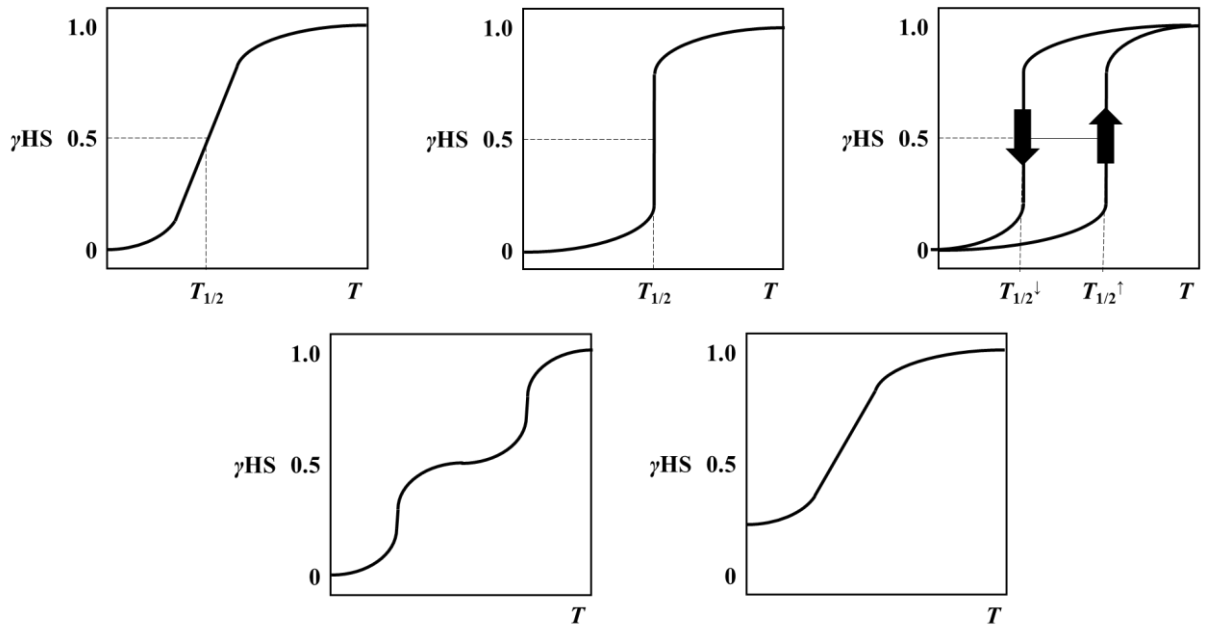

Figure 7. Schematic representation of possible spin transition plotted as the HS mole fraction against the temperature: a) gradual, b) abrupt, c) abrupt with hysteresis, d) stepwise and e) incomplete. $T_{1/2}$ represents the temperature, where equal amounts of HS and LS molecules are present in the sample (γHS = 0.5).

Many different methods such as magnetic susceptibility measurement, Mössbauer spectroscopy, X-ray diffraction, optical spectroscopy as well as IR and Raman spectroscopy offer the possibility to study the temperature dependence of the spin transition in Fe(II) SCO complexes, due to the pronounced electronic, magnetic and structural changes.[56,116,128]

The measurement of **temperature-dependent magnetic susceptibility** χ is nowadays one of the most common techniques to follow the thermally induced spin transition in solid state by using a SQUID (Superconducting Quantum Interference Device) magnetometer. The SQUID magnetometer is based on superconducting loops with Josephson junctions and enables the possibility to measure extremely low magnetic fields. Thus, this measurement technique is highly sensitive towards a change of the magnetic susceptibility χ, allowing sample sizes of single crystals as well as milligram scales. Additionally, customized sample holders allow the measurement under inertgas atmosphere, pressure and light irradiation. The change of the magnetic susceptibility χ in SCO compounds arises from the changing number of unpaired electrons upon switching between the different electronic states. This is especially pronounced in Fe(II) complexes, where the spin transition occurs between the diamagnetic LS ($S = 0$) and the strongly paramagnetic HS ($S = 2$) state. By plotting the χT product versus the temperature, the spin transition curves are directly obtained, often resembling the ideal characteristic ones as shown in Figure 7.[33,96,116,128] To compare the experimentally obtained data with theoretical values, the effective magnetic moments μ_{eff} of the respective spin state can be calculated by using the spin-only formalism (Equation 1.6), with the Landé factor $g \approx 2$, the total spin S and the Bohr magneton μ_B.[94,129]

$$\mu_{eff} = g\sqrt{S(S+1)}\mu_B \tag{1.6}$$

The resulting effective magnetic moment μ_{eff} is in fact related to the χT product (Equation 1.7), with the Boltzmann constant k_B, the Avogadro number N_A and the Bohr magneton μ_B.[94]

$$\mu_{eff} = \sqrt{\frac{3k_B}{N_A{\mu_B}^2}\chi T} = 2.827915\sqrt{\chi T} \tag{1.7}$$

The experimental data are usually slightly higher than the calculated ones for Fe(II) in the HS state, since the orbit contribution to the magnetic moment is not taken into account by the formalism described above.

In solution, the temperature dependency of the magnetic susceptibility can be followed by the **Evans NMR method**.[79,117,130–135] This method is especially well suited to study the influence of electronic modifications to the ligand on the SCO behavior, because cooperative effects are negligible in solution. Specialized double-walled NMR tubes are used to measure the NMR spectra of the SCO sample in deuterated solvents. The outer tube is filled with the dissolved sample while in the inner tube the deuterated solvent is placed as reference. As a consequence of the additional magnetic field of the paramagnetic substance, the NMR solvent signals corresponding to the outer tube will be shifted by $\Delta\nu$ compared to those of the inner tube. With $\Delta\nu$, the mass of the paramagnetic sample m, the frequency of the spectrometer ν as well as the density of the pure deuterated solvent $\rho_{solvent}$ and the sample solution ρ_{sample} the magnetic mass susceptibility of the paramagnetic sample $\chi_{m,sample}$ can be calculated (Equation 1.8).[79]

$$\chi_{m,sample} = \frac{3\Delta\nu}{4\pi\nu m} + \chi_{m,solvent} + \chi_{m,solvent}\frac{\rho_{solvent}-\rho_{sample}}{m} \quad (1.8)$$

Single-crystal X-ray diffraction is another valuable analysis technique, which can be used to detect and analyze the SCO phenomenon. Already mentioned in previous chapters, the spin transition goes along with the redistribution of electrons between the antibonding e_g and the non- to weak-bonding t_{2g} orbitals, which will affect the metal-ligand donor atom bond lengths. Again, for Fe(II) this change is most pronounced resulting in a coordination bond length difference of Δr(Fe-L) ≈ 0.2 Å between the HS and the LS state. The different states can be detected by measuring the crystal structure of the SCO sample before and after the transition temperature $T_{1/2}$. The change of bond lengths during the spin transition directly alters the geometry of the complex leading to a more distorted octahedral coordination environment in the HS state for Fe(II) compared to the almost ideal octahedral coordination sphere in the LS state, which is a result of the isomeric electron distribution in the d-orbitals. The distortion of a Fe(II)-{N_6} coordination sphere can be described by the octahedral distortion parameter Σ (sum of the deviation from 90° of the 12 cis-N-Fe-N angles φ_i in the FeN6 coordination sphere).

$$\Sigma = \sum_{i=1}^{12}|90° - \varphi_i| \quad (1.9)$$

This parameter was firstly introduced by *Hendrickson* to measure small deviations of the coordination geometry in Fe(II) HS complexes[136] and adopted by *Guionneau* to assign rough values to the HS and the LS state in Fe(II) SCO compounds.[137] Thus, complexes in the HS state usually have values of Σ>100° whereas in the LS states Σ<80°. Furthermore, single-crystal X-ray diffraction structure analysis gives the possibility to determine intermolecular interactions in the solid state such as hydrogen bonding or π-π-stacking of aromatic moieties in the ligand backbone. Short- and long-range interactions have a significant influence on the cooperativity and therefore on the SCO properties.[116,128,138]

Another well suited measurement technique to study the SCO behavior of Fe(II) complexes is the **Mössbauer spectroscopy**, which was firstly used by *König et al*. in 1966.[50] The Mössbauer spectroscopy is based on the recoil-free resonant absorption and emission of gamma rays in solids and two important values can be obtained which differ significantly for the HS and the LS state in Fe(II) SCO complexes. Namely, the isomer shift δ, giving information about the oxidation and spin state of the Mössbauer absorber, and the quadrupole splitting ΔE_Q, providing information about the electronic environment around the Mössbauer-active element. Typical Mössbauer spectra for Fe(II) in the HS state show an isomer shift of δ^{HS} ≈ 1 mms^{-1} and a large quadrupole splitting of $\Delta E_Q{}^{HS}$ ≈ 2 – 3 mms^{-1}, whereas for the LS state these parameters are generally smaller with δ^{LS}≤0.5 mms^{-1}and of $\Delta E_Q{}^{LS}$≤1 mms^{-1}. If both spin states are present at a given temperature and the time-scale of the HS→LS relaxation is slower than the Mössbauer time window (10^{-7} s for ^{57}Fe), it is possible to distinguish the two subspectra even though they strongly overlap. Further, the area fractions of the resonance lines are proportional to the concentration of the respective spin state and can be fitted using the Lorentzian fit.[96,116,128,139]

Since the SCO in Fe(II) complexes is often accompanied by a color change when switching between the different electronic states (thermochromism), the thermal spin transition phenomenon can be followed by the naked eye or even more precisely by using **UV/Vis spectroscopy**. If the color of a SCO complex is solely attributed to the d-d transitions, it follows that the LS state is usually intensively colored and the HS state mostly colorless. This can be explained by looking again at the Tanabe-Sugano diagram (Figure 4). The only spin allowed d-d transition in the HS state ($^5T_2 \rightarrow {}^5E$) is located in the near infrared region (800–900 nm) whereas the two spin allowed transition in the LS state ($^1A_1 \rightarrow {}^1T_1$, 500–700 nm and $^1A_1 \rightarrow {}^1T_2$, 300–400 nm) appears in the visible region. The reason for the coloration is that the ligand field strength Δ_O in the LS state is larger compared to the HS state and therefore higher energetic radiation is necessary for excitation. Consequently, upon cooling a SCO sample the band for the HS state decreases while the two bands for the LS are increasing. Additionally, information about the ligand field strength Δ_O can be extracted as well as possible irradiation band to observe the LIESST effect.[33,56,58,93,128]

The temperature-dependent spin transition in Fe(II) SCO materials can also be monitored by **vibrational spectroscopy** such as IR or Raman spectroscopy. Key feature for these techniques are the changes of the metal-ligand donor atom bond lengths. The corresponding Fe-L vibration band can be found in the range of 500 to 250 cm^{-1} for a Fe(II)-{N_6} complex and should show the greatest difference when changing the electronic state. However, these bands are often hard to assign since there are a lot of bands in the so-called "finger print" region arising from various different vibration modes in the solid state. More suitable to follow the thermally induced SCO phenomenon are vibrational modes of coordinating ligands that are directly linked to the coordination bond modes, for example the C-N stretching vibrations of coordinating pseudohalide anions as they appear in the region of 2200–2000 cm^{-1}.[56,99,116,140–142]

A thermal SCO can also be interpreted as a first order phase transition which is cooperatively propagating through the solid state.[99] Hence, it can be monitored by **differential scanning calorimetry** (DSC). A DSC measurement can be used to determine the transition temperature $T_{1/2}$ because the excessive heat capacity C_P is observed as a peak at this temperature, which is a result of the enthalpy and entropy changes during the spin transition. Depending on the peak size, the different thermal transition types can be directly seen. Namely, a broad signal corresponds to a gradual SCO and a sharp signal to an abrupt one. Furthermore, by integration over the peak area in the C_P vs. T plot, the values for the enthalpy change ΔH and the entropy change ΔS can be calculated because the change in free Gibbs energy ΔG equals zero at $T_{1/2}$.[33,39,128,141,143–147]

These are by far the most common techniques to investigate the thermal SCO behavior in Fe(II) complexes but there are some more which come in handy in special cases.[39,116,128] They will not be discussed in detail but should be mentioned: **Electron Paramagnetic Resonance spectroscopy** (EPR),[148–152] **X-ray Absorption Spectroscopy** (XAS),[153–156] **Positron Annihilation Spectroscopy** (PAS),[157,158] **Muon Spin Relaxation** (μSR),[159–162] and **Nuclear Resonance Scattering** (NRS).[163–165]

1.2.5 Some aspects regarding the difference between Fe(II) and Co(II) SCO complexes

This chapter emphasizes in a more detailed way on the differences between Fe(II) and Co(II) complexes even though some were already mentioned before.

In Fe(II) complexes the SCO has a huge influence on the properties, because in the HS state the antibonding e_g orbitals are occupied by two electrons ($t_{2g}^4e_g^2$), while in the LS state only the non- or weak-bonding t_{2g} orbitals are occupied ($t_{2g}^6e_g^0$). This results in the aforementioned drastic changes of for example the magnetic susceptibility ($S^{HS} = 2$, $S^{LS} = 0$) or the metal-ligand donor atom bond lengths (Δr(Fe-L) ≈ 0.2 Å). The property changes in Co(II) are much less pronounced. The transition takes place between the ^{2}E (LS) and the $^4T_1$ (HS) state with the corresponding electronic configurations $t_{2g}^6 e_g^1$ and $t_{2g}^5e_g^2$. As a consequence, the change of the metal-ligand donor atom distance is smaller with Δr(Co-L) ≈ 0.10 Å, because in both electronic states the antibonding e_g orbitals are occupied.[74,75,166] Since the molecular volume changes in Co(II) compounds is less pronounced during the spin transition, cooperative interactions, which help to propagate local distortions through the solid, are usually less important.[74] Thus, the probability of the occurrence of a thermal hysteresis is less expected. In fact, the vast majority of the Co(II) complexes showing SCO behavior exhibit a gradual transition. Consistent with the above mentioned, the magnitude of both thermodynamic parameters, the enthalpy change ΔH and the entropy change ΔS is smaller.[166] The smaller entropy difference ΔS for Co(II) SCO complexes, which can be calculated with Equation 1.4, as well as the possibility of spin state mixing through spin-orbit coupling causes a lower activation barrier compared to Fe(II) SCO compound. This results in spin interconversion between the HS and the LS state induced by smaller changes of external stimuli.[75,166] Another important difference is the respective contribution of the Jahn-Teller effect. The HS state of an Fe(II) SCO complex is influenced solely to a very small extent while the LS state of a Co(II) SCO compound is strongly affected, which results in trigonal or tetragonal distortions.[74] The most important method to characterize a thermally induced SCO in Co(II) complexes is the temperature-dependent magnetic susceptibility measurement, as it is also for Fe(II). However, the evaluation is more difficult for Co(II) ions. The LS state has one unpaired electron (S = 1/2) and the χT product can be calculated by using the spin only formalism (χT ≈ 0.38 cm^3Kmol^{-1}, Equation 1.6 and 1.7) which is usually very close to the experimentally obtained data, independent of different local geometries. The spin-only value for the HS state with three unpaired electrons (S = 3/2) state is calculated as χT ≈ 1.88 cm^3Kmol^{-1}. But the experimental values can deviate drastically from this value, due to the orbital angular moment of the $^4T_1$ state and the resulting spin-orbit coupling which contributes to the magnetic moment.[39,74–76,166] According to the spectrochemical series of metal ions, the contribution to the ligand field strength Δ_O is smaller in Co(II) compared to Fe(II) ions and can be explained by the higher spin pairing energy of the former.[40,41,166,167] Thus, to obtain SCO complexes with Co(II), ligands with stronger ligand field strength are necessary which is especially well studied for the bis(terpyridine) systems.[75]

1.3 Influences on the SCO behavior

1.3.1 Ligand design

The ligand field strength Δ_O appropriate in energy to the used metal ion plays a significant role for observing SCO behavior. As already mentioned, every metal ion in a specific oxidation state has an individual natural splitting of the d-orbitals, thus there are only a few suitable donor sets to exhibit the spin transition. Although the SCO research field now exists for almost 60 years, there is still no rational approach to predict the exact ligand field and often the ligand field strength Δ_O need to be adjusted, since it does not solely depend on the type of donor atom sets.[96,116,128,168]

One approach to modify the ligand field is the replacement of chelating ligands by coordinating counter ions, which directly alters the ligand field strength Δ_O. From an empirical point of view, for mixed heteroleptic complexes $[MA_nB_{(6-n)}]$ the rule of the "averaged environment" applies, which illustrates that the Δ_O (10 Dq) values of mixed complexes can be approximated by a linear relationship between Δ_O values for the homoleptic complexes $[MA_6]$ and $[MB_6]$ (Equation 1.10).[94]

$$\Delta_O\left(\left[MA_nB_{(6-n)}\right]\right) = \frac{n}{6}\Delta_O([MA_6]) + \frac{(6-n)}{6}\Delta_O([MB_6]) \qquad (1.10)$$

A prime example is the Fe(II) complex $[Fe^{II}(\mathbf{phen})_3]^{2+}$ which is in the LS state at room temperature, independent of the non-coordinating anions. Substitution of one of the bidentate phenanthroline ligands for two NCS^- ions results in the first known Fe(II) SCO complex $[Fe^{II}(\mathbf{phen})_2(NCS)_2]$, which was reported by *Baker* and *Bobonich* in 1964.[49] Another example is given by *Zarembowitch* in 1990. The complex $[Fe^{II}(\mathbf{py})_4(NCS)_2]$ (with **py** = pyridine) is in the HS state at room temperature and does not show a spin transition until very low temperatures. However, by substituting two pyridine molecules for either a 2,2'-bipyrimidine (**bpym**) or a 1,10-phenanthroline (**phen**) molecule, which naturally has a stronger ligand field strength Δ_O, the resulting complexes $[Fe^{II}(\mathbf{py})_2(\mathbf{bpym})(NCS)_2]$ and $[Fe^{II}(\mathbf{py})_2(\mathbf{phen})(NCS)_2]$ exhibit thermally induced abrupt SCO behavior. In addition, the **bpym** complex even shows a small thermal hysteresis.[169,170] In both examples NCS^- has been used as coordinating anion. However, there are many other pseudohalides such as NCO^-, $NCBH_3^-$, $NCSe^-$, CN^- or $(CN)_2N^-$, which differ in ligand field strength Δ_O and thus allow fine tuning of the SCO properties. For example *Brooker et al* reported a shift of the spin transition temperature $T_{1/2}$ of the SCO complex $[Fe^{II}(\mathbf{L})_2(X)_2]$ (with $X = NCS^-$, $NCSe^-$ and $NCBH_3^-$ and **L** = 4-p-tolyl-3-(2-pyrazinyl)-5-(2-pyridyl)-1,2,4-triazole) upon variation of the coordinating counter ions. By increasing the ligand field strength Δ_O of the pseudohalide anions ($NCS^- < NCSe^- < NCBH_3^-$) $T_{1/2}$ is shifted to higher temperatures.[171] This effect is well documented in literature.[99,110,172–177]

Another way to vary the ligand field can be achieved by adding substituents to the ligand system, either to add steric hindrance or to effect the electronic properties of the donor atoms by incorporating electron-donating or electron-withdrawing groups. As the electronic state correlates with the metal-ligand bond length, the addition of a bulky substituent close to the donor atom leads to steric hindrance between the metal center and the ligand. Thus, the coordination geometry will be distorted and the HS state will be favored. This approach can be used to change the spin state of the system. Here again the complex $[Fe^{II}(\mathbf{phen})_3]^{2+}$ serves as an excellent example. Functionalization in the 2-position of the phenanthroline ligand by substituting the proton atom for the sterically hindered methyl group leads to an extension of the Fe-N bond length and thus to stabilization of the HS state at room temperature. Although the σ-donor strength of the nitrogen donor atom increases due to the positive inductive effect (+I-effect) of the CH_3 group, the steric hindrance of the methyl substituent has the greater influence on the ligand field. Furthermore, the complex with the methylated phenanthroline ligand shows SCO behavior when cooled.[178,179] Similar behavior was found in other ligand systems as well.[55,180–182]
The effect of electron-donating or electron-withdrawing groups on the SCO behavior was nicely demonstrated by *Halcrow et al.*[183] They used the complex $[Fe^{II}(\mathbf{bpp})_2]^{2+}$ (with **bpp** = 2,6-di(pyrazol-2-yl)pyridine) to generalize a relationship between ligand substituents and spin state by replacing the hydrogen atom on the 4-position in the pyridine ring, para to the nitrogen donor atom, as well as on 4-position in the pyrazole, meta to the nitrogen donor atom, for substituents with different electronic properties. They were able to correlate the transition temperature $T_{1/2}$ of twenty-five different substituted complexes to the relevant Hammett parameter[184], which basically takes into account mesomeric and inductive effects of the substituents. The study was performed on complex solutions with the Evans NMR method because in solution, crystal-packing effects can be neglected and thus the spin state is only dependent on the electronic nature of the ligand. As a result, substitution at the pyridine ring with electron-withdrawing groups or at the pyrazole ring with electron-donating groups stabilizes the LS state. However, the authors emphasize that there is no generality to the question whether electron-donating or electron-withdrawing groups will stabilize either exclusively the HS or the LS state. The spin state depends on the position of the substituent within the ligand backbone and the competing influence of opposing metal to ligand σ- and π-bonding effects.[183]

Further possibilities to modify the ligand field strength Δ_O of the ligand are the replacement of six-membered heteroaromatic rings by five-membered ones, the replacement of aromatic by aliphatic donating moieties or varying the chelating ring size. All these modifications result in different strain within the ligand backbones as well as an alteration of the σ-donor and π-acceptor character of the system[96,185] Recently, a nice example has been given by *Brooker*.[135] Substitution of the pyridine moieties in the side arms of the **TDPT** ligand (4-Tolyl-3,5-di(2-pyridyl)-4*H*-1,2,4-triazole) for thiazoles (**TDTT** = 4-Tolyl-3,5-di(2-thiazolyl)-4*H*-1,2,4-triazole) resulted in the complex $[Fe^{II}(\mathbf{TDTT})_3](BF_4)_2$. While the complex with the **TDPT** ligand remains in the HS state, the new complex with the **TDTT** ligand shows SCO behavior.

1.3.2 Cooperativity

Even though there are many possibilities to design the ligand systems and thus vary the ligand field strength Δ_O to ultimately reach SCO behavior at room temperature with a wide thermal hysteresis as final goal for future applications, the properties in the solid state are not predictable. DSC measurements show that a spin transition can be seen as a first order phase transition that propagates through the material, which originates from the change of coordination bond lengths.[99] Cooperative effects have a significant impact on this propagation and often influence the type of the spin transition or even the appearance. As mentioned earlier, weak cooperativity results in a gradual or incomplete SCO behavior whereas strong communication leads to abrupt transitions and possibly to the occurrence of a thermal hysteresis.[33,128,186,187] The cooperativity in the solid state can be enhanced intermolecularly by classical and non-classical hydrogen bonding directly between the complexes or facilitated by non-coordinating solvent molecules or non-coordinating counter ions. Further, the communication can be mediated by van der Waals' contacts via π-π-stacking of aromatic moieties in the ligand backbone and there are also some examples of lone pair-π and halogen bonding interactions.[33,142,188–190]

The effect of cooperativity on the properties and the shape of a spin transition can be investigated when comparing the SCO behavior of a crystalline compound to its behavior in solution. In solution the SCO complexes as well as the solvent molecules and the coordinating anion are randomly disordered and thus the complexes act as isolated molecules whereas in the solid state the aforementioned cooperative interactions lead to a systematic orientation of the complexes which enables communication.[117] Alternatively, the intermolecular communication between the SCO metal ions can be suppressed by metal dilution with other transition metals which are not SCO-active or at least not with the chosen ligand system (Zn(II), Ni(II), Mn(II) or Co(II)). In the doped material, the intermolecular interactions are still available but the propagation of the phase transition in the SCO-active metal ions will be buffered by complexes bearing the foreign metal ions, which do not show any structural change. As an example, the SCO complex $[Fe^{II}(2\text{-}\mathbf{pic})_3](Cl)_2 \cdot EtOH$ (with **pic** = picolylamine), reported 1967 by *Renovitch* and *Baker*, shows an abrupt spin transition at about 115 K.[191] Single-crystal structure analysis revealed hydrogen bonding interactions mediated by the solvent molecules.[192] Successively replacing Fe(II) with Zn(II) ions, which have isostructural complex cations, resulted in a series of mixed complexes with the chemical composition of $[Fe^{II}_xZn^{II}_{1-x}(2\text{-}\mathbf{pic})_3](Cl)_2 \cdot EtOH$ with x ranging from 0.0007 to 1. Upon decreasing Fe(II) concentration, the spin transition becomes more gradual and the transition temperature $T_{1/2}$ is shifted to lower temperatures. At very high dilution with about one percent of Fe(II), the spin transition curve can be described by the Boltzmann distribution, normally observed for complex solutions, where cooperativity is practically non-existent.[193] This work was the first to show clearly the existence of cooperative elastic interactions in the solid state and the effect of these interactions on the SCO behavior, leading to further metal dilution studies in other SCO complexes.[128,194–198] Additionally, due to the importance of cooperative effects in solid SCO materials a theoretical approach, the so-called "Mainz Model" based on pure mechanical communication between the spin-carrying metal centers was developed by *Spiering* and *Willenbacher*.[199,200]

1.3.3 Solvent and non-coordinating anion effects

The intermolecular interactions in the solid material rarely occur directly between the complex molecules but are mostly mediated by non-coordinating anions and solvent molecules. Classical and non-classical hydrogen bonding leads to short contacts between the complex cations and non-coordinating molecules and the formation of intermolecular interaction pathways. Furthermore, hydrogen bonding can have a relayed effect on the ligand field due to a small change in the electron density of the coordinating ligand. Thus, the non-coordinating anions and solvent molecules embedded in the crystal lattice can drastically effect the SCO properties, resulting in a shift of the transition temperature $T_{1/2}$, a different shape of the transition curve or even in a total absence of any spin transition. This influence is hardly predictable and makes systematic studies of the relation between intermolecular interactions and the SCO behavior inevitable.

Again the $[Fe^{II}(2\text{-}\mathbf{pic})_3](Cl)_2 \cdot EtOH$ SCO complex is a nice example to introduce the effect of non-coordinating anions as well as solvent molecules on the SCO properties. By replacing the chloride in the former complex for bromide or iodide, the spin transition is less abrupt and complete in the mentioned order. Furthermore, changing the co-crystallized ethanol molecules in the chloride complex for methanol results in a more gradual SCO near 150 K. In the case of the monohydrate complex it leads to the occurrence of a 90 K wide thermal hysteresis with the two transition temperatures of $T_{1/2}{}^{\downarrow} = 200$ K and $T_{1/2}{}^{\uparrow} = 290$ K. However, the dehydrated sample does not show any SCO properties.[116,128,201–203] The importance of hydrogen bonding on the SCO has later been intensively studied by *Gütlich et al.* by isotopic exchange of hydrogen for deuterium and ^{14}N for ^{15}N in various positions within the 2-picolylamine ligand system as well as in the solvent molecules. This work clarified that the spin transition is only affected when isotopic substitution is performed on atoms directly involved in the hydrogen bonding network, which was confirmed by other studies as well.[39,116,204,205] Besides the presented complex, there are many other examples in literature showing the influence of the solvent molecules as well as non-coordinating anions and their incorporation in hydrogen bonding interaction pathways on the properties of different SCO compounds.[206–212]

Another example is given by *Brooker et al*.[213] They were able to show that the variation of the solvent molecules by reversible single-crystal to single-crystal transformation leads to distinguishable magnetic properties and to different colors of the Fe(II) complexes. The transformation processes were facilitated by exposure to vapors of different solvent molecules (acetonitrile, ethanol and water). Remarkably, crystal transformation is reversible even though the Fe(II) complexes with coordinating acetonitrile and ethanol molecules are dinuclear whereas the Fe(II) compound with coordinating water molecules is a 1D chain. The varying nuclearity is explained by two different bridging modes of the ligand. While the MeCN complex is dark red and shows hysteretic SCO behavior, the orange EtOH complex and the yellow H_2O complex remain in the HS state over the whole measured temperature region.[213] Usually, such sensing of guest molecules, which renders these compounds promising candidates for application as chemical sensors, is observed for porous Metal Organic Frameworks (MOFs). There are also many examples of MOFs that show guest-dependent SCO behavior.[214–218]

1.4 Polynuclear Fe(II) SCO complexes

In the previous chapters, the general concepts and many phenomena of SCO behavior were explained mainly for mononuclear compounds. However, in the 1980s the focus within the research field shifted towards SCO materials with higher nuclearity. Multinuclear compounds are in advantage to mononuclear complexes because they potentially exhibit intramolecular cooperative effects additionally to the intermolecular interactions such as hydrogen bonding and π-π-stacking. The direct connection of SCO-active metal centers via organic molecules can lead to increased cooperativity and thus to more abrupt transitions and the occurrence of wide thermal hysteresis. In this regard, a large number of SCO materials where the spin switching metal centers are embedded in discrete polynuclear structures or in coordination polymers, have been synthesized and investigated.[85–88]

1.4.1 Fe(II) coordination polymers

Among the coordination polymers the Fe(II)-1,2,4-triazole system has proven to be a perfect candidate for designing 1D chains, 2D layers or 3D networks.[70] In fact, one of the most promising materials for future applications is the 1D polymer with the chemical composition $[Fe^{II}(\mathbf{Rtrz})_3]A_2 \cdot$solvent (with **Rtrz** = 4-R-1,2,4-triazole and A = mono negative non-coordinating anion) because there are some examples showing large thermal hysteresis around room temperature and strong thermochromism.[13,87,219] Within these chains the Fe(II) ions are bridged by three 1,2,4-triazole molecules. Substitution at the 4-position of the ligands as well as changing the counter ions and the solvent molecules allows the investigation of different intermolecular interactions and thus different SCO behavior. Despite the great research interest in such compounds due to the potential application as memory or display devices outlined by *Kahn*,[13] the poor crystallinity makes structural characterization of those compound very difficult. It is mostly limited to X-ray absorption as well as powder diffraction experiments and comparison to related structural characterized structures as discussed in a number of reviews.[220–223] The incorporation of these coordination polymers into technologically convenient substrates such as composites, gels, nanoparticles or liquid-crystalline materials has been successful. However, up until now they have never been used in commercially available devices.[87] Coupling two triazole ligands at the 4-position results in SCO materials with a 2D layer structure. In the $[Fe^{II}(\mathbf{btr})_2(NCS)_2]\cdot H_2O$ (with **btr** = 4,4'-bis-1,2,4-triazole) coordination polymer, the Fe(II) are bridged by four 4,4'-bis-1,2,4-triazole ligands which are coordinating in plane whereas two NCS^- anions in the apical positions, trans to each other, fill the octahedral coordination sphere. The layers are connected via weak van der Waals contacts and hydrogen bonding interactions between the water molecules and the non-coordinating nitrogen atoms of the ligand. This compound was the first example, showing abrupt SCO behavior and a 25 K wide thermal hysteresis centered around 134 K in a 2D network, and still remains a model material in SCO research.[224,225] Furthermore, replacing the coordinating NCS^- anions for non-coordinating ClO_4^- resulted in a 3D network where each Fe(II) ions is coordinated by six 4,4'-bis-1,2,4-triazole ligands and is bridged to six other Fe(II) centers. The compound with the chemical composition $[Fe^{II}(\mathbf{btr})_3](ClO_4)_2$ shows a two-step

SCO behavior with a plateau region centered around 200 K after 50% of the Fe(II) have changed the spin state.[226] Besides the 1,2,4-triazole ligand there are many other possible ligand systems such as fused tetrazoles or pyridines with different lengths and functionalities within the organic linkers resulting in two- or three-dimensional networks which exhibit SCO behavior.[70,87] Additionally, metal organic frameworks of the Hofmann-type are excellent examples of coordination polymers that show SCO properties, which can be varied by host guest chemistry in these porous materials.[88]

1.4.2 Dinuclear Fe(II) SCO complexes

Coordination polymers have proven to be excellent candidates to propagate local distortion as a result of a spin transition throughout the solid state. Consequently, they often show abrupt SCO behavior with the occurrence of wide thermal hysteresis. However, there are many difficulties regarding these materials. Indeed, the limited control over the overall structure of such compounds, the reproducibility of chemical and physical properties and more importantly the poor crystallinity and thus the structural characterization, makes the full understanding of the SCO properties within such coordination polymers a very challenging task.
Considering these facts, the research in SCO compounds with discrete nuclearity, which combine the advantages of the intramolecular cooperative interactions of SCO coordination polymers with the easier structural characterization, has increased. There are many discrete oligomeric SCO compounds ranging from dinuclear to octanuclear synthesized by supramolecular self-assembly strategies or by incorporation of the metal ions in rational designed multidentate chelating ligands. The *supramolecular* approach benefits from the rather easy synthesis by combining commercially available or easily synthesized capping and bridging ligands in precise ratios with metal ions while the nuclearity is controlled via the geometrical requirements of the metal center and the denticity of the ligands. The main disadvantage of this route is that side products can form due to rearrangement of the ligands and/or the presence of dynamic equilibria between different possible nuclearities and thus prediction of the final compound is not straightforward. The other approach of rational designing chelating ligands has the advantage that the nuclearity is controlled by the number of binding pockets within the ligand system. Further, this route offers the possibility to systematically investigate material properties by variation of the ligand backbones. However, the main problem is the often required multistep organic synthesis that sometimes is very time consuming and challenging.[86,119,168]

Among the polynuclear SCO compounds the dimeric structural motif is most valuable. It is the simplest and smallest unit of two interacting spin switching metal centers allowing for systematic investigations of intra- and intermolecular cooperative interactions. Furthermore, the dinuclear complexes with two SCO-active centers may exhibit a two-step spin transition leading to three accessible states ([HS-HS], [HS-LS] and [LS-LS]), which potentially allow higher information storage capacities and complex operations based on trinary logic.[67,227,228] The intermediate state can be displayed either by a 1:1 mixture of molecules in the [HS-HS] and [LS-LS] state or by isolated molecules with one of the two SCO-active metal ions being in the LS state while the other is in the HS state. The possibility of an intermediate spin state led

to an increased interest in dimeric SCO compounds. However, not all dinuclear complexes exhibit multistep SCO behavior. Whether the spin transition occurs directly in one-step [HS-HS]→[LS-LS] or in a two-step manner via the intermediate spin state [HS-HS]→[HS-LS]→[LS-LS] depends on the enthalpy difference between the mixed [HS-LS] state and the halfway point between the enthalpies of the [HS-HS] and the [LS-LS] state 1/2Δ*H*. If the [HS-LS] state lies in energy between the [HS-HS] and 1/2Δ*H*, the spin transition occur directly from the [HS-HS] to the [LS-LS] state (Figure 8 a). Thus, the more the mixed spin state is stabilized in energy relative to 1/2Δ*H* meaning closer in energy to the [LS-LS] state, the more likely a step-wise transition takes place (Figure 8 b). However, if the energy gap between the [HS-LS] and the [LS-LS] is too small, the system will remain trapped in the intermediate spin state and no second spin transition to the ground state is observable (Figure 8 c). This phenomenological model was introduced by *Kahn* and *Zarembowitch* and was proven to be applicable in many cases.[229–234]

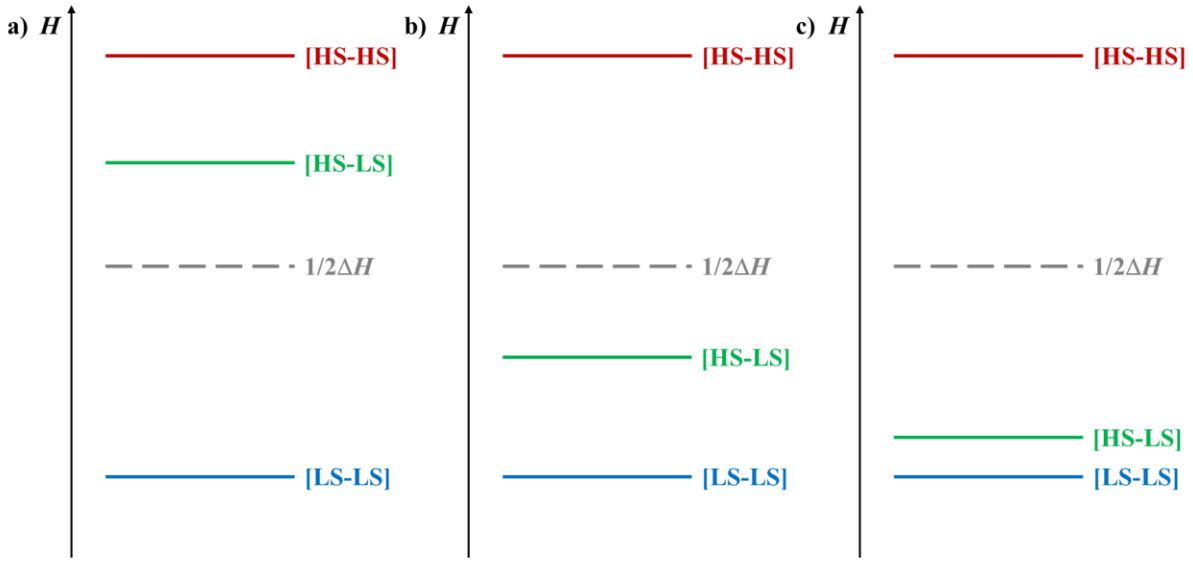

Figure 8. Representation of [HS-HS], [HS-LS] and [LS-LS] enthalpies relative to each other for a one-step spin transition from the [HS-HS] to the [LS-LS] state (a), for a two-step spin transition via the intermediate [HS-LS] state (b) and for a one-step transition from the [HS-HS] to the [HS-LS] state (c) according to the phenomenological model of *Kahn* and *Zarembowitch*.[229]

The first bimetallic Fe(II) SCO complex $[Fe^{II}_2(\mathbf{bpym})(\mathbf{bzp})_2(NCS)_4]$ (with **bpym** = 2,2'-bipyrimidine and **bzp** = bromazepam) was reported 1987 by *Real et al.* showing a spin transition between 260 and 220 K from the [HS-HS] to the intermediate [HS-LS] state.[65] Further investigation of related ligand systems led to the synthesis and characterization of $[Fe^{II}_2(\mathbf{bpym})(\mathbf{bt})_2(NCS)_4]$ (with **bt** = 2,2'-bis-1,3-thiazole) in 1992. Within this dinuclear complex each Fe(II) ion is coordinated by two NCS^- anions and one bidentate bis-thiazole ligand and bridged by the bipyrimidine ligand providing the $\{N_6\}$ coordination environment. This compound shows for the first time abrupt two-step thermal SCO

([HS-HS]→[HS-LS]→[LS-LS]) behavior within a dimeric structural motif. Based on calorimetric and Mössbauer measurements, *Real et al.* proposed that the intermediate spin state is displayed by discrete [HS-LS] and thus both metal ions undergo spin transition separately at slightly different temperature.[229] Furthermore, they suggested that the synergistic interplay between intra- and intermolecular cooperative interactions is the key factor whether the intermediate state consists of a 1:1 mixture of [HS-HS] and [LS-LS] molecules or of localized [HS-LS] molecules. The final evidence for the existence of localized molecules with one Fe(II) in the HS and one in the LS state in the intermediate state was given by *Ksenofontov et al.* by using applied field Mössbauer spectroscopy. With this measurement method they were able to distinguish two different HS signals for the Fe(II) ions belonging either to the [HS-HS] or the [HS-LS] state.[235]

Almost twenty years after the discovery of the first bimetallic Fe(II) complex showing two-step SCO behavior, in 2005 *Klingele et al.* were the first observing localized [HS-LS] molecules crystallographically (Figure 9, left).[236] By using the bis-tridentate bridging ligand **PMAT** (4-amino-3,5-bis{[(2-pyridylmethyl)amino]methyl}-4*H*-1,2,4-triazole), which is strongly predestinated to build the dimeric structure motif, they were able to synthesize the bimetallic compound $[Fe^{II}_2(\mathbf{PMAT})_2](BF_4)_4 \cdot H_2O$. The complex exhibits an abrupt spin transition from the [HS-HS] to the [HS-LS] state centered around $T_{1/2} = 224$ K investigated by temperature-dependent magnetic moment measurement (Figure 9, right). The crystal structure of the complex cation $[Fe^{II}_2(\mathbf{PMAT})_2]^{4+}$ recorded at 123 K shows two crystallographically distinguishable Fe(II) ions with different Fe-N bond lengths corresponding to the HS (Fe(2)) and the LS (Fe(1)) state.

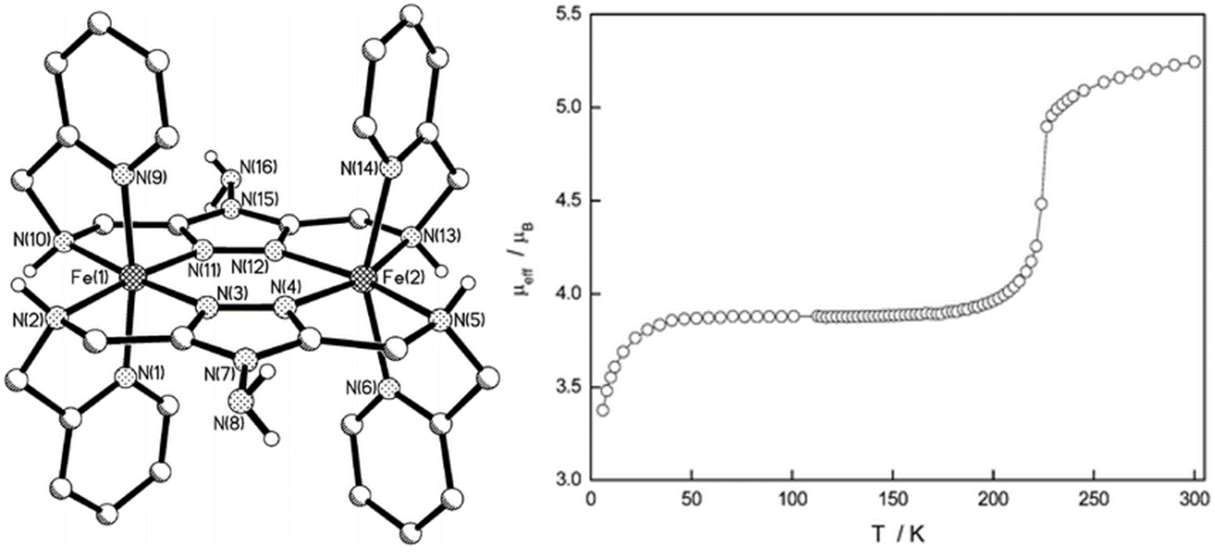

Figure 9. Crystal structure of the complex cation of $[Fe^{II}_2(\mathbf{PMAT})_2](BF)_4 \cdot H_2O$ with one Fe(II) in the LS (Fe(1)) and one in the HS (Fe(2)) state, resulting in the [HS-LS] state for the complex, measured at 123 K (left) and the temperature dependency of its magnetic moment in the range of 4–300 K (right). Reproduced from literature[236] with the permission from the Royal Society Of Chemistry.

This crystallographical differentiation was possible due to a molecular symmetry breaking. In the [HS-HS] state an inversion center is located between the two metal centers and the asymmetric unit consists of one half of the dinuclear complex whereas in the [HS-LS] state the inversion center is in-between two cations and a whole complex molecule is part of the asymmetric unit. The [HS-LS] state remains trapped until very low temperatures and no spin transition to the [LS-LS] state is observable.[236] Replacing the amino function in the 4-position of the 1,2,4-triazole moiety by other substituents resulted in similar bimetallic Fe(II) complexes. Despite the fact that the substitution is remote from the donor atoms, the synthesized compounds show very different SCO properties. However, none of the complexes exhibited the second potential spin transition to the [LS-LS]. The authors explained the inhibited conversion [HS-LS]↛[LS-LS] by strain between the metal ions arising from the rigidity and the wide biting angle of the ligand systems.[236,237] Only recently, substitution of the amino linkages for thioether linkages between the 1,2,4-triazole unit and the pyridine rings in the side arms resulted in new complexes with the chemical composition $[Fe^{II}_2(\mathbf{PSRT})_2](BF_4)_4$ (**PSRT** = 4-R-3,5-bis{[(2-pyridylmethyl)thio]methyl}-4*H*-1,2,4-triazole). By variation of the substituents in the 4-position, they were able to observe a spin transition to the [LS-LS] with the phenyl substituent.[79]

Inspired by the work of *Brooker et al.* our work group started in 2013 to investigate structural and electronic influences of the bridging unit on the SCO behavior.[210,211,238–240] *Herold et al.* reported in 2015 on the synthesis and characterization of new symmetric dinuclear complexes $[Fe^{II}_2(\mathbf{PMTD})_2](X)_4\cdot$solvent (with X = BF_4^-, ClO_4^- and $F_3CSO_3^-$) based on the **PMTD** (2,5-bis[(2-pyridylmethyl)amino]methyl-1,3,4-thiadiazole) ligand (Figure 10, left). The **PMTD** ligand is isostructural to the **PMAT** ligand and has two tridentate $\{N_3\}$ binding pockets, only the 1,2,4-triazole bridging unit was substituted for 1,3,4-thiadiazole. The basic idea here is that by exchanging the nitrogen atom in the triazole for the larger sulphur atom, the strain in the dimeric complex will be reduced and the ligand field strength Δ_O will be increased. According to these changes, the [LS-LS] state should be thermally accessible and stabilized at low temperatures, which was not possible with the related **PMAT** ligand. In fact, all three complexes are in the [LS-LS] state as revealed by single-crystal X-ray structure analysis recorded at 173 K. Unfortunately, they stay in the ground state until room temperature as shown by magnetic susceptibility measurements. Only above room temperature, a rise in the χT product indicates a possible gradual spin transition to the [HS-LS] state.[238,239] Small differences between the three complexes can be explained by the different intermolecular interactions in the solid state attributed to the incorporation of the various non-coordinating counter ions. Additionally, *Herold et al.* investigated the influence of solvent molecules on the SCO properties in the case of $[Fe^{II}_2(\mathbf{PMTD})_2](BF_4)_4\cdot$4DMF (Figure 10, right).[210,239] The complex remains in the [LS-LS] ground state until room temperature. When heated to 400 K solvent loss results in an abrupt one-step spin transition for the complex molecules directly from the [LS-LS] to the [HS-HS] state. However, the desolvated complex $[Fe^{II}_2(\mathbf{PMTD})_2](BF_4)_4$ shows a rather gradual SCO event to the [HS-LS] state upon cooling and remains trapped in this state until very low temperatures, inhibiting the possible second spin transition to the [LS-LS]. The stabilization of the [LS-LS] state in the DMF complex is explained by intermolecular hydrogen bonding between the complex cations and the DMF molecules which

also increases the ligand field strength Δ_O.[210] Further modifications of the **PMTD** ligand system performed by *Herold*, either for electronic or steric reasons, resulted in different bimetallic complexes, but the dimeric compounds stayed in the [HS-HS] state and the SCO properties were lost in all cases.[239]

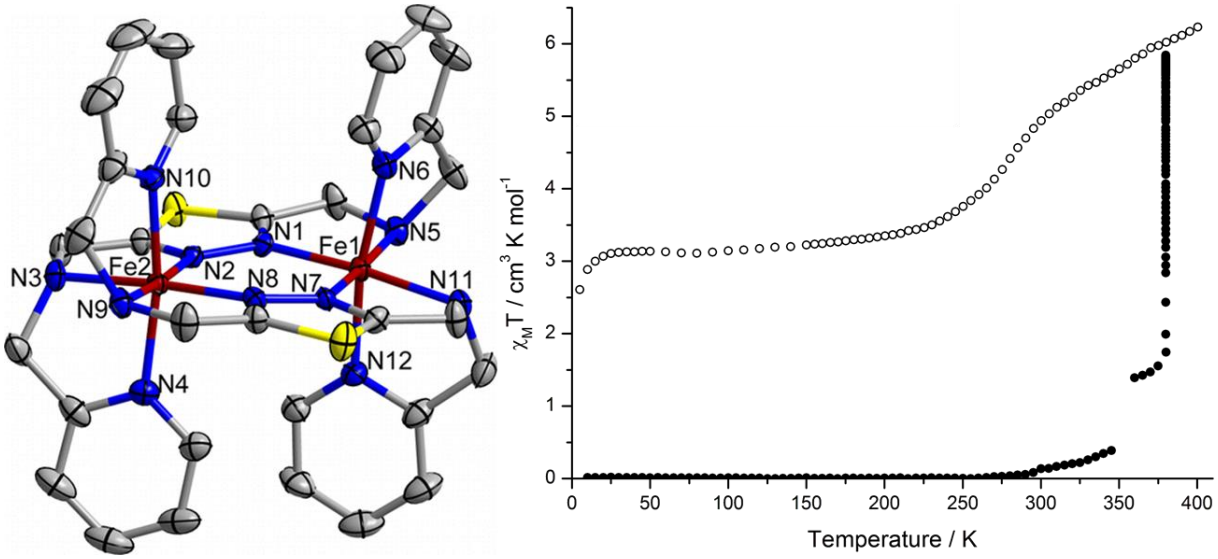

Figure 10. Crystal structure of the complex cation of $[Fe^{II}_2(\mathbf{PMTD})_2](BF)_4 \cdot 4DMF$ with thermal ellipsoids recorded at 173 K (color code: Fe dark red, N blue, S yellow and C grey) (left) and the temperature dependency of the χT product in the range of 2–400 K for $[Fe^{II}_2(\mathbf{PMTD})_2](BF_4)_4 \cdot 4DMF$ (filled dots) and for $[Fe^{II}_2(\mathbf{PMTD})_2](BF_4)_4$ (empty dots) (right). The figure was reproduced from literature[210] with the permission from the American Chemical Society.

More recently, *Bittner* described the synthesis of an asymmetric 1,3,4-thiadiazole ligand (**PBPMTD** = 2-(2-pyridyl)-5-[*N*,*N*-bis(2-pyridylmethyl)amino]methyl-1,3,4-thiadiazole). With this ligand he generated a series of dinuclear Fe(II) SCO complexes varying in the non-coordinating counter ions and the solvent molecules. $[Fe^{II}_2(\mathbf{PBPMTD})_2](BF_4)_4 \cdot$solvent was obtained as microcrystalline needles from a vapour diffusion of diethyl ether, hexane and cyclohexane (1:1:1) to an acetone complex solution. The freshly prepared complex yielded a two-step SCO behavior with two rather gradual spin transitions centered around 305 and 187 K, as shown by temperature-dependent magnetic susceptibility measurements (Figure 11, top). Interestingly, remeasuring of the sample resulted in a more abrupt two-step SCO and both spin transitions were shifted to higher temperatures ($T_{1/2}$ = 333 K and 204 K), which is ascribed to stronger intermolecular interactions due to the loss of solvent molecules. However, this could not be proven. Due to a poor crystallinity no structural characterization was possible. An analogue complex $[Fe^{II}_2(\mathbf{PBPMTD})_2](BF_4)_4 \cdot 0.5H_2O \cdot MeNO_2$ was obtained as single crystals suitable for X-ray structure analysis. The structure analysis of the complex was performed at two different temperatures (250 and 120 K) to get an insight into the structure of the different spin states. Both structures show a vast network of hydrogen bonding mainly between the complex cations and the non-coordinating anions leading to intermolecular cooperative

interaction pathways, while the solvent molecules interactions can almost be neglected. The high temperature structure reveals the [HS-HS] states at 250 K, which fits the DFT optimized structure. At 120 K the author suggests the complex being in the [HS-LS] state arising from a 1:1 mixture of [HS-HS] and [LS-LS] molecules after comparison with the calculated structures for the [HS-HS] and the [LS-LS] state. No magnetic data of this complex could be obtained due to the lack of crystalline material. It is noteworthy, that the two solvatomorphs of the tetrafluoroborate complexes cannot directly be compared since the different solvent content most likely results in different crystal packing. Similar solvent dependent SCO behavior was observed for the complex with perchlorate as non-coordinating anion $[Fe^{II}_2(\mathbf{PBPMTD})_2](ClO_4)_4\cdot$solvent. The freshly prepared sample shows a direct one-step spin transition from the [LS-LS] to the [HS-HS] state centered around room temperature when heated from 2–400 K and after solvent loss an abrupt two-step SCO [HS-HS]→[HS-LS]→[LS-LS] event occurs upon subsequent cooling (Figure 11, bottom).[241]

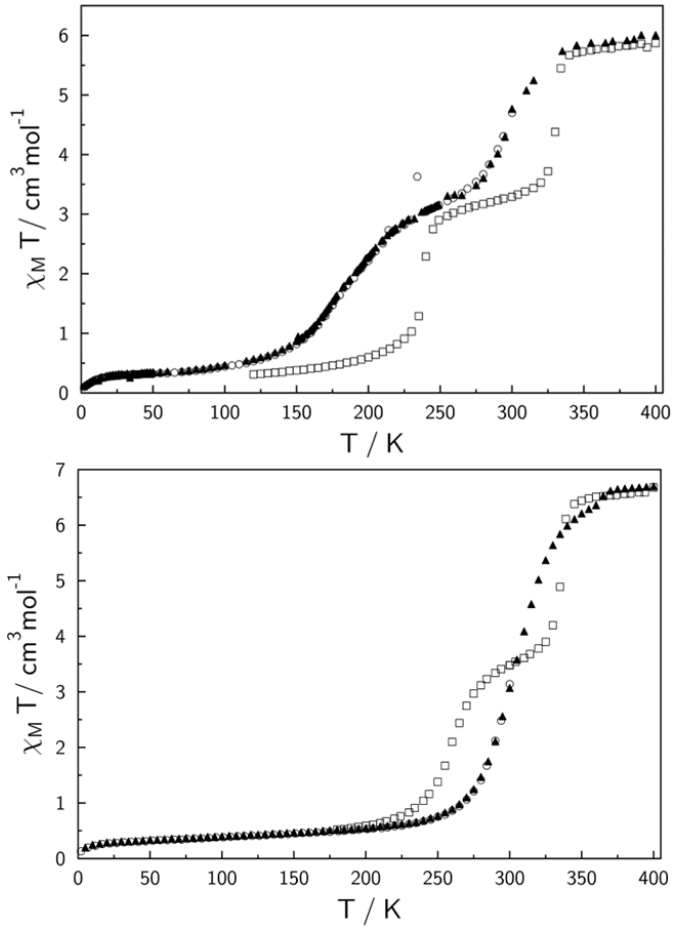

Figure 11. Top: Temperature-dependent magnetic susceptibility data of $[Fe^{II}_2(\mathbf{PBPMTD})_2](BF_4)_4\cdot$solvent. The freshly prepared sample was measured from 300–2 K (empty dots) and subsequently from 2–400 K (filled triangles) while the dried sample was recorded 14 days later (empty squares). Bottom: Temperature-dependent magnetic susceptibility data of $[Fe^{II}_2(\mathbf{PBPMTD})_2](ClO_4)_4\cdot$solvent. The freshly prepared sample was measured from 300–2 K (open circles) and subsequently heated from 2–400 K (filled triangles) and cooled from 400–175 K (empty squares). Reproduced from literature[241] with the permission of *Bittner*.

Köhler et al. reported the first dinuclear Fe(II) SCO complexes $[Fe^{II}_2(\mathbf{PMOD})_2](X_4)_4\cdot$solvent (with $X = BF_4^-$, ClO_4^- and $F_3CSO_3^-$) based on the isostructural **PMOD** ligand (2,5-bis[(2-pyridylmethyl)amino]methyl-1,3,4-oxadiazole) (Figure 12, left).[211,240] The tetrafluoroborate complex remains in the [HS-HS] within the measured temperature range of 2 to 300 K while the perchlorate compound shows an abrupt spin transition to the [HS-LS] state around 150 K, which is also explained in analogy to the **PMAT** system of *Brooker* by strong tension in the ligand backbone. Interestingly, the triflate complex shows the same spin transition but it is shifted to higher temperatures with the occurrence of thermal hysteresis. The authors correlate the strong anion dependency with the degree of intermolecular cooperativity between the complex cations and the non-coordinating anions (Figure 12, right).[211] Ongoing investigations were performed by *Eppelsheimer* who replaced the pyridine functionalities in the side arms for imidazole groups to further increase the intermolecular connectivity through additional hydrogen bonding possibilities. In fact, the synthesized dimeric complexes of the type $[Fe^{II}_2(\mathbf{I^2MOD})_2](X_4)_4\cdot$solvent (with $X = BF_4^-$, ClO_4^- and $F_3CSO_3^-$) based on the modified oxadiazole ligand **I²MOD** (2,5-bis[(1*H*-imidazol-2-ylmethyl)amino]methyl-1,3,4-oxadiazole, the superscript 2 stands for the connection between the imidazole group and the ligand backbone) shows an extended hydrogen bonding network, but the imidazole derivatives do not show any spin transition and remain in the [HS-HS] state, which is ascribed to the lower ligand field strength Δ_O of the **I²MOD** compared to the **PMOD** ligand.[242]

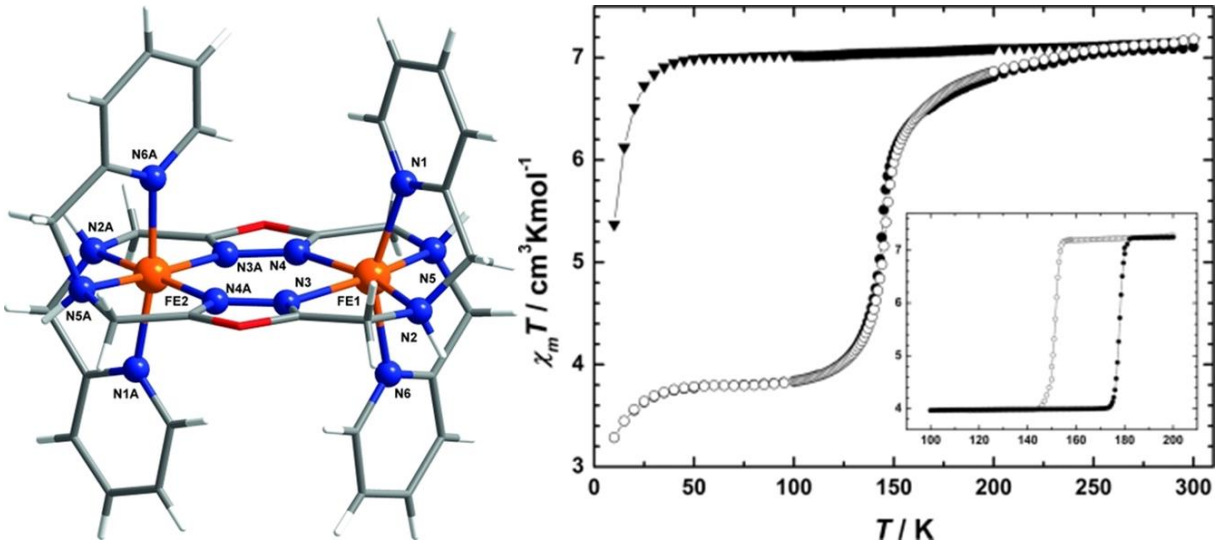

Figure 12. Crystal structure of the complex cation of $[Fe^{II}_2(\mathbf{PMOD})_2](ClO_4)_4\cdot$4MeCN, being in the [HS-LS] state, recorded at 100 K (color code: Fe orange, N blue, O red, C grey and H white) (left) and the temperature dependency of the χT product in the range of 2–300 K for $Fe^{II}_2(\mathbf{PMOD})_2](BF_4)_4\cdot$2MeCN (triangles) and for $[Fe^{II}_2(\mathbf{PMOD})_2](ClO_4)_4\cdot$4MeCN (dots) as well as in the range of 100–200 K for $[Fe^{II}_2(\mathbf{PMOD})_2](F_3CSO_3)_4\cdot$2MeCN (dots, small picture). The filled symbols represent the cooling mode while the empty symbols account for the heating (right). The figure was reproduced from literature[211] with permission from John Wiley & Sons, Inc.

Concluding, these studies together with many others in literature nicely demonstrate that the synergistic inter- and intramolecular interactions strongly influences the SCO behavior of bimetallic complexes. In many cases, the intermolecular interactions can be systematically varied to alter the type of the spin transition due to the formation of hydrogen bonding networks between complexes and solvent molecules and/or non-coordinating anions. The intramolecular interactions are adjusted by ligand design and some reports relate the occurrence of a two-step spin transition to the strain between the SCO-active metal ions. However, it remains difficult to predictably fine-tune or even control SCO behavior (including step-wise transitions, transition temperature $T_{1/2}$ or hysteresis). Intermolecular effects such as crystal packing and/or hydrogen bonding mediated by solvent molecules or anions can dominate ligand field effects in the solid state. Hence, designing new ligand systems for dinuclear SCO complexes and thus providing better insight in the delicate interplay between these different cooperative interactions is still highly desired. Only by fully understanding and thus rational controlling of all these potential influences on the SCO properties, future application in sensors, data storages, displays or actuators can be envisaged.[85,86,119]

1.5 Objectives and scope of this thesis

The previous chapters provide an insight in the SCO phenomenon, its occurrence, its different transition types, its advantages, its potential applications and its possible drawbacks, especially for mononuclear and dinuclear compounds. This research field has rapidly developed in the past decades and it has been shown that cooperative interactions, meaning the "communication" between the spin-carrying metal ions, effectively propagate the local distortions which accompany the spin transition throughout the solid state and lead to more abrupt transition and in some cases to the occurrence of thermal hysteresis. Abrupt spin transitions and especially thermal hysteresis is strongly recommended for future applications since it offers bistability, allowing the system to be in two different states within a certain range of external stimuli depending on its history, and thus a memory effect. The cooperativity can either be enhanced intermolecularly by, for example, hydrogen bonding networks between the complex cations, often facilitated by solvent molecules or non-coordinating anions, or intermolecularly by bridging metal ions via multidentate organic ligand systems. Despite the numerous studies concerning the origin of cooperativity between the SCO-active metal centers, the prediction of its behavior in the solid state solely from rational designing SCO complexes is hardly possible.

The previous work of *Herold* and *Bittner* of our group nicely demonstrated the potential of 1,3,4-thiadiazole bridging ligands to generate bimetallic complexes showing solvent-dependent SCO behavior (Chapter 1.4.2).[210,238,239,241] However, for $[Fe^{II}_2(\mathbf{PMTD})_2](BF_4)_4 \cdot 4DMF$ the three possible spin states ([HS-HS, [HS-LS] and [LS-LS]) were accessible only upon solvent loss while the other **PMTD** based complexes, synthesized by *Herold*, showed gradual spin transition only above room temperature not even reaching the intermediate [HS-LS] state. Further, the $[Fe^{II}_2(\mathbf{PBPMTD})_2](X)_4 \cdot$solvent systems (with $X = BF_4^-$ and ClO_4^-) of *Bittner*

could not be fully characterized due to the lack of crystalline material suitable for X-ray structure analysis and thus the origin of the various SCO behavior could only be estimated.

Based on these previously obtained results, the major goal of this work was the modification of the **PMTD** ligand. The new ligands should then be used to synthesize new dinuclear complexes possibly stabilizing the [HS-HS] state at elevated temperatures, ultimately exhibiting two-step SCO behavior with all three possible spin states thermally accessible ([HS-HS]→[HS-LS]→[LS-LS]). Furthermore, the origin of the SCO properties should be investigated to provide a better understanding of competing cooperative intra- and intermolecular interactions in the solid state by correlating their magnetic to the structural properties. The modification followed two different approaches. On one hand the substitution of the six-membered pyridine donor moieties in the side arms for five-membered *N*-heterocycles with a second heteroatom within the aromatic ring should increase the biting angle between the amine linkages and the heterocycle and weaken the ligand field strength Δ_O. This should result in a larger binding pocket for the metal ions and in an extension of the metal-ligand donor atom bond lengths, which favors the HS state. In addition, by varying the position and the nature of the second heteroatom within the pentamerous unit the electronic and structural properties of the ligand can be subtly altered, which gives the possibility to fine-tune the ligand field strength Δ_O and possibly change the intermolecular interaction pathways. On the other hand replacing the amino linkages for thioether linkages should lead to longer C-S bonds compared to the C-N bonds thus rendering greater flexibility to the ligand. This could possibly result in the population of the [HS-LS] and/or the [HS-HS] state at elevated temperatures (Figure 13).

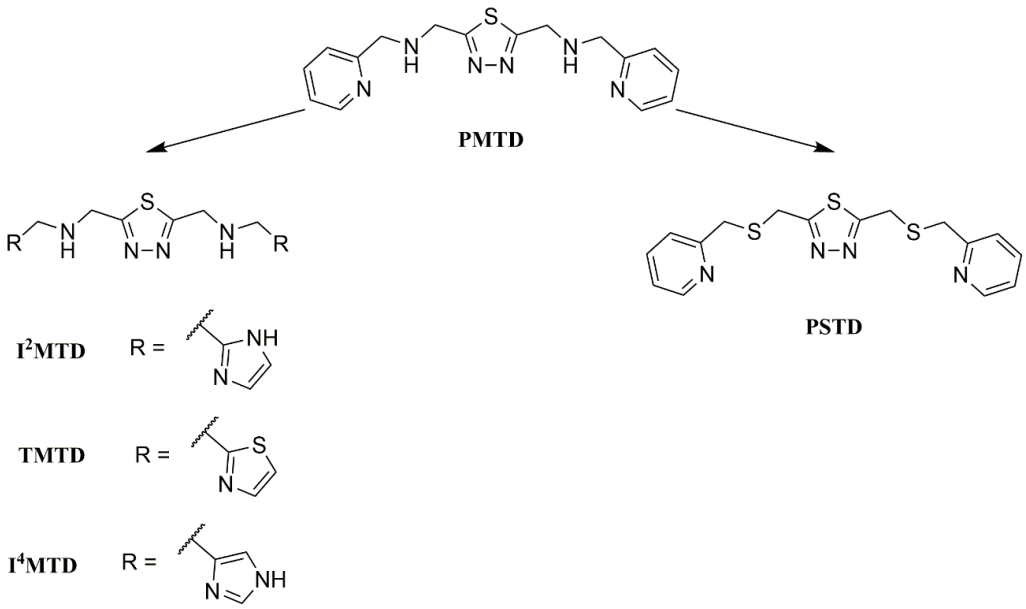

Figure 13. The intended ligand systems for this thesis. **I²MTD** (2,5-bis[(1*H*-imidazol-2-ylmethyl)amino]methyl-1,3,4-thiadiazole), **TMTD** (2,5-bis[(thiazol-2-ylmethyl)amino]methyl-1,3,4-thiadiazole), **I⁴MTD** (2,5-bis[(1*H*-imidazol-4-ylmethyl)amino]methyl-1,3,4-thiadiazole) and **PSTD** (2,5-bis[(2-pyridylmethyl)thio]methyl-1,3,4-thiadiazole).

The present Chapter 1 gives an introduction and an overview of the relevant literature of SCO, which is necessary to follow and understand the results presented in this thesis.

Chapter 2 describes the synthesis and characterization of the novel ligands **I^{2}MTD** and **TMTD** and the new dinuclear complexes obtained based on these two bridging ligands. Depending on the ligand and on the non-coordinating counter ions, these complexes show different magnetic properties ranging from a temperature-independent [HS-HS] state, over a one-step spin transition, towards a two-step SCO behavior. In fact, for one of the complexes all three spin states ([HS-HS], [HS-LS] and [LS-LS]) are subsequently accessible simply by varying the temperature. This two-step spin crossover is accompanied by two crystallographic phase transitions upon slow cooling. This results in unambiguously identifiable [HS-LS] Fe(II) pairs for the mixed [HS-LS] state. However, upon rapid cooling of the sample no phase transition was detected and the [HS-LS] state is a superposition of HS and LS Fe(II) ions in the complex cation. These results are presented by thorough interpretation of the data obtained by temperature-dependent magnetic susceptibility measurements, single-crystal X-ray structure analysis and Mössbauer measurements. The salient feature of this paper is the cooling rate dependency of the single-crystal diffraction experiment for the observability of the phase transition associated with the SCO behavior.

Chapter 3 covers the synthesis and characterization of three novel dinculear Fe(II) complexes based on the **I^{4}MTD** bridging ligand. Temperature-dependent magnetic susceptibility measurements revealed that two complexes stay in the [HS-HS] state until very low temperatures while the third complex shows a spin transition from the [HS-HS] to the [HS-LS]. The intermediate [HS-LS] is displayed by a 1:1 mixture of [HS-HS] and [LS-LS] molecules, which are arranged in layers, containing solely [HS-HS] or [LS-LS] complexes. These layers are clearly separated from each other by solvent molecules and counter ions proven by single-crystal X-ray structure analysis. The different magnetic behavior is attributed to different crystal packings in the complexes arising from the incorporation of the different non-coordinating anions. This paper is a nice example for crystal packing effects dominating over the ligand field strength Δ_O the SCO properties in the solid state.

Chapter 4 presents the synthesis and characterization of the new thioether-linked **PSTD** bridging ligand. The ligand was used to generate bimetallic Fe(II) complexes, resulting in a mononuclear complex in which two ligands are coordinating the Fe(II) metal center with only one of the tridentate coordination pocket. The Fe(II) compound stays in the LS state until above room temperature. Based on this result, a mononuclear Co(II) complex was synthesized. This complex is isostructural to the previous one but show gradual SCO behavior. The characterization and interpretation of the properties have been done on the basis of temperature-dependent magnetic susceptibility measurements and single-crystal X-ray structure analysis. To our knowledge, this is the first Co(II) SCO complex with a $\{N_4S_2\}$ donor atom set.

Finally, Chapter 5 summarizes all the obtained results and will provide an outlook.

1.6 References

[1] H.-P. Schlemmer, *Radiologe* **2005**, *45*, 356–362.
[2] W. Plass, *Chemie unserer Zeit* **1998**, *32*, 323–333.
[3] J. S. Miller, A. J. Epstein, *Angew. Chem.* **1994**, *106*, 399–432.
[4] A. Dei, D. Gatteschi, C. Sangregorio, L. Sorace, *Acc. Chem. Res.* **2004**, *37*, 827–835.
[5] R. Sessoli, D. Gatteschi, A. Caneschi, M. A. Novak, *Nature* **1993**, *365*, 141–143.
[6] K. Katoh, H. Isshiki, T. Komeda, M. Yamashita, *Coord. Chem. Rev.* **2011**, *255*, 2124–2148.
[7] R. Vincent, S. Klyatskaya, M. Ruben, W. Wernsdorfer, F. Balestro, *Nature* **2012**, *488*, 357–360.
[8] K. Hymas, A. Soncini, *Phys. Rev. B* **2019**, *99*, 245404.
[9] D. M. Adams, D. N. Hendrickson, *J. Am. Chem. Soc.* **1996**, *118*, 11515–11528.
[10] N. S. Hush, A. T. Wong, G. B. Bacskay, J. R. Reimers, *J. Am. Chem. Soc.* **1990**, *112*, 4192–4197.
[11] A. Aviram, *Int. J. Quantum Chem.* **1992**, *42*, 1615–1624.
[12] O. Kahn, J. Kröber, C. Jay, *Adv. Mater.* **1992**, *4*, 718–728.
[13] O. Kahn, C. J. Martinez, *Science* **1998**, *279*, 44–48.
[14] Y. Garcia, V. Ksenofontov, P. Gütlich, *Hyperfine Interact.* **2002**, *139–140*, 543–551.
[15] C. M. Varma, *Rev. Mod. Phys.* **1976**, *48*, 219–238.
[16] J. P. Fackler, in *Encycl. Inorg. Chem.*, John Wiley & Sons, Ltd, Chichester, UK, **2006**.
[17] P. Day, N. S. Hush, R. J. . Clark, *Philos. Trans. R. Soc. A Math. Phys. Eng. Sci.* **2008**, *366*, 5–14.
[18] M. B. Robin, P. Day, in *Adv. Inorg. Chem. Radiochem.* (Eds.: H.J. Emeléus, A.G. Sharpe), Academic Press, **1968**, pp. 247–422.
[19] C. G. Pierpont, *Coord. Chem. Rev.* **2001**, *216–217*, 99–125.
[20] D. N. Hendrickson, C. G. Pierpont, in *Spin Crossover Transition Metal Compdounds II* (Eds.: P. Gütlich, H.A. Goodwin), Springer, Berlin, Heidelberg, **2004**, pp. 63–95.
[21] A. C. Cope, A. C. Haven, F. L. Ramp, E. R. Trumbull, *J. Am. Chem. Soc.* **1952**, *74*, 4867–4871.
[22] J. Hankache, O. S. Wenger, *Chem. Rev.* **2011**, *111*, 5138–5178.
[23] A. Heckmann, C. Lambert, *Angew. Chem. Int. Ed.* **2012**, *51*, 326–392.
[24] R. M. Buchanan, C. G. Pierpont, *J. Am. Chem. Soc.* **1980**, *102*, 4951–4957.
[25] M. W. Lynch, D. N. Hendrickson, B. J. Fitzgerald, C. G. Pierpont, *J. Am. Chem. Soc.* **1981**, *103*, 3961–3963.
[26] M. W. Lynch, D. N. Hendrickson, B. J. Fitzgerald, C. G. Pierpont, *J. Am. Chem. Soc.* **1984**, *106*, 2041–2049.
[27] O.-S. Jung, D. H. Jo, Y.-A. Lee, B. J. Conklin, C. G. Pierpont, *Inorg. Chem.* **1997**, *36*, 19–24.
[28] A. Caneschi, A. Dei, *Angew. Chem. Int. Ed.* **1998**, *37*, 3005–3007.
[29] G. Speier, Z. Tyeklár, P. Tóth, E. Speier, S. Tisza, A. Rockenbauer, A. M. Whalen, N. Alkire, C. G. Pierpont, *Inorg. Chem.* **2001**, *40*, 5653–5659.
[30] R. D. Schmidt, D. A. Shultz, J. D. Martin, *Inorg. Chem.* **2010**, *49*, 3162–3168.
[31] R. D. Schmidt, D. A. Shultz, J. D. Martin, P. D. Boyle, *J. Am. Chem. Soc.* **2010**, *132*, 6261–6273.
[32] T. Tezgerevska, K. G. Alley, C. Boskovic, *Coord. Chem. Rev.* **2014**, *268*, 23–40.
[33] P. Gütlich, A. Hauser, H. Spiering, *Angew. Chemie Int. Ed. English* **1994**, *33*, 2024–2054.
[34] S. Brooker, *Chem. Soc. Rev.* **2015**, *44*, 2880–2892.

[35] M. D. Manrique-Juárez, S. Rat, L. Salmon, G. Molnár, C. M. Quintero, L. Nicu, H. J. Shepherd, A. Bousseksou, *Coord. Chem. Rev.* **2016**, *308*, 395–408.
[36] O. Sato, *Acc. Chem. Res.* **2003**, *36*, 692–700.
[37] O. Sato, *Nat. Chem.* **2016**, *8*, 644–656.
[38] J. Linares, E. Codjovi, Y. Garcia, *Sensors* **2012**, *12*, 4479–4492.
[39] P. Gütlich, *Eur. J. Inorg. Chem.* **2013**, *2013*, 581–591.
[40] J. S. Griffith, L. E. Orgel, *Q. Rev. Chem. Soc.* **1957**, *11*, 381.
[41] Y. Garcia, P. Gütlich, in *Spin Crossover Transition Metal Compdounds II* (Eds.: P. Gütlich, H.A. Goodwin), Springer, Berlin, Heidelberg, **2004**, pp. 49–62.
[42] L. Cambi, L. Szegö, *Berichte der Dtsch. Chem. Gesellschaft (A B Ser.* **1931**, *64*, 2591–2598.
[43] L. Cambi, L. Szegö, *Berichte der Dtsch. Chem. Gesellschaft (A B Ser.* **1933**, *66*, 656–661.
[44] L. Cambi, L. Malatesta, *Berichte der Dtsch. Chem. Gesellschaft (A B Ser.* **1937**, *70*, 2067–2078.
[45] A. White, R. Roper, E. Kokot, H. Waterman, R. Martin, *Aust. J. Chem.* **1964**, *17*, 294.
[46] A. H. Ewald, R. L. Martin, E. Sinn, A. H. White, *Inorg. Chem.* **1969**, *8*, 1837–1846.
[47] B. N. Figgis, G. E. Toogood, *J. Chem. Soc. Dalton Trans.* **1972**, 2177.
[48] A. H. Ewald, R. L. Martin, I. G. Ross, A. H. White, *Proc. R. Soc. London. Ser. A. Math. Phys. Sci.* **1964**, *280*, 235–257.
[49] W. A. Baker, H. M. Bobonich, *Inorg. Chem.* **1964**, *3*, 1184–1188.
[50] E. König, K. Madeja, *Chem. Commun. (London)* **1966**, *0*, 61–62.
[51] E. Koenig, K. Madeja, *Inorg. Chem.* **1967**, *6*, 48–55.
[52] R. C. Stoufer, D. H. Busch, W. B. Hadley, *J. Am. Chem. Soc.* **1961**, *83*, 3732–3734.
[53] R. Hogg, R. G. Wilkins, *J. Chem. Soc.* **1962**, 341–350.
[54] E. König, *Coord. Chem. Rev.* **1968**, *3*, 471–495.
[55] H. A. Goodwin, *Coord. Chem. Rev.* **1976**, *18*, 293–325.
[56] P. Gütlich, in *Metal Complexes. Structure and Bonding*, Springer, Berlin, Heidelberg, **1981**, pp. 83–195.
[57] S. Decurtins, P. Gütlich, C. P. Köhler, H. Spiering, A. Hauser, *Chem. Phys. Lett.* **1984**, *105*, 1–4.
[58] S. Decurtins, P. Gutlich, K. M. Hasselbach, A. Hauser, H. Spiering, *Inorg. Chem.* **1985**, *24*, 2174–2178.
[59] J. H. Ammeter, R. Bucher, N. Oswald, *J. Am. Chem. Soc.* **1974**, *96*, 7833–7835.
[60] M. E. Switzer, R. Wang, M. F. Rettig, A. H. Maki, *J. Am. Chem. Soc.* **1974**, *96*, 7669–7674.
[61] W. Kläui, *J. Chem. Soc. Chem. Commun.* **1979**, 700.
[62] P. G. Sim, E. Sinn, *J. Am. Chem. Soc.* **1981**, *103*, 241–243.
[63] D. M. Halepoto, D. G. L. Holt, L. F. Larkworthy, G. J. Leigh, D. C. Povey, G. W. Smith, *J. Chem. Soc. Chem. Commun.* **1989**, 1322.
[64] D. M. Halepoto, D. G. L. Holt, L. F. Larkworthy, D. C. Povey, G. W. Smith, G. J. Leigh, *Polyhedron* **1989**, *8*, 1821–1822.
[65] A. Real, J. Zarembowitch, O. Kahn, X. Solans, *Inorg. Chem.* **1987**, *26*, 2939–2943.
[66] G. Vos, R. A. Le Febre, R. A. G. De Graaff, J. G. Haasnoot, J. Reedijk, *J. Am. Chem. Soc.* **1983**, *105*, 1682–1683.
[67] E. Breuning, M. Ruben, J. Lehn, F. Renz, Y. Garcia, V. Ksenofontov, P. Gütlich, E. Wegelius, K. Rissanen, *Angew. Chem. Int. Ed.* **2000**, *39*, 2504–2507.
[68] M. Shatruk, A. Dragulescu-Andrasi, K. E. Chambers, S. A. Stoian, E. L. Bominaar, C. Achim, K. R. Dunbar, *J. Am. Chem. Soc.* **2007**, *129*, 6104–6116.
[69] M. B. Duriska, S. M. Neville, B. Moubaraki, J. D. Cashion, G. J. Halder, K. W.

Chapman, C. Balde, J.-F. Létard, K. S. Murray, C. J. Kepert, et al., *Angew. Chem. Int. Ed.* **2009**, *48*, 2549–2552.
[70] Y. Garcia, V. Niel, M. C. Muñoz, J. A. Real, in *Spin Crossover Transition Metal Compdounds I* (Eds.: P. Gütlich, H.A. Goodwin), Springer, Berlin, Heidelberg, **2004**, pp. 229–257.
[71] J. G. Haasnoot, G. Vos, W. L. Groeneveld, *Zeitschrift für Naturforsch. B* **1977**, *32*, 1421–1430.
[72] M. NIHEI, T. SHIGA, Y. MAEDA, H. OSHIO, *Coord. Chem. Rev.* **2007**, *251*, 2606–2621.
[73] D. J. Harding, P. Harding, W. Phonsri, *Coord. Chem. Rev.* **2016**, *313*, 38–61.
[74] I. Krivokapic, M. Zerara, M. L. Daku, A. Vargas, C. Enachescu, C. Ambrus, P. Tregenna-Piggott, N. Amstutz, E. Krausz, A. Hauser, *Coord. Chem. Rev.* **2007**, *251*, 364–378.
[75] S. Hayami, Y. Komatsu, T. Shimizu, H. Kamihata, Y. H. Lee, *Coord. Chem. Rev.* **2011**, *255*, 1981–1990.
[76] R. G. Miller, S. Narayanaswamy, J. L. Tallon, S. Brooker, *New J. Chem.* **2014**, *38*, 1932.
[77] H. Toftlund, J. J. McGarvey, in *Spin Crossover Transition Metal Compdounds I* (Eds.: P. Gütlich, H.A. Goodwin), Springer, Berlin, Heidelberg, **2004**, pp. 151–166.
[78] B. Weber, *Coord. Chem. Rev.* **2009**, *253*, 2432–2449.
[79] R. W. Hogue, H. L. C. Feltham, R. G. Miller, S. Brooker, *Inorg. Chem.* **2016**, *55*, 4152–4165.
[80] J. S. Costa, C. Balde, C. Carbonera, D. Denux, A. Wattiaux, C. Desplanches, J.-P. Ader, P. Gütlich, J.-F. Létard, *Inorg. Chem.* **2007**, *46*, 4114–4119.
[81] P. Gütlich, H. A. Goodwin, *Spin Crossover in Transition Metal Compounds I*, Springer Berlin Heidelberg, Berlin, Heidelberg, **2004**.
[82] P. Gütlich, H. A. Goodwin, *Spin Crossover in Transition Metal Compounds II*, Springer Berlin Heidelberg, Berlin, Heidelberg, **2004**.
[83] P. Gütlich, H. A. Goodwin, *Spin Crossover in Transition Metal Compounds III*, Springer Berlin Heidelberg, Berlin, Heidelberg, **2004**.
[84] M. A. Halcrow, *Spin-Crossover Materials: Properties and Applications*, John Wiley & Sons Ltd, Oxford, UK, **2013**.
[85] J. Olguín, S. Brooker, in *Spin-Crossover Mater. Prop. Appl.* (Ed.: M.A. Halcrow), John Wiley & Sons Ltd, Oxford, UK, **2013**, pp. 77–120.
[86] R. W. Hogue, S. Singh, S. Brooker, *Chem. Soc. Rev.* **2018**, *47*, 7303–7338.
[87] M. Carmen Muñoz, J. Antonio Real, in *Spin-Crossover Mater. Prop. Appl.* (Ed.: M.A. Halcrow), John Wiley & Sons Ltd, Oxford, UK, **2013**, pp. 121–146.
[88] Z.-P. Ni, J.-L. Liu, M. N. Hoque, W. Liu, J.-Y. Li, Y.-C. Chen, M.-L. Tong, *Coord. Chem. Rev.* **2017**, *335*, 28–43.
[89] K. Senthil Kumar, M. Ruben, *Coord. Chem. Rev.* **2017**, *346*, 176–205.
[90] M. Ruben, K. S. Kumar, *Angew. Chem.* **2019**, ange.201911256.
[91] R. L. Mössbauer, *Zeitschrift für Phys.* **1958**, *151*, 124–143.
[92] R. L. Mössbauer, *Naturwissenschaften* **1958**, *45*, 538–539.
[93] A. Hauser, in *Spin Crossover Transition Metal Compdounds I* (Eds.: P. Gütlich, H.A. Goodwin), Springer, Berlin/Heidelberg, **2004**, pp. 49–58.
[94] L. H. Gade, *Koordinationschemie*, Wiley, **2012**.
[95] F. Hund, *Zeitschrift für Phys.* **1927**, *40*, 742–764.
[96] P. Gütlich, Y. Garcia, H. A. Goodwin, *Chem. Soc. Rev.* **2000**, *29*, 419–427.
[97] Y. Tanabe, S. Sugano, *J. Phys. Soc. Japan* **1954**, *9*, 766–779.
[98] C. K. Jørgensen, *Discuss. Faraday Soc.* **1958**, *26*, 110–115.
[99] M. Sorai, S. Seki, *J. Phys. Chem. Solids* **1974**, *35*, 555–570.

[100] E. Konig, G. Ritter, S. K. Kulshreshtha, *Chem. Rev.* **1985**, *85*, 219–234.
[101] V. Ksenofontov, A. B. Gaspar, P. Gütlich, in *Spin Crossover Transition Metal Compdounds III* (Eds.: P. Gütlich, H.A. Goodwin), Springer, Berlin, Heidelberg, **2004**, pp. 23–64.
[102] T. Granier, B. Gallois, J. Gaultier, J. A. Real, J. Zarembowitch, *Inorg. Chem.* **1993**, *32*, 5305–5312.
[103] J. Jeftic, R. Hinek, S. C. Capelli, A. Hauser, *Inorg. Chem.* **1997**, *36*, 3080–3087.
[104] V. Ksenofontov, G. Levchenko, H. Spiering, P. Gütlich, J.-F. Létard, Y. Bouhedja, O. Kahn, *Chem. Phys. Lett.* **1998**, *294*, 545–553.
[105] J. A. Real, A. B. Gaspar, M. C. Muñoz, *Dalt. Trans.* **2005**, 2062.
[106] J.-F. Létard, L. Capes, G. Chastanet, N. Moliner, S. Létard, J.-A. Real, O. Kahn, *Chem. Phys. Lett.* **1999**, *313*, 115–120.
[107] P. Gütlich, Y. Garcia, T. Woike, *Photoswitchable Coordination Compounds*, **2001**.
[108] M. Marchivie, P. Guionneau, J. A. K. Howard, G. Chastanet, J. F. Létard, A. E. Goeta, D. Chasseau, *J. Am. Chem. Soc.* **2002**, *124*, 194–195.
[109] C. Bressler, C. Milne, V.-T. Pham, A. ElNahhas, R. M. van der Veen, W. Gawelda, S. Johnson, P. Beaud, D. Grolimund, M. Kaiser, et al., *Science* **2009**, *323*, 489–492.
[110] J. Klingele, D. Kaase, M. Schmucker, Y. Lan, G. Chastanet, J.-F. Létard, *Inorg. Chem.* **2013**, *52*, 6000–6010.
[111] A. Hauser, *Chem. Phys. Lett.* **1986**, *124*, 543–548.
[112] A. Hauser, *Coord. Chem. Rev.* **1991**, *111*, 275–290.
[113] A. Hauser, in *Spin Crossover Transition Metal Compdounds II* (Eds.: P. Gütlich, H.A. Goodwin), Springer, Berlin, Heidelberg, **2004**, pp. 155–198.
[114] J.-F. Létard, G. Chastanet, P. Guionneau, C. Desplanches, in *Spin-Crossover Mater. Prop. Appl.* (Ed.: M.A. Halcrow), John Wiley & Sons Ltd, Oxford, UK, **2013**, pp. 475–506.
[115] J.-F. Létard, *J. Mater. Chem.* **2006**, *16*, 2550–2559.
[116] P. Gütlich, H. A. Goodwin, in *Spin Crossover Transition Metal Compdounds I* (Eds.: P. Gütlich, H.A. Goodwin), Springer, Berlin/Heidelberg, **2004**, pp. 1–47.
[117] M. P. Shores, C. M. Klug, S. R. Fiedler, in *Spin-Crossover Mater. Prop. Appl.* (Ed.: M.A. Halcrow), John Wiley & Sons Ltd, Oxford, UK, **2013**, pp. 281–301.
[118] K. Ridier, G. Molnár, L. Salmon, W. Nicolazzi, A. Bousseksou, *Solid State Sci.* **2017**, *74*, A1–A22.
[119] K. S. Murray, *Eur. J. Inorg. Chem.* **2008**, *2008*, 3101–3121.
[120] N. Ortega-Villar, M. Muñoz, J. Real, *Magnetochemistry* **2016**, *2*, 16.
[121] G. N. Newton, M. Nihei, H. Oshio, *Eur. J. Inorg. Chem.* **2011**, 3031–3042.
[122] M. Steinert, B. Schneider, S. Dechert, S. Demeshko, F. Meyer, *Inorg. Chem.* **2016**, *55*, 2363–2373.
[123] N. Sasaki, T. Kambara, *Phys. Rev. B* **1989**, *40*, 2442–2449.
[124] T. Buchen, P. Guetlich, H. A. Goodwin, *Inorg. Chem.* **1994**, *33*, 4573–4576.
[125] N. Moliner, A. B. Gaspar, M. C. Muñoz, V. Niel, J. Cano, J. A. Real, *Inorg. Chem.* **2001**, *40*, 3986–3991.
[126] M. Marchivie, P. Guionneau, J. F. Létard, D. Chasseau, J. A. K. Howard, *J. Phys. Chem. Solids* **2004**, *65*, 17–23.
[127] V. Gómez, C. Sáenz de Pipaón, P. Maldonado-Illescas, J. C. Waerenborgh, E. Martin, J. Benet-Buchholz, J. R. Galán-Mascarós, *J. Am. Chem. Soc.* **2015**, *137*, 11924–11927.
[128] P. Gütlich, A. B. Gaspar, Y. Garcia, *Beilstein J. Org. Chem.* **2013**, *9*, 342–391.
[129] E. Riedel, C. Janiak, *Anorganische Chemie*, De Gruyter, **2015**.
[130] D. F. Evans, *J. Chem. Soc.* **1959**, 2003–2005.
[131] C. J. O'Connor, in *Mol. Magn. Mater.* (Eds.: M.M. Turnbull, T. Sugimoto, L.K.

Thompson), American Chemical Society, **1996**, pp. 44–66.
[132] N. Ortega-Villar, A. L. Thompson, M. C. Muñoz, V. M. Ugalde-Saldívar, A. E. Goeta, R. Moreno-Esparza, J. A. Real, *Chem. - A Eur. J.* **2005**, *11*, 5721–5734.
[133] C. Reus, K. Ruth, S. Tüllmann, M. Bolte, H.-W. Lerner, B. Weber, M. C. Holthausen, M. Wagner, *Eur. J. Inorg. Chem.* **2011**, *2011*, 1709–1718.
[134] M. Milek, F. W. Heinemann, M. M. Khusniyarov, *Inorg. Chem.* **2013**, *52*, 11585–11592.
[135] S. Singh, S. Brooker, *Inorg. Chem.* **2020**, *59*, 1265–1273.
[136] J. K. McCusker, A. L. Rheingold, D. N. Hendrickson, *Inorg. Chem.* **1996**, *35*, 2100–2112.
[137] P. Guionneau, M. Marchivie, G. Bravic, J.-F. Létard, D. Chasseau, in *Spin Crossover Transition Metal Compdounds II* (Eds.: P. Gütlich, H.A. Goodwin), Springer, Berlin, Heidelberg, **2004**, pp. 97–128.
[138] P. Guionneau, *Dalt. Trans.* **2014**, *43*, 382–393.
[139] P. Gütlich, *Zeitschrift für Anorg. und Allg. Chemie* **2012**, *638*, 15–43.
[140] J.-P. Tuchagues, A. Bousseksou, G. Molnár, J. J. McGarvey, F. Varret, in *Spin Crossover Transition Metal Compdounds III* (Eds.: P. Gütlich, H.A. Goodwin), Springer, Berlin, Heidelberg, **2004**, pp. 84–103.
[141] R. Kulmaczewski, J. Olguín, J. A. Kitchen, H. L. C. Feltham, G. N. L. Jameson, J. L. Tallon, S. Brooker, *J. Am. Chem. Soc.* **2014**, *136*, 878–881.
[142] G. A. Craig, J. S. Costa, O. Roubeau, S. J. Teat, H. J. Shepherd, M. Lopes, G. Molnár, A. Bousseksou, G. Aromí, *Dalt. Trans.* **2014**, *43*, 729–737.
[143] M. Sorai, in *Spin Crossover Transition Metal Compdounds III* (Eds.: P. Gütlich, H.A. Goodwin), Springer, Berlin, Heidelberg, **2004**, pp. 153–170.
[144] R. Boča, M. Boča, H. Ehrenberg, H. Fuess, W. Linert, F. Renz, I. Svoboda, *Chem. Phys.* **2003**, *293*, 375–395.
[145] H. L. C. Feltham, C. Johnson, A. B. S. Elliott, K. C. Gordon, M. Albrecht, S. Brooker, *Inorg. Chem.* **2015**, *54*, 2902–2909.
[146] S. Hora, H. Hagiwara, *Inorganics* **2017**, *5*, 49.
[147] W.-B. Chen, J.-D. Leng, Z.-Z. Wang, Y.-C. Chen, Y. Miao, M.-L. Tong, W. Dong, *Chem. Commun.* **2017**, *53*, 7820–7823.
[148] J. Zarembowitch, O. Kahn, *Inorg. Chem.* **1984**, *23*, 589–593.
[149] M. D. Timken, S. R. Wilson, D. N. Hendrickson, *Inorg. Chem.* **1985**, *24*, 3450–3457.
[150] C. Cantin, J. Kliava, Y. Servant, L. Sommier, O. Kahn, *Appl. Magn. Reson.* **1997**, *12*, 87–93.
[151] H. Daubric, J. Kliava, P. Guionneau, D. Chasseau, J.-F. Létard, O. Kahn, *J. Phys. Condens. Matter* **2000**, *12*, 5481–5494.
[152] I. V. Ovchinnikov, T. A. Ivanova, A. N. Turanov, R. R. Garipov, *Phys. Solid State* **2009**, *51*, 2058–2063.
[153] Y. Garcia, P. J. van Koningsbruggen, G. Bravic, P. Guionneau, D. Chasseau, G. L. Cascarano, J. Moscovici, K. Lambert, A. Michalowicz, O. Kahn, *Inorg. Chem.* **1997**, *36*, 6357–6365.
[154] A. Michalowicz, J. Moscovici, J. Charton, F. Sandid, F. Benamrane, Y. Garcia, *J. Synchrotron Radiat.* **2001**, *8*, 701–703.
[155] J. Okabayashi, S. Ueno, Y. Wakisaka, T. Kitazawa, *Inorg. Chim. Acta* **2015**, *426*, 142–145.
[156] A. Y. Mohamed, M. Lee, K. Kitase, T. Kitazawa, J. Y. Kim, D. Y. Cho, *Crystals* **2018**, *8*, DOI 10.3390/cryst8110433.
[157] A. Vértes, K. Süvegh, R. Hinek, P. Gütlich, *Hyperfine Interact.* **1994**, *84*, 483–489.
[158] Y. Nagai, H. Saito, T. Hyodo, A. Vértes, K. Süvegh, *Phys. Rev. B* **1998**, *57*, 14119–14122.

[159] S. J. Campbell, V. Ksenofontov, Y. Garcia, J. S. Lord, Y. Boland, P. Gütlich, *J. Phys. Chem. B* **2003**, *107*, 14289–14295.
[160] S. J. Blundell, F. L. Pratt, T. Lancaster, I. M. Marshall, C. A. Steer, S. L. Heath, J.-F. Létard, T. Sugano, D. Mihailovic, A. Omerzu, *Polyhedron* **2003**, *22*, 1973–1980.
[161] O. Roubeau, P. C. M. Gubbens, D. Visser, M. Blaauw, P. Dalmas De Réotier, A. Yaouanc, J. G. Haasnoot, J. Reedijk, S. Sakarya, U. A. Jayasooriya, et al., *Chem. Phys. Lett.* **2004**, *395*, 177–181.
[162] Y. Garcia, S. J. Campbell, J. S. Lord, P. Gütlich, *Inorg. Chim. Acta* **2008**, *361*, 3577–3585.
[163] H. Grünsteudel, H. Paulsen, W. Meyer-Klaucke, H. Winkler, A. X. Trautwein, H. F. Grünsteudel, A. Q. R. Baron, A. I. Chumakov, R. Rüffer, H. Toftlund, *Hyperfine Interact.* **1998**, *113*, 311–317.
[164] H. Winkler, A. I. Chumakov, A. X. Trautwein, in *Spin Crossover Transition Metal Compdounds III* (Eds.: P. Gütlich, H.A. Goodwin), Springer, Be, **2004**, pp. 137–152.
[165] G. Félix, M. Mikolasek, H. Peng, W. Nicolazzi, G. Molnár, A. I. Chumakov, L. Salmon, A. Bousseksou, *Phys. Rev. B* **2015**, *91*, 024422.
[166] H. A. Goodwin, in *Spin Crossover Transition Metal Compdounds II* (Eds.: P. Gütlich, H.A. Goodwin), Springer, Berlin, Heidelberg, **2004**, pp. 23–47.
[167] E. König, S. Kremer, *Theor. Chim. Acta* **1971**, *23*, 12–20.
[168] K. S. Murray, C. J. Kepert, in *Spin Crossover Transition Metal Compdounds I* (Eds.: P. Gütlich, H.A. Goodwin), Springer, Berlin, Heidelberg, **2004**, pp. 195–228.
[169] I. Søtofte, S. E. Rasmussen, S. J. Cyvin, J. Brunvoll, G. Hagen, *Acta Chem. Scand.* **1967**, *21*, 2028–2040.
[170] R. Claude, J. A. Real, J. Zarembowitch, O. Kahn, L. Ouahab, D. Grandjean, K. Boukheddaden, F. Varret, A. Dworkin, *Inorg. Chem.* **1990**, *29*, 4442–4448.
[171] R. W. Hogue, R. G. Miller, N. G. White, H. L. C. Feltham, G. N. L. Jameson, S. Brooker, *Chem. Commun.* **2014**, *50*, 1435–1437.
[172] N. Moliner, M. C. Muñoz, S. Létard, J.-F. Létard, X. Solans, R. Burriel, M. Castro, O. Kahn, J. A. Real, *Inorg. Chim. Acta* **1999**, *291*, 279–288.
[173] N. Moliner, A. B. Gaspar, M. C. Muñoz, V. Niel, J. Cano, J. A. Real, *Inorg. Chem.* **2001**, *40*, 3986–3991.
[174] J. Klingele, D. Kaase, M. H. Klingele, J. Lach, *Dalt. Trans.* **2012**, *41*, 1397–1406.
[175] H. S. Scott, T. M. Ross, N. F. Chilton, I. A. Gass, B. Moubaraki, G. Chastanet, N. Paradis, J.-F. Lètard, K. R. Vignesh, G. Rajaraman, et al., *Dalt. Trans.* **2013**, *42*, 16494.
[176] S. Zheng, M. A. Siegler, O. Roubeau, S. Bonnet, *Inorg. Chem.* **2014**, *53*, 13162–13173.
[177] X.-R. Wu, H.-Y. Shi, R.-J. Wei, J. Li, L.-S. Zheng, J. Tao, *Inorg. Chem.* **2015**, *54*, 3773–3780.
[178] H. Goodwin, R. Sylva, *Aust. J. Chem.* **1968**, *21*, 83.
[179] H. Goodwin, E. Kucharski, A. White, *Aust. J. Chem.* **1983**, *36*, 1115.
[180] M. G. Simmons, L. J. Wilson, *Inorg. Chem.* **1977**, *16*, 126–130.
[181] E. C. Constable, G. Baum, E. Bill, R. Dyson, R. van Eldik, D. Fenske, S. Kaderli, D. Morris, A. Neubrand, M. Neuburger, et al., *Chem. - A Eur. J.* **1999**, *5*, 498–508.
[182] J. Elhaïk, D. J. Evans, C. A. Kilner, M. A. Halcrow, *Dalt. Trans.* **2005**, 1693–1700.
[183] L. J. Kershaw Cook, R. Kulmaczewski, R. Mohammed, S. Dudley, S. A. Barrett, M. A. Little, R. J. Deeth, M. A. Halcrow, *Angew. Chem. Int. Ed.* **2016**, *55*, 4327–4331.
[184] C. Hansch, A. Leo, R. W. Taft, *Chem. Rev.* **1991**, *91*, 165–195.
[185] M. A. Halcrow, *Chem. Soc. Rev.* **2011**, *40*, 4119.
[186] J. A. Real, A. B. Gaspar, V. Niel, M. C. Muñoz, *Coord. Chem. Rev.* **2003**, *236*, 121–141.
[187] J.-F. Létard, G. Chastanet, O. Nguyen, S. Marcén, M. Marchivie, P. Guionneau, D. Chasseau, P. Gütlich, *Monatshefte für Chemie / Chem. Mon.* **2003**, *134*, 165–182.

[188] N. Nassirinia, S. Amani, S. J. Teat, O. Roubeau, P. Gamez, *Chem. Commun.* **2014**, *50*, 1003–1005.
[189] L. J. Kershaw Cook, H. J. Shepherd, T. P. Comyn, C. Baldé, O. Cespedes, G. Chastanet, M. A. Halcrow, *Chem. - A Eur. J.* **2015**, *21*, 4805–4816.
[190] J.-Y. Li, C.-T. He, Y.-C. Chen, Z.-M. Zhang, W. Liu, Z.-P. Ni, M.-L. Tong, *J. Mater. Chem. C* **2015**, *3*, 7830–7835.
[191] G. A. Renovitch, W. A. Baker, *J. Am. Chem. Soc.* **1967**, *89*, 6377–6378.
[192] M. Mikami, M. Konno, Y. Saito, *Chem. Phys. Lett.* **1979**, *63*, 566–569.
[193] M. Sorai, J. Ensling, P. Gütlich, *Chem. Phys.* **1976**, *18*, 199–209.
[194] T. Tayagaki, A. Galet, G. Molnár, M. Carmen Muñoz, A. Zwick, K. Tanaka, J. A. Real, A. Bousseksou, *J. Phys. Chem. B* **2005**, *109*, 14859–14867.
[195] S. Zheng, M. A. Siegler, J. Sánchez Costa, W.-T. Fu, S. Bonnet, *Eur. J. Inorg. Chem.* **2013**, *2013*, 1033–1042.
[196] N. Paradis, G. Chastanet, F. Varret, J.-F. Létard, *Eur. J. Inorg. Chem.* **2013**, *2013*, 968–974.
[197] C. Baldé, C. Desplanches, F. Le Gac, P. Guionneau, J.-F. Létard, *Dalt. Trans.* **2014**, *43*, 7820.
[198] C. Baldé, C. Desplanches, J. François Létard, G. Chastanet, *Polyhedron* **2017**, *123*, 138–144.
[199] N. Willenbacher, H. Spiering, *J. Phys. C Solid State Phys.* **1988**, *21*, 1423–1439.
[200] H. Spiering, N. Willenbacher, *J. Phys. Condens. Matter* **1989**, *1*, 10089–10105.
[201] M. Sorai, J. Ensling, K. M. Hasselbach, P. Gütlich, *Chem. Phys.* **1977**, *20*, 197–208.
[202] H. Köppen, E. W. Müller, C. P. Köhler, H. Spiering, E. Meissner, P. Gütlich, *Chem. Phys. Lett.* **1982**, *91*, 348–352.
[203] L. Wiehl, G. Kiel, C. P. Köhler, H. Spiering, P. Gütlich, *Inorg. Chem.* **1986**, *25*, 1565–1571.
[204] P. Gütlich, H. Köppen, H. G. Steinhäuser, *Chem. Phys. Lett.* **1980**, *74*, 475–480.
[205] A. Bousseksou, L. Tommasi, G. Lemercier, F. Varret, J.-P. Tuchagues, *Chem. Phys. Lett.* **1995**, *243*, 493–499.
[206] R. N. Sylva, H. A. Goodwin, *Aust. J. Chem.* **1967**, *20*, 479–496.
[207] O. Kahn, *Curr. Opin. Solid State Mater. Sci.* **1996**, *1*, 547–554.
[208] A. Galet, A. B. Gaspar, M. C. Muñoz, J. A. Real, *Inorg. Chem.* **2006**, *45*, 4413–4422.
[209] C. M. Klug, A. M. McDaniel, S. R. Fiedler, K. A. Schulte, B. S. Newell, M. P. Shores, *Dalt. Trans.* **2012**, *41*, 12577–12585.
[210] C. F. Herold, S. I. Shylin, E. Rentschler, *Inorg. Chem.* **2016**, *55*, 6414–6419.
[211] C. Köhler, E. Rentschler, *Eur. J. Inorg. Chem.* **2016**, *2016*, 1955–1960.
[212] I. Galadzhun, I. Capel Berdiell, N. Shahid, M. A. Halcrow, *CrystEngComm* **2019**, *21*, 6330–6334.
[213] S. Rodríguez-Jiménez, H. L. C. Feltham, S. Brooker, *Angew. Chem. Int. Ed.* **2016**, *55*, 15067–15071.
[214] G. J. Halder, C. J. Kepert, B. Moubaraki, K. S. Murray, J. D. Cashion, *Science* **2002**, *298*, 1762–1765.
[215] J. Cirera, *Rev. Inorg. Chem.* **2014**, *34*, 199–216.
[216] C. Bartual-Murgui, A. Akou, C. Thibault, G. Molnár, C. Vieu, L. Salmon, A. Bousseksou, *J. Mater. Chem. C* **2015**, *3*, 1277–1285.
[217] C. H. Pham, J. Cirera, F. Paesani, *J. Am. Chem. Soc.* **2016**, *138*, 6123–6126.
[218] A. Tissot, X. Kesse, S. Giannopoulou, I. Stenger, L. Binet, E. Rivière, C. Serre, *Chem. Commun.* **2019**, *55*, 194–197.
[219] J. Kröber, E. Codjovi, O. Kahn, F. Grolière, C. Jay, *J. Am. Chem. Soc.* **1993**, *115*, 9810–9811.

[220] J. G. Haasnoot, *Coord. Chem. Rev.* **2000**, *200–202*, 131–185.
[221] G. Aromí, L. A. Barrios, O. Roubeau, P. Gamez, *Coord. Chem. Rev.* **2011**, *255*, 485–546.
[222] O. Roubeau, *Chem. - A Eur. J.* **2012**, *18*, 15230–15244.
[223] L. G. Lavrenova, O. G. Shakirova, *Eur. J. Inorg. Chem.* **2013**, 670–682.
[224] W. Vreugdenhil, J. H. Van Diemen, R. A. G. De Graaff, J. G. Haasnoot, J. Reedijk, A. M. Van Der Kraan, O. Kahn, J. Zarembowitch, *Polyhedron* **1990**, *9*, 2971–2979.
[225] A. Ozarowski, B. R. McGarvey, A. Mislankar, J. E. Drake, Y. Shunzhong, *Inorg. Chem.* **1991**, *30*, 3167–3174.
[226] Y. Garcia, O. Kahn, L. Rabardel, B. Chansou, L. Salmon, J. P. Tuchagues, *Inorg. Chem.* **1999**, *38*, 4663–4670.
[227] M. Ruben, E. Breuning, J.-P. Gisselbrecht, J.-M. Lehn, *Angew. Chem.* **2000**, *39*, 4139–4142.
[228] J.-F. Létard, P. Guionneau, L. Goux-Capes, in *Spin Crossover Transition Metal Compdounds III* (Eds.: P. Gütlich, H.A. Goodwin), Springer, Berlin/Heidelberg, **2004**, pp. 221–249.
[229] J. A. Real, H. Bolvin, A. Bousseksou, A. Dworkin, O. Kahn, F. Varret, J. Zarembowitch, *J. Am. Chem. Soc.* **1992**, *114*, 4650–4658.
[230] J. A. Real, I. Castro, A. Bousseksou, M. Verdaguer, R. Burriel, M. Castro, J. Linares, F. Varret, *Inorg. Chem.* **1997**, *36*, 455–464.
[231] V. Ksenofontov, A. B. Gaspar, V. Niel, S. Reiman, J. A. Real, P. Gütlich, *Chem. - A Eur. J.* **2004**, *10*, 1291–1298.
[232] S. Zein, S. A. Borshch, *J. Am. Chem. Soc.* **2005**, *127*, 16197–16201.
[233] A. B. Gaspar, M. C. Muñoz, J. A. Real, *J. Mater. Chem.* **2006**, *16*, 2522–2533.
[234] J. Cirera, E. Ruiz, *J. Mater. Chem. C* **2015**, *3*, 7954–7961.
[235] V. Ksenofontov, H. Spiering, S. Reiman, Y. Garcia, A. . Gaspar, N. Moliner, J. . Real, P. Gütlich, *Chem. Phys. Lett.* **2001**, *348*, 381–386.
[236] M. H. Klingele, B. Moubaraki, J. D. Cashion, K. S. Murray, S. Brooker, *Chem. Commun.* **2005**, *2*, 987–989.
[237] J. A. Kitchen, J. Olguín, R. Kulmaczewski, N. G. White, V. A. Milway, G. N. L. Jameson, J. L. Tallon, S. Brooker, *Inorg. Chem.* **2013**, *52*, 11185–11199.
[238] C. F. Herold, L. M. Carrella, E. Rentschler, *Eur. J. Inorg. Chem.* **2015**, *2015*, 3632–3636.
[239] C. F. Herold, Spin Crossover Systems Based on 1,3,4-Thiadiazoles, PhD Thesis, Johannes Gutenberg University, Mainz, **2016**.
[240] C. Köhler, Spin Crossover Behavior of 1,3,4-Oxadiazole Based Dinuclear Iron(II) Complexes, PhD Thesis, Johannes Gutenberg University, Mainz, **2016**.
[241] D. Bittner, 1,3,4-Thiadiazole Based Bis-Multidentate Ligands for Bridged Bimetallic Complexes with Individually Adjustable Coordination Pockets, PhD Thesis, Johannes Gutenberg University, Mainz, **2018**.
[242] J. Eppelsheimer, Eisen(II) Spin-Crossover Verbindungen Mit 1,3,4-Oxadiazol-Brückenliganden, Master Thesis, Johannes Gutenberg University, Mainz, **2017**.

2. Phase Trapping in Multistep Spin Crossover compound

This chapter describes the synthesis and characterization of six novel dinuclear Fe(II) complexes based on the new tris-bidentate **I²MTD** (2,5-bis[(1*H*-imidazol-2-ylmethyl)amino]methyl-1,3,4-thiadiazole) and **TMTD** (2,5-bis[(thiazol-2-ylmethyl)amino]methyl-1,3,4-thiadiazole) ligands. Depending on the ligand and the various non-coordinating anions, these complexes show distinct different magnetic behavior. The properties and their origin were investigated by single-crystal X-ray structure analysis, magnetic susceptibility measurements and Mössbauer spectroscopy. The results are presented as scientific article previously published in Inorganic Chemistry. Reprinted with the permission from:

F. Fürmeyer, L. M. Carrella, V. Ksenofontov, A. Möller, E. Rentschler, *Inorg. Chem.* **2020**, *59*, 2843–2852. DOI: 10.1021/acs.inorgchem.9b03170.

Author contribution.
Fabian Fürmeyer designed the synthesis, synthesized and characterized the ligands and the complexes. He gathered and analyzed the magnetic data. Single-crystal X-ray diffraction measurements were performed by Dr. D[redacted] S[redacted] and [redacted]. The structure solutions and the refinement of the data was done by Dr. Luca M. Carrella. Mössbauer spectroscopy data was collected by Dr. Vadim Ksenofontov and analyzed by him and Prof. Dr. Angela Möller. The manuscript was written by Fabian Fürmeyer and improved with the help of all other authors. Finally, Eva Rentschler had the overall supervision in the interpretation of the data throughout the manuscript process. All authors have read and agreed to the published version of the manuscript.

‘Phase Trapping in Multistep Spin Crossover Compound’

Fabian Fürmeyer, Luca M. Carrella, Vadim Ksenofontov, Angela Möller and Eva Rentschler*

2.1 Graphical Abstract

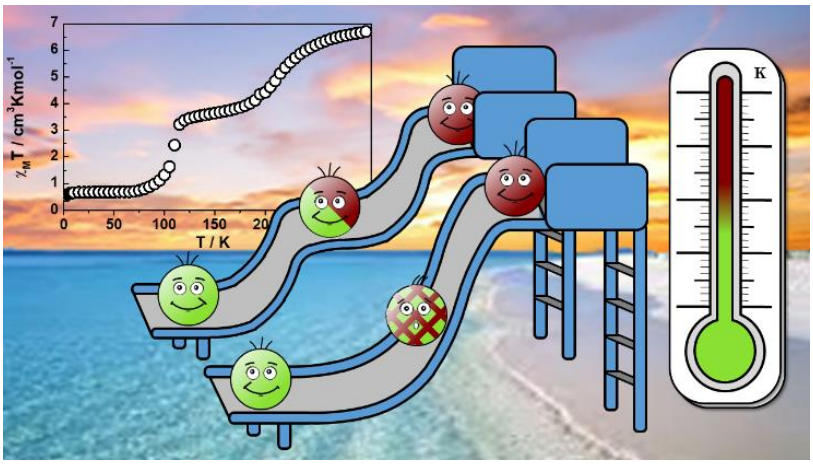

2.2 Abstract

The dimeric motif is the smallest unit for two interacting spin centers allowing for systematic investigations of cooperative interactions. As spin transition compounds, dinuclear complexes are of particular interest, since they potentially reveal a two-step spin crossover (SCO), switching between the high spin – high spin [HS-HS], the high spin – low spin [HS-LS], and the low spin – low spin [LS-LS] states. Herein, we report the synthesis and characterization of six dinuclear iron(II) complexes $[Fe^{II}_2(\mu_2\text{-}\mathbf{L^1})_2](BF_4)_4$ (**C1**), $[Fe^{II}_2(\mu_2\text{-}\mathbf{L^1})_2](ClO_4)_4$ (**C2**), $[Fe^{II}_2(\mu_2\text{-}\mathbf{L^1})_2](F_3CSO_3)_4$ (**C3**), $[Fe^{II}_2(\mu_2\text{-}\mathbf{L^2})_2](BF_4)_4$ (**C4**), $[Fe^{II}_2(\mu_2\text{-}\mathbf{L^2})_2](BF_4)_4$ (**C5**) and $[Fe^{II}_2(\mu_2\text{-}\mathbf{L^2})_2](BF_4)_4$ (**C6**), based on the 1,3,4-thiadiazole (TDA) bridging motif. The two novel bis-tridentate ligands (**L**$^{\mathbf{1}}$ = 2,5-bis{[(1*H*-imidazol-2-ylmethyl)-amino]-methyl}-1,3,4-thiadiazole and **L**$^{\mathbf{2}}$ = 2,5-bis{[(thiazol-2-ylmethyl)-amino]-methyl}-1,3,4-thiadiazole) were employed in the presence of iron(II) salts with the different counter ions. Upon varying ligands and counter ions we were able to change the magnetic properties of the complexes from a temperature-independent [HS-HS] spin state over an one-step spin transition towards a two-step SCO. When cooled slowly from room temperature, the two-step SCO goes along with two distinct phase transitions, and in the intermediate mixed [HS-LS] state distinct HS/LS pairs can be identified unambiguously. In contrast, rapid cooling precludes a crystallographically observable phase transition. For the mixed [HS-LS] state Mössbauer spectroscopy confirms a statistical (random) orientation of adjacent [HS-LS]•[HS-LS]•[HS-LS] chains.

2.3 Introduction

Spin crossover (SCO) describes the transition between two different electronic states, the so-called high spin (HS) and low spin (LS) states, which can be induced by external stimuli such as temperature, pressure, or light irradiation. The resulting changes of the optical and the magnetic properties of compounds containing switchable spin centers renders them highly promising candidates for future application. On the basis of the molecular switching ability of these inorganic materials, they are discussed for high-density data storage, sensing, or display devices.[1–4]

Among the reported SCO materials with several different metal ions ($3d^4$–$3d^7$), iron(II) compounds ($3d^6$) are the far most investigated ones. When switched between the different electronic states, a significant difference in the magnetic moment between the diamagnetic LS (S = 0) and the paramagnetic HS (S = 2) occurs. Upon (un)occupying antibonding σ^*-orbitals huge changes in the average Fe-N bond distance are observed possibly leading to phase transition for the crystal structure.[3,5–7] For future applications, the presence of a wide thermal hysteresis of the spin transition in solid state is advantageous. It is known that the abruptness and the occurrence of such a hysteresis is strongly dependent on the cooperativity of the spin-carrying metal centers. Cooperativity can be enhanced either intramolecularly by bridging the metal ions via organic ligand systems or intermolecularly by hydrogen bonding between the complex molecules or π-π-stacking interactions of neighboring aromatic functionalities in the ligand backbone. The cooperative interactions can be facilitated even with the assistance of solvent molecules or non-coordinating anions.[3,8–13] Polynuclear complexes were anticipated to propagate efficiently local distortions throughout the material due to their high connectivity. In fact, SCO coordination polymers often show large thermal hysteresis.[1,14–16] However, there are many challenges associated with these systems such as a limited control over the nuclearity of the formed complexes, the reproducibility of samples, as well as the full characterization via crystallographic techniques. Considering these facts, the dimeric structural motif is most valuable. It is the simplest and smallest system of two interacting SCO centers suitable for systematic investigations of intra- and intermolecular cooperative interactions. Furthermore, dinuclear complexes represent the first synthetic step toward new functional polynuclear nanomaterials. Finally, dinuclear complexes are of particular interest, since they may show two-step spin crossover switching between the [HS-HS], the [HS-LS], and the [LS-LS] states. For three accessible states a higher data storage capacity and the applicability of complex mathematical operations based on trinary logic can be envisaged.[17,18] Since the first report of a two-step SCO behavior in dinuclear iron(II) complexes in 1987 by Kahn et al. only a few examples examining this phenomena have been reported. Most of them are using different ligands that bridge the metal ions and the ones that complete the coordination sphere.[19–30] This is probably due to the difficulty of designing ligands that simultaneously act as a bridge and induce an appropriate ligand field strength.

Brooker and co-workers are among the first who reported dinuclear SCO compounds using solely one ligand based on the 1,3,4-triazole motif as well as substituted derivatives of it, always keeping the core of the ligand intact. These chelate ligands provide two tridentate pockets and are perfectly suitable to bridge two metal centers in dinuclear complexes.[31–36] Our group has

been working on the synthesis and characterization of symmetric dinuclear iron(II) complexes with 1,3,4-thiadiazole (TDA) and 1,3,4-oxadiazole (ODA) bridging ligands. In previous studies we demonstrated the influence of counter ions as well as solvate molecules on the intra- and intermolecular cooperativity and on the magnetic hysteresis.[37–39] For the latter, recent reports show the key influence of the cooling rate on the width of the hysteresis.[40,41] We figured out that the cooling rate is not only crucial for the magnetic properties but as well for crystallographic differentiation of the HS and LS iron(II) ions in the mixed [HS-LS] state. This crystallographic distinction was first reported by Brooker in 2005[31] and for a two-step SCO compound by Murray et al. in 2006.[27] Herein we report for the first time a discrete two-step SCO behavior accompanied by two phase transitions. On the one hand, when slowly cooled (e.g., often applied during physical properties studies) in the mixed [HS-LS] state the HS and LS iron(II) ions can be identified unambiguously. On the other hand, fast cooling or quenching (which is usually done in single X-ray diffraction studies) leads to no observable phase transition and to a superposition of the HS and LS iron(II) ions. This crystallographic superposition of HS and LS iron(II) ions in the [HS-LS] state is reported in several examples.[22,25,28–30,42] However, until now no satisfying reasoning to that observation is given.

2.4 Experimental Section

2.4.1 Genral Methods and Materials

All chemicals were purchased from Alfa Aesar, Deutero, Fisher Chemicals, TCI, Sigma-Aldrich, and Acros Organics and used without further purification. Absolute solvents were dried according to literature known procedures and used freshly distilled.[43] The NMR spectra were recorded at room temperature with a Bruker Avance DSX 400 and analyzed with the program MestReNova.[44] Magnetic susceptibility measurements were performed on a Quantum Design SQUID magnetometer MPMSXL in a temperature range between 2 and 400 K with an applied field of 1 kOe. Field desorption (FD) mass spectra as well as elemental analyses (C, H, and N) were measured at the microanalytical laboratories of the Johannes Gutenberg University Mainz. X-ray diffraction data were collected at 100, 120, 160, 193, 240, and 250 K with a STOE IPDS 2T at the Johannes Gutenberg University Mainz and at 100 K with a STOE STADIVARI at STOE & Cie GmbH in Darmstadt. The structures were solved with ShelXT[45] and refined with ShelXL[46] implemented in the program Olex2.[47] [57]Mössbauer spectra were recorded using the gas-flow N_2 cryostat with He-exchange gas. The Mössbauer spectrometer is operating in the velocity range from −4 to +4 mm/s (constant acceleration mode) equipped with a ^{57}Co(Rh) source. The spectra were fitted using the Lorentzian analysis of the program Recoil.[48] **Caution!** *The prepared perchlorate complexes are potentially explosive. Even though no explosions occurred, only small amounts should be prepared and handled with care.*

2.4.2 Ligand Synthesis

1,2-Bis(chloroacetyl)hydrazine and 2,5-bis-(chloromethyl)-1,3,4-thiadiazole (**1**) were prepared as described in literature.[37] 2,5-Bis(azidomethyl)-1,3,4-thiadiazole (**2**) and 2,5-bis(aminomethyl)-1,3,4-thiadiazole (**3**) were prepared according to modified synthesis in literature.[49,50] The ligands (**L^1** = 2,5-bis{[(1*H*-imidazol-2-ylmethyl)-amino]-methyl}-1,3,4-thiadiazole and **L^2** = 2,5-bis{[(thiazol-2-ylmethyl)-amino]-methyl}-1,3,4-thiadiazole) were synthesized based on a modified reductive amination known in literature.[51]

2,5-Bis(azidomethyl)-1,3,4-thiadiazole (2). A suspension of 2,5-bis(chloromethyl)-1,3,4-thiadiazole (**1**) (3.60 g, 19.7 mmol, 1.0 equiv), sodium azide (5.10 g, 78.8 mmol, 4.0 equiv), and 18-crown 6 (0.50 g, 1.9 mmol, 0.1 equiv) in acetone (40 mL) was stirred at room temperature for 19 h. The solvent was removed under reduced pressure, and the resulting crude product was purified by column chromatography (SiO_2, dichloromethane/diethyl ether 4:1) to give the pure product as yellow oil. Yield: 3.11 g (15.9 mmol, 81.0%) ^{1}H-NMR (400 MHz, $CDCl_3$, 25 °C): δ = 4.80 (s, 4H, C*H*$_2$) ppm. ^{13}C-NMR (100 MHz, $CDCl_3$, 25 °C): δ = 167.0 (*C*, TDA), 48.8 (*C*H$_2$) ppm. FD-MS ($CHCl_3$): *m*/*z* (%) = 196.08 (100) [M$^+$], 197.07 (16) [M+H$^+$].

2,5-Bis(aminomethyl)-1,3,4-thiadiazole (3). 2,5-Bis-(azidomethyl)-1,3,4-thiadiazole (**2**) (5.14 g, 26.2 mmol, 1.0 equiv) was dissolved in tetrahydrofuran (THF; 280 mL), and triphenylphosphine (16.52 g, 63.0 mmol, 2.4 equiv) and water (14 mL) were added. The solution was stirred at room temperature for 24 h. The solvent was removed under reduced pressure. The resulting orange brown oil was purified by column chromatography (SiO_2). First residual triphenylphosphane and formed triphenylphosphane oxide were eluated with chloroform/methanol (2:1). The pure product as orange solid was isolated by adding triethylamine (1%) to the former solvent mixture. Yield: 3.78 g (26.2 mmol, quant). ^{1}H-NMR (400 MHz, $CDCl_3$, 25 °C): δ = 4.21 (s, 4H, C*H*$_2$), 1.78 (s, 4H, N*H*$_2$) ppm. ^{13}C-NMR (100 MHz, $CDCl_3$, 25 °C): δ = 173.9 (*C*, TDA), 41.5 (*C*H$_2$) ppm. FD-MS ($CHCl_3$): *m*/*z* (%) = 288.66 (85) [(2M)$^+$], 432.59 (100) [(3M)$^+$], 576.49 (33) [(4M)$^+$].

2,5-Bis{[(1*H*-imidazol-2-ylmethyl)-amino]-methyl}-1,3,4-thiadiazole (L^1). 1*H*-Imidazol-2-carbaldehyde (**4a**) (847 mg, 8.80 mmol, 2.1 equiv) was dissolved in methanol (80 mL). To this solution 2,5-bis(aminomethyl)-1,3,4-thiadiazole (**3**) (615 mg, 4.20 mmol, 1.0 equiv) in methanol (20 mL), sodium cyanoborohydride (1320 mg, 21.00 mmol, 5.0 equiv) and acetic acid (528 mg, 8.80 mmol, 2.1 equiv) were added. The solution was refluxed for 18 h, and then the solvent was removed under reduced pressure. The resulting oil was purified by column chromatography (SiO_2, chloroform/methanol 2:1) to give the pure product as brown solid. Yield: 898 mg (2.95 mmol, 70.3%). ^{1}H-NMR (400 MHz, $CDCl_3$, 25 °C): δ = 6.97 (s, 4H, *H*-4, *H*-5, Imz), 4.14 (s, 4H, C*H*$_2$, TDA), 3.89 (s, 4H, C*H*$_2$, Imz) ppm. ^{13}C-NMR (100 MHz, $CDCl_3$, 25 °C): δ = 174.2 (*C*, TDA), 147.7 (*C*-2, Imz), 122.8 (*C*-4, *C*-5 Imz), 48.1 (*C*H$_2$, Imz), 46.5 (*C*H$_2$, TDA) ppm. FD-MS (MeOH): *m*/*z* (%) = 305.20 (100) [M+H$^+$], 327.23 (44) [M+Na$^+$].

2,5-Bis{[(thiazol-2-ylmethyl)-amino]-methyl}-1,3,4-thiadiazole (L^2). Thiazol-2-carbaldehyde (**4b**) (2.38 g, 21.00 mmol, 2.1 equiv), 2,5-bis(aminomethyl)-1,3,4-thiadiazole (**3**) (1.44 mg, 10.00 mmol, 1.0 equiv), sodium cyanoborohydride (3.14 g, 50.00 mmol, 5.0 equiv), and acetic acid (1.26 g, 21:00 mmol, 2.1 equiv) were dissolved in methanol (200 mL). The solution was refluxed and monitored by thin-layer chromatography (TLC) (chloroform/methanol 2:1). After disappearance of **3** the solvent was removed under reduced pressure. The resulting oil was purified by column chromatography (SiO_2, chloroform/methanol 19:1) to give the pure product as brown orange solid. Yield: 1.90 g (5.61 mmol, 56.1%). ^{1}H-NMR (400 MHz, $CDCl_3$, 25 °C): δ = 7.71 (d, 2H, $^3J_{H\text{-}H}$ = 3.3 Hz, *H*-4, Ta), 7.52 (d, 2H, $^3J_{H\text{-}H}$ = 3.3 Hz, *H*-5, Ta), 4.24 (s, 4H, C*H*$_2$, TDA), 4.17 (s, 4H, C*H*$_2$, Ta) ppm. ^{13}C-NMR (100 MHz, $CDCl_3$, 25 °C): δ = 174.6 (*C*, TDA), 173.5 (*C*-2, Ta), 143.1 (*C*-4, Ta), 121.0 (*C*-5, Ta), 50.7 (*C*H$_2$, Ta), 48.3 (*C*H$_2$, TDA) ppm. FD-MS (MeOH): *m*/*z* (%) = 339.01 (28) [M+H$^+$], 676.46 (100) [(2M)$^+$].

2.4.3 General Synthesis of Complexes $[Fe^{II}_2(\mu_2\text{-}L^{1,2})_2](X)_4$.

All complex reactions were performed under nitrogen atmosphere in a glovebox. To an orange solution of the ligand (0.10 mmol) in absolute acetonitrile/methanol (2:1, 2 mL) a solution of the corresponding iron(II) salt [0.10 mmol, $Fe(BF_4)_2{\cdot}6H_2O$, $Fe(ClO_4)_2{\cdot}xH_2O$, or $Fe(F_3CSO_3)_2$] in absolute acetonitrile (2 mL) was added. The reddish to brownish solutions were exposed to vapor diffusion of absolute diethyl ether or absolute tetrahydrofuran, and after several weeks crystals suitable for X-ray diffraction or microcrystalline solids were obtained.

$[Fe^{II}_2(\mu_2\text{-}L^1)_2](BF_4)_4{\cdot}2/3THF{\cdot}1/3(2MeCN)$ (C1). $Fe(BF_4)_2{\cdot}6H_2O$ (34 mg) and 2,5-bis{[(1*H*-imidazol-2-ylmethyl)-amino]-methyl}-1,3,4-thiadiazole (**L^1**, 30 mg) were used to obtain **C1** (33 mg, 57.7%) as light brown crystals suitable for X-ray diffraction. $C_{28}H_{39.3}B_4F_{16}Fe_2N_{16.65}O_{0.67}S_2$ $[Fe^{II}_2(\mu_2\text{-}L^1)_2](BF_4)_4{\cdot}2/3THF{\cdot}1/3(2MeCN)$ (1143.13): calcd. C 29.43, H 3.47, N 20.40; found (after drying in vacuo) C 29.28, H 3.04, N 20.39.

$[Fe^{II}_2(\mu_2\text{-}L^1)_2](ClO_4)_4$ (C2). $Fe(ClO_4)_2{\cdot}xH_2O$ (27 mg) and 2,5-bis{[(1*H*-imidazol-2-ylmethyl)-amino]-methyl}-1,3,4-thiadiazole (**L^1**, 30 mg) were used to obtain **C2** (33 mg, 59.0%) as light brown microcrystalline powder. $C_{24}H_{32}Cl_4Fe_2N_{16}O_{16}S_2$ $[Fe^{II}_2(\mu_2\text{-}L^1)_2](ClO_4)_4$ (1118.23): calcd. C 25.78, H 2.88, N 20.04; found (after drying in vacuo) C 25.43, H 2.73, N 20.01.

$[Fe^{II}_2(\mu_2\text{-}L^1)_2](F_3CSO_3)_4{\cdot}2/3THF{\cdot}1/3(2MeCN)$ (C3). $Fe(F_3CSO_3)_2$ (35 mg) and 2,5-bis{[(1*H*-imidazol-2-ylmethyl)-amino]-methyl}-1,3,4-thiadiazole (**L^1**, 30 mg) were used to obtain **C3** (28 mg, 40.2%) as dark brown crystals suitable for X-ray diffraction. $C_{32}H_{39.3}F_{12}Fe_2N_{16.7}O_{12.7}S_6$ $[Fe^{II}_2(\mu_2\text{-}L^1)_2](F_3CSO_3)_4{\cdot}2/3THF{\cdot}1/3(2MeCN)$ (1392.13): calcd. C 27.61, H 2.85, N 16.77; found (after drying in vacuo) C 27.38, H 2.61, N 16.78.

[$Fe^{II}_2(\mu_2$-$L^2)_2$](BF$_4$)$_4$·3MeCN (C4). Fe(BF$_4$)$_2$·6H$_2$O (34 mg) and 2,5-bis{[(thiazol-2-ylmethyl)-amino]-methyl}-1,3,4-thiadiazole (**L^2**, 34 mg) were used to obtain **C4** (14 mg, 24.7%) as brown crystals suitable for X-ray diffraction. $C_{24}H_{28}B_4F_{16}Fe_2N_{12}S_6$ [$Fe^{II}_2(\mu_2$-**L^2**$)_2$](BF$_4$)$_4$ (1135.84): calcd. C 25.38, H 2.48, N 14.80; found (after drying in vacuo) C 25.43, H 2.21, N 14.82.

[$Fe^{II}_2(\mu_2$-$L^2)_2$](ClO$_4$)$_4$·3MeCN (C5). Fe(ClO$_4$)$_2$·xH$_2$O (27 mg) and 2,5-bis{[(thiazol-2-ylmethyl)-amino]-methyl}-1,3,4-thiadiazole (**L^2**, 34 mg) were used to obtain **C5** (29 mg, 48.8%) as brown crystals suitable for X-ray diffraction. $C_{24}H_{28}Cl_4Fe_2N_{12}O_{16}S_6$ [$Fe^{II}_2(\mu_2$-**L^2**$)_2$](ClO$_4$)$_4$ (1186.41): calcd. C 24.30, H 2.38, N 14.17; found (after drying in vacuo) C 24.69, H 2.37, N 14.04.

[$Fe^{II}_2(\mu_2$-$L^2)_2$](F$_3$CSO$_3$)$_4$·2MeCN (C6). Fe(F$_3$CSO$_3$)2(35 mg) and 2,5-bis{[(thiazol-2-ylmethyl)-amino]-methyl}-1,3,4-thiadiazole (**L^2**, 34 mg) were used to obtain **C6** (28 mg, 19.1%) as dark brown crystals suitable for X-ray diffraction. $C_{30}H_{31}F_{12}Fe_2N_{13}O_{12}S_{10}$ [$Fe^{II}_2(\mu_2$-**L^2**$)_2$](F$_3$CSO$_3$)$_4$·MeCN (1425.93): calcd. C 25.27, H 2.19, N 12.77; found (after drying in vacuo) C 25.20, H 2.11, N 12.80.

2.5 Results and Discussion

2.5.1 Synthesis

The synthesis of the ligands (**L^1** and **L^2**) is presented in Scheme 1. The preparation of the 2,5-bis(chloromethyl)-1,3,4-thiadiazole (**1**) we reported previously.[37] 2,5-Bis(azidomethyl)-1,3,4-thiadiazole (**2**) was synthesized by a nucleophilic substitution of the chloride with sodium azide in the presence of an 18-crown 6.[49] 2,5-Bis-(aminomethyl)-1,3,4-thiadiazole (**3**) was prepared from **2** in a Staudinger reaction.[50] The ligands (**L^1** = 2,5-bis{[(1*H*-imidazol-2-ylmethyl)-amino]-methyl}-1,3,4-thiadiazole and **L^2** = 2,5-bis{[(thiazol-2-ylmethyl)-amino]-methyl}-1,3,4-thiadiazole) were synthesized in a reductive amination reaction of the precursor **3**. The imine was formed by reacting **3** with the respective aldehyde {1*H*-imidazole-2-carbaldehyde (**4a**, Imz) and thiazole-2-carbaldehyde (**4b**, Ta)} and then in situ reduced with sodium cyanoborohydride to the desired ligands (**L^1** and **L^2**) in total yields of 56.9% (**L^1**) and 45.5% (**L^2**) over three steps.[51]

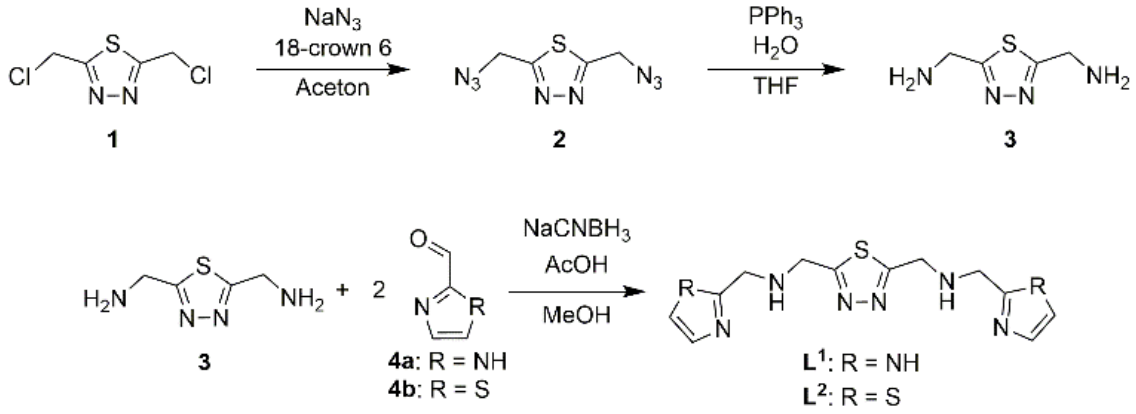

Scheme 1. Synthesis of the ligands $\mathbf{L^1}$ and $\mathbf{L^2}$ starting from 2,5-bis(chloromethyl)-1,3,4-thiadiazole (**1**).

The compounds $Fe^{II}_2(\mu_2\text{-}\mathbf{L^{1,2}})_2](X)_4$ (with X = BF_4^-, ClO_4^-, and $F_3CSO_3^-$) were synthesized in a stoichiometric reaction between the ligand ($\mathbf{L^1}$ or $\mathbf{L^2}$) and the corresponding iron(II) salt. The compounds were obtained as single crystals (**C1**, **C4**–**C6**), suitable for X-ray diffraction experiments, or as microcrystalline solids (**C2** and **C3**). The synthesis was facilitated under nitrogen atmosphere by vapor diffusion of absolute diethyl ether or absolute tetrahydrofuran in complex solutions of absolute acetonitrile and absolute methanol (5:1 volume ratio).

2.5.2 Crystal Structures

The complex $[Fe^{II}_2(\mu_2\text{-}\mathbf{L^1})_2](BF_4)_4\cdot 2/3THF\cdot 1/3(2MeCN)$ (**C1**) crystallizes in the triclinic space group $P\bar{1}$ at 193 K. The crystal structure contains two distinguishable complex cations with two crystallographic different iron(II) centers–one per cation (Figures S15 and S16 in Supporting Information). Each cation consists of two metal centers bridged by two ligand molecules ($\mathbf{L^1}$) via the two nitrogens of the thiadiazole backbone. The two imidazolyl groups in the side arms of the ligand are coordinating in a *cis*-axial manner (Figure 1), and the iron(II) ions are coordinated by six nitrogen donor atoms in distorted octahedral geometries.

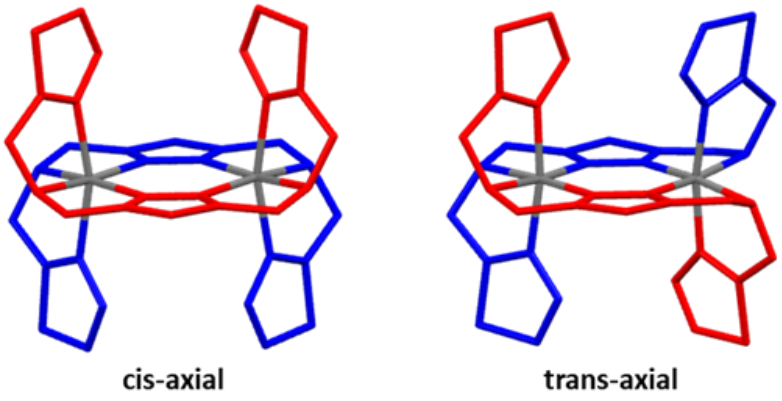

Figure 1. Sketch of the two possible binding modes for the obtained complexes.

The average Fe-N bond length is 2.200 Å (Fe1)/2.196 Å (Fe2), and the octahedral distortion parameter Σ (sum of the deviation from 90° of the 12 *cis*-N-Fe-N angles in the FeN_6 coordination sphere) equals 115.3° for both iron(II) (Fe1 and Fe2). These values are typical for iron(II) in HS state.[52,53] For more detailed information on bond lengths and angles see Table S1 (Supporting Information) for **C1** (for **C4**–**C6** see Table 1). The crystal structure further comprises four non-coordinating tetrafluoroborate ($BF4^-$) anions per cation, which counterbalance the charge. The voids between two complex cations are partially filled with non-coordinating solvent molecules (Figure S15 in Supporting Information). Complexes $[Fe^{II}_2(\mu_2\text{-}\mathbf{L^1})_2](ClO_4)_4$(**C2**) and $[Fe^{II}_2(\mu_2\text{-}\mathbf{L^1})_2](F_3CSO_3)_4$ (**C3**) could be obtained only as microcrystalline solids. However, from the IR spectra we assume that **C1**–**C3** have the same complex cation structures. All IR spectra are very similar except for the bands assigned to the different counter ions (see Supporting Information). Elemental analyses confirm the composition of the complexes as $[Fe^{II}_2(\mu_2\text{-}\mathbf{L^1})_2](ClO_4)_4$ (**C2**) and $[Fe^{II}_2(\mu_2\text{-}\mathbf{L^1})_2](F_3CSO_3)_4$ (**C3**). Likewise to the previous described complex (**C1**), the complexes $[Fe^{II}_2(\mu_2\text{-}\mathbf{L^2})_2](BF_4)_4\cdot 3MeCN$ (**C4**), $[Fe^{II}_2(\mu_2\text{-}\mathbf{L^2})_2](ClO_4)_4\cdot 3MeCN$ (**C5**), and $[Fe^{II}_2(\mu_2\text{-}\mathbf{L^2})_2](F_3CSO_3)_4\cdot 2MeCN$ (**C6**) consist of two iron(II) ions bridged by two ligand molecules. The binding mode of the ligand $\mathbf{L^2}$ for complexes **C4**, **C5**, and **C6** is different. While in **C4** and **C5** a *cis*-axial mode is realized, in **C6** the *trans*-axial mode is present (see Figure 1). However, for our system, as well as for similar ligands forming dinuclear complexes, there seems no easy control over the *cis*- or *trans*-axial coordination mode of theligand. Hydrogen networking of the anions (tetrafluoroborate **C4**, perchlorate **C5**, triflate **C6**) with the complex cations leads to the formation of one-dimensional (1D) chains (Figure S17 in Supporting Information). Additionally, acetonitrile solvent molecules are present in the crystal structure. The different hydrogen-bonded anions lead to various intermolecular distances between the complex cations and to an ecliptic (**C4** and **C5**) or to a staggered (**C6**) orientation of the complex cations along the 1D chain (Figure S18 in Supporting Information).

Table 1. Selected bond lengths [Å], N-Fe-N bond angles [deg] and the octahedral distortion parameter Σ [deg] for the compounds **C4**–**C6**[a].

	C4 (@ 120 K)	**C4** (@ 240 K)	**C5** (@ 100 K)	**C5** (@ 160 K) slow cooldown	**C5** (@ 160 K) quenching	**C5** (@ 250 K)	**C6** (@ 100 K)
Fe-N_{TDA}[b]	**LS** 1.979(5)/1.960(6) **HS** 2.120(4)/2.127(6)	2.115(3)	2.008(4)	**LS** 2.028(7)/1.985(5) **HS** 2.070(7)/2.129(5)	2.062(2)	2.129(2)	1.922(4), 1.929(4)/ 1.929(4), 1.932(4)/ 1.930(4), 1.934(4) 1.930(4), 1.941(4)
Fe-$N_{Imz/Ta}$[b]	**LS** 1.991(5)/1.977(5) **HS** 2.122(5)/2.134(5)	2.113(3)	2.097(4)	**LS** 1.969(6)/1.970(6) **HS** 2.145(6)/2.130(6)	2.049(6)	2.126(2)	1.959(5), 1.969(5)/ 1.968(5), 1.978(5)/ 1.968(5), 1.973(5)/ 1.967(5), 1.968(5)
Fe-N_{NH}[b]	**LS** 2.071(5)/2.082(5) **HS** 2.213(5)/2.212(5)	2.223(3)	2.014(4)	**LS** 2.041(7)/2.072(6) **HS** 2.269(7)/2.228(6)	2.136(6)	2.244(3)	2.024(4), 2.049(4)/ 2.059(4), 2.060(4)/ 2.057(4), 2.062(4)/ 2.051(4), 2.053(4)
ave Fe-N	**LS** 2.014/2.006 **HS** 2.152/2.158	2.150	2.040	**LS** 2.013/2.009 **HS** 2.161/2.162	2.082	2.166	1.978/1.988/ 1.987/1.985
ave *cis* N-Fe-N	**LS** 90.0/90.0 **HS** 90.4/90.5	90.2	90.12	**LS** 90.1/90.0 **HS** 90.3/90.5	90.2	90.3	90.0/90.0/ 90.0/90.0
ave *trans* N-Fe-N	**LS** 1733.9/173.7 **HS** 166.6/161.1	169.1	171.8	**LS** 174.3/173.9 **HS** 167.3/166.0	170.2	168.4	174.2/172.6/ 173.2/173.6
Σ[b,c]	**LS** 65.48/64.86 **HS** 100.01/105.05	97.05	72.22	**LS** 64.51/68.19 **HS** 113.27/104.05	82.48	100.68	57.09/60.82// 61.43/58.74

[a]For compounds **C4** and **C5** the values are given for different temperatures. [b]Fe1/Fe2/Fe3/Fe4. [c]Octahedral distortion parameter Σ (sum of the deviation from 90° of the 12 *cis*-N-Fe-N angles in the FeN_6 coordination sphere).

2.5.3 Magnetic Susceptibility Measurements

Variable-temperature magnetic susceptibility measurements were performed on freshly prepared crystalline as well as on dried samples of **C1**–**C6** in the temperature range of 2–400 K with an external magnetic field of 1000 Oe (0.1 T). It is noteworthy that solvent loss upon drying did not lead to different magnetic behavior for freshly prepared and dried samples (see Figures S29 and S30 in Supporting Information). Compound **C5**, though, is an exception. Here, solvent deficiency (dried sample) clearly leads to the disappearance of the SCO behavior. Thus, it is necessary to ensure that, for the magnetic studies, only freshly prepared samples are used. All magnetic studies were performed with a heating and cooling rate of 1.5 K/min.

The temperature-dependent magnetic susceptibility data of the samples $[Fe^{II}_2(\mu_2\text{-}\mathbf{L^1})_2](X)_4$ (with X = BF_4^-, ClO_4^-, and $F_3CSO_3^-$) **C1**–**C3** are shown in Figure S29 (in Supporting Information). In all three complexes the iron(II) centers are in the HS state at 300 K as indicated by $\chi_M T$ values between 6.52 and 6.61 cm^3Kmol^{-1} per dinuclear complexes depending on the different counter ions. The value for one iron(II) dimer with two non-interacting HS iron ions is calculated as 6.00 cm^3Kmol^{-1} by using the spin-only formalism. The iron(II) centers remain in the [HS-HS] state over the whole measured temperature range. Only below 50 K the $\chi_M T$ values rapidly decrease to a final value between 0.36 and 0.52 cm^3Kmol^{-1} at 2 K. This overall temperature-dependent behavior is consistent with the presence of weak anti-ferromagnetic exchange interactions between the two iron(II) ions in the dimer. These results further confirm that **C2** and **C3** are similar to **C1** regarding the complex cations.

The magnetic data for $[Fe^{II}_2(\mu_2\text{-}\mathbf{L^2})_2](X)_4$ (with X = BF_4^-, ClO_4^-, and $F_3CSO_3^-$) **C4**–**C6** are shown in Figure 2. At low temperature compound **C4** shows a $\chi_M T$ value of 3.65 cm^3Kmol^{-1}, which accounts for an [HS-LS] state in accordance with the single X-ray structure analysis for 120 K (described below) that showed one iron(II) center in the HS state and one in the LS state for the complex cation. By raising the temperature to 180 K the $\chi_M T$ value remains almost constant. Between 180 and 220 K an abrupt increase of the $\chi_M T$ product occurs, which reaches a value of 6.08 cm^3Kmol^{-1} at 220 K. This can be explained by an abrupt spin transition of the complexes from the [HS-LS] to the [HS-HS] state with a transition temperature of $T_{1/2}$ = 200 K. At low temperature, the $\chi_M T$ value of **C5** is ~0.65 cm^3Kmol^{-1} per dinuclear complex, consistent with almost all iron(II) centers being in the LS state. Thus, the thermodynamic stable state for **C5** is the [LS-LS] state. The remaining magnetic susceptibility can account for 16% of the complex cations being in the [HS-LS]. The magnetic data are consistent with the crystallographically obtained values at 100 K (see next chapter). When heated, an abrupt SCO occurs between 90 and 120 K resulting in a plateau region from 120 until 180 K with a $\chi_M T$ of ~3.64 cm^3Kmol^{-1} (at 160 K). This means that, in this transition with $T_{1/2}$ of 105 K, one iron(II) cation per dimer is switching from LS to HS state. The second SCO transition starting at 180 K is more gradual and takes place over a temperature range of 70 K with $T_{1/2}$ of 215 K. The $\chi_M T$ value rises to 6.70 cm^3Kmol^{-1} at 300 K, consistent with the complex being in the [HS-HS] state. The magnetic susceptibility data of **C6** finally show a fully diamagnetic ground state ([LS-LS]) at low temperatures. Again, this is in good agreement with the information obtained from the Fe-N bond lengths and the octahedral distortion parameter from single-crystal structure analysis. By raising the temperature, the $\chi_M T$ product rapidly increases above 300 K to a final value of 5.04 cm^3Kmol^{-1} at 400 K as a result of a gradual one-step SCO from the diamagnetic

[LS-LS] to the paramagnetic [HS-HS] state. The spin transition is not complete until the measurement limit of 400 K. The obtained value corresponds to ~77% of the iron(II) centers being in the HS state.

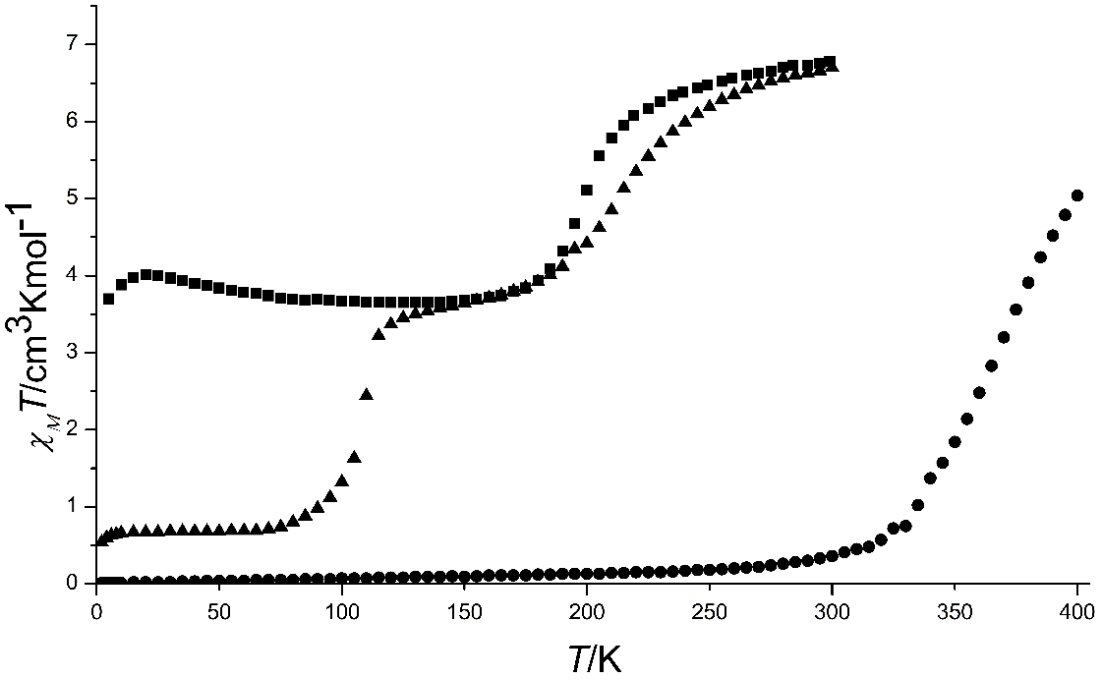

Figure 2. $\chi_M T$ vs T data for the compounds **C4** (■), **C5** (▲), and **C6** (●). The data are given per dinuclear iron(II) molecule.

All here described spin-change phenomena occur without any observation of magnetic hysteresis. The $\chi_M T$ versus T plots are indistinguishable for the measurements when heated or cooled with a cooling/heating rate of 1.5 K/min. The distinguished SCO properties of **C4**–**C6** reflect different intermolecular interactions that we attribute for our ligand system to the various counter ions in the structures, which lead to different distances between the complex cations. For **C5** the intermolecular distance of 4.380 Å (at 250 K) between the complex cations is slightly larger than in **C4**, leading to the observed two-step SCO behavior. The strong rigidity of **C4** due to the smaller intermolecular distance of 4.363 Å (at 240 K) leads basically to the full loss of the switching ability for the second iron(II) center. Thus, the complex remains in the [HS-LS] state until very low temperatures, although we could observe a spin transition of the second iron(II) ion for a small amount of dinuclear molecules (less than 30%) upon very slow cooling (0.1 K/min). **C6** has the largest intermolecular distance of 4.642 Å, thus showing the lowest level of rigidity, which allows the system to reach the thermodynamic favored [LS-LS] state in one-step already above room temperature. Furthermore, because of the trans-axial coordination of the ligand in compound **C6** the iron(II) ions are almost perfectly coordinated in an octahedral environment. The *cis* and *trans* N-Fe-N angles are close to 90° and 180°, which is highly preferred by the thermodynamic favored [LS] state.

2.5.4 Crystallographic Observation of Phase Transition

For $[Fe^{II}_2(\mu_2\text{-}\mathbf{L^2})_2](ClO_4)_4 \cdot 3MeCN$ (**C5**), which shows a twostep SCO, we investigated the change of the crystal structure in dependence of the temperature. **C5** crystallizes in the monoclinic space group *C*2/*m* at 250 K, where only one–fourth of the complex cation with one independent iron(II) ion is part of the asymmetric unit (Figure 3). The dimeric complex cation is generated by symmetry (Figure S21 in Supporting Information). The *C*2-axis runs through the Fe-Fe trajectory of the dimer, while the inversion center is located between the two iron(II) ions. The average (ave) Fe-N distance is 2.166 Å, and the octahedral distortion parameter is $\Sigma = 100.68°$. Both values correspond to an iron(II) ion in the HS state, which accounts for the [HS-HS] state at this temperature.

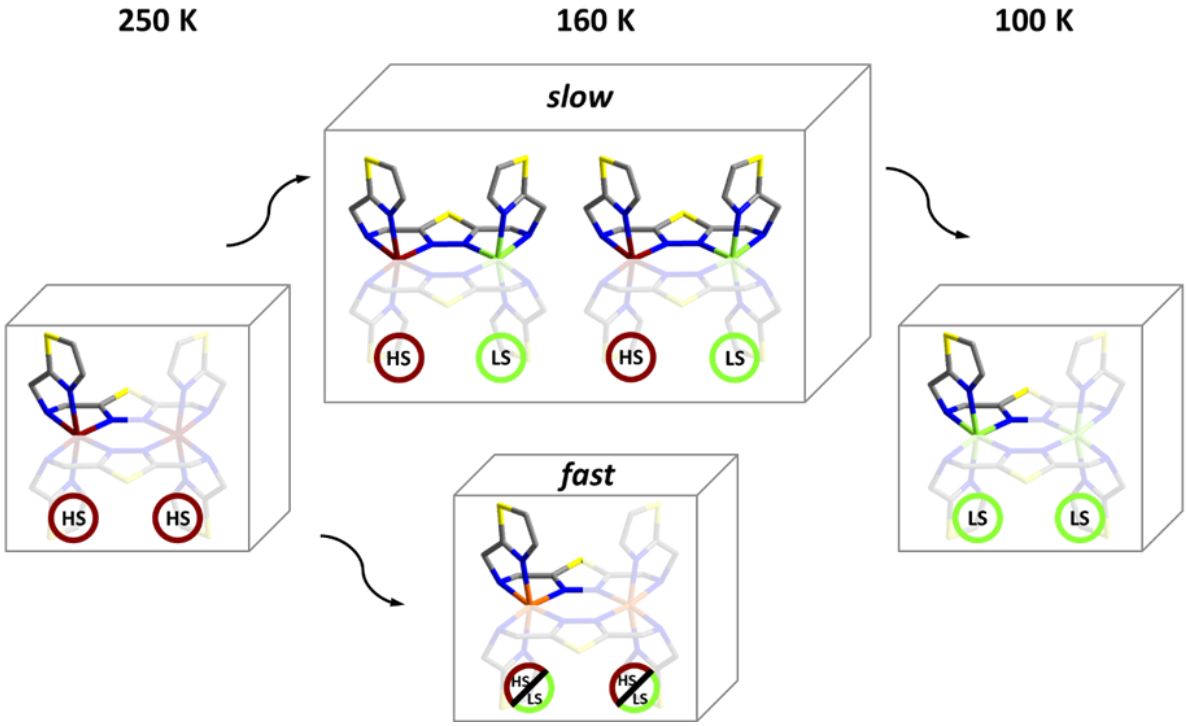

Figure 3. Schematic representation of the SCO and phase transition at different temperatures and different cooling rates for **C5**. The asymmetric unit is depicted in bold, while the symmetry-generated part of the dimeric cationic complex is kept translucent.

When the temperature is slowly lowered to 160 K, a phase transition is observed, and the space group changes to *I*2/*a*. For better comparison with the high, low temperature and the quenched structure, the space group setting *C*2/*c* was selected. The cell volume is nearly quadrupled from 2549.1(5) to 9866.2(6) $Å^3$. Now the asymmetric unit consists of two times half complex cations with in total four independent iron(II) ions (Figures S22–S24 in Supporting Information). In contrast to the structure at 250 K only the *C*2-axis runs through the Fe-Fe trajectory of the dimeric cations, while the inversion centers are next to the dimers. Consequently, two independent iron ions per dimer exist (Figure 4a).

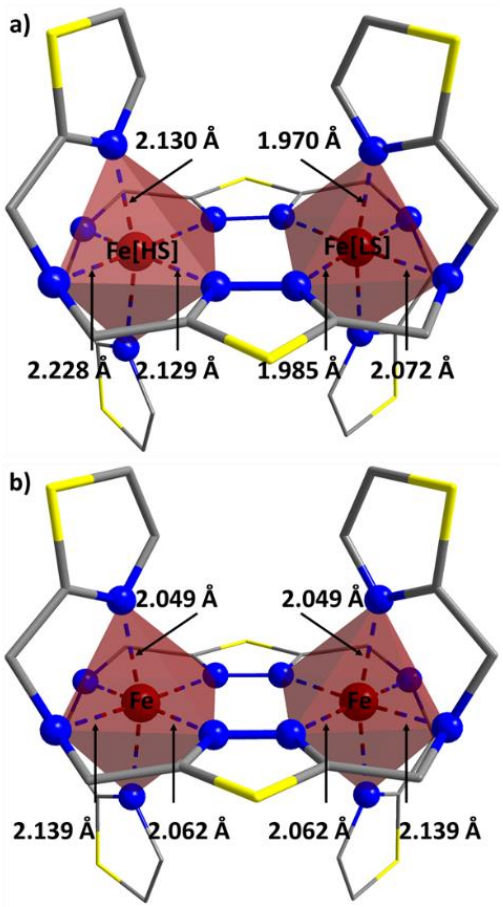

Figure 4. Crystal structures for the two different complex cations of **C5** with Fe-N bond lengths at 160 K. (a) Slow cooldown: two crystallographic distinguishable iron(II) ions. (b) Quenching or rapid cooling: two crystallographic indistinguishable iron(II) ions. Hydrogens, solvent molecules, and counter ions were omitted for clarity. Color code: Fe dark red, N blue, S yellow, and C gray.

The average Fe-N distances for $Fe2^{[LS]}$ and $Fe3^{[LS]}$ decrease from 2.166 to 2.012 Å and to 2.009 Å, while for $Fe1^{[HS]}$ and $Fe4^{[HS]}$ the distances remain nearly the same with 2.161 and 2.162 Å, respectively. Similarly, the octahedral distortion parameters for $Fe2^{[LS]}$ and $Fe3^{[LS]}$ decrease from Σ = 100.68° to Σ = 64.51° and 68.19° and remain rather constant for $Fe1^{[HS]}$ and $Fe4^{[HS]}$ with Σ = 113.27° and 104.05°. The change for $Fe2^{[LS]}$ and $Fe3^{[LS]}$ is typical for Fe(II) centers switching from the HS state to the LS state. Now, each complex cation possesses one iron(II) ion in the HS and one iron(II) ion in the LS state. Along the 1D chain this leads to an ordered orientation of the cations ([HS-LS]•[HS-LS]•[HS-LS]) (Figure S17 in Supporting Information). However, the next neighbor 1D chains are arranged in an antiparallel way (Figure 5). The spin transition that occurs between 250 and 160 K from the [HS-HS] to the [HS-LS] state is accompanied by a phase transition from *C*2/*m* to *I*2/*a*. Further, slow cooling to 100 K leads to a second phase transition accompanied by a space group change back to *C*2/*m* (Figure S26 in Supporting Information). Again, only one–fourth of the complex cation with one independent Fe(II) ion is part of the asymmetric unit. The average Fe-N distance shrinks to 2.040 Å, and the octahedral distortion parameter goes to Σ = 72.22°. This corresponds to the

iron(II) ions being in the LS state. However, the values are slightly higher than the ones expected for all iron(II) centers being in the [LS] state.[52,53] This indicates that a small percentage of the metal ions stays in the [HS] state at this temperature and that the SCO is not complete, as it is confirmed also by magnetic measurements, discussed above. To conclude, a second SCO transition takes place between 160 and 100 K, switching almost all [HS-LS] dimers to the [LS-LS] state. In strong contrast to the slow cooling procedure, fast cooling (quenching) of the compound from 250 to 160 K by mounting the crystal directly under the cold nitrogen stream leads to no observable phase transition. The space group does not change, and the complex stays in the monoclinic space group *C*2/*m* (Figure S25 in Supporting Information). Similar to the structures measured at 250 and 100 K, just one–fourth of the complex cation is part of the asymmetric unit. The average Fe-N distance is 2.082 Å, and the octahedral distortion parameter is Σ = 82.48° (Figure 4b). Both values are between the HS and the LS values in the discrete [HS-LS] state of the previous measurement obtained from the slow cooling procedure. This means that the cooling rate is crucial to observe the phase transition, which is associated with the SCO behavior (Figure 3). Both cooling modes lead to an orientation of the distinct HS/LS dimers along the 1D chain ([HS-LS]•[HS-LS]•[HS-LS]). The 1D chains are oriented antiparallel after slow cooling. In contrast, fast cooling (quenching) leads to no orientation of the 1D chains (Figure 5).

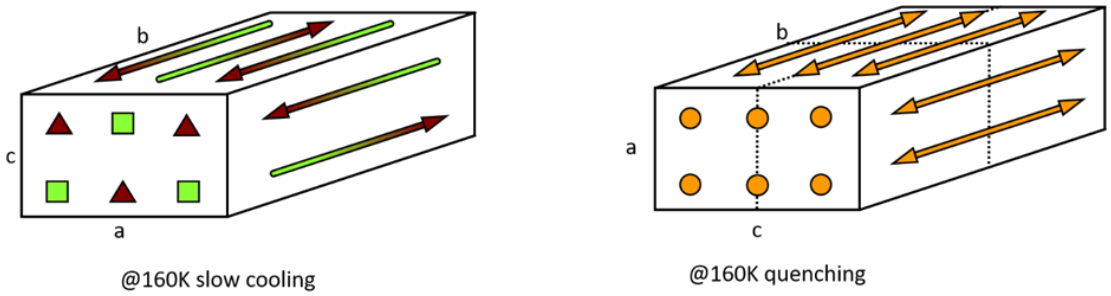

Figure 5. Schematic representation of the orientation of the 1D chains after slow cooling (left) and quenching (right). In the slow-cooled structure the HS iron(II) ions within the HS-LS dimers are pointing toward the head of the arrow (red). Fast cooling leads to a randomized orientation of the 1D chains (orange).

The compound $[Fe^{II}_2(\mu_2\text{-}\mathbf{L^2})_2](BF_4)_4\cdot 3MeCN$ (**C4**) crystallizes in the monoclinic space group *I*2/*m* at 240 K, with one–fourth of the complex cation and one independent iron(II) ion being part of the asymmetric unit (Figure S19 in Supporting Information). The average Fe-N distance is 2.150 Å, and the octahedral distortion parameter Σ is 97.05°. Both values account for an iron(II) ion in the [HS], which reveals the [HS-HS] state at this temperature. When slowly cooled the space group changes to *I*2/*a* at 120 K, while the cell volume is nearly quadrupled (2469.8(10) to 9515.2(8) Å^3). Likewise to **C5** now two times one–half complex cations with four independent iron(II) ions are part of the asymmetric unit (see Figure S20 in Supporting Information). In each complex cation one iron(II) ion is in the [HS] state, and the other one is in the [LS] state. The average Fe-N distance for the LS iron(II) ion is 2.010 Å, and the average

octahedral distortion parameter Σ is 65.17°. For the HS iron(II) ion the average Fe-N distance is 2.155 Å, and Σ is 102.53°. The position of the HS and LS iron(II) centers in each cation is statistically disordered by 15%. Thus, a spin transition occurs between 240 and 120 K from the [HS-HS] to the [HS-LS] state. Further cooling leads to no additional phase transition or SCO. The rapid cooling measurement was also done for **C4**. However, the phase transition, which accompanies the SCO while slow cooling, also takes place while quenching.
The crystal structure of complex **C6** was measured at 100 K (Figures S27 and S28 in the Supporting Information). The asymmetric unit of **C6** contains two complex cations with four slightly different coordinated iron(II) centers. Contrary to the other obtained structures, the ligand is coordinating in a *trans*-axial manner (see Figure 1) with one side arm up and one down. This coordination mode of the ligand results in average Fe-N distances ranging from 1.978 to 1.988 Å for the four different iron(II) ions. The average octahedral distortion parameter values Σ range from 57.09° to 61.43°, respectively. The average *cis* N-Fe-N angle values of 90° and the average *trans* N-Fe-N angle values of 172.6°–174.2° resemble an almost perfect octahedral coordination sphere compared to the previous described structures (see Table 1). These values are typical for iron(II) ions in the [LS] state.
By a direct comparison of **C1** and **C4** the slightly different electronic and geometric properties of $\mathbf{L^1}$ and $\mathbf{L^2}$ can clearly be seen. The average Fe-N distance is a little bit longer for the former compound, but the octahedral average values for the Fe-N distance and the octahedral distortion parameter Σ differ drastically (**C1**: 115.26° and **C4**: 97.05°). Thus, it is very unlikely that **C1** shows any SCO behavior.

2.5.5 Mössbauer Studies

A freshly prepared sample of **C5** was further investigated by using ^{57}Fe Mössbauer spectroscopy. In Figure 6 we show six spectra recorded in the cooling/heating mode sequence: (a) quenched from room temperature to 130 K and measured at 154 K; (b) further quenched to 79 K; (c) heated to 260 K; (d) slowly cooled to 81 K; (e) heated to 153 K; and (f) fast cooled within 11 min to 81 K. Table 2 lists the fitted hyperfine parameters of the individual HS and LS subspectra to the experimental data. The spectra (c) and (d) show mainly one signal, accounting for the pure [HS-HS] ($Fe^{HS(1)}$) state at 260 K and the pure [LS-LS] ($Fe^{LS(1)}$) at 81 K (after slow cooling), respectively. This is in accordance with the magnetic and crystallographic data. To further investigate the interesting results obtained by single-crystal structure analysis, two Mössbauer spectra were recorded at the plateau region (Figure 6a,e). The spectrum at 153 K recorded after slow cooling from 260 K and the spectrum at 154 K obtained after quenching are quite similar. Both spectra show a doublet that can be assigned to an iron(II) ion in the LS state ($Fe^{LS(2)}$). However, the quadrupole splittings indicate that, in both cases, the neighboring ion in the dimer must be an HS iron(II) ion. In fact, both spectra show a second doublet, which can be attributed to an iron(II) ion in the HS state ($Fe^{HS(2)}$). These values for the HS and the LS iron(II) ions are neither identical with the values for the HS iron(II) ions in the [HS-HS] state nor with the values for the LS iron(II) ions in the [LS-LS] state. Thus, the spin state at the plateau region clearly can be assigned to localized [HS-LS] dimers. Interestingly, in the spectrum of the quenched sample a second HS doublet is observed ($Fe^{HS(3)}$). The appearance of this second HS doublet in the quenched sample is explained by the randomized orientation of

the 1D chain. In fact, the relative orientation of the 1D chains to each other is different. In case of the slow cooling, the 1D chains are aligned antiparallel, while quenching leads to a randomized orientation (see Figure 5). The different interchain neighbors have a clear influence on the local environment of the iron(II) ions, leading to mainly two different HS doublets. For the iron(II) ions in the LS state two doublets are expected, as well. However, the resolution limit does not allow to distinguish between the Fe^{LS} components due to the small quadrupole splitting. The two additional spectra at ~80 K (Figure 6b,f) show the possibility to stabilize the [HS-LS] state even at very low temperatures. The randomized or ordered phase is maintained upon rapid cooling from the plateau region, dependent on its initial phase. However, the right cooling rate is crucial for this observation. Indeed, the spectrum at 79 K (Figure 6b) after quenching from 154 K shows only a small difference to the one recorded at 154 K (Figure 6a). This observation was further confirmed by magnetic susceptibility measurements conducted with a cooling rate of 10 K/min (see Figure S31 in Supporting Information). In contrast, the spectra at 81 K (Figure 6f) after cooling from 153 K within 11 min show a second LS signal ($Fe^{LS(1)}$). Despite the high cooling rate, a partial transition to the [LS-LS] ($Fe^{LS(1)}$) takes place. Now, 14% of the dimers are in the [LS-LS] state. Overall, the hyperfine parameters obtained from Lorentzian fittings of the Mössbauer spectra for the respective Fe^{HS} and Fe^{LS} sites (Table 2) are in good agreement with the reported ones in the literature.[23,27–29,37,39]

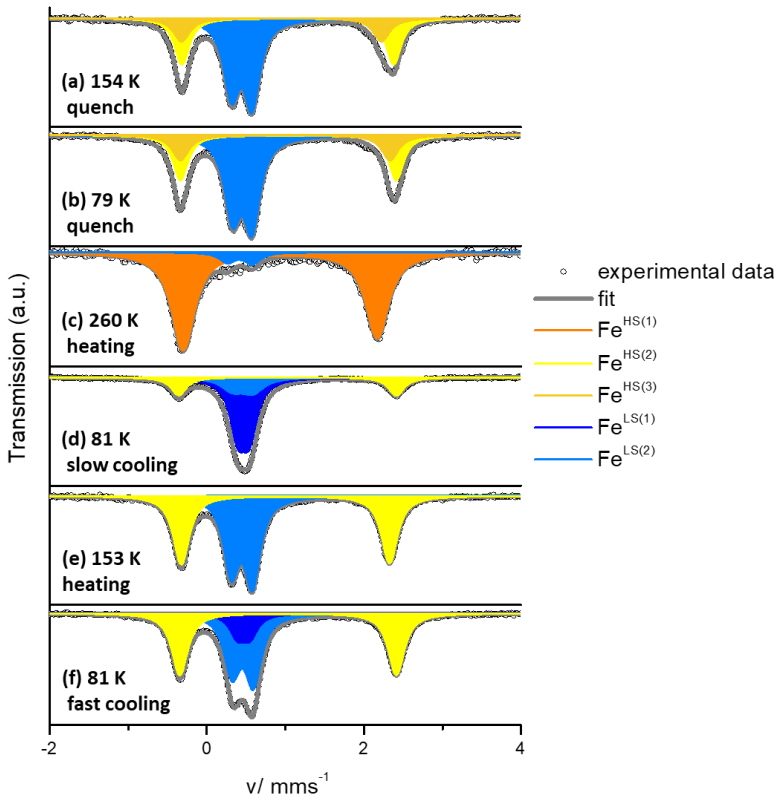

Figure 6. Mössbauer spectra recorded for **C5** at the given temperatures. The temperature sequence starts from 293 K and is referenced chronologically (a–f) by intermediate quenching, heating, or cooling mode. Three different HS- and two LS-subspectra are depicted. Color code: $Fe^{HS(1)}$ in [HS-HS] dimer orange; $Fe^{LS(1)}$ in [LS-LS] dimer dark blue; $Fe^{HS(2)}$ in [HS-LS] dimer (interchain ordered) yellow; $Fe^{HS(3)}$ in [HS-LS] dimer (interchain disordered) dark yellow; and $Fe^{LS(2)}$ in [HS-LS] dimer blue.

Table 2. Chemical shifts (δ) quadrupole splittings (Δ), and site populations for all measured Mössbauer spectra of **C5**.

spectra	site	assignment	δ	Δ	site population, %	T, K
(a)	$Fe^{HS(2)}$	HS-LS	1.03(1)	2.70(3)	30.4	154
	$Fe^{HS(3)}$	HS-LS	0.95(3)	2.54(6)	17.0	
	$Fe^{LS(2)}$	HS-LS	0.45(1)	0.26(1)	52.6	
(b)	$Fe^{HS(2)}$	HS-LS	1.04(1)	2.75(2)	28.2	79
	$Fe^{HS(3)}$	HS-LS	1.00(1)	2.67(5)	17.5	
	$Fe^{LS(2)}$	HS-LS	0.45(1)	0.25(2)	54.3	
(c)	$Fe^{HS(1)}$	HS-HS	0.94(1)	2.47(1)	92.7	260
	$Fe^{LS(2)}$	HS-LS	0.42(1)	0.32(1)	7.34	
(d)	$Fe^{LS(1)}$	LS-LS	0.47(1)	0.15(1)	58.3	81
	$Fe^{HS(2)}$	HS-LS	1.03(1)	2.77(1)	20.8	
	$Fe^{LS(2)}$	HS-LS	0.46(1)	0.26(1)	20.9	
(e)	$Fe^{HS(2)}$	HS-LS	1.00(1)	2.65(1)	47.6	153
	$Fe^{LS(2)}$	HS-LS	0.46(1)	0.26(1)	52.4	
(f)	$Fe^{HS(2)}$	HS-LS	1.04(1)	2.76(1)	42.8	81
	$Fe^{LS(2)}$	HS-LS	0.46(1)	0.27(1)	43.0	
	$Fe^{LS(1)}$	LS-LS	0.47(1)	0.16(1)	14.2	

2.6 Conclusion

We synthesized and characterized six new dinuclear iron(II) complexes in all of which the two metal ions are μ_2-bridged by two new bis-tridentate 1,3,4-thiadiazole ligands. While the complexes formed from a thiadiazole ligand with imidazole side-arms remain in the [HS-HS] state over the whole temperature range, different spin crossover properties were observed for **C4**, **C5**, and **C6** bearing thiazole side arms. We attribute the origin of the various spin crossover behavior to the different intermolecular distances between the complex cations originating from different counteranions. By reducing the volume of the anion the intermolecular distances shrink, destabilizing the [LS-LS] state. Thus, **C6** ($F_3CSO_3^-$, with the largest volume) shows a spin crossover transition from the [LS-LS] state above room temperature, while for **C4** (BF_4^-) the [LS-LS] is not reached even at very low temperatures. Here, an abrupt transition between the [HS-LS] and [HS-HS] is observed. Only for **C5** (ClO_4^-) all three spin states ([LS-LS], [HS-LS], [HS-HS]) are accessible. The two-step spin crossover is accompanied by two phase transitions when slowly cooled. In the mixed [HS-LS] state distinct [HS-LS] iron(II) pairs can be identified unambiguously. Remarkably, upon rapid cooling or quenching no phase transition is detected, and the [HS-LS] state is a superposition of HS and LS iron(II) ions in the complex cation. Mössbauer studies for **C5** support these findings. To summarize, we found that the cooling rate is crucial to observe the phase transition associated with the SCO behavior. This finding is important for the further understanding of SCO behavior. Notably, special attention should be paid when comparing results of physical properties studies (mostly slow cooling) and crystallographic measurements (usually fast cooling or quenching).

2.7 Associated Content

Supporting Information

The supporting Information is available free of charge at https://pubs.acs.org/doi/10.1021/acs.inorgchem.9b03170.

^{1}H and ^{13}C NMR spectra of **2**, **3**, $\mathbf{L^1}$, and $\mathbf{L^2}$; IR spectra of dried **C1**−**C6**; X-ray diffraction measurements; magnetic data.

Accession Codes

CCDC 1949841−1949845 and 1959864−1959867 contain the supplementary crystallographic data for this paper. These data can be obtained free of charge via www.ccdc.cam.ac.uk/data_request/cif, or by emailing data_request@ccdc.cam.ac.uk, or by contacting The Cambridge Crystallographic Data Centre, 12 Union Road, Cambridge CB2 1EZ, UK; fax: +441223 336033.

2.8 Author Information

Corresponding author

Eva Rentschler — *Department of Chemistry, Johannes Gutenberg University Mainz, Mainz 55128, Gemany*; orcid.org/0000-0003-1431-3641; Email: rentschler@uni-mainz.de

Authors

Fabian Fürmeyer — *Department of Chemistry, Johannes Gutenberg University Mainz, Mainz 55128, Gemany*

Luca M. Carrella — *Department of Chemistry, Johannes Gutenberg University Mainz, Mainz 55128, Gemany*

Vadim Ksenofontov — *Department of Chemistry, Johannes Gutenberg University Mainz, Mainz 55128, Gemany*

Angela Möller — *Department of Chemistry, Johannes Gutenberg University Mainz, Mainz 55128, Gemany*; orcid.org/0000-0002-3323-6998

Complete contact information is available at: https://pubs.acs.org/10.1021/acs.inorgchem.9b03170

Notes

The Authors declare no competing financial interest.

2.9 Acknowledgments

Dedicated to P[redacted] G[redacted] on the occasion of his 85th birthday. Dr. D. S[redacted] is kindly acknowledged for measuring the crystal structures of **C1**, **C4**, and **C5** at all given temperatures. We want to thank [redacted] for collecting the crystallographic data of **C6** at 100 K. A.M. and V.K. acknowledge support by the [redacted].

2.10 References

(1) Kahn, O. Spin-Transition Polymers: From Molecular Materials Toward Memory Devices. *Science* **1998**, *279* (5347), 44–48.
(2) Létard, J.-F.; Guionneau, P.; Goux-Capes, L. Towards Spin Crossover Applications. In *Spin Crossover in Transition Metal Compounds III*; Springer-Verlag: Berlin, Germany, 2006; Vol. *1*, pp 221−249. DOI: 10.1007/b95429.
(3) Gütlich, P.; Hauser, A.; Spiering, H. Thermisch Und Optisch Schaltbare Eisen(II)-Komplexe. *Angew*. *Chem*. **1994**, *106* (20), 2109−2141.
(4) Bousseksou, A.; Molnár, G.; Salmon, L.; Nicolazzi, W. Molecular Spin Crossover Phenomenon: Recent Achievements and Prospects. *Chem*. *Soc*. *Rev*. **2011**, *40* (6), 3313−3335.
(5) Gütlich, P.; Garcia, Y.; Goodwin, H. A. Spin Crossover Phenomena in Fe(II) Complexes. *Chem*. *Soc*. *Rev*. **2000**, *29* (6), 419−427.
(6) Gütlich, P.; Goodwin, H. A. Spin Crossover─An Overall Perspective. In *Spin Crossover in Transition Metal Compounds I*; Springer-Verlag: Berlin, Germany, 2004; Vol. *1*, pp 1−47. DOI: 10.1007/b13527.
(7) Capel Berdiell, I.; Kulmaczewski, R.; Cespedes, O.; Halcrow, M. A. An Incomplete Spin Transition Associated with a Z ′=1→ Z ′=24 Crystallographic Symmetry Breaking. *Chem*. *- Eur*. *J*. **2018**, *24* (20),5055−5059.
(8) Enachescu, C.; Stoleriu, L.; Nishino, M.; Miyashita, S.; Stancu, A.; Lorenc, M.; Bertoni, R.; Cailleau, H.; Collet, E. Theoretical Approach for Elastically Driven Cooperative Switching of Spin- Crossover Compounds Impacted by an Ultrashort Laser Pulse. *Phys*. *Rev*. *B*: *Condens*. *Matter Mater*. *Phys*. **2017**, *95* (22), 224107.
(9) Pavlik, J.; Boča, R. Established Static Models of Spin Crossover. *Eur*. *J*. *Inorg*. *Chem*. **2013**, *2013* (5−6), 697−709.
(10) Barrios, L. A.; Peyrecave-Lleixà, E.; Craig, G. A.; Roubeau, O.; Teat, S. J.; Aromí, G. Unusual Crystal Packing in a Family of [Fe{2,6-Bis(Pyrazol-3-Yl)Pyridine} 2] 2+ Compounds and the Effect on the Occurrence of Spin Crossover and Its Cooperative Character. *Eur*. *J*. *Inorg*. *Chem*. **2014**, *2014* (35), 6013−6021.
(11) Halcrow, M. A. Structure:Function Relationships in Molecular Spin-Crossover Complexes. *Chem*. *Soc*. *Rev*. **2011**, *40* (7), 4119.
(12) Seredyuk, M.; Muñoz, M. C.; Castro, M.; Romero-Morcillo, T.; Gaspar, A. B.; Real, J. A. Unprecedented Multi-Stable Spin Crossover Molecular Material with Two Thermal Memory Channels. *Chem*. *- Eur*. *J*. **2013**, *19* (21), 6591−6596.

(13) Valverde- Muñoz, F. J.; Seredyuk, M.; Meneses-Sánchez, M.; Muñoz, M. C.; Bartual-Murgui, C.; Real, J. A. Discrimination between Two Memory Channels by Molecular Alloying in a Doubly Bistable Spin Crossover Material. *Chem. Sci*. **2019**, *10* (13), 3807−3816.
(14) Kahn, O.; Kröber, J.; Jay, C. Spin Transition Molecular Materials for Displays and Data Recording. *Adv. Mater*. **1992**, *4* (11),718−728.
(15) Kröber, J.; Codjovi, E.; Kahn, O.; Grolière, F.; Jay, C. A Spin Transition System with a Thermal Hysteresis at Room Temperature. *J. Am. Chem. Soc*. **1993**, *115* (21), 9810−9811.
(16) Hogue, R. W.; Singh, S.; Brooker, S. Spin Crossover in Discrete Polynuclear Iron (II) Complexes. *Chem. Soc. Rev*. **2018**, *47* (19), 7303−7338.
(17) Ruben, M.; Breuning, E.; Gisselbrecht, J.-P.; Lehn, J.-M. Multilevel Molecular Electronic Species: Electrochemical Reduction of a [2×2] CoII4 Grid-Type Complex by 11 Electrons in 10 Reversible Steps. *Angew. Chem., Int. Ed*. **2000**, *39* (22), 4139−4142.
(18) Breuning, E.; Ruben, M.; Lehn, J.; Renz, F.; Garcia, Y.; Ksenofontov, V.; Gütlich, P.; Wegelius, E.; Rissanen, K. Spin Crossover in a Supramolecular Fe4II [2×2] Grid Triggered by Temperature, Pressure, and Light. *Angew. Chem., Int. Ed*. **2000**, *39* (14), 2504−2507.
(19) Real, A.; Zarembowitch, J.; Kahn, O.; Solans, X. Magnetic Interaction and Spin Transition in Iron(II) Dinuclear Compounds. Crystal Structure of (.Mu.-2,2'-Bipyrimidine)Bis[(2,2'-Bipyrimidine)Bis(Thiocyanato)Iron(II)]. *Inorg. Chem*. **1987**, *26* (18), 2939−2943.
(20) Real, J. A.; Bolvin, H.; Bousseksou, A.; Dworkin, A.; Kahn, O.; Varret, F.; Zarembowitch, J. Two-Step Spin Crossover in the New Dinuclear Compound [Fe(Bt)(NCS)2]2bpym, with Bt = 2,2'-Bi-2-Thiazoline and Bpym = 2,2'-Bipyrimidine: Experimental Investigation and Theoretical Approach. *J. Am. Chem. Soc*. **1992**, *114* (12), 4650–4658.
(21) Murray, K. S. Advances in Polynuclear Iron(II), Iron(III) and Cobalt(II) Spin-Crossover Compounds. *Eur. J. Inorg. Chem*. **2008**, *2008* (20), 3101−3121.
(22) Schneider, C. J.; Cashion, J. D.; Chilton, N. F.; Etrillard, C.; Fuentealba, M.; Howard, J. A. K.; Létard, J.-F.; Milsmann, C.; Moubaraki, B.; Sparkes, H. A.; et al. Spin Crossover in a 3,5-Bis(2-Pyridyl)-1,2,4-Triazolate-Bridged Dinuclear Iron(II) Complex [{Fe(NCBH 3)(Py)} 2 (μ-L 1) 2]-Powder versus Single Crystal Study. *Eur. J. Inorg. Chem*. **2013**, *2013* (5−6), 850−864.
(23) Real, J. A.; Castro, I.; Bousseksou, A.; Verdaguer, M.; Burriel, R.; Castro, M.; Linares, J.; Varret, F. Spin Crossover in the 2,2'-Bipyrimidine- (Bpym-) Bridged Iron(II) Complexes [Fe(L)(NCX)2]2 (Bpym) (L = 2, 2'-Bithiazoline (Bt) and Bpym; X = S, Se). X-Ray Absorption Spectroscopy, Magnetic Susceptibility, Calorimetric, and Mössbauer Spectroscopy Studie. *Inorg. Chem*. **1997**, *36* (3), 455−464.
(24) Real, J. A.; Gaspar, A. B.; Niel, V.; Muñoz, M. C. Communication between Iron(II) Building Blocks in Cooperative Spin Transition Phenomena. *Coord. Chem. Rev*. **2003**, *236* (1−2), 121−141.
(25) Ortega-Villar, N.; Thompson, A. L.; Muñoz, M. C.; Ugalde-Saldívar, V. M.; Goeta, A. E.; Moreno-Esparza, R.; Real, J. A. Solidand Solution-State Studies of the Novel μ-Dicyanamide-Bridged Dinuclear Spin-Crossover System {[(Fe(Bztpen)]2[μ-N(CN)2]}-(PF6)3·n H2O. *Chem. - Eur. J*. **2005**, *11* (19), 5721−5734.
(26) Gaspar, A. B.; Muñoz, M. C.; Real, J. A. Dinuclear Iron (ii) Spin Crossover Compounds: Singular Molecular Materials for Electronics. *J. Mater. Chem*. **2006**, *16* (26), 2522−2533.

(27) Amoore, J. J. M.; Kepert, C. J.; Cashion, J. D.; Moubaraki, B.; Neville, S. M.; Murray, K. S. Structural and Magnetic Resolution of a Two-Step Full Spin-Crossover Transition in a Dinuclear Iron(II) Pyridyl-Bridged Compound. *Chem. - Eur. J.* **2006**, *12* (32), 8220−8227.
(28) Verat, A. Y.; Ould-Moussa, N.; Jeanneau, E.; Le Guennic, B.; Bousseksou, A.; Borshch, S. A.; Matouzenko, G. S. Ligand Strain and the Nature of Spin Crossover in Binuclear Complexes: Two-Step Spin Crossover in a 4,4′-Bipyridine-Bridged Iron(II) Complex [{Fe(Dpia)-(NCS) 2 } 2 (4,4′-Bpy)] (Dpia = di(2-Picolyl)Amine; 4,4′-Bpy = 4,4′-Bipyridine). *Chem. - Eur. J.* **2009**, *15* (39), 10070−10082.
(29) Matouzenko, G. S.; Jeanneau, E.; Yu Verat, A.; Bousseksou, A. Spin Crossover and Polymorphism in a Family of 1,2-Bis(4-Pyridyl)Ethene-Bridged Binuclear Iron(II) Complexes. A Key Role of Structural Distortions. *Dalt. Trans.* **2011**, *40* (37), 9608.
(30) Matouzenko, G. S.; Jeanneau, E.; Verat, A. Y.; de Gaetano, Y. The Nature of Spin Crossover and Coordination Core Distortion in a Family of Binuclear Iron(II) Complexes with Bipyridyl-Like Bridging Ligands. *Eur. J. Inorg. Chem.* **2012**, *2012* (6), 969−977.
(31) Klingele, M. H.; Moubaraki, B.; Cashion, J. D.; Murray, K. S.; Brooker, S. The First X-Ray Crystal Structure Determination of a Dinuclear Complex Trapped in the [Low Spin−High Spin] State: [FeII 2 (PMAT) 2](BF 4) 4 ·DMF. *Chem. Commun.* **2005**, *2* (8), 987−989.
(32) Klingele, M. H.; Moubaraki, B.; Murray, K. S.; Brooker, S. Synthesis and Some First-Row Transition-Metal Complexes of the 1,2,4-Triazole-Based Bis(Terdentate) Ligands TsPMAT and PMAT. *Chem. - Eur. J.* **2005**, *11* (23), 6962−6973.
(33) Bhattacharjee, A.; Ksenofontov, V.; Kitchen, J. A.; White, N. G.; Brooker, S.; Gütlich, P. Effect of Pressure and Light on the Spin Transition Behavior of the Dinuclear Iron(II) Compound [FeII2-(PMAT)2](BF4)4·DMF. *Appl. Phys. Lett.* **2008**, *92* (17), 174104.
(34) Grunert, C. M.; Reiman, S.; Spiering, H.; Kitchen, J. A.; Brooker, S.; Gütlich, P. Mixed Spin-State [HS-LS] Pairs in a Dinuclear Spin-Transition Complex: Confirmation by Variable-Temperature 57Fe Mössbauer Spectroscopy. *Angew. Chem., Int. Ed.* **2008**, *47* (16), 2997−2999.
(35) Kitchen, J. A.; White, N. G.; Jameson, G. N. L. L.; Tallon, J. L.; Brooker, S. Effect of Counteranion X on the Spin Crossover Properties of a Family of Diiron(II) Triazole Complexes [Fe II 2 (PMAT) 2](X) 4. *Inorg. Chem.* **2011**, *50* (10), 4586−4597.
(36) Hogue, R. W.; Feltham, H. L. C.; Miller, R. G.; Brooker, S. Spin Crossover in Dinuclear N 4 S 2 Iron(II) Thioether−Triazole Complexes: Access to [HS-HS], [HS-LS], and [LS-LS] States. *Inorg. Chem.* **2016**, *55* (9), 4152−4165.
(37) Herold, C. F.; Carrella, L. M.; Rentschler, E. A Family of Dinuclear Iron(II) SCO Compounds Based on a 1,3,4-Thiadiazole Bridging Ligand. *Eur. J. Inorg. Chem.* **2015**, *2015* (22), 3632−3636.
(38) Herold, C. F.; Shylin, S. I.; Rentschler, E. Solvent-Dependent SCO Behavior of Dinuclear Iron(II) Complexes with a 1,3,4-Thiadiazole Bridging Ligand. *Inorg. Chem.* **2016**, *55* (13), 6414−6419.
(39) Köhler, C.; Rentschler, E. The First 1,3,4-Oxadiazole Based Dinuclear Iron(II) Complexes Showing Spin Crossover Behavior with Hysteresis. *Eur. J. Inorg. Chem.* **2016**, *2016* (13−14), 1955−1960.

(40) Kulmaczewski, R.; Olguín, J.; Kitchen, J. A.; Feltham, H. L. C.; Jameson, G. N. L.; Tallon, J. L.; Brooker, S. Remarkable Scan Rate Dependence for a Highly Constrained Dinuclear Iron(II) Spin Crossover Complex with a Wide Thermal Hysteresis Loop. *J. Am. Chem. Soc.* **2014**, *136* (3), 878−881.
(41) Brooker, S. Spin Crossover with Thermal Hysteresis: Practicalities and Lessons Learnt. *Chem. Soc. Rev.* **2015**, *44* (10), 2880−2892.
(42) de Gaetano, Y.; Jeanneau, E.; Verat, A. Y.; Rechignat, L.; Bousseksou, A.; Matouzenko, G. S. Ligand-Induced Distortions and Magneto-Structural Correlations in a Family of Dinuclear Spin Crossover Compounds with Bipyridyl-Like Bridging Ligands. *Eur. J. Inorg. Chem.* **2013**, *2013* (5−6), 1015−1023.
(43) Eaborn, C. Purification of Laboratory Chemicals. *J. Organomet. Chem.* **1981**, *213* (2), C62.
(44) Cobas, J. C.; Sardina, F. J. Nuclear Magnetic Resonance Data Processing. MestRe-C: A Software Package for Desktop Computers. *Concepts Magn. Reson.* **2003**, *19A* (2), 80−96.
(45) Sheldrick, G. M. SHELXT−Integrated Space-Group and Crystal-Structure Determination. *Acta Crystallogr., Sect. A: Found. Adv.* **2015**, *71* (1), 3−8.
(46) Sheldrick, G. M. Crystal Structure Refinement with SHELXL. *Acta Crystallogr., Sect. C: Struct. Chem.* **2015**, *71* (Md), 3−8.
(47) Dolomanov, O. V.; Bourhis, L. J.; Gildea, R. J.; Howard, J. A. K.; Puschmann, H. OLEX2: A Complete Structure Solution, Refinement and Analysis Program. *J. Appl. Crystallogr.* **2009**, *42* (2), 339−341.
(48) Lagarec, K.; Rancourt, D. *Recoil User Manual─Mossbauer Spectral Analysis Software for Windows*; 1998.
(49) Kun, S.; Nagy, G. Z.; Tóth, M.; Czecze, L.; Van Nhien, A. N.; Docsa, T.; Gergely, P.; Charavgi, M.-D.; Skourti, P. V.; Chrysina, E. D.; et al. Synthesis of Variously Coupled Conjugates of D-Glucose, 1,3,4-Oxadiazole, and 1,2,3-Triazole for Inhibition of Glycogen Phosphorylase. *Carbohydr. Res.* **2011**, *346* (12), 1427−1438.
(50) Lebeau, L.; Oudet, P.; Mioskowski, C. Synthesis of New Phospholipids Linked to Steroid-Hormone Derivatives Designed for Two-Dimensional Crystallization of Proteins. *Helv. Chim. Acta* **1991**, *74* (8), 1697−1706.
(51) Dangerfield, E. M.; Plunkett, C. H.; Win-Mason, A. L.; Stocker, B. L.; Timmer, M. S. M. Protecting-Group-Free Synthesis of Amines: Synthesis of Primary Amines from Aldehydes via Reductive Amination. *J. Org. Chem.* **2010**, *75* (16), 5470−5477.
(52) Guionneau, P.; Marchivie, M.; Bravic, G.; Létard, J.-F.; Chasseau, D. Structural Aspects of Spin Crossover. Example of the [FeIILn(NCS)2] Complexes. In *Spin Crossover in Transition Metal Compounds II*; Springer-Verlag: Berlin, Germany, 2012; pp 97−128. DOI: 10.1007/b95414.
(53) Kitchen, J. A.; Olguín, J.; Kulmaczewski, R.; White, N. G.; Milway, V. A.; Jameson, G. N. L.; Tallon, J. L.; Brooker, S. Effect of N4 -Substituent Choice on Spin Crossover in Dinuclear Iron(II) Complexes of Bis-Terdentate 1,2,4-Triazole-Based Ligands. *Inorg. Chem.* **2013**, *52* (19), 11185−11199.

2.11 Supporting Information

2.11.1 NMR Spectroscopy

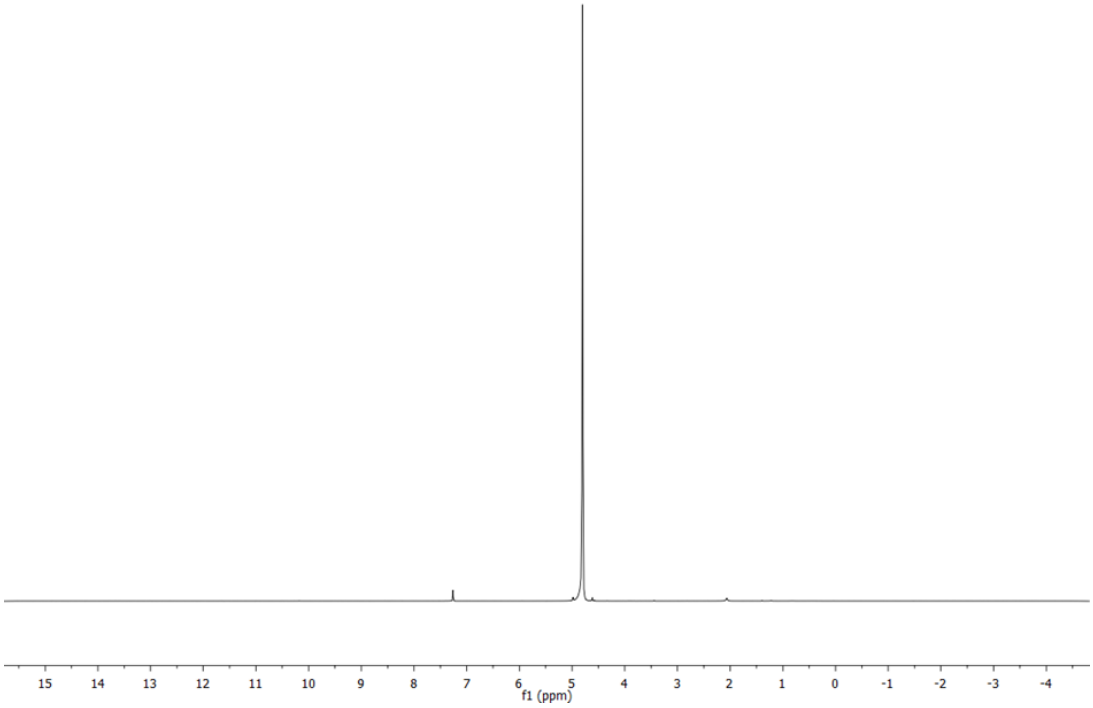

Figure S1. ^{1}H-NMR of 2,5-bis(azidomethyl)-1,3,4-thiadiazole (**2**).

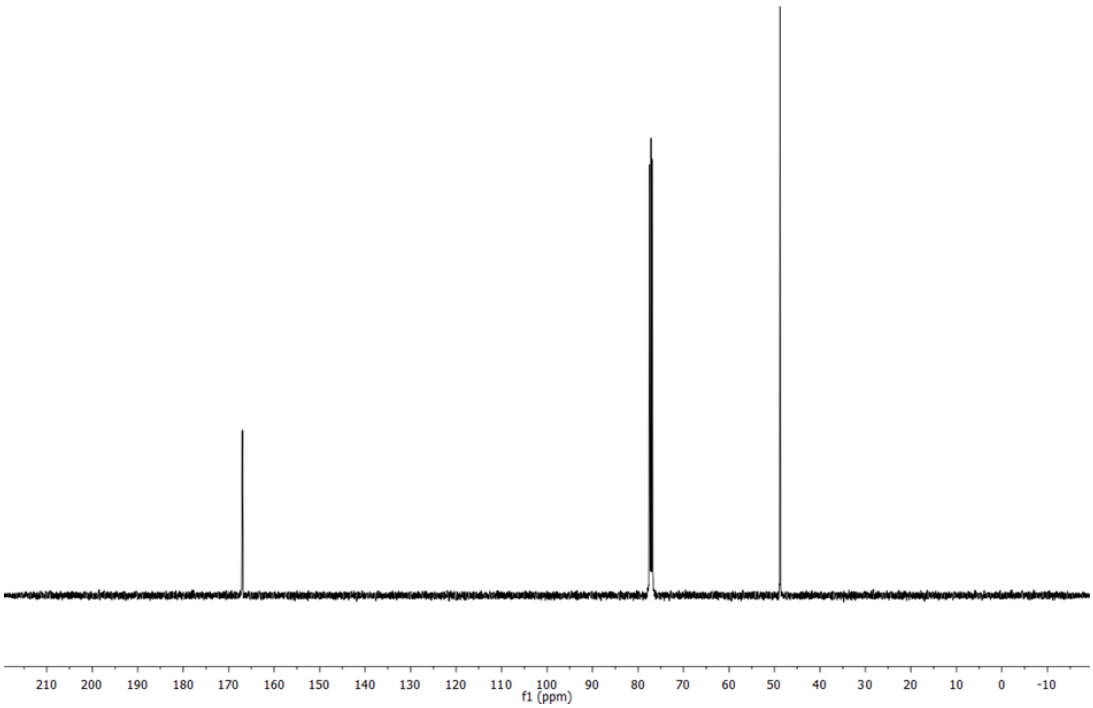

Figure S2. ^{13}C-NMR 2,5-bis(azidomethyl)-1,3,4-thiadiazole (**2**).

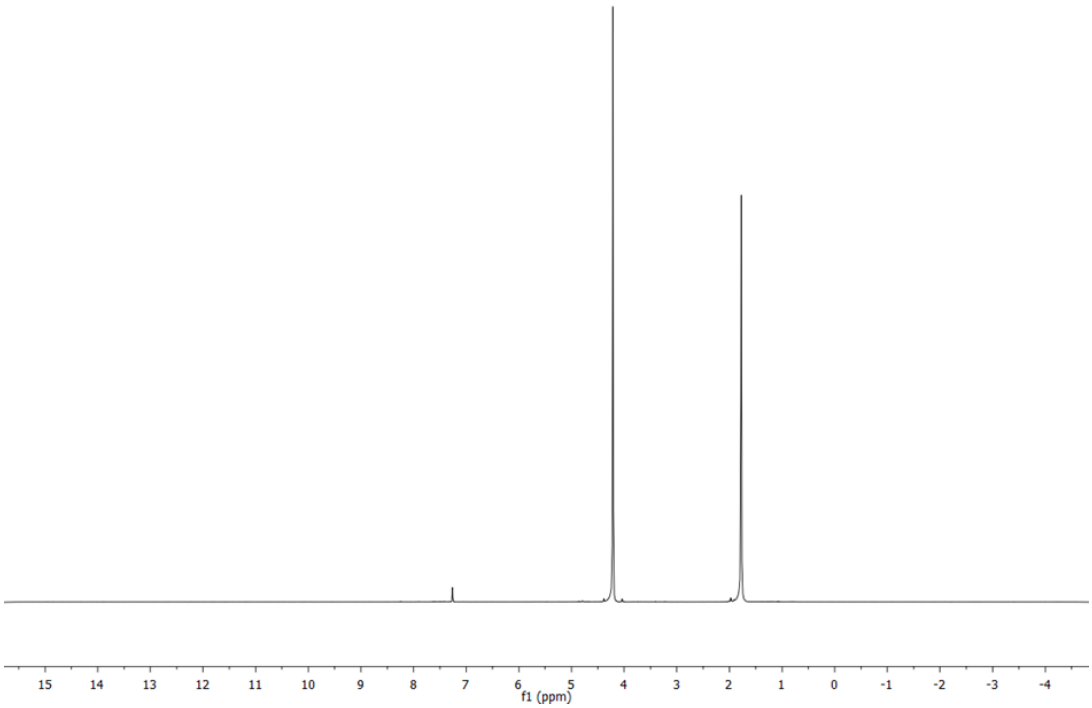

Figure S3. ^{1}H-NMR of 2,5-bis(aminomethyl)-1,3,4-thiadiazole (**3**).

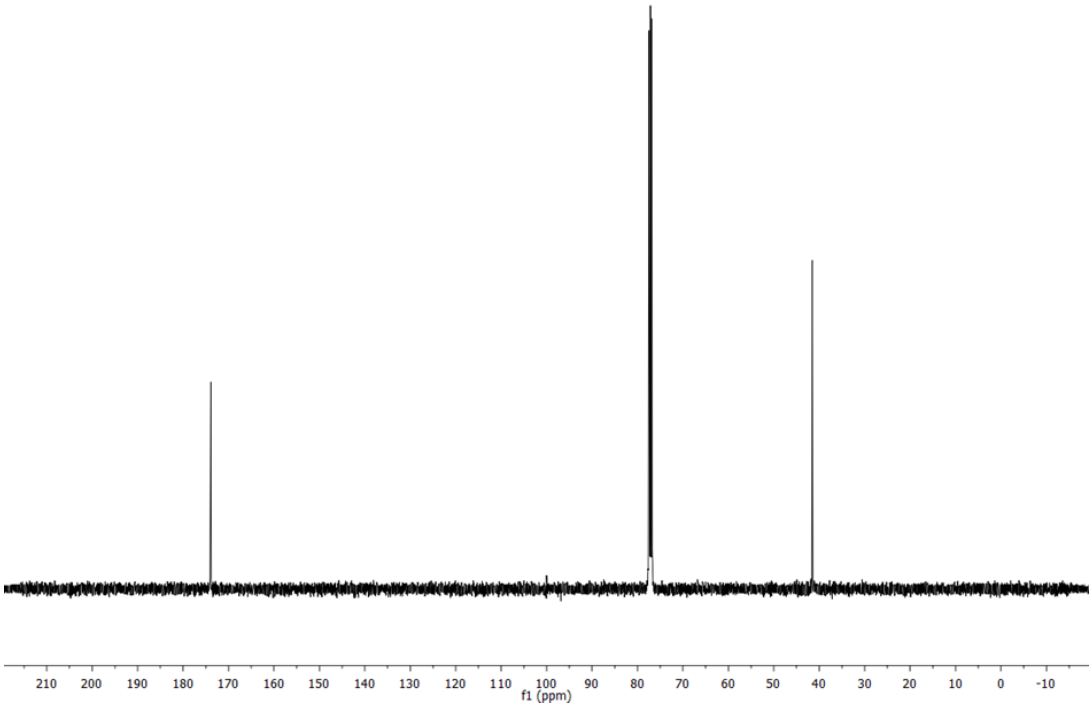

Figure S4. ^{13}C-NMR of 2,5-bis(aminomethyl)-1,3,4-thiadiazole (**3**).

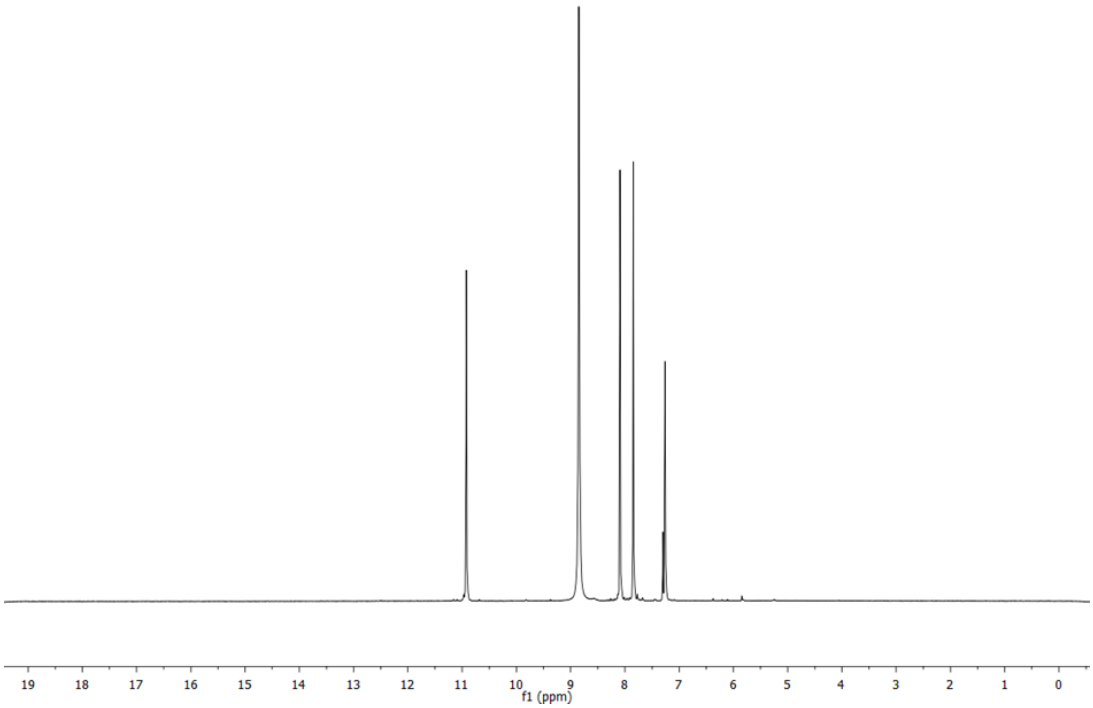

Figure S5. ^{1}H-NMR of 2,5-bis{[(1*H*-imidazol-2-ylmethyl)-amino]-methyl}-1,3,4-thiadiazole (**L^{1}**).

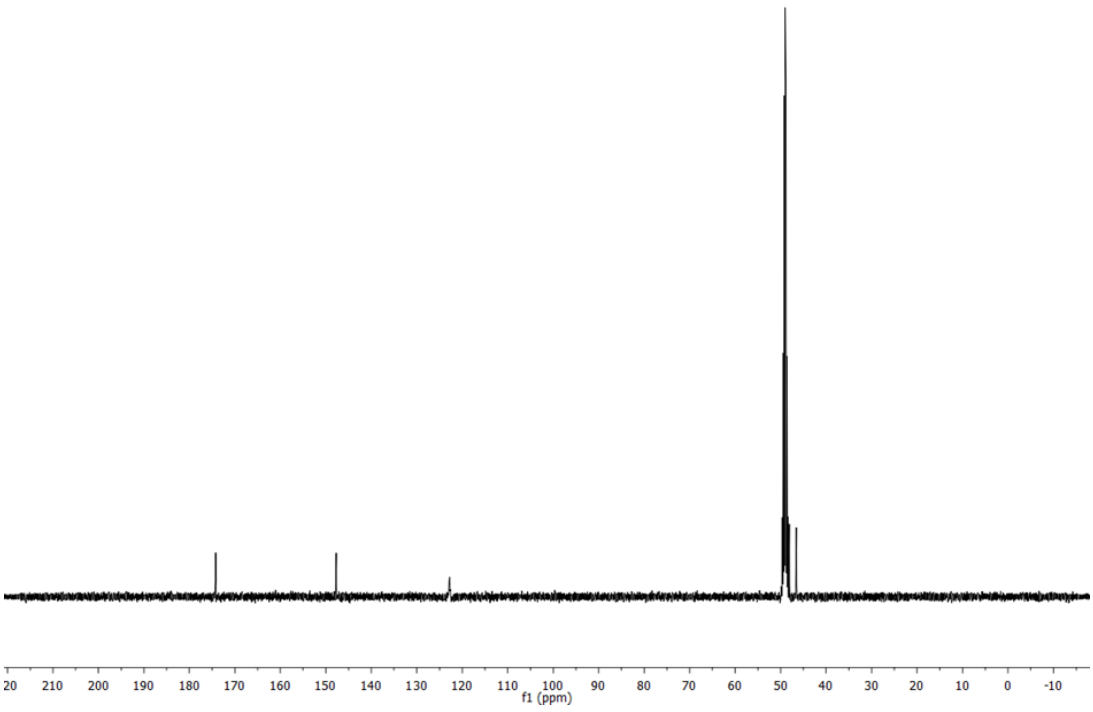

Figure S6. ^{13}C-NMR of 2,5-bis{[(1*H*-imidazol-2-ylmethyl)-amino]-methyl}-1,3,4-thiadiazole (**L^{1}**).

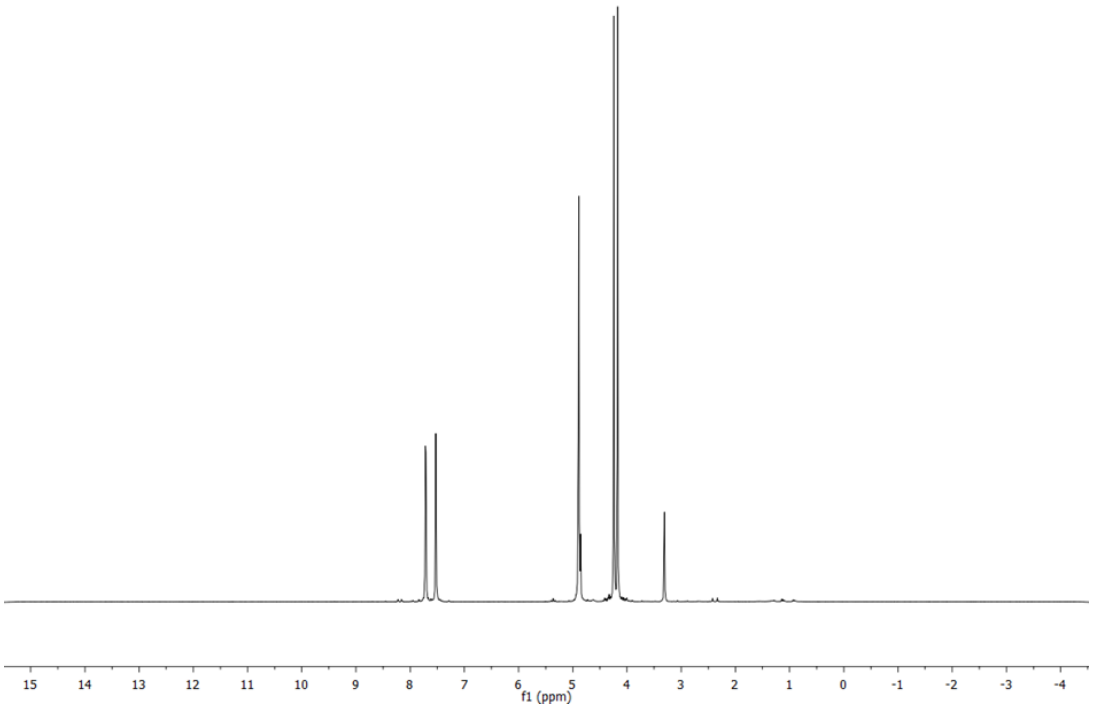

Figure S7. ^{1}H-NMR of 2,5-bis{[(thiazol-2-ylmethyl)-amino]-methyl}-1,3,4-thiadiazole (**L^{2}**).

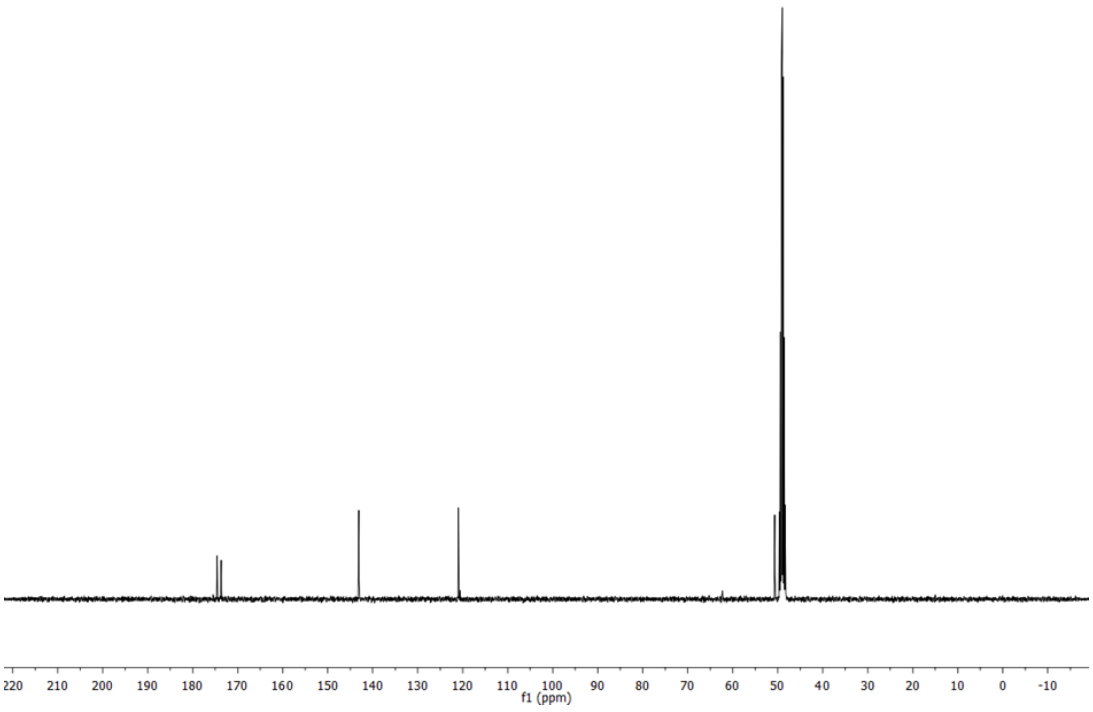

Figure S8. ^{13}C-NMR of 2,5-bis{[(thiazol-2-ylmethyl)-amino]-methyl}-1,3,4-thiadiazole (**L^{2}**).

2.11.2 IR Spectroscopy

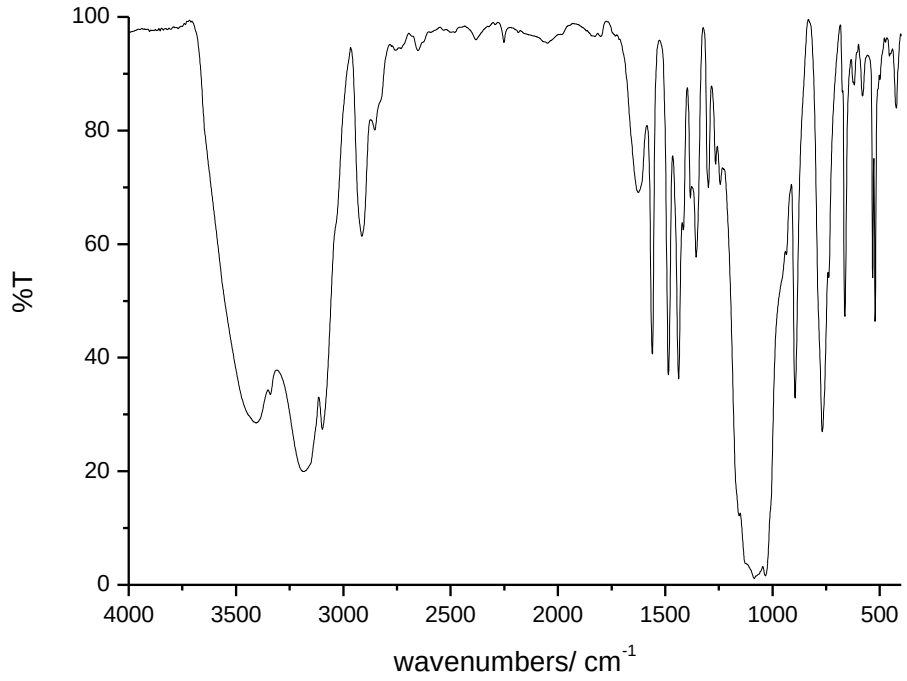

Figure S9. IR spectrum of dried $[Fe^{II}_2(\mu_2\text{-}\mathbf{L^1})_2](BF_4)_4$ (**C1**).

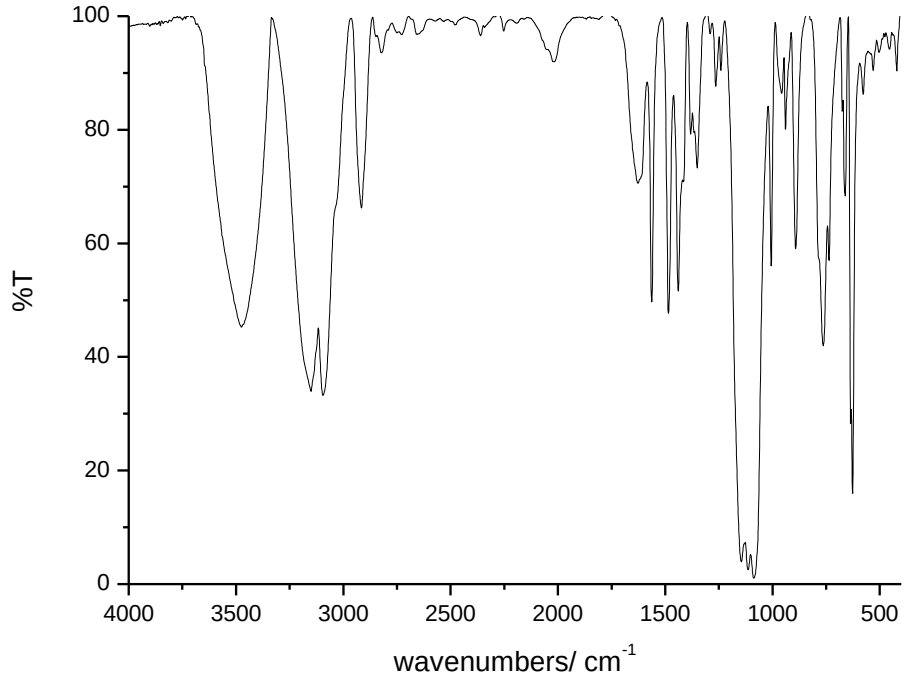

Figure S10. IR spectrum of dried $[Fe^{II}_2(\mu_2\text{-}\mathbf{L^1})_2](ClO_4)_4$ (**C2**).

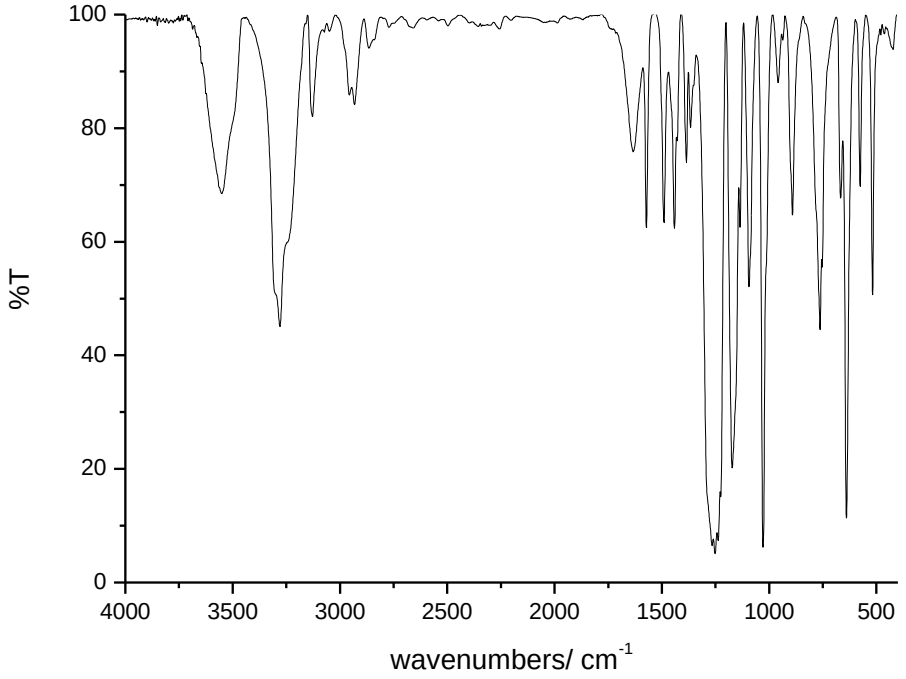

Figure S11. IR spectrum of dried $[Fe^{II}_2(\mu_2\text{-}\mathbf{L^1})_2](F_3CSO_3)_4$ (**C3**).

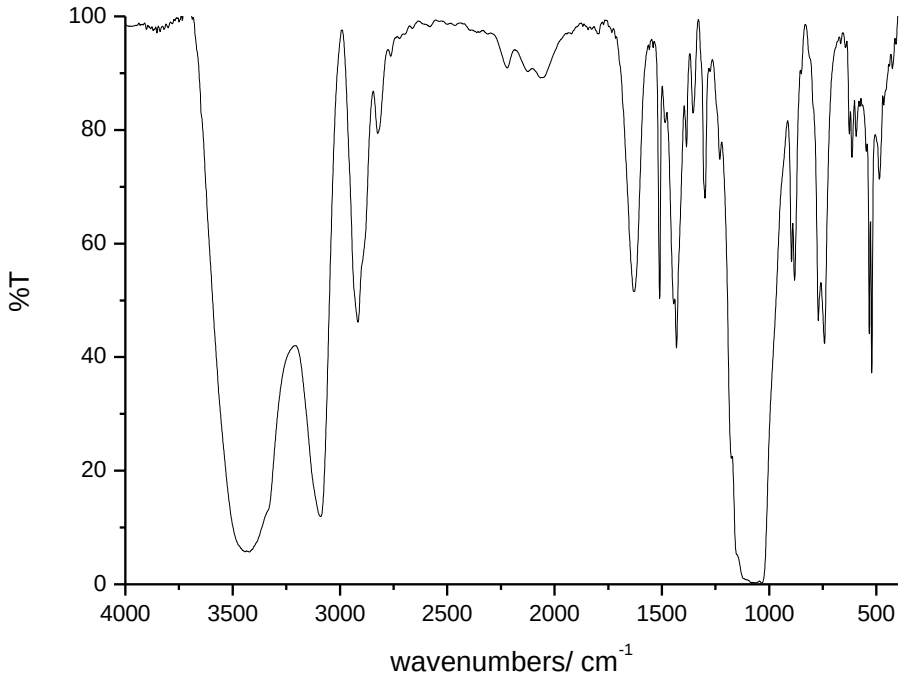

Figure S12. IR spectrum of dried $[Fe^{II}_2(\mu_2\text{-}\mathbf{L^2})_2](BF_4)_4$ (**C4**).

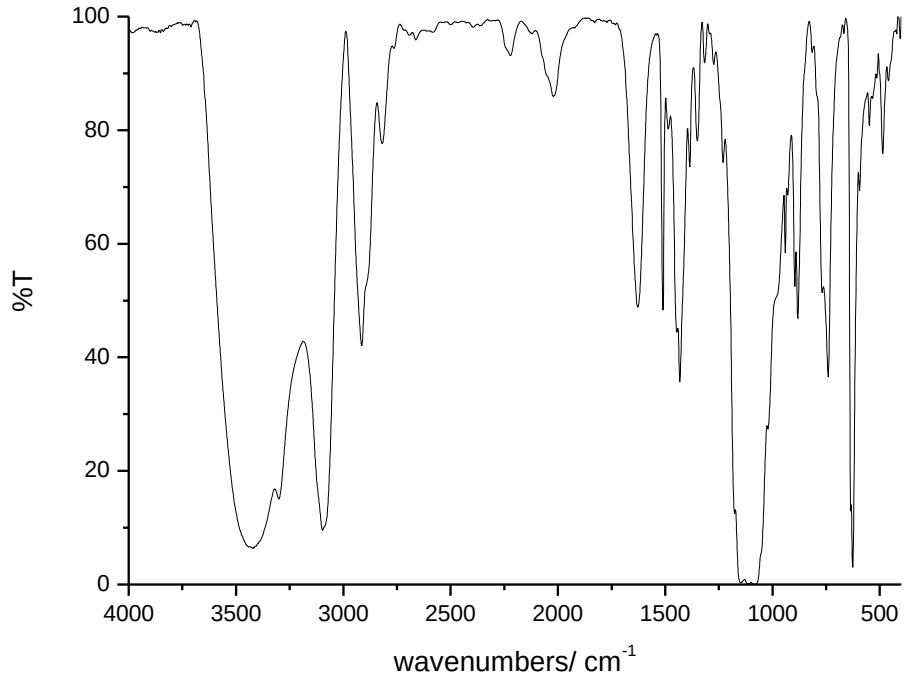

Figure S13. IR spectrum of dried $[Fe^{II}_2(\mu_2\text{-}\mathbf{L^2})_2](ClO_4)_4$ (**C5**).

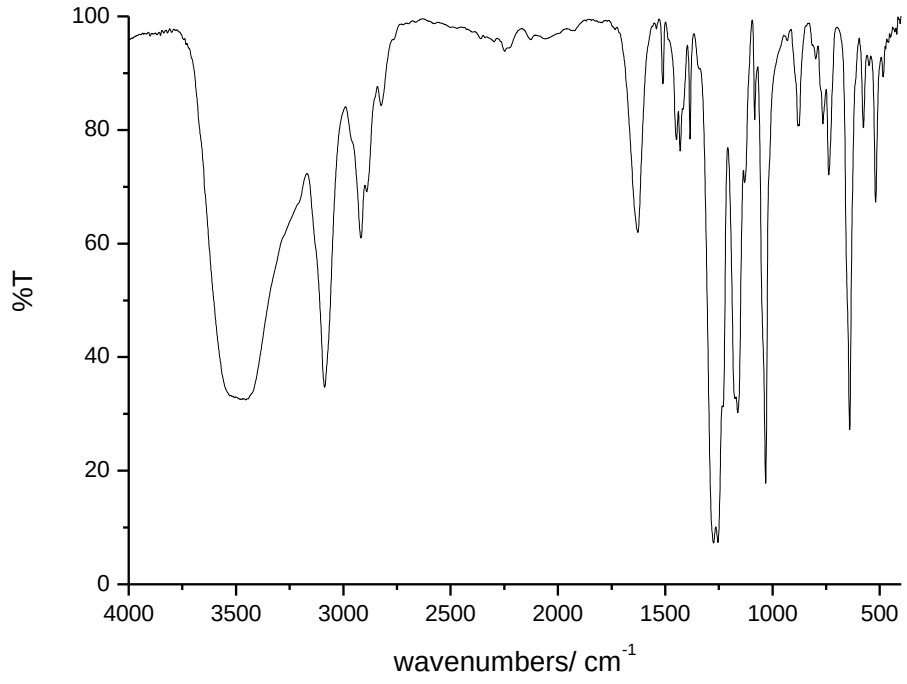

Figure S14. IR spectrum of dried $[Fe^{II}_2(\mu_2\text{-}\mathbf{L^2})_2](F_3CSO_3)_4$ (**C6**).

2.11.3 X-ray Diffraction Measurements

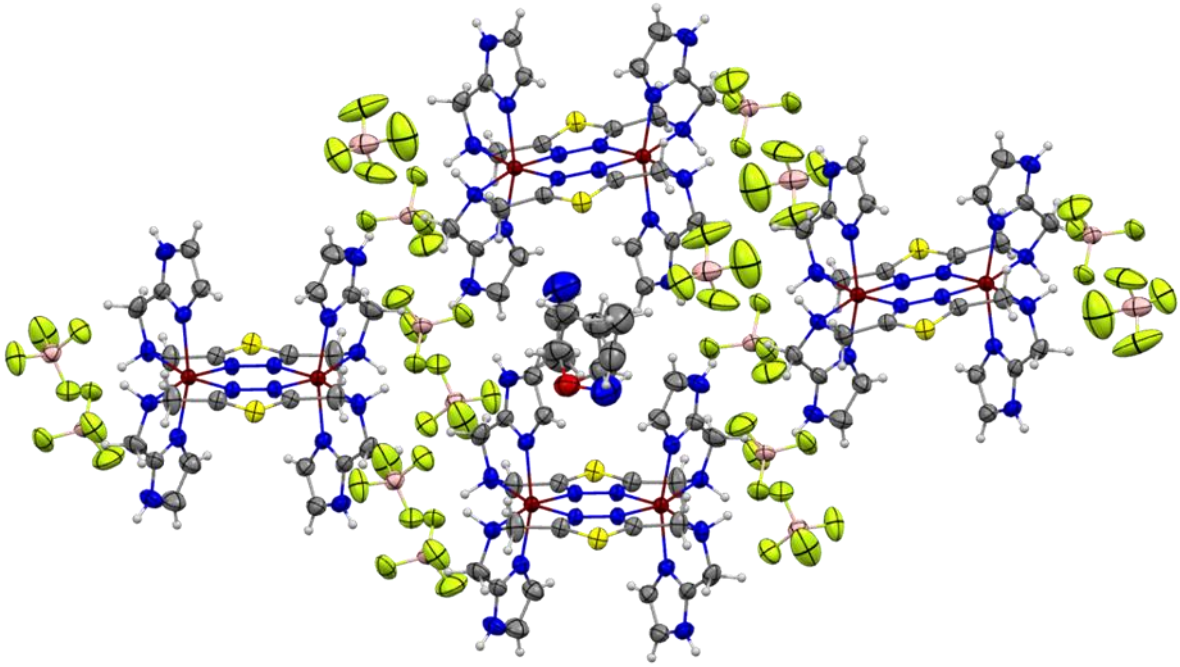

Figure S15. Packing of the molecules in complex $[Fe^{II}_2(\mu_2\text{-}\mathbf{L^1})_2](BF_4)_4 \cdot 2/3THF \cdot 1/3(2MeCN)$ (**C1**) with thermal ellipsoids. Color code: Fe dark red, N blue, S yellow, C grey, H white, O red, B pink and F light green.

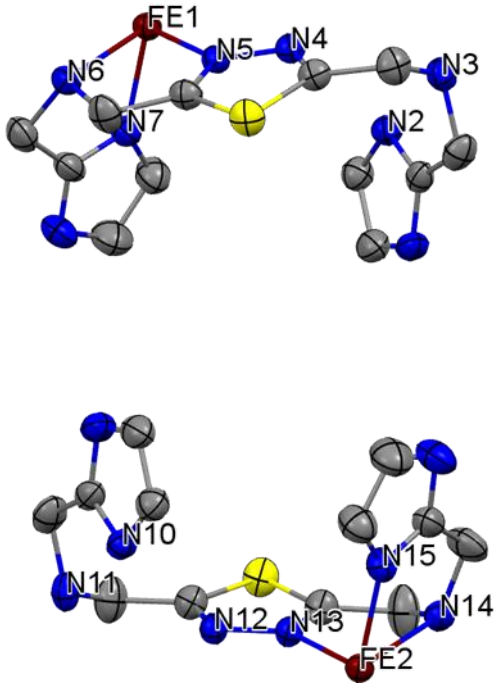

Figure S16. Asymmetric unit of $[Fe^{II}_2(\mu_2\text{-}\mathbf{L^1})_2](BF_4)_4 \cdot 2/3THF \cdot 1/3(2MeCN)$ (**C1**) without hydrogens, solvent molecules and counter ions. Color code: Fe dark red, N blue, S yellow and C grey.

Table S1. Selected bond lengths [Å], N-Fe-N bond angles [°] and the octahedral distortion parameter Σ[°] for the compound **C1** at 193 K.

	C1 (@ 193 K)
Fe-N_{TDA}[a]	2.150(3), 2.185(3)/ 2.169(3), 2.172(3)
Fe-$N_{Imz/Ta}$[a]	2.096(4), 2.111(4)/ 2.084(4), 2.090(4)
Fe-N_{NH}[a]	2.313(3), 2.342(3)/ 2.321(3), 2.343(4)
ave Fe-N	2.200/2.196
ave *cis* N-Fe-N[a]	90.3/90.4
ave *trans* N-Fe-N[a]	167.1/167.0
Σ[a][b]	115.26/115.30

[a] Fe1/Fe2. [b] Octahedral distortion parameter Σ (sum of the deviation from 90° of the 12 cis-N-Fe-N angles in the FeN6 coordination sphere)

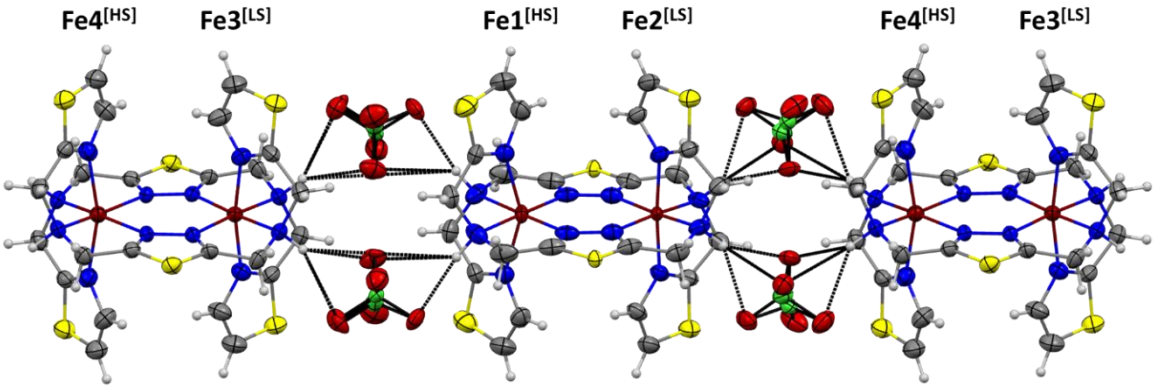

Figure S17. Representation of the 1D chain for **C5** (@160 K, slow cooling). The dimers along the chain are ordered in the same way ([HS-LS]•[HS-LS]•[HS-LS]). This figure is representative for all formed 1D chains with the different counter ions (**C4** – **C6**) although the intermolecular distances differ. Solvent molecules and non-bridging counter ions have been omitted for clarity. Hydrogen bonds are shown as black dashed lines. Color code: Fe dark red, N blue, S yellow, C grey, H white, O red and Cl green.

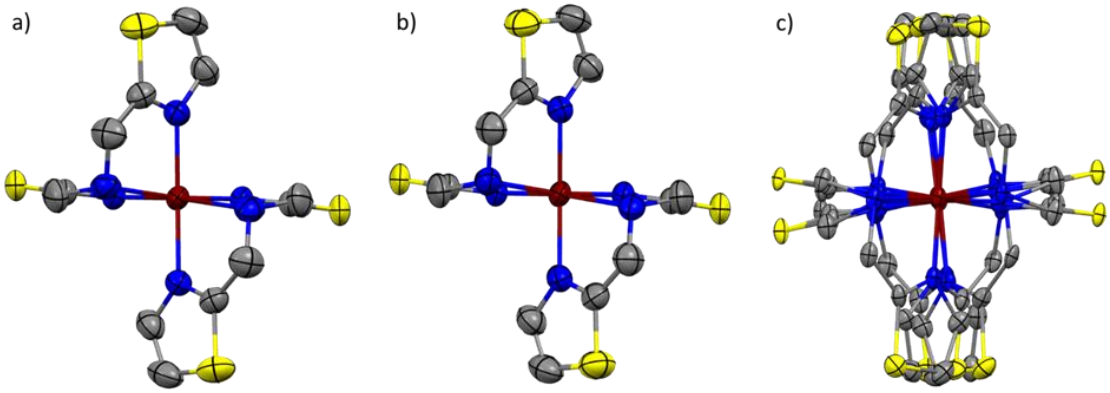

Figure S18. Different orientation of the complex cations of **a)** $[Fe^{II}_2(\mu_2\text{-}\mathbf{L^2})_2](BF_4)_4\cdot 3MeCN$ (**C4**), **b)** $[Fe^{II}_2(\mu_2\text{-}\mathbf{L^2})_2](ClO_4)_4\cdot 3MeCN$ (**C5**) and **c)** $[Fe^{II}_2(\mu_2\text{-}\mathbf{L^2})_2](F_3CSO_3)_4\cdot 2MeCN$ (**C6**) along the 1D chain. Hydrogens, solvent molecules and counter ions have been omitted for clarity. Color code: Fe dark red, N blue, S yellow and C grey.

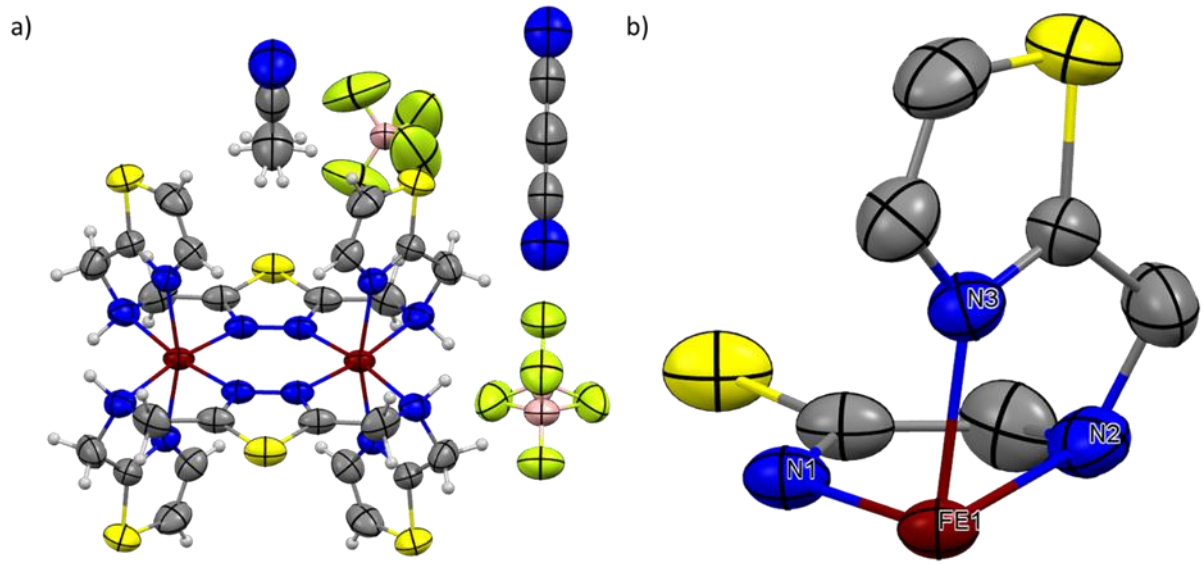

Figure S19. a) Molecular structure of $[Fe^{II}_2(\mu_2\text{-}\mathbf{L}^2)_2](BF_4)_4\cdot 3MeCN$ (**C4**) with thermal ellipsoids at 240 K. **b)** Asymmetric unit without hydrogens, solvent molecules and counter ions. Color code: Fe is dark red, N blue, S yellow, C grey, H white, B pink and F light green.

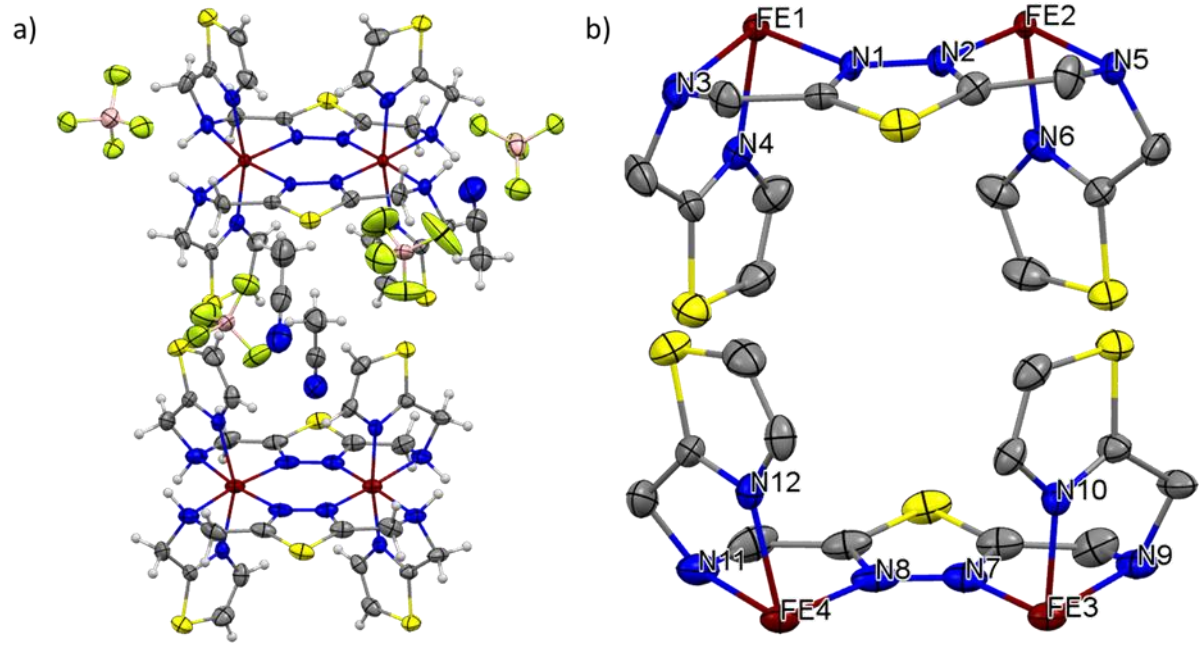

Figure S20. a) Molecular structure of $[Fe^{II}_2(\mu_2\text{-}\mathbf{L}^2)_2](BF_4)_4\cdot 3MeCN$ (**C4**) with thermal ellipsoids at 120 K. **b)** Asymmetric unit without hydrogens, solvent molecules and counter ions. Color code: Fe dark red, N blue, S yellow, C grey, H white, B pink and F light green.

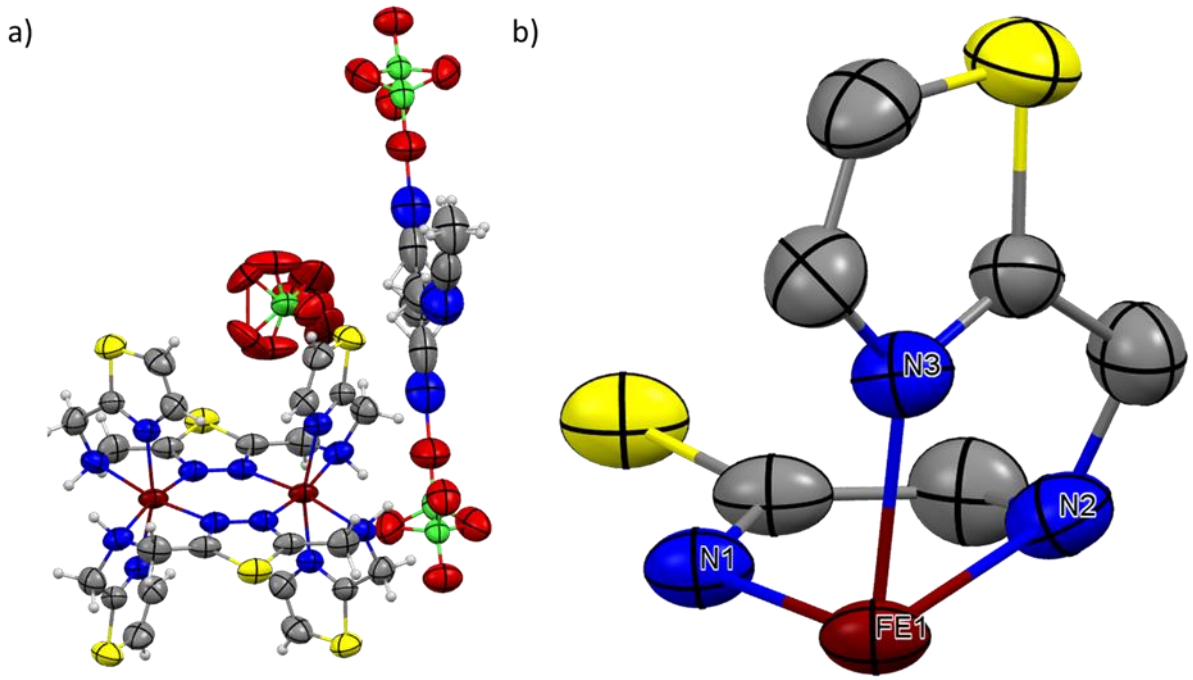

Figure S21. a) Molecular structure of $[Fe^{II}_2(\mu_2\text{-}\mathbf{L}^2)_2](ClO_4)_4 \cdot 3MeCN$ (**C5**) with thermal ellipsoids at 250 K. **b)** Asymmetric unit without hydrogens, solvent molecules and counter ions. Color code: Fe dark red, N blue, S yellow, C grey, H white, O red and Cl green.

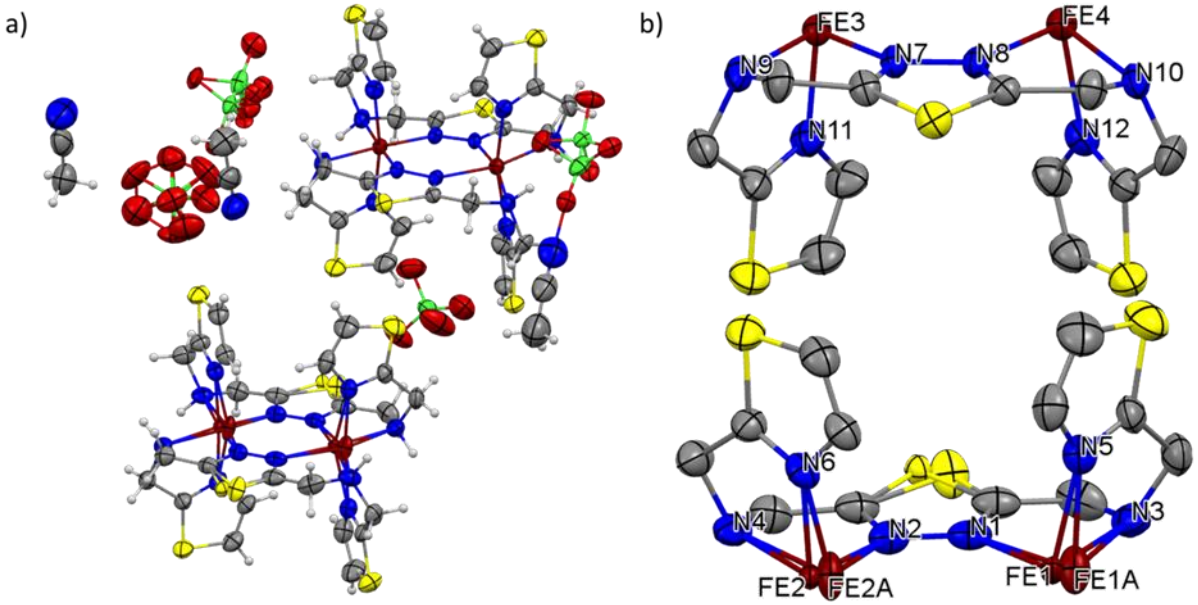

Figure S22. a) Molecular structure of $[Fe^{II}_2(\mu_2\text{-}\mathbf{L}^2)_2](ClO_4)_4 \cdot 3MeCN$ (**C5**) with thermal ellipsoids at 160 K after slow cooling. **b)** Asymmetric unit without hydrogens, solvent molecules and counter ions. Color code: Fe dark red, N blue, S yellow, C grey, H white, O red and Cl green.

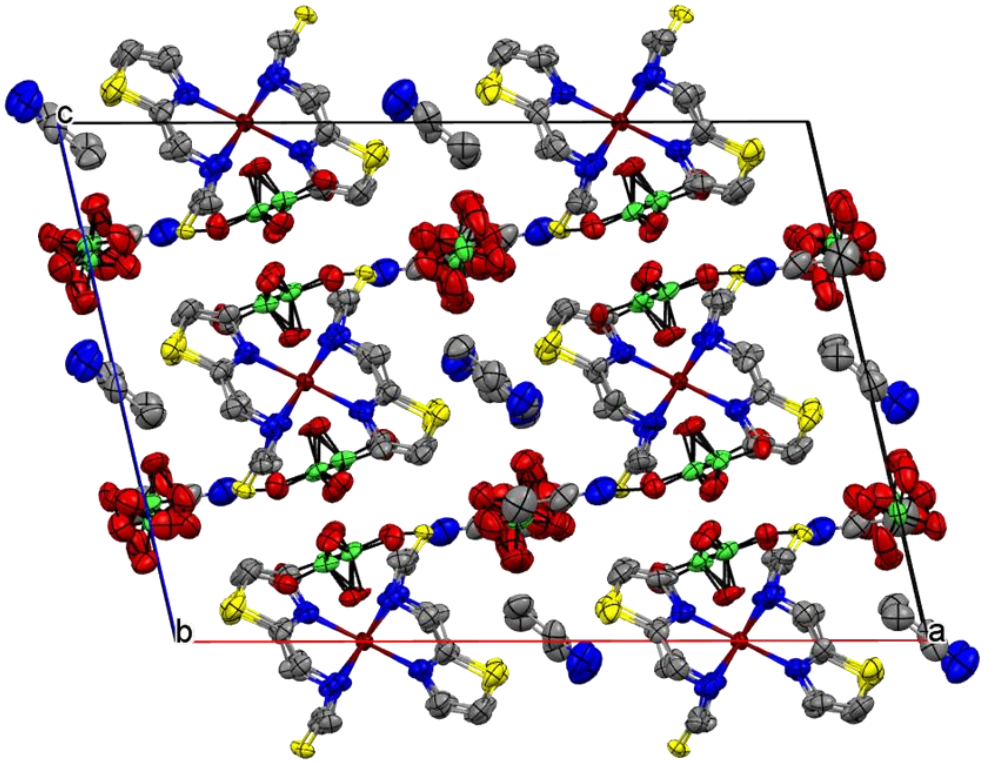

Figure S23. Packing of $[Fe^{II}_2(\mu_2\text{-}\mathbf{L^2})_2](ClO_4)_4 \cdot 3MeCN$ (**C5**) along b-axis with thermal ellipsoids at 160 K after slow cooling. Hydrogens have been omitted for clarity. Color code: Fe dark red, N blue, S yellow, C grey, O red and Cl green.

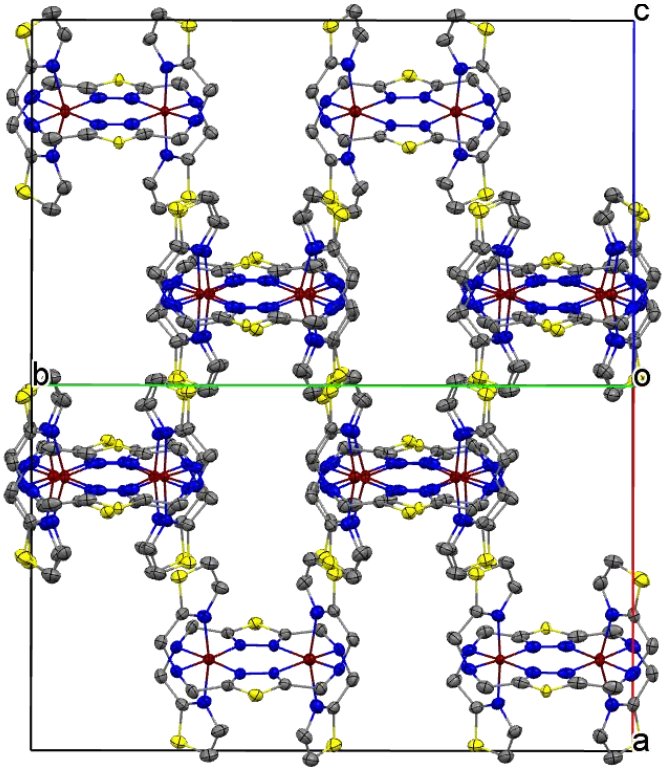

Figure S24. Packing of $[Fe^{II}_2(\mu_2\text{-}\mathbf{L^2})_2](ClO_4)_4 \cdot 3MeCN$ (**C5**) along the bisecting between a and c with thermal ellipsoids at 160 K after slow cooling. Hydrogens, solvent molecules and counter ions have been omitted for clarity. Color code: Fe dark red, N blue, S yellow, C grey.

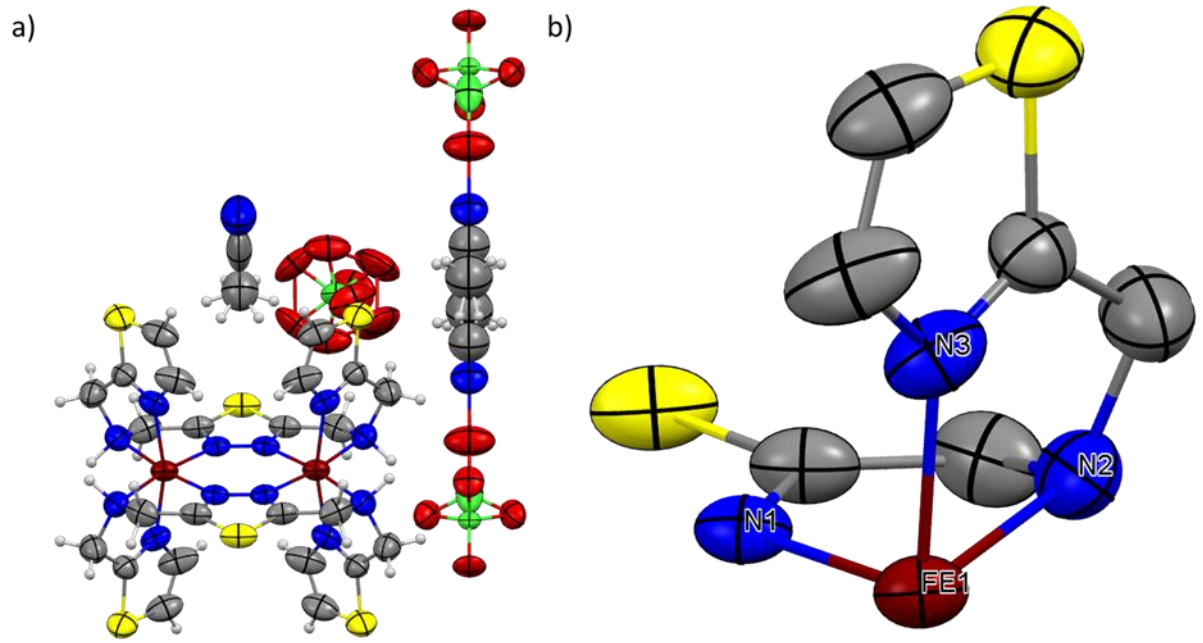

Figure S25. a) Molecular structure of $[Fe^{II}_2(\mu_2\text{-}\mathbf{L}^2)_2](ClO_4)_4\cdot 3MeCN$ (**C5**) with thermal ellipsoids at 160 K after quenching. **b)** Asymmetric unit without hydrogens, solvent molecules and counter ions. Color code: Fe dark red, N blue, S yellow, C grey, H white, O red and Cl green.

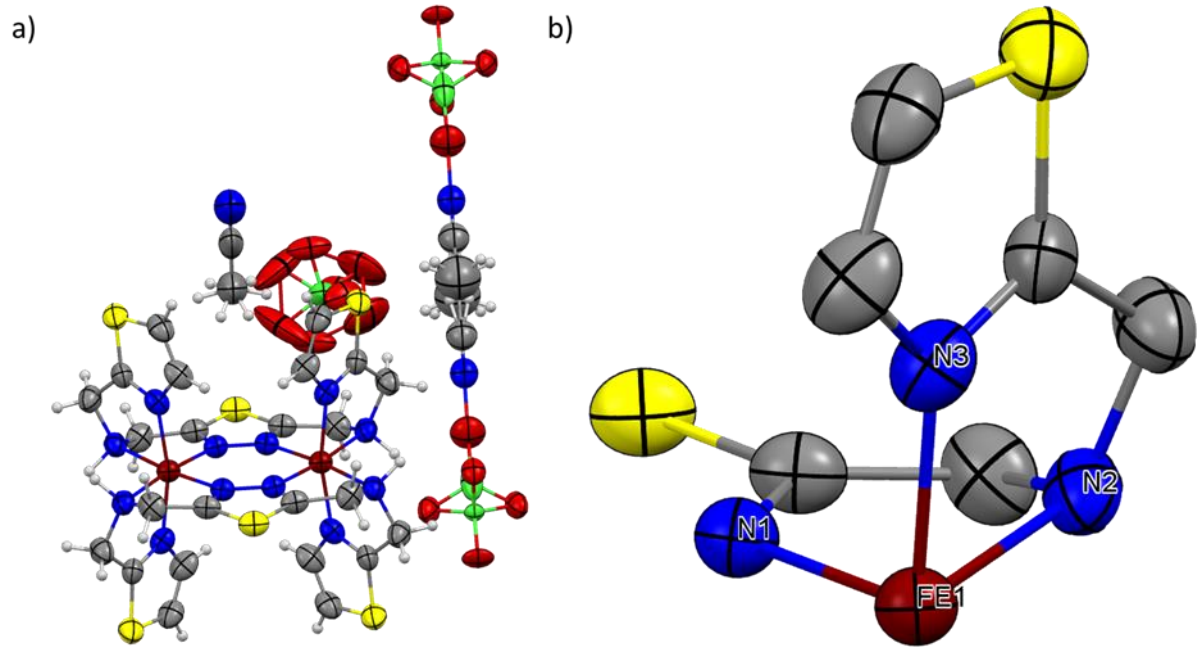

Figure S26. a) Molecular structure of $[Fe^{II}_2(\mu_2\text{-}\mathbf{L}^2)_2](ClO_4)_4\cdot 3MeCN$ (**C5**) with thermal ellipsoids at 100 K. **b)** Asymmetric unit without hydrogens, solvent molecules and counter ions. Color code: Fe dark red, N blue, S yellow, C grey, H white, O red and Cl green.

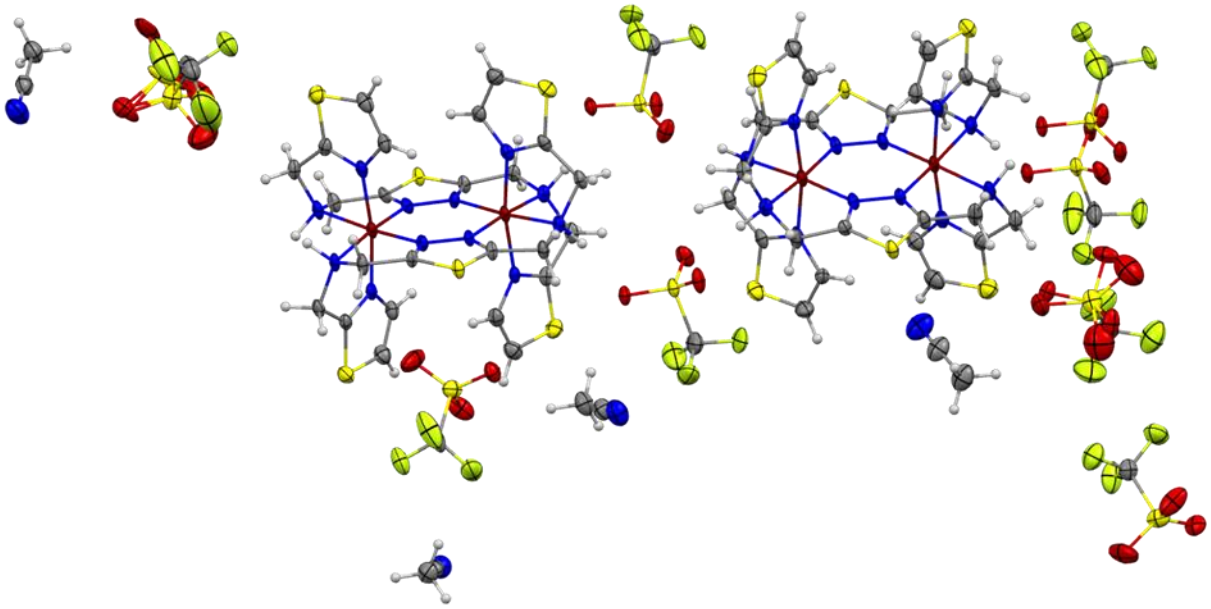

Figure S27. Molecular structure of $[Fe^{II}_2(\mu_2\text{-}\mathbf{L}^2)_2](F_3CSO_3)_4\cdot 2MeCN$ (**C6**) with thermal ellipsoids at 100 K. Color code: Fe dark red, N blue, S yellow, C grey, H white, O red and F light green.

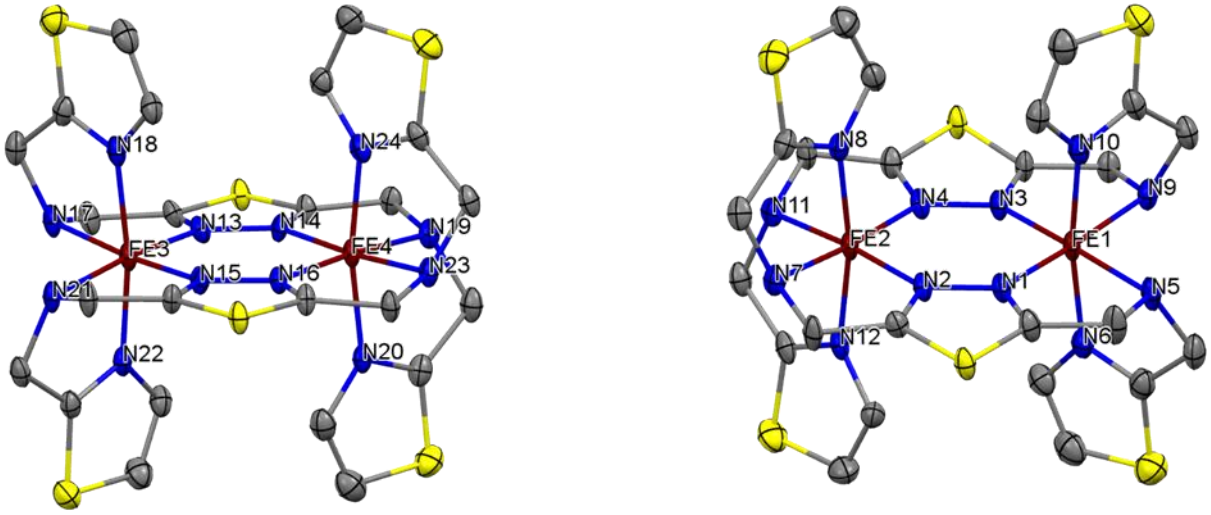

Figure S28. Asymmetric unit of $[Fe^{II}_2(\mu_2\text{-}\mathbf{L}^2)_2](F_3CSO_3)_4\cdot 2MeCN$ (**C6**) without Hydrogens, solvent molecules and counter ions. Color code: Fe dark red, N blue, S yellow and C grey.

Table S2. Crystallographic parameters for all discussed crystal structures of **C1** – **C6**

	C1	**C4** (@120 K)	**C4** (@240 K)	**C5** (@100 K)	**C5** (@160 K)–1	**C5** (@160 K)–1'	**C5** (@160 K)–2	**C5** (@250 K)	**C6** (@100 K)
formula	C28 H39.34 B4 F16 Fe2 N16.65 O0.67 S2	C60 H74 B8 F32 Fe4 N30 S12	C30 H37 B4 F16 Fe3 N15 S6	C30 H37 Cl4 Fe2 N15 O16 S6	C60 H74 Cl8 Fe4 N30 O32 S12	C60 H74 Cl8 Fe4 N30 O32 S12	C30 H37 Cl4 Fe2 N15 O16 S6	C30 H37 Cl4 Fe2 N15 O16 S6	C64 H68 F24 Fe4 N28 O24 S20
molar weight [g/mol]	1143.13	2518.09	1259.04	1309.6	2619.21	2619.21	1309.6	1309.6	2934.06
crystal system	triclinic	monoclinic	monoclinic	monoclinic	monoclinic	monoclinic	monoclinic	monoclinic	triclinic
space group	*P*-1	*I*2/*a*	*I*2/*m*	*C*2/*m*	*I*2/*a*	*C*2/*c*	*C*2/*m*	*C*2/*m*	*P*-1
a/Å	12.0375(7)	16.7167(7)	13.004(3)	17.0993(10)	23.9111(8)	26.0447(9)	17.006(2)	16.9633(18)	14.1442(16)
b/Å	13.0822(7)	24.8024(13)	12.609(3)	12.3564(9)	24.9799(10)	24.9799(10)	12.4677(17)	12.6415(17)	27.6210(19)
c/Å	14.6807(8)	23.5826(11)	16.117(3)	12.8089(8)	16.9439(6)	16.9439(6)	12.898(2)	13.2025(14)	23.975(3)
α /°	91.122(4)	90	90	90	90	90	90	90	96.402(9)
β /°	103.133(4)	103.305(4)	110.83(3)	116.817(4)	102.872(3)	116.490(3)	116.051(10)	115.795(7)	101.108(8)
γ /°	98.453(3)	90	90	90	90	90	90	90	110.374(10)
V/Å^3	2222.6(2)	9515.2(8)	2469.8(10)	2415.3(3)	9866.2(6)	9866.3(7)	2456.9	2549.1(5)	5392.1(11)
Z	2	4	2	2	4	4	2	2	4
T/K	193(2)	120(2)	240(2)	100(2)	160(2)	160(2)	160(2)	250(2)	100(2)
$\rho_{calcd.}$ [g/cm^3]	1.707	1.758	1.693	1.801	1.763	1.763	1.770	1.706	1.807
μ [mm^{-1}]	0.863	0.982	0.946	1.165	1.141	1.141	1.145	1.104	1.036
R(int)	0.0324	0.0250	0.0184	0.0265	0.0361	0.0361	0.0394	0.0173	0.0543
S	1.027	1.070	1.046	1.123	1.050	1.040	1.141	1.090	1.030
R1 (l > 2σ (l))	0.6120	0.1067	0.0616	0.0740	0.0921	0.0922	0.0978	0.0525	0.0626
wR2 (all data)	0.1843	0.3077	0.1794	0.1859	0.2777	0.2817	0.2471	0.1586	0.1714

2.11.4 Magnetic Data

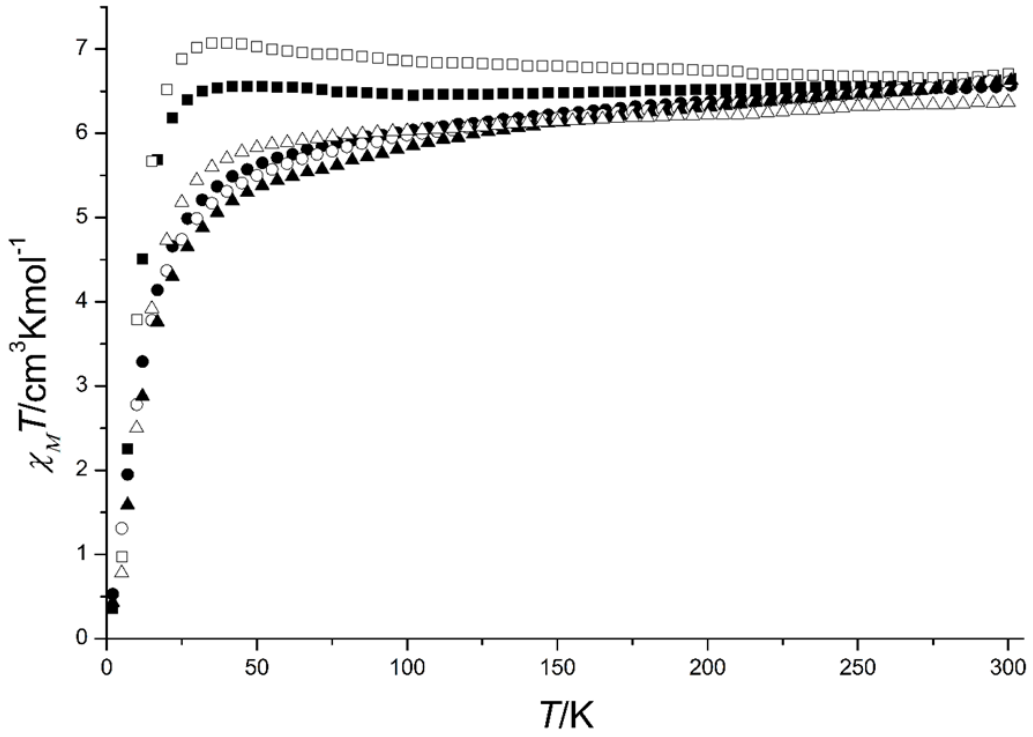

Figure S29. $\chi_M T$ vs T data for the compound **C1** (freshly prepared: filled squares; dried: open squares), **C2** (freshly prepared: filled triangles; dried: open triangles) and **C3** (freshly prepared: filled dots; dried: open dots). The Data is given per dinuclear iron(II) molecule.

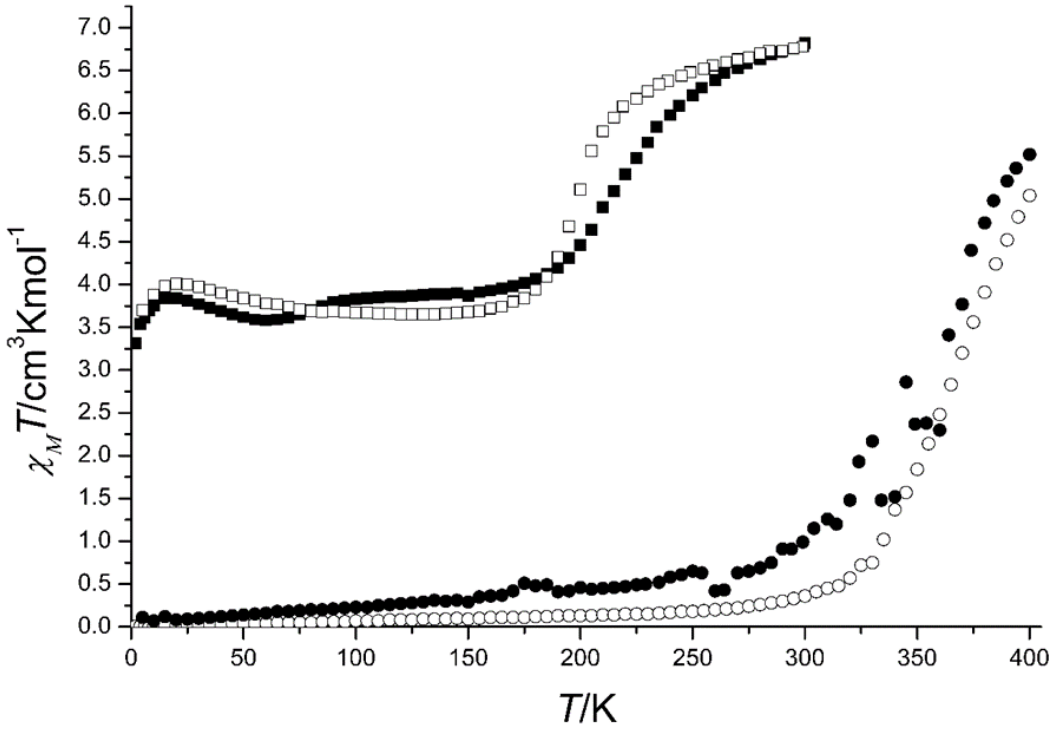

Figure S30. $\chi_M T$ vs T data for the compound **C4** (freshly prepared: filled squares; dried: open squares), and **C6** (freshly prepared: filled dots; dried: open dots). The Data is given per dinuclear iron(II) molecule.

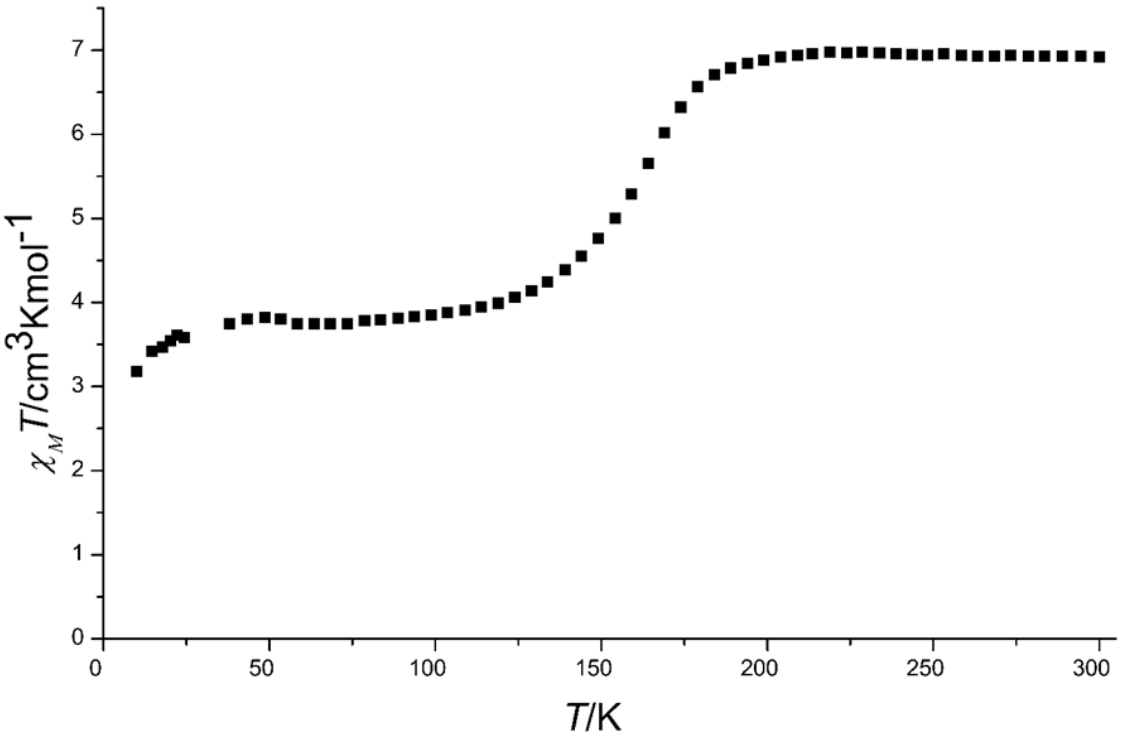

Figure S31. $\chi_M T$ vs T data for **C5** in sweeping mode with a cooling rate of 10 K/ min. The Data is given per dinuclear iron(II) molecule.

2.12 Additional Results

This chapter covers the crystal structures of **C2** and **C3**, which unfortunately could only be obtained after the acceptance of the publication. $[Fe^{II}_2(\mu_2\text{-}\mathbf{L^1})_2](ClO_4)_4{\cdot}2Et_2O$ **C2** crystalizes in the space group $P\bar{1}$ at 120 K and $[Fe^{II}_2(\mu_2\text{-}\mathbf{L^1})_2](F_3CSO_3)_4{\cdot}2/3(2MeCN){\cdot}1/3(Et_2O)$ **C3** in $P2_1/n$ at 173 K. The two iron(II) ions in both complex cations are coordinated by two ligand molecules in the *cis*-axial manner, similar to **C1** (Figure AR1 and Figure AR2). For both crystal structures, the asymmetric unit contains one-half of the complex cation. The average Fe-N bond lengths of 2.179 Å (**C2**) and 2.186 Å (**C3**) as well as the octahedral distortion parameters of 103.57° (**C2**) and 108.42° (**C3**) account for an iron(II) ion in the HS state. Thus, the dimeric complex cations are in the [HS-HS] at the measured temperatures. The crystal structures further compromise four non-coordinating anions per complex cation (ClO_4^- or $F_3CSO_3^-$) and solvent molecules. Detailed information about bond lengths and the crystal parameters of **C2** and **C3** are given in Table AR1 and Table AR2.

Table AR1. Selected bond lengths [Å] and bond angles [°] and the octahedral distortion parameter Σ [°] for **C2** and **C3**.

Selected Parameters[a]	**C2** (@120 K)	**C3** (@173 K)
Fe-N_{TDA}	2.131(3), 2.149(3)	2.145(2), 2.159(2)
Fe-N_{Imz}	2.101(3), 2.105(3)	2.098(2), 2.107(2)
Fe-N_{NH}	2.290(3), 2.300(3)	2.299(2), 2.306(2)
ave Fe-N	2.179	2.186
ave *cis* N-Fe-N	90.2	90.2
ave *trans* N-Fe-N	168.6	168.3
Σ	103.57	108.42

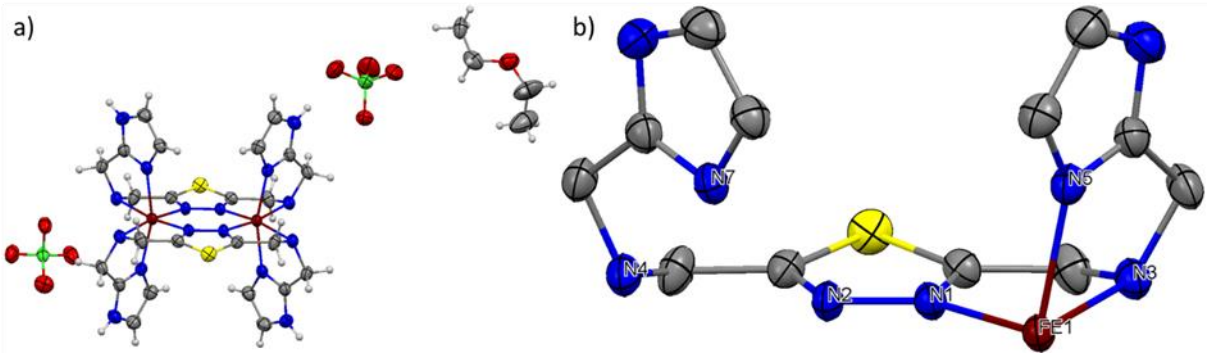

Figure AR1. a) Molecular structure of $[Fe^{II}_2(\mu_2\text{-}\mathbf{L^1})_2](ClO_4)_4{\cdot}2Et_2O$ (**C2**) with thermal ellipsoids at 120 K. **b)** Asymmetric unit without hydrogens, solvent molecules and counter ions. Color code: Fe dark red, N blue, S yellow, C grey, H white, O red and Cl green.

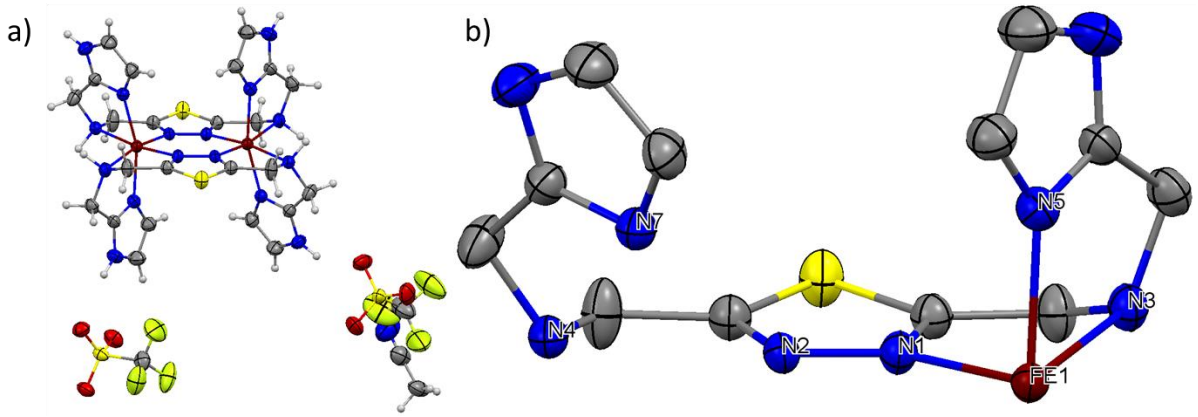

Figure AR2. a) Molecular structure of $[Fe^{II}_2(\mu_2\text{-}\mathbf{L^1})_2](F_3CSO_3)_4 \cdot 2/3(2MeCN) \cdot 1/3(Et_2O)$ (**C3**) with thermal ellipsoids at 173 K. **b)** Asymmetric unit without hydrogens, solvent molecules and counter ions. Color code: Fe dark red, N blue, S yellow, C grey, H white, O red and F light green.

Table AR2. Crystallographic parameters for **C2** and **C3**.

	C2 (@120 K)	**C3** (@173 K)
formula	C32 H48 Cl4 Fe2 N16 O18 S2	C32 H39.33 F12 Fe2 N17.33 O12.33 S6
molar weigth [g/mol]	1262.48	1396.14
crystal system	Triclinic	monoclinic
space group	*P*-1	$P2_1/n$
a/Å	10.6283(6)	10.6125(3)
b/Å	10.5458(5)	12.5033(4)
c/Å	12.5477(7)	20.2563(5)
α/°	93.794(4)	90
β/°	106.320(4)	90.944(2)
γ/°	108.281(4)	90
V/Å^3	1263.10(12)	2687.47(13)
Z	1	2
T/K	120(2)	137(2)
$\rho_{calcd.}$ [g/cm^3]	1.66	1.695
μ [mm^{-1}]	0.954	0.885
R(int)	0.0256	0.0425
S	1.040	1.025
R1 (l > 2σ (l))	0.0677	0.0517
wR2 (all data)	0.2070	0.1496

3. 2D Layer Arrangement of Solely [HS-HS] or [LS-LS] Molecules in the [HS-LS] State of a Dinuclear Fe(II) Spin Crossover Complex

In this chapter the synthesis and characterization of the novel bridging ligand **I^{4}MTD** (2,5-bis[(1*H*-imidazol-4-ylmethyl)amino]methyl-1,3,4-thiadiazole), which was used to generate a series of three new bimetallic iron(II) complexes [Fe^{II}_2(**I^{4}MTD**)$_2$](X)$_4$·solvents with the respective counter ions ($F_3CSO_3^-$, ClO_4^- and BF_4^-) and different solvent content. The compounds have been magnetically and structurally investigated, while it has been observed that the tetrafluoroborate complex shows SCO behavior. The different properties are accounted to crystal packing effects in the solid state. The results are presented as scientific article previously published in Crystals. Reprinted with the permission from:

F.Fürmeyer, L.M. Carrella, E. Rentschler, *Crystals* **2020**, *10*(6), 488.

Author contribution

Fabian Fürmeyer designed and performed the synthesis of the ligand and the complexes. He also performed the IR spectroscopy as well as collected and prepared the samples for elemental analysis and SQUID magnetometry. Luca M. Carrella collected the single-crystal X-ray structure data and performed the refinement of the structures. Evaluation of the magnetic and structural data was done by Fabian Fürmeyer. The manuscript was written by Fabian Fürmeyer while important input was added by Luca M. Carrella and Eva Rentschler. Finally, Eva Rentschler had the overall supervision in the interpretation of the data throughout the manuscript process. All authors have read and agreed to the published version of the manuscript.

‘2D Layer Arrangement of Solely [HS-HS] or [LS-LS] Molecules in the [HS-LS] State of A Dinuclear Fe(II) Spin Crossover Complex’

Fabian Fürmeyer, Luca M. Carrella and Eva Rentschler*

Department of Chemistry, Johannes Gutenberg University Mainz, Duesbergweg 10–14, 55128 Mainz; Germany; fuermeyer@uni-mainz.de (F.F.); carrella@uni-mainz.de (L.M.C.)
***** Correspondence: rentschler@uni-mainz.de

Received: 13 April 2020; Accepted: 8 May 2020; Published: 31 May 2020.

Keywords: spin crossover; dinuclear complex; [HS-LS]; 1,3,4-thiadiazole; iron(II); magnetism; single-crystal structure analysis

3.1 Abstract

Herein we report the synthesis and characterization of three new dinuclear iron(II) complexes $[Fe^{II}_2(\mathbf{I^4MTD})_2](F_3CSO_3)_4$ (**C1**), $[Fe^{II}_2(\mathbf{I^4MTD})_2](ClO_4)_4$ (**C2**) and $[Fe^{II}_2(\mathbf{I^4MTD})_2](BF_4)_4$ (**C3**) based on the novel ligand (**I^{4}MTD** = 2,5-bis{[(1*H*-**i**midazol-**4**-yl**m**ethyl)amino]methyl}-1,3,4-**t**hia**d**iazole). Magnetic susceptibility measurements and single-crystal structure analysis show that the iron(II) spin centers for all complexes are in the high spin state at high temperatures. While the magnetic data of air-dried samples confirm the [HS-HS] state for **C1** and **C2** down to very low temperature, for **C3**, a gradual spin crossover is observed below 150 K. The crystal structure of **C3**·THF at 100 K shows that a spin transition from [HS-HS] to an intermediate state takes place, which is a 1:1 mixture of discrete [HS-HS] and [LS-LS] molecules, as identified unambiguously by crystallography. The different SCO properties of **C1**–**C3** can be attributed to crystal packing effects in the solid state.

3.2 Introduction

The growing interest and the necessity of miniaturizing processes lead to multiple research areas in the past decades [1]. The ability to switch between different states at the molecular scale, thus exhibiting molecular bistability, renders spin crossover (SCO) compounds highly promising candidates for memory storage devices, sensors, actuators or displays [2–11]. Complexes of first-row transition metal ions with an electron configuration of d^4–d^7 can either be in the high spin [HS] or in the low spin [LS] state, depending on the octahedral field splitting (Δ_O) and the spin pairing energy (P). Switching between these two states by external stimuli such as the change of temperature, pressure or light is called SCO [12–14]. Iron(II) complexes

in the N_6 coordination environment are by far the most investigated SCO compounds. Their d^6 electron configuration allows switching between a diamagnetic LS state (S = 0) and a paramagnetic HS state (S = 2). Occupying or, vice versa, complete depopulating of the antibonding e_g* orbitals gives rise to a large change in the average Fe-N bond length. This allows the investigation of SCO in iron(II) compounds by standard methods such as temperature-dependent magnetic measurements and X-ray crystallography. Since the interest in SCO is mainly due to the possible application as a molecular switch in information storage or sensors, the research focus is on a complete, abrupt and hysteretic spin switch [1,15–17]. In the solid state, the abrupt change in the properties upon switching and even more, the occurrence of a thermal SCO hysteresis strongly depends on the cooperativity between the spin centers. This is highly favored by intermolecular hydrogen bridges and π–π interactions between the ligand backbones. However, an even better tool to improve cooperativity is to take advantage of intramolecular covalent linking of the metal centers in polymeric compounds [1,3,13,18–21]. Drawbacks are here the difficulties to control the polymerization that hampers crystallization. This can be overcome with oligonuclear compounds. Especially, dinuclear compounds are of particular interest due to the easier control of synthesis and characterization [19,22–25]; furthermore, dinuclear complexes offer the possibility of addressing three accessible states ([HS-HS], [HS-LS] and [LS-LS]) [26], which opens the chance for higher information storage capacities and mathematical operations based on trinary logic [27–29]. In 2005, Brooker reported the dinuclear triazole bridged iron(II) complex $[Fe^{II}_2(\mathbf{PMAT})_2](BF_4)_4$ (**PMAT** = 3,5-bis{[(2-**p**yridyl**m**ethyl)amino]methyl}-4-**a**mino-4*H*-1,2,4-**t**riazole) (Figure 1) that shows a spin switch from the [HS-HS] state at high temperature to an [HS-LS] state at lower temperatures [30]. Our group reported the synthesis and characterization of symmetric dinuclear complexes incorporating the **PMTD** (2,5-bis[(2-**p**yridyl**m**ethyl)amino]methyl-1,3,4-**t**hia**d**iazole, Figure 1) and **PMOD** ligand (2,5-bis[(2-**p**yridyl**m**ethyl)amino]methyl-1,3,4-**o**xa**d**iazole, Figure 1) which both show spin crossover in dependence of the solvent and non-coordinating counter ions used [31–33]. Like the **PMAT** ligand, the bridging bis-tridentate ligands **PMTD** and **PMOD** provide six donor atoms, respectively, allowing for octahedral coordination of both iron(II) ions. Recently, we reported six new dinuclear iron(II) complexes based on two new 1,3,4-thiadiazole bridging ligands (**I^{2}MTD** = 2,5-bis{[(1*H*-**i**midazol-**2**-yl**m**ethyl)amino]methyl}-1,3,4-**t**hia**d**iazole and **TMTD** = 2,5-bis{[(**t**hiazol-2-yl-**m**ethyl)amino]methyl}-1,3,4-**t**hia**d**iazole, Figure 1). For the complex $[Fe^{II}_2(\mathbf{TMTD})_2](ClO_4)_4\cdot 3MeCN$ a two-step spin crossover is observed that is accompanied by two distinct phase transitions. While slow cooling leads to distinguishable HS/LS pairs in the mixed [HS-LS] state, rapid cooling leads to a superposition of the HS and LS iron(II) ions in the [HS-LS] state. Thus, quenching prevents the phase transition to be observable crystallographically. In contrast, all complexes with the **I^{2}MTD** ligand remain in the [HS-HS] state until very low temperatures [34]. We now report on the modification of the **I^{2}MTD** ligand by changing the binding of the imidazolyl heteroaromatic ring to the thiadiazole backbone. The novel **I^{4}MTD** (2,5-bis{[(1*H*-**i**midazol-**4**-yl**m**ethyl)amino]methyl}-1,3,4-**t**hia**d**iazole, Figure 1) was synthesized and characterized. The purpose of this modification was to investigate the intermolecular cooperative interaction pathways of the dinuclear complexes bridged by the **I^{4}MTD** ligand compared to the **I^{2}MTD** based complexes. Since the position of the protonated nitrogen atom in the imidazolyl ring is changed, different hydrogen bonding is expected. We

synthesized and characterized three new bimetallic iron(II) complexes $[Fe^{II}_2(\mathbf{I^4MTD})_2](X)_4$ (with X = BF_4^-, ClO_4^- and $F_3CSO_3^-$), which exhibit distinct different hydrogen bonding networks via the non-coordinating counter ions, resulting in different magnetic properties.

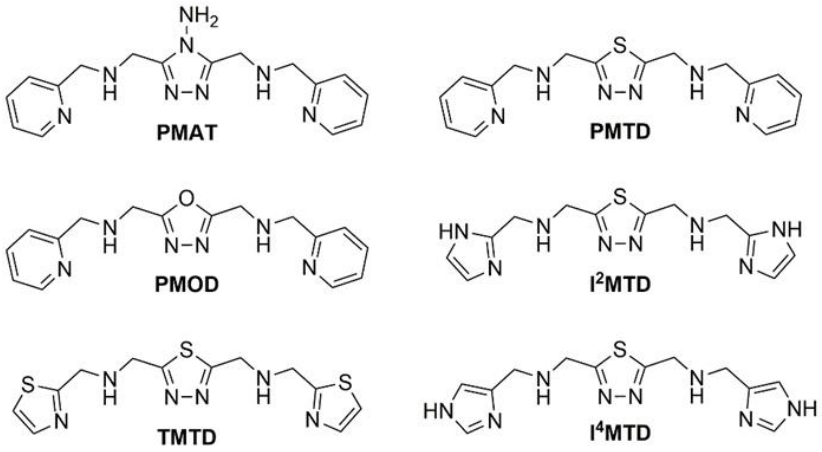

Figure 1. Summary of the ligand systems mentioned in the introduction.

3.3 Experimental Section

3.3.1 General Methods and Materials

All chemicals were purchased as commercially available from Alfa Aesar (Thermo Fisher (Kandel) GmbH, Kandel, Rhineland-Palatinate, Germany), Deutero (Deutero GmbH, Kastellaun, Rhineland-Palatinate, Germany), TCI (TCI Deutschland GmbH, Eschborn, Hesse, Germany), Sigma-Aldrich (Sigma-Aldrich Chemie GmbH, Munich, Bavaria, Germany) and Acros Organics (Thermo Fisher Scientific, Geel, Belgium) and used without further purificationas described in the literature [35]. ^{1}H- and ^{13}C-NMR spectra were recorded at room temperature on a Bruker Avance DSX 400 and analyzed with the program MestReNova (Mestrelab Research, Santiago de Compostela, Spain) [36]. Variable-temperature magnetic susceptibility data for bulk crystalline to powderous samples were measured from 2 to 300 K and in an applied field of 1 kOe with a Quantum Design SQUID magnetometer MPMSXL. FD mass spectrometry measurements and elemental analysis (C, H, N) were performed at the microanalytical laboratories of Johannes Gutenberg University Mainz. Single-crystal X-ray diffraction data were collected at 100 K, 173 K and 200 K with a STOE STADIVARI at the Johannes Gutenberg University Mainz. The structures were solved with ShelXT [37] and refined with ShelXL [38] implemented in the program Olex^2 (OlexSys Ltd., Durham, United Kingdom) [39]. CCDC-1995090-1995093 contains the supplementary crystallographic data for this paper. These data can be obtained free of charge from the Cambridge Crystallographic Data Centre via www.ccdc.cam.ac.uk/data_request/cif. **Caution!** The prepared perchlorate complexes are potentially explosive. Even though no explosions occurred, only small amounts should be prepared and handled with care.

3.3.2 Ligand synthesis

1,2-Bis(chloroacetyl)hydrazine, 2,5-bis(chloromethyl)-1,3,4-thiadiazole, 2,5-bis(azidomethyl)-1,3,4-thiadiazole and 2,5-bis(aminomethyl)-1,3,4-thiadiazole (**1**) were prepared according to literature-known procedures [31,34]. The ligand (**I^{4}MTD** = 2,5-Bis{[(1*H*-**i**midazol-**4**-yl**m**ethyl)amino]methyl}-1,3,4-**t**hia**d**iazole) was synthesized based on similar reductive amination recently published by us [34].

2,5-Bis{[(1*H*-imidazol-4-ylmethyl)amino]methyl}-1,3,4-thiadiazole (I^{4}MTD)
A solution of 1*H*-Imidazol-4-carbaldehyde (**2**) (2.02 g, 21.00 mmol, 2.1 equiv.), 2,5-bis(aminomethyl)-1,3,4-thiadiazole (**1**) (1.44 g, 10.00 mmol, 1.0 equiv.), sodium cyanoborohydride (3.14 g, 50.00 mmol, 5.0 equiv.), and acetic acid (1.26 g, 21.00 mmol, 2.1 equiv.) in methanol (200 mL) was refluxed and followed with TLC (chloroform/methanol 2:1) until the disappearance of **1**. After removal of the solvent under reduced pressure, the obtained oil was purified by column chromatography (SiO_2, chloroform/methanol 2:1). The brown and oily product crystallized upon drying under reduced pressure. The product could not be separated from small impurities. Yield: 2.80 g (9.20 mmol, 92.0%). ^{1}H-NMR (400 MHz, $CDCl_3$, 25 °C): δ = 7.64 (s, 2H, *H*-2, Imz), 6.99 (s, 2H, *H*-5, Imz), 4.14 (s, 4H, CH_2, TDA), 3.80 (s, 4H, CH_2, Imz) ppm. ^{13}C-NMR (100 MHz, $CDCl_3$, 25 °C): δ = 174.2 (*C*, TDA), 136.8 (*C*-4, Imz), 136.5 (*C*-2, Imz), 118.6 (*C*-5, Imz), 47.7 (*C*, TDA), 45.7 (*C*, Imz) ppm. FD-MS (MeOH): *m/z*(%) = 304.05 (100) [(M+H)$^+$], 327.05 (23) [(M+Na)$^+$].

3.3.3 General complex synthesis of [Fe$^{II}_2$(I^{4}MTD)$_2$](X)$_4$

The complex syntheses were carried out in a glovebox under nitrogen atmosphere and exclusion of water and oxygen. After a solution of the ligand (**I^{4}MTD**, 0.10 mmol) in absolute acetonitrile/methanol (2:1, 2 mL) was added to a solution of the corresponding iron(II) salt (0.10 mmol, $Fe(BF_4)_2{\cdot}6H_2O$, $Fe(ClO_4)_2{\cdot}xH_2O$ or $Fe(F_3CSO_3)_2$) in absolute acetonitrile (2 mL) the resulting yellowish to orange complex solutions were exposed to vapor diffusion of absolute diethyl ether or absolute tetrahydrofuran. After several days to weeks, crystals have formed, which were suitable for single-crystal X-ray studies.

[Fe$^{II}_2$(I^{4}MTD)$_2$](F$_3$CSO$_3$)$_4$·solvents (C1)
$Fe(F_3CSO_3)_2$ (35 mg) and 2,5-bis{[(1*H*-imidazol-4-ylmethyl)amino]methyl}-1,3,4-thiadiazole (**I^{4}MTD**, 30 mg) were used to obtain **C1** (23 mg, 33.6%) as yellow crystals. $C_{28}H_{32}F_{12}Fe_2N_{16}O_{12}S_6$ [Fe$^{II}_2$(**I^{4}MTD**)$_2$](F$_3$CSO$_3$)$_4$ (1316.50): calcd. C 25.54 H 2.45 N 17.02; found (after air-drying) C 25.17 H 2.15 N 16.61.

[Fe$^{II}_2$(I^{4}MTD)$_2$](ClO$_4$)$_4$·THF (C2)
$Fe(ClO_4)_2{\cdot}xH_2O$ (27 mg) and 2,5-bis{[(1*H*-imidazol-4-ylmethyl)amino]methyl}-1,3,4-thiadiazole (**I^{4}MTD**, 30 mg) were used to obtain **C2** (26 mg, 45.6%) as yellow crystals $C_{24}H_{32}Cl_4Fe_2N_{16}O_{16}S_2$ [Fe$^{II}_2$(**I^{4}MTD**)$_2$](ClO$_4$)$_4$·(1118.22): calcd. C 25.78 H 2.88N 20.04; found (after air-drying) C 26.48 H 2.61 N20.52.

$[Fe^{II}_2(I^4MTD)_2](BF_4)_4 \cdot THF$ (C3)
$Fe(BF_4)_2 \cdot 6H_2O$ (34 mg) and 2,5-bis{[(1*H*-imidazol-4-ylmethyl)amino]methyl}-1,3,4-thiadiazole (**I^4MTD**, 30 mg) were used to obtain **C3** (26 mg, 43.7%) as yellow crystals. $C_{24}H_{32}B_4F_{16}Fe_2N_{16}S_2$ $[Fe^{II}_2(I^4MTD)_2](BF_4)_4$ (1067.66): calcd. C 27.00 H 3.02 N 20.99; found (after air-drying) C 26.67 H 2.59 N 20.97.

3.4 Results and Discussion

3.4.1 Synthesis

The synthesis of the precursor molecule 2,5-bis(aminomethyl)-1,3,4-thiadiazole (**1**) was previously reported by us [34]. The ligand (**I^4MTD** = 2,5-bis{[(1*H*-**i**midazol-**4**-yl**m**ethyl)amino]methyl}-1,3,4-**t**hia**d**iazole) was synthesized according to a published reductive amination [34] by reacting **1** with 1*H*-imidazole-4-carbaldehyde (**2**) followed by an in situ reduction of the formed imine to the respective amine with sodium cyanoborohydride. The reaction scheme for the synthesis of the ligand (**I^4MTD**) is shown in Scheme 1.

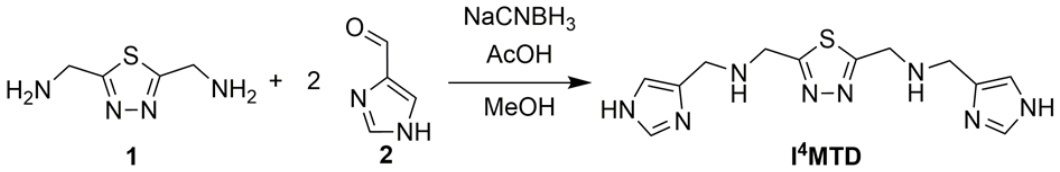

Scheme 1. Synthesis of the ligand (**I^4MTD**) starting from 2,5-bis(aminomethyl)-1,3,4-thiadiazole (**1**).

The complexes $[Fe^{II}_2(I^4MTD)_2](F_3CSO_3)_4$ (**C1**), $[Fe^{II}_2(I^4MTD)_2](ClO_4)_4$ (**C2**) and $[Fe^{II}_2(I^4MTD)_2](BF_4)_4$ (**C3**) were synthesized in stoichiometric reactions of the ligand (**I^4MTD**) with the respective iron(II) salt $Fe^{II}(F_3CSO_3)_2$, $Fe^{II}(ClO_4)_2 \cdot xH_2O$ or $Fe^{II}(BF_4)_2 \cdot 6H_2O$. Single crystals suitable for X-ray diffraction have been obtained by vapor diffusion of diethyl ether or tetrahydrofuran into complex solutions of acetonitrile and methanol (5:1 volume ratio). The syntheses were performed under nitrogen atmosphere using absolute solvents to prevent oxidation of the iron(II) ions.

3.4.2 Crystal structures

The crystal structures of the complexes $[Fe^{II}_2(I^4MTD)_2](F_3CSO_3)_4 \cdot Et_2O/2MeCN$ (**C1**$\cdot Et_2O/2MeCN$, @173 K), $[Fe^{II}_2(I^4MTD)_2](ClO_4)_4 \cdot THF$ (**C2**$\cdot$THF, @173 K) and $[Fe^{II}_2(I^4MTD)_2](BF_4)_4 \cdot THF$ (**C3**$\cdot$THF, @100 and 200 K) all have the centrosymmetric $[Fe_2L_2]^{4+}$ complex cation in common. The two iron(II) centers are bridged by two ligand molecules via the two nitrogen donor atoms of the thiadiazole moiety. The two ligands provide an N_6 octahedral environment for each metal center. Despite the possibility of *cis*- or *trans*-axial

coordination of the ligand, as shown for compounds with related ligands [30,31,34,40], all here described complexes feature the *cis*-axial coordination (see Figure 2). The crystal structures comprise four respective anions counterbalancing the charge. For **C2** and **C3**, the non-coordinating solvent molecule included is tetrahydrofuran. For **C1**, the electron density can be interpreted as either one diethyl ether molecule or two acetonitrile molecules per cation. The highly disordered solvent molecules were treated with SQUEEZE [41] in the program Olex^2 [39]. The formula $[Fe^{II}_2(\mathbf{I^4MTD})_2](F_3CSO_3)_4\cdot$solvent (**C1**·solvent) is used throughout the paper. All crystallographic parameters are given in Table S1.

C1 is found to be in the monoclinic space group *C*2/*c* (@173 K), **C2** in the triclinic space group $P\bar{1}$ (@173 K) and **C3** in the orthorhombic group *Pbca* (@200 K). For all three structures, one half of the complex cation is part of the asymmetric unit and the full cation is symmetry generated by an inversion center located between the two metal centers in the bimetallic complex. The average Fe-N bond lengths of 2.188 Å (**C1**·solvents), 2.192 Å (**C2**·THF) and 2.187 Å (**C3**·THF, @200 K), account for an iron(II) ion in the HS state, resulting in the [HS-HS] state for the whole complex molecule at the given temperatures. This is further confirmed by the octahedral distortion parameters Σ (sum of the deviation from 90° of the 12 *cis*-N-Fe-N angles in the FeN_6 coordination sphere) of 108.0° (**C1**·solvents), 105.3° (**C2**·THF) and 116.5° (**C3**·THF, @200 K) [5,12,13,42]. Information on bond lengths and angles of **C1**–**C3** are summarized in Table 1.

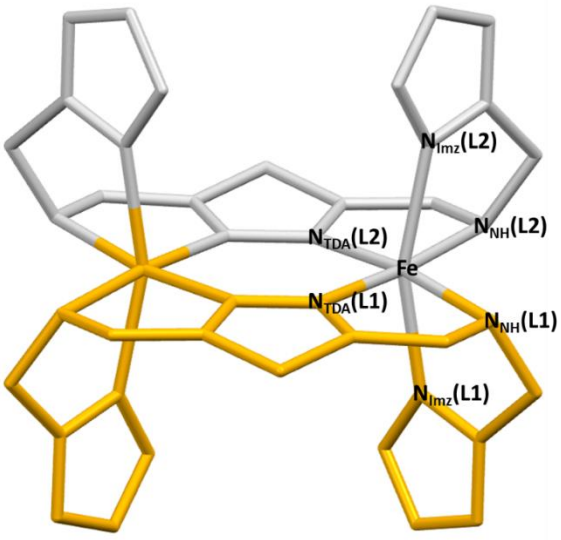

Figure 2. Sketch of the centrosymmetric complex cation $[Fe^{II}_2(\mathbf{I^4MTD})_2]^{4+}$, showing the *cis*-coordination of the ligand as well as octahedral coordination environment for the iron(II) ions.

Table 1. Selected bond lengths (Å), N-Fe-N bond angles (°) and the octahedral distortion parameter Σ[°] for the compounds **C1**–**C3**. For compound **C3** the values are given for different temperatures.

Selected Parameters [a] [b]	**C1·Solvents (@173 K)**	**C2·THF (@173 K)**	**C3·THF (@100 K)**	**C3·THF (@200 K)**
Fe-N_{TDA}(L1)	2.157(2)	2.150(2)	**LS** 1.967(8)/ **HS** 2.147(8)	2.154(2)
Fe-N_{TDA}(L2)	2.161(2)	2.174(2)	**LS** 1.971(7)/ **HS** 2.170(8)	2.158(2)
Fe-N_{NH}(L1)	2.298(2)	2.296(2)	**LS** 2.055(8)/ **HS** 2.239(7)	2.255(2)
Fe-N_{NH}(L2)	2.304(2)	2.297(2)	**LS** 2.103(8)/ **HS** 2.290(8)	2.301(2)
Fe-N_{Imz}(L1)	2.106(2)	2.114(2)	**LS** 1.995(8)/ **HS** 2.131(7)	2.132(2)
Fe-N_{Imz}(L2)	2.104(2)	2.120(2)	**LS** 1.958(8)/ **HS** 2.124(7)	2.122(2)
av. Fe-N	2.188	2.192	**LS** 2.008/ **HS** 2.184	2.187
av. *cis* N-Fe-N	90.2	90-2	**LS** 90.0/ **HS** 90.2	90.2
av. *trans* N-Fe-N	169.5	169.5	**LS** 172.9/ **HS** 168.1	168.2
Σ[c]	108.0	105.3	**LS** 69.5 **HS** 115.6	116.5

[a] N_{TDA} = donor atom on thiadiazole; N_{Imz} = donor atom on imidazole; N_{NH} = amine donor atom. [b] Fe1/Fe2. [c] Octahedral distortion parameter Σ (sum of the deviation from 90° of the 12 *cis*-N-Fe-N angles in the FeN_6 coordination sphere).

Variable-temperature magnetic susceptibility measurements have been performed for all complexes (see below). For **C3**, a partial spin state switching below 150 K was observed. To elucidate this finding, we decided to investigate the X-ray data at lower temperatures. Thus, the single-crystal X-ray data were collected for **C3**·THF at 100 K. The yellow crystal turned red during cooling, but also got fine cracks, which lowers the quality of the crystallographic data. However, a phase transition was seen unambiguously when lowering the temperature to 100 K. The space group changed from orthorhombic *Pbca* (@200 K) to monoclinic $P2_1/c$ (@100 K). The asymmetric unit of the monoclinic phase consists now of two half complex cations with two crystallographic independent iron(II) ions; one per cation (Figure 3).

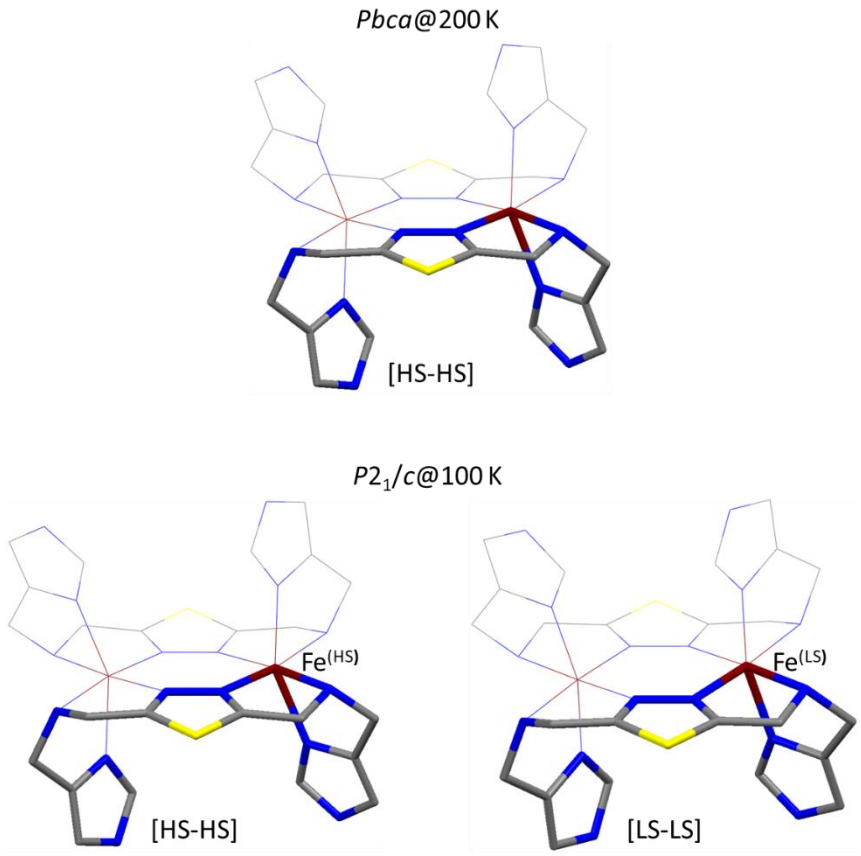

Figure 3. Crystallographic independent complex cations for **C3**·THF at 200 (**top**) and 100 K (**bottom**). The asymmetric units are depicted in bold, while the second half of the cations (wireframe) are symmetry generated. The orientation of the molecules and the labeling is the same as for Figure 2. Hydrogens, solvent molecules and cations are omitted for clarity. Color code: Fe dark red, N blue, S yellow, C gray.

For one complex cation in the asymmetric unit, the iron(II) ion (Fe^{HS}) stays in the HS state. The average Fe-N bond length of 2.184 Å and the octahedral distortion Σ of 115.6° remain almost the same as in the structure obtained at 200 K (2.187 Å and 116.3°), confirming a localized [HS-HS] dimer. For the other complex cation, the average Fe-N bond lengths and the octahedral distortion parameter Σ for the iron(II) ion (Fe^{LS}) decrease to 2.008 Å and 69.5°, which accounts for a localized [LS-LS] complex cation. Thus, a spin transition occurs between 200 and 100 K from the [HS-HS] to the mixed [HS/LS] state, which is a 1:1 mixture of localized dimers either in the [HS-HS] or in the [LS-LS] state (Figure 3). The crystallographic differentiation, whether the [HS-LS] state is realized by discrete [HS-LS] molecules or it composes from a 1:1 mixture of [HS-HS] and [LS-LS] molecules, is not possible in most cases due to higher symmetry in the space group. In centrosymmetric molecular structures, a superposition of the HS and LS iron(II) ions might be observed [43–49]. Fortunately, this is not the case for **C3**, where at low temperatures the dimeric spin crossover complexes can be clearly identified as either [HS-HS] or [LS-LS] molecules.

However, to get a better understanding of why **C3**·THF shows SCO while **C1**·solvents and **C2**·THF do not, we have to take a closer look at the crystal packing, which has a crucial influence on the SCO behavior [3,25,42,50].

Along the crystallographic *c*-axis in **C3**·THF (@200 K), the dinuclear [HS-HS] molecules are arranged in two-dimensional layers formed by hydrogen bonds between the amine protons and the fluorine atoms of the tetrafluoroborate ions (Figure 4, bottom). These layers are separated by 3.11 Å and non-coordinating tetrahydrofuran solvent molecules, as well as tetrafluoroborate counter ions which are located between the layers (Figure 4, top). However, there is no cooperative interaction pathway via hydrogen bonding between the two layers. When lowering the temperature, the occurring SCO phenomenon, ([HS-HS]→[HS-LS]) is accompanied by a phase transition and the space group changes from *Pbca* to $P2_1/c$. At low temperatures, the complex cations in every second layer are switched to the [LS-LS] state, resulting in alternating layers of either [LS-LS] or [HS-HS] molecules. This layered arrangement of molecules solely in the HS or in the LS is rare and we found only a few examples in the literature for which the spin crossover is accompanied by shrinking or expanding of one distinguished crystallographic axis [51–56]. Note that although the direction of the stacking does not change, the crystallographic *c*-axis of the high-temperature space group *Pbca* turns to be the *a*-axis in $P2_1/c$ (Figures 4 and 5). While the intramolecular bond lengths and angles for the iron(II) centers change significantly when going from the HS to the LS state, the intermolecular hydrogen bridges between the dimers in each layer do not change significantly. Thus, to give way to the overall reduced required space for [LS-LS] dimers, compared to the [HS-HS] ones, the stacking changes. With the SCO the interlayer diameter reduces by 0.3 Å from 3.110 Å to 2.804 Å. This drastic impact of the phase transition on only one of the crystallographic axes results inevitably to the small cracks in the crystal.

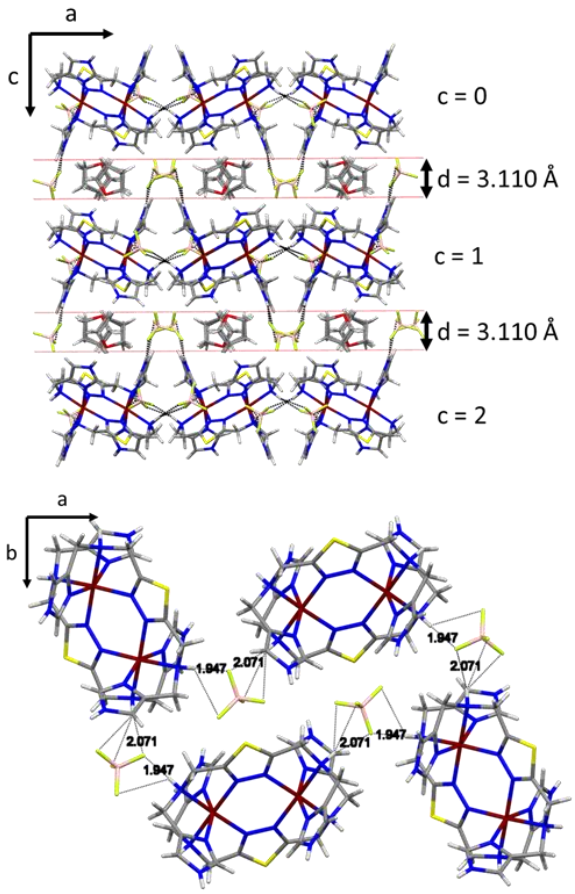

Figure 4. Crystal packing and hydrogen bonding (black dashed lines) toward neighboring anions in **C3**·THF at 200 K (space group *Pbca*). **Top.** View along the crystallographic *b*-axis. **Bottom.** View along the crystallographic *c*-axis. Solvent molecules, as well as non-bridging counter ions, have been omitted for clarity. Color code: Fe dark red, N blue, S yellow, C gray, B pink, F green and H white.

For **C1** and **C2**, the dinuclear complex cations show hydrogen bonding between the amino or the imidazolyl groups and the respective counter anions triflate or perchlorate (Figures S8 and S10). While for **C1**, a three-dimensional network is realized for **C2** intertwined layers are formed. In both cases, the molecules are quite densely packed in the solid state and there is basically no “space” to compensate for bond lengths and volume changes that come together with a spin transition. Thus, single-crystal structure analysis reveals that it is very unlikely that **C1** and **C2** show any SCO behavior.

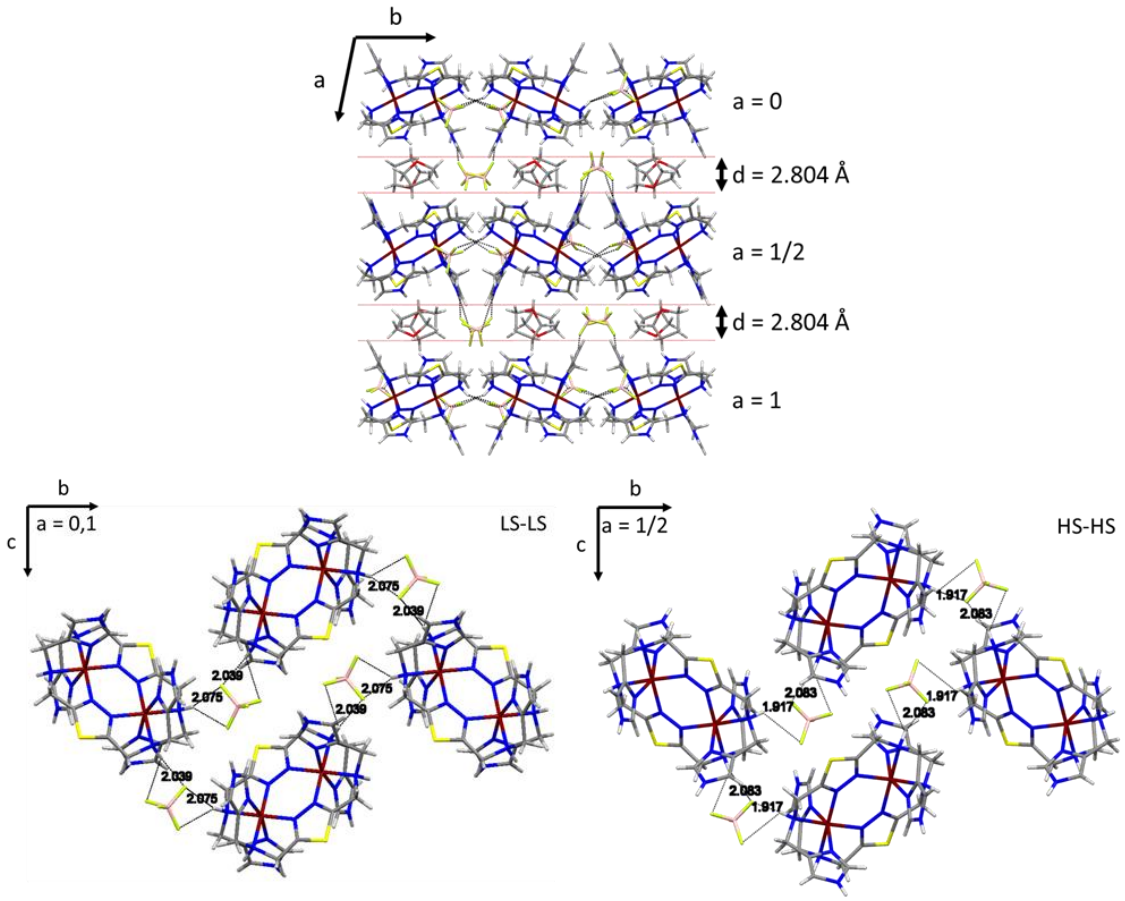

Figure 5. Crystal packing and hydrogen bonding (black dashed lines) toward neighboring anions in C3·THF at 100 K (space group P21/c). **Top**. View along the crystallographic c-axis. **Bottom**. View along the crystallographic a-axis. **Left**. Layer with only [LS-LS] molecules. **Right**. Layer with [HS-HS] molecules. Solvent molecules, as well as non-bridging counter ions, have been omitted for clarity. Color code: Fe dark red, N blue, S yellow, C gray, B pink, F green and H white.

3.4.3 Variable-Temperature Magnetic Susceptibility Measurements

Variable-temperature magnetic susceptibility measurements were performed on microcrystalline to powderous air-dried samples of **C1**–**C3** in the temperature range of 2–300 K in an applied magnetic field of 1000 Oe (0.1 T) (Figures 6 and S12). It is important to mention that the freshly prepared crystalline samples of **C1**–**C3** almost immediately lose crystallinity, when exposed to air, explained by the loss of the volatile solvents (diethyl ether or tetrahydrofuran). Thus, we did not succeed to obtain magnetic data of freshly prepared crystalline samples. The magnetic studies were performed with a cooling/heating rate of 1.5 K/min and the $\chi_M T$ *vs* T plots are indistinguishable for the measurements when heated or cooled. In all three compounds **C1**–**C3**, the dimers are in the [HS-HS] state at 300 K as indicated by $\chi_M T$ values between 6.54 and 6.96 cm^3Kmol^{-1} per complex cation varying with the counter ions. All measured values are slightly higher than the calculated one for an iron(II) dimer with two non-interacting HS iron(II) ions of 6.00 cm^3Kmol^{-1} using the spin-only formalism.

However, this difference is expected, as the spin-only formula does not account for any orbital angular momentum. Upon lowering the temperature, the $\chi_M T$ values for **C1** and **C2** remain almost invariant, indicating that the iron(II) ions remain in the HS state down to low temperature. Below 50 K, for both complexes, the $\chi_M T$ value decreases which can be explained by the presence of weak anti-ferromagnetic exchange interactions between the iron(II) ions and/or by the zero-field splitting of the S = 2 state. For **C3**, the $\chi_M T$ value remains high until about 150 K before it drops to ~4.40 cm^3Kmol^{-1}. The resulting small plateau between 70 and 50 K can be explained by a gradual spin transition of a major part of the dimers (calculated to 70%) from the [HS-HS] to the [HS-LS] state. The decrease of the $\chi_M T$ value for **C3** below 50 K is again explained with the presence of weak anti-ferromagnetic exchange interactions between the HS iron(II) ions in the remaining [HS-HS] dimers and/or by the zero-field splitting of the S = 2 state. The difference between the magnetic data and the single-crystal structure analysis (described above) of **C3** is explained by the loss of the volatile solvent molecules and thus by the loss of crystallinity upon air-drying of the sample. The effect of the solvent loss on the magnetic data is shown in Figure S13 in the supporting information.

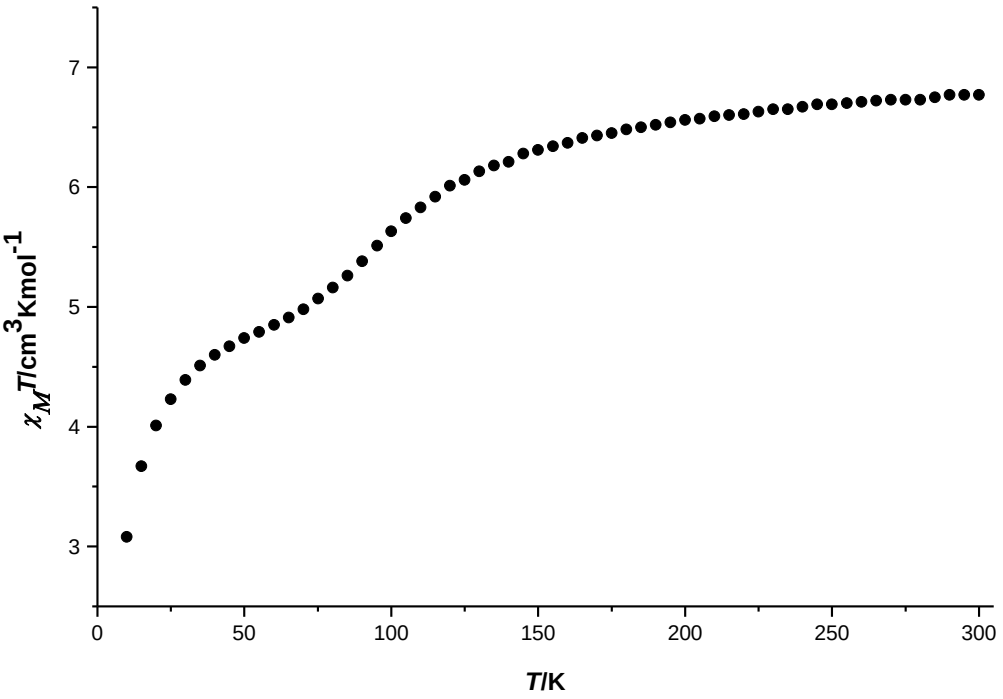

Figure 6. $\chi_M T$ vs T data for the compound **C3**. The data are given per dinuclear iron(II) molecule.

3.5 Conclusion

Concluding, we synthesized the new bis-tridentate 1,3,4-thiadiazole bridging ligand (**I^{4}MTD** = 2,5-Bis{[(1*H*-**i**midazol-**4**-yl**m**ethyl)amino]methyl}-1,3,4-**t**hia**d**iazole, from which we obtained a series of three potentially SCO active dinuclear iron(II) complexes ([Fe^{II}_2(**I^{4}MTD**)$_2$](X)$_4$ with X = $F_3CSO_3^-$ (**C1**), ClO_4^- (**C2**) and BF_4^- (**C3**)). Magnetic susceptibility measurements and single-crystal structure analysis revealed a temperature-independent [HS-HS] state for **C1** and **C2**. In contrast, magnetic data for **C3** showed a gradual spin transition below 200 K suggesting an intermediate [HS-LS] state at low temperatures. However, single-crystal X-ray analysis proved the supposed intermediate spin state to be a 1:1 mixture of [HS-HS] and [LS-LS] molecules. While the local ligand field strength for the iron(II) ions is the same in all three complexes, very clearly, different crystal packing causes the different spin switching properties of the complexes. For **C1** and **C2**, three-dimensional hydrogen bridged networks or strongly intertwined layers of iron(II) dimer molecules are found. In contrast, the dimers in **C3** arrange in two-dimensional layers that are well separated by the non-coordinating counter ions and solvent molecules. The SCO is accompanied by a crystallographic phase transition that accounts for the molecular re-arrangement. With this, the interlayer spacing is already reduced by 0.3 Å although only the molecules in every second 2D layer change the spin state. At 100 K alternating layers of [HS-HS] and [LS-LS] dimers are observed in the crystal structure. In magnetic data obtained from the bulk sample, an average "[HS-LS]" state is featured. Thus, our results clearly underline the importance of investigations of SCO phenomena using complementary methods.

Supplementary Materials: The following are available online at www.mdpi.com/xxx/s1, **Figure S1.** ^{1}H-NMR of 2,5-bis{[(1*H*-imidazol-4-ylmethyl)amino]methyl}-1,3,4-thiadiazole (**I^{4}MTD**)., **Figure S2.** ^{13}C-NMR of 2,5-bis{[(1*H*-imidazol-4-ylmethyl)amino]methyl}-1,3,4-thiadiazole (**I^{4}MTD**)., **Figure S3.** Field desorption mass spectrum of 2,5-bis{[(1*H*-imidazol-4-ylmethyl)amino]methyl}-1,3,4-thiadiazole (**I^{4}MTD**)., **Figure S4.** IR spectrum of air-dried [Fe^{II}_2(**I^{4}MTD**)$_2$](F_3CSO_3)$_4$ (**C1**)., **Figure S5.** IR spectrum of air-dried [Fe^{II}_2(**I^{4}MTD**)$_2$](ClO_4)$_4$ (**C2**)., **Figure S6.** IR spectrum of air-dried [Fe^{II}_2(**I^{4}MTD**)$_2$](BF_4)$_4$ (**C3**)., **Figure S7.** Molecular structure of [Fe^{II}_2(**I^{4}MTD**)$_2$](F_3CSO_3)$_4$·solvents (**C1**·solvents) with thermal ellipsoids at 173 K. Solvent molecules could not be solved. Color code: Fe is dark red, N blue, S yellow, C grey, H white, O red and F light green., **Figure S8.** Crystal packing and hydrogen bonding (black dashed lines) via anions in [Fe^{II}_2(**I^{4}MTD**)$_2$](F_3CSO_3)$_4$·solvents (**C1**·solvents) at 173 K. Non-bridging counter ions have been omitted for clarity. **a)** View along crystallographic *b*-axis. **b)** View along crystallographic *a*-axis. Color code: Fe is dark red, N blue, S yellow, C grey, H white, O red and F light green., **Figure S9.** Molecular structure of [Fe^{II}_2(**I^{4}MTD**)$_2$](ClO_4)$_4$·THF (**C2**·THF) with thermal ellipsoids at 173 K. Color code: Fe is dark red, N blue, S yellow, C grey, H white, O red and Cl green., **Figure S10.** Crystal packing and hydrogen bonding (black dashed lines) via anions in [Fe^{II}_2(**I^{4}MTD**)$_2$](ClO_4)$_4$·THF (**C2**·THF) at 173 K. Non-bridging counter ions and solvent molecules have been omitted for clarity. **a)** View along crystallographic *a*-axis. **b)** View along the angle bisector of the crystallographic *a*- and *b*-axis. Color code: Fe is dark red, N blue, S yellow, C grey, H white, O red and Cl green., **Figure S11.**

Molecular structure of $[Fe^{II}_2(\mathbf{I^4MTD})_2](BF_4)_4\cdot THF(\mathbf{C3}\cdot THF)$ with thermal ellipsoids at **a)** 200 K and **b)** 100 K. Color code: Fe is dark red, N blue, S yellow, C grey, H white, O red, B pink and F light green., **Figure S12.** $\chi_M T$ vs T data for the air-dried compounds **C1** (squares) and **C2** (triangles). The data are given per dinuclear iron(II) molecule, **Figure S13.** $\chi_M T$ vs T data for **C3** for a freshly taken sample measured from 10 – 300 K after direct low-temperature freezing within the magnetometer (filled squares), subsequently measured from 300 - 10 K (empty squares) and for a dried sample from 10 – 300 K after heating the sample to 400 K for 2 hours (filled circles). The data are given per dinuclear iron(II) molecule., **Table S1.** Crystallographic parameters for all discussed crystal structures of **C1** – **C3**.

Author contributions: F.F. performed the synthesis and characterization of the ligand and the complexes. F.F. measured and analyzed the magnetic data. L.M.C. performed the X-ray acquisition data and analysis. F. F. and E.R. finalized the manuscript with contributions from L.M.C. All authors have read and agreed to the published version of the manuscript.

Funding: This research received no external funding.

Conflicts of Interest The authors declare no conflicts of interest.

3.6 References

1. Kahn, O.; Martinez, C.J. Spin-Transition Polymers: From Molecular Materials Toward Memory Devices. *Science* **1998**, *279*, 44–48, doi:10.1126/science.279.5347.44.
2. Bousseksou, A.; Molnár, G.; Salmon, L.; Nicolazzi, W. Molecular spin crossover phenomenon: Recent achievements and prospects. *Chem. Soc. Rev.* **2011**, *40*, 3313–3335, doi:10.1039/c1cs15042a.
3. Halcrow, M.A. Structure:function relationships in molecular spin-crossover complexes. *Chem. Soc. Rev.* **2011**, *40*, 4119, doi:10.1039/c1cs15046d.
4. Linares, J.; Codjovi, E.; Garcia, Y. Pressure and Temperature Spin Crossover Sensors with Optical Detection. *Sensors* **2012**, *12*, 4479–4492, doi:10.3390/s120404479.
5. Gütlich, P.; Gaspar, A.B.; Garcia, Y. Spin state switching in iron coordination compounds. *Beilstein J. Org. Chem.* **2013**, *9*, 342–391, doi:10.3762/bjoc.9.39.
6. Halcrow, M.A. *Spin-Crossover Materials: Properties and Applications*; Halcrow, M.A., Ed.; John Wiley & Sons Ltd: Oxford, UK, 2013; ISBN 9781118519301.
7. Gütlich, P. Spin Crossover - Quo Vadis? *Eur. J. Inorg. Chem.* **2013**, *2013*, 581–591, doi:10.1002/ejic.201300092.
8. Manrique-Juárez, M.D.; Rat, S.; Salmon, L.; Molnár, G.; Quintero, C.M.; Nicu, L.; Shepherd, H.J.; Bousseksou, A. Switchable molecule-based materials for micro- and nanoscale actuating applications: Achievements and prospects. *Coord. Chem. Rev.* **2016**, *308*, 395–408, doi:10.1016/j.ccr.2015.04.005.
9. Sato, O. Dynamic molecular crystals with switchable physical properties. *Nat. Chem.* **2016**, *8*, 644–656, doi:10.1038/nchem.2547.

10. Senthil Kumar, K.; Ruben, M. Emerging trends in spin crossover (SCO) based functional materials and devices. *Coord. Chem. Rev.* **2017**, *346*, 176–205, doi:10.1016/j.ccr.2017.03.024.
11. Ruben, M.; Kumar, K.S. Sublimable Spin Crossover Complexes: From Spin-State Switching to Molecular Devices. *Angew. Chemie* **2019**, ange.201911256, doi:10.1002/ange.201911256.
12. Gütlich, P.; Hauser, A.; Spiering, H. Thermal and Optical Switching of Iron(II) Complexes. *Angew. Chemie Int. Ed. English* **1994**, *33*, 2024–2054, doi:10.1002/anie.199420241.
13. Gütlich, P.; Goodwin, H.A. Spin Crossover—An Overall Perspective. In *Spin Crossover in Transition Metal Compounds I*; Gütlich, P., Goodwin, H.A., Eds.; Springer: Berlin/Heidelberg, 2004; Vol. 1, pp. 1–47.
14. Hauser, A. Ligand Field Theoretical Considerations. In *Spin Crossover in Transition Metal Compounds I*; Gütlich, P., Goodwin, H.A., Eds.; Springer: Berlin/Heidelberg, 2004; pp. 49–58.
15. Kröber, J.; Codjovi, E.; Kahn, O.; Grolière, F.; Jay, C. A Spin Transition System with a Thermal Hysteresis at Room Temperature. *J. Am. Chem. Soc.* **1993**, *115*, 9810–9811, doi:10.1021/ja00074a062.
16. Brooker, S. Spin crossover with thermal hysteresis: practicalities and lessons learnt. *Chem. Soc. Rev.* **2015**, *44*, 2880–2892, doi:10.1039/C4CS00376D.
17. Ridier, K.; Molnár, G.; Salmon, L.; Nicolazzi, W.; Bousseksou, A. Hysteresis, nucleation and growth phenomena in spin-crossover solids. *Solid State Sci.* **2017**, *74*, A1–A22, doi:10.1016/j.solidstatesciences.2017.10.014.
18. Galet, A.; Gaspar, A.B.; Muñoz, M.C.; Real, J.A. Influence of the counterion and the solvent molecules in the spin crossover system [Co(4-terpyridone)2]Xp·nH2O. *Inorg. Chem.* **2006**, *45*, 4413–4422, doi:10.1021/ic060090u.
19. Real, J.A.; Gaspar, A.B.; Niel, V.; Muñoz, M.C. Communication between iron(II) building blocks in cooperative spin transition phenomena. *Coord. Chem. Rev.* **2003**, *236*, 121–141, doi:10.1016/S0010-8545(02)00220-5.
20. Carmen Muñoz, M.; Antonio Real, J. Polymeric Spin-Crossover Materials. In *Spin-Crossover Materials: Properties and Applications*; Halcrow, M.A., Ed.; John Wiley & Sons Ltd: Oxford, UK, 2013; pp. 121–146 ISBN 9781119998679.
21. Wu, X.-R.; Shi, H.-Y.; Wei, R.-J.; Li, J.; Zheng, L.-S.; Tao, J. Coligand and Solvent Effects on the Architectures and Spin-Crossover Properties of (4,4)-Connected Iron(II) Coordination Polymers. *Inorg. Chem.* **2015**, *54*, 3773–3780, doi:10.1021/ic5029542.
22. Gaspar, A.B.; Muñoz, M.C.; Real, J.A. Dinuclear iron(<scp>ii</scp>) spin crossover compounds: singular molecular materials for electronics. *J. Mater. Chem.* **2006**, *16*, 2522–2533, doi:10.1039/B603488H.
23. Murray, K.S. Advances in Polynuclear Iron(II), Iron(III) and Cobalt(II) Spin-Crossover Compounds. *Eur. J. Inorg. Chem.* **2008**, *2008*, 3101–3121, doi:10.1002/ejic.200800352.
24. Olguín, J.; Brooker, S. Spin-Crossover in Discrete Polynuclear Complexes. In *Spin-Crossover Materials: Properties and Applications*; Halcrow, M.A., Ed.; John Wiley & Sons Ltd: Oxford, UK, 2013; pp. 77–120 ISBN 9781119998679.
25. Hogue, R.W.; Singh, S.; Brooker, S. Spin crossover in discrete polynuclear iron(ii) complexes. *Chem. Soc. Rev.* **2018**, *47*, 7303–7338, doi:10.1039/c7cs00835j.

26. Real, J.A.; Bolvin, H.; Bousseksou, A.; Dworkin, A.; Kahn, O.; Varret, F.; Zarembowitch, J. Two-step spin crossover in the new dinuclear compound [Fe(bt)(NCS)2]2bpym, with bt = 2,2'-bi-2-thiazoline and bpym = 2,2'-bipyrimidine: experimental investigation and theoretical approach. *J. Am. Chem. Soc.* **1992**, *114*, 4650–4658, doi:10.1021/ja00038a031.
27. Ruben, M.; Breuning, E.; Gisselbrecht, J.-P.; Lehn, J.-M. Multilevel Molecular Electronic Species: Electrochemical Reduction of a [2×2] CoII4 Grid-Type Complex by 11 Electrons in 10 Reversible Steps. *Angew. Chemie* **2000**, *39*, 4139–4142, doi:10.1002/1521-3773(20001117)39:22<4139::AID-ANIE4139>3.0.CO;2-Y.
28. Breuning, E.; Ruben, M.; Lehn, J.; Renz, F.; Garcia, Y.; Ksenofontov, V.; Gütlich, P.; Wegelius, E.; Rissanen, K. Spin Crossover in a Supramolecular Fe4II [2×2] Grid Triggered by Temperature, Pressure, and Light. *Angew. Chemie Int. Ed.* **2000**, *39*, 2504–2507, doi:10.1002/1521-3773(20000717)39:14<2504::AID-ANIE2504>3.0.CO;2-B.
29. Létard, J.-F.; Guionneau, P.; Goux-Capes, L. Towards Spin Crossover Applications. In *Spin Crossover in Transition Metal Compounds III*; Gütlich, P., Goodwin, H.A., Eds.; Springer: Berlin/Heidelberg, 2004; Vol. 1, pp. 221–249.
30. Klingele, M.H.; Moubaraki, B.; Cashion, J.D.; Murray, K.S.; Brooker, S. The first X-ray crystal structure determination of a dinuclear complex trapped in the [low spin–high spin] state: [Fe II 2 (PMAT) 2](BF 4) 4 ·DMF. *Chem. Commun.* **2005**, *2*, 987–989, doi:10.1039/B415891A.
31. Herold, C.F.; Carrella, L.M.; Rentschler, E. A Family of Dinuclear Iron(II) SCO Compounds Based on a 1,3,4-Thiadiazole Bridging Ligand. *Eur. J. Inorg. Chem.* **2015**, *2015*, 3632–3636, doi:10.1002/ejic.201500483.
32. Herold, C.F.; Shylin, S.I.; Rentschler, E. Solvent-dependent SCO Behavior of Dinuclear Iron(II) Complexes with a 1,3,4-Thiadiazole Bridging Ligand. *Inorg. Chem.* **2016**, *55*, 6414–6419, doi:10.1021/acs.inorgchem.6b00163.
33. Köhler, C.; Rentschler, E. The First 1,3,4-Oxadiazole Based Dinuclear Iron(II) Complexes Showing Spin Crossover Behavior with Hysteresis. *Eur. J. Inorg. Chem.* **2016**, *2016*, 1955–1960, doi:10.1002/ejic.201501278.
34. Fürmeyer, F.; Carrella, L.M.; Ksenofontov, V.; Möller, A.; Rentschler, E. Phase Trapping in Multistep Spin Crossover Compound. *Inorg. Chem.* **2020**, *59*, 2843–2852, doi:10.1021/acs.inorgchem.9b03170.
35. Eaborn, C. Purification of Laboratory Chemicals. *J. Organomet. Chem.* **1981**, *213*, C62, doi:10.1016/S0022-328X(00)82974-5.
36. Cobas, J.C.; Sardina, F.J. Nuclear magnetic resonance data processing. MestRe-C: A software package for desktop computers. *Concepts Magn. Reson.* **2003**, *19A*, 80–96, doi:10.1002/cmr.a.10089.
37. Sheldrick, G.M. SHELXT – Integrated space-group and crystal-structure determination. *Acta Crystallogr. Sect. A Found. Adv.* **2015**, *71*, 3–8, doi:10.1107/S2053273314026370.
38. Sheldrick, G.M. Crystal structure refinement with SHELXL. *Acta Crystallogr. Sect. C Struct. Chem.* **2015**, *71*, 3–8, doi:10.1107/S2053229614024218.
39. Dolomanov, O. V.; Bourhis, L.J.; Gildea, R.J.; Howard, J.A.K.; Puschmann, H. OLEX2 : a complete structure solution, refinement and analysis program. *J. Appl. Crystallogr.* **2009**, *42*, 339–341, doi:10.1107/S0021889808042726.

40. Hogue, R.W.; Feltham, H.L.C.; Miller, R.G.; Brooker, S. Spin Crossover in Dinuclear N 4 S 2 Iron(II) Thioether–Triazole Complexes: Access to [HS-HS], [HS-LS], and [LS-LS] States. *Inorg. Chem.* **2016**, *55*, 4152–4165, doi:10.1021/acs.inorgchem.5b02851.
41. van der Sluis, P.; Spek, A.L. BYPASS: an effective method for the refinement of crystal structures containing disordered solvent regions. *Acta Crystallogr. Sect. A Found. Crystallogr.* **1990**, *46*, 194–201, doi:10.1107/S0108767389011189.
42. Kitchen, J.A.; Olguín, J.; Kulmaczewski, R.; White, N.G.; Milway, V.A.; Jameson, G.N.L.; Tallon, J.L.; Brooker, S. Effect of N 4 -Substituent Choice on Spin Crossover in Dinuclear Iron(II) Complexes of Bis-Terdentate 1,2,4-Triazole-Based Ligands. *Inorg. Chem.* **2013**, *52*, 11185–11199, doi:10.1021/ic4014416.
43. Ortega-Villar, N.; Thompson, A.L.; Muñoz, M.C.; Ugalde-Saldívar, V.M.; Goeta, A.E.; Moreno-Esparza, R.; Real, J.A. Solid- and Solution-State Studies of the Novel μ-Dicyanamide-Bridged Dinuclear Spin-Crossover System {[(Fe(bztpen)]2[μ-N(CN)2]}(PF6)3·n H2O. *Chem. - A Eur. J.* **2005**, *11*, 5721–5734, doi:10.1002/chem.200500171.
44. Gaspar, A.B.; Ksenofontov, V.; Reiman, S.; Gütlich, P.; Thompson, A.L.; Goeta, A.E.; Muñoz, M.C.; Real, J.A. Mössbauer Investigation of the Photoexcited Spin States and Crystal Structure Analysis of the Spin-Crossover Dinuclear Complex [{Fe(bt)(NCS)2}2bpym] (bt=2,2′-Bithiazoline, bpym=2,2′-Bipyrimidine). *Chem. - A Eur. J.* **2006**, *12*, 9289–9298, doi:10.1002/chem.200600559.
45. Verat, A.Y.; Ould-Moussa, N.; Jeanneau, E.; Le Guennic, B.; Bousseksou, A.; Borshch, S.A.; Matouzenko, G.S. Ligand Strain and the Nature of Spin Crossover in Binuclear Complexes: Two-Step Spin Crossover in a 4,4′-Bipyridine-Bridged Iron(II) Complex [{Fe(dpia)(NCS) 2 } 2 (4,4′-bpy)] (dpia=di(2-picolyl)amine; 4,4′-bpy=4,4′-bipyridine). *Chem. - A Eur. J.* **2009**, *15*, 10070–10082, doi:10.1002/chem.200900921.
46. Matouzenko, G.S.; Jeanneau, E.; Yu. Verat, A.; Bousseksou, A. Spin crossover and polymorphism in a family of 1,2-bis(4-pyridyl)ethene-bridged binuclear iron(ii) complexes. A key role of structural distortions. *Dalt. Trans.* **2011**, *40*, 9608, doi:10.1039/c1dt10312a.
47. Matouzenko, G.S.; Jeanneau, E.; Verat, A.Y.; de Gaetano, Y. The Nature of Spin Crossover and Coordination Core Distortion in a Family of Binuclear Iron(II) Complexes with Bipyridyl-Like Bridging Ligands. *Eur. J. Inorg. Chem.* **2012**, *2012*, 969–977, doi:10.1002/ejic.201101178.
48. de Gaetano, Y.; Jeanneau, E.; Verat, A.Y.; Rechignat, L.; Bousseksou, A.; Matouzenko, G.S. Ligand-Induced Distortions and Magneto-Structural Correlations in a Family of Dinuclear Spin Crossover Compounds with Bipyridyl-Like Bridging Ligands. *Eur. J. Inorg. Chem.* **2013**, *2013*, 1015–1023, doi:10.1002/ejic.201200711.
49. Schneider, C.J.; Cashion, J.D.; Chilton, N.F.; Etrillard, C.; Fuentealba, M.; Howard, J.A.K.; Létard, J.-F.; Milsmann, C.; Moubaraki, B.; Sparkes, H.A.; et al. Spin Crossover in a 3,5-Bis(2-pyridyl)-1,2,4-triazolate-Bridged Dinuclear Iron(II) Complex [{Fe(NCBH 3)(py)} 2 (μ-L 1) 2] - Powder versus Single Crystal Study. *Eur. J. Inorg. Chem.* **2013**, *2013*, 850–864, doi:10.1002/ejic.201201075.

50. Singh, S.; Brooker, S. Extension of Azine-Triazole Synthesis to Azole-Triazoles Reduces Ligand Field, Leading to Spin Crossover in Tris-L Fe(II). *Inorg. Chem.* **2020**, *59*, 1265–1273, doi:10.1021/acs.inorgchem.9b02993.
51. Chernyshov, D.; Hostettler, M.; Törnroos, K.W.; Bürgi, H.-B. Ordering Phenomena and Phase Transitions in a Spin-Crossover Compound—Uncovering the Nature of the Intermediate Phase of[Fe(2-pic)3]Cl2·EtOH. *Angew. Chemie Int. Ed.* **2003**, *42*, 3825–3830, doi:10.1002/anie.200351834.
52. Yamada, M.; Ooidemizu, M.; Ikuta, Y.; Osa, S.; Matsumoto, N.; Iijima, S.; Kojima, M.; Dahan, F.; Tuchagues, J.-P. Interlayer Interaction of Two-Dimensional Layered Spin Crossover Complexes [Fe II H 3 L Me][Fe II L Me]X (X - = ClO 4 - , BF 4 - , PF 6 - , AsF 6 - , and SbF 6 - ; H 3 L Me = Tris[2-(((2-methylimidazol-4-yl)methylidene)amino)ethyl]amine). *Inorg. Chem.* **2003**, *42*, 8406–8416, doi:10.1021/ic034439e.
53. Yamada, M.; Hagiwara, H.; Torigoe, H.; Matsumoto, N.; Kojima, M.; Dahan, F.; Tuchagues, J.P.; Re, N.; Iijima, S. A variety of spin-crossover behaviors depending on the counter anion: Two-dimensional complexes constructed by NH···Cl- hydrogen bonds, [FeIIH3LMe]Cl·X (X = PF 6-, AsF6-, SbF6-, CF3SO3-; H3L Me = tris[2-{[(2methylimi... *Chem. - A Eur. J.* **2006**, *12*, 4536–4549, doi:10.1002/chem.200500972.
54. Sheu, C.-F.; Pillet, S.; Lin, Y.-C.; Chen, S.-M.; Hsu, I.-J.; Lecomte, C.; Wang, Y. Magnetostructural Relationship in the Spin-Crossover Complex t-{Fe(abpt) 2 [N(CN) 2] 2 }: Polymorphism and Disorder Phenomenon. *Inorg. Chem.* **2008**, *47*, 10866–10874, doi:10.1021/ic800879c.
55. Li, B.; Wei, R.-J.; Tao, J.; Huang, R.-B.; Zheng, L.-S.; Zheng, Z. Solvent-Induced Transformation of Single Crystals of a Spin-Crossover (SCO) Compound to Single Crystals with Two Distinct SCO Centers. *J. Am. Chem. Soc.* **2010**, *132*, 1558–1566, doi:10.1021/ja909695f.
56. Luan, J.; Zhou, J.; Liu, Z.; Zhu, B.; Wang, H.; Bao, X.; Liu, W.; Tong, M.L.; Peng, G.; Peng, H.; et al. Polymorphism-dependent spin-crossover: Hysteretic two-step spin transition with an ordered [HS-HS-LS] intermediate phase. *Inorg. Chem.* **2015**, *54*, 5145–5147, doi:10.1021/acs.inorgchem.5b00629.

3.7 Supporting Information

3.7.1 NMR Spectroscopy

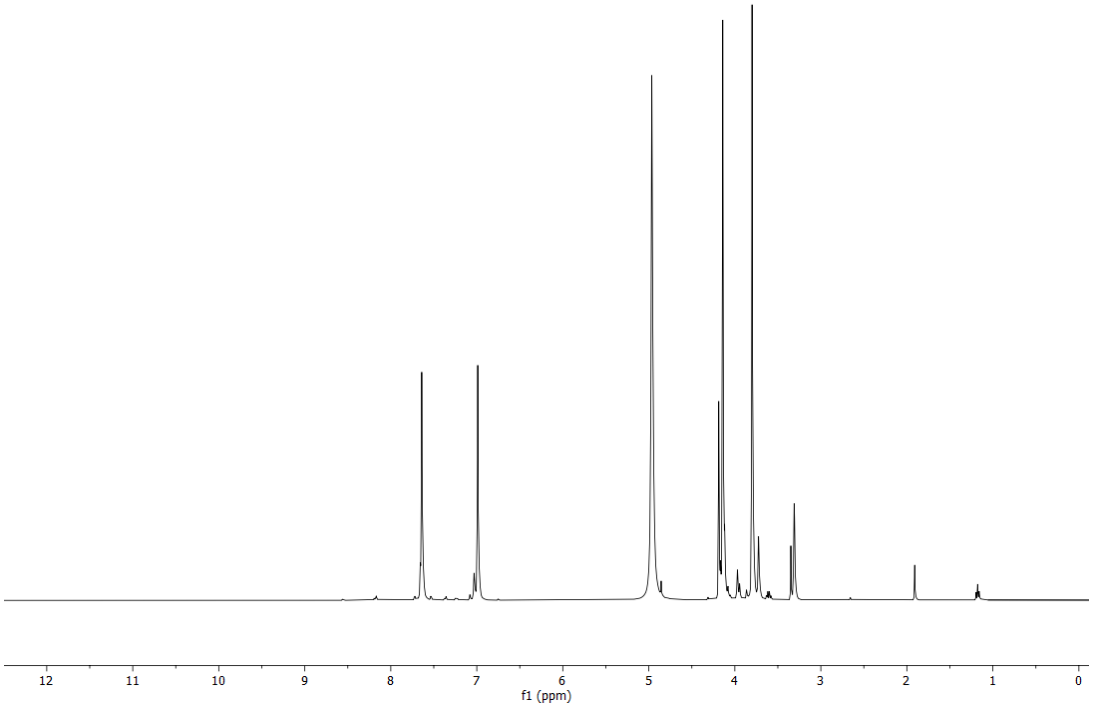

Figure S1. ^{1}H-NMR of 2,5-bis{[(1*H*-imidazol-4-ylmethyl)amino]methyl}-1,3,4-thiadiazole (**I^{4}MTD**).

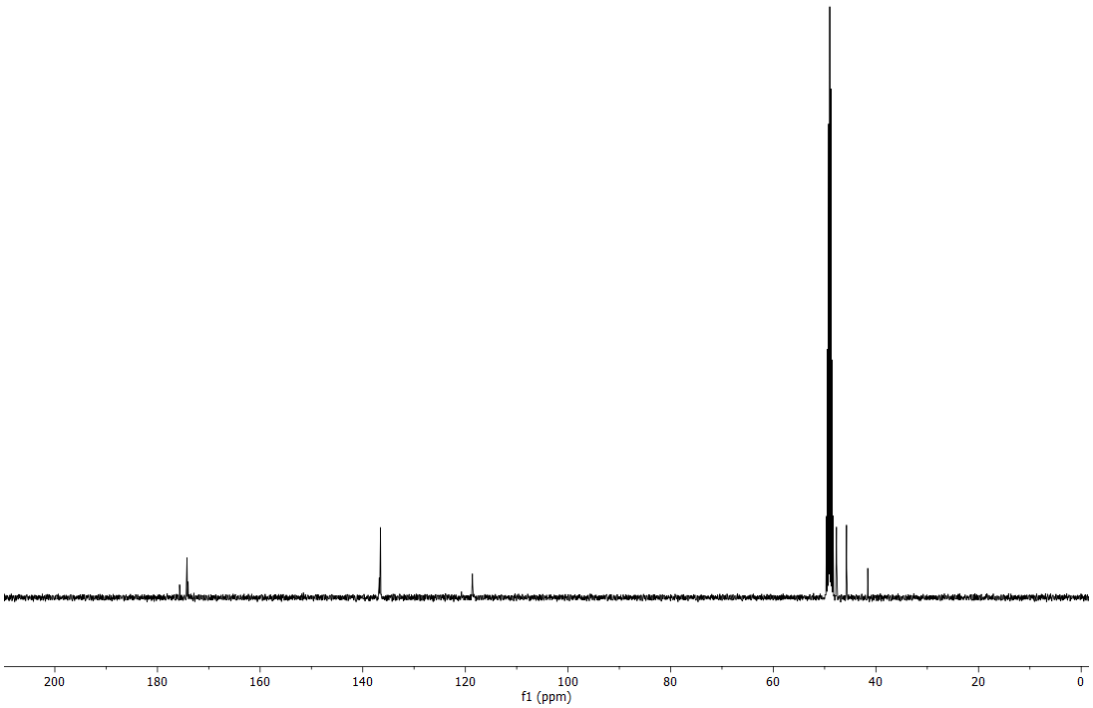

Figure S2. ^{13}C-NMR of 2,5-bis{[(1*H*-imidazol-4-ylmethyl)amino]methyl}-1,3,4-thiadiazole (**I^{4}MTD**).

3.7.2 Mass Spectrometry

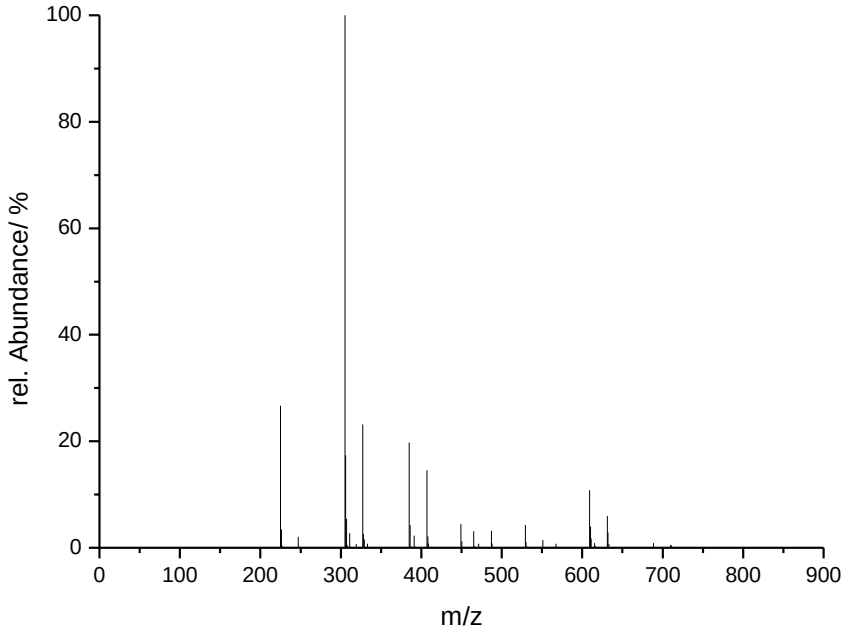

Figure S3. Field desorption mass spectrum of 2,5-bis{[(1*H*-imidazol-4-ylmethyl)amino]methyl}-1,3,4-thiadiazole (**I^{4}MTD**).

3.7.3 IR Spectroscopy

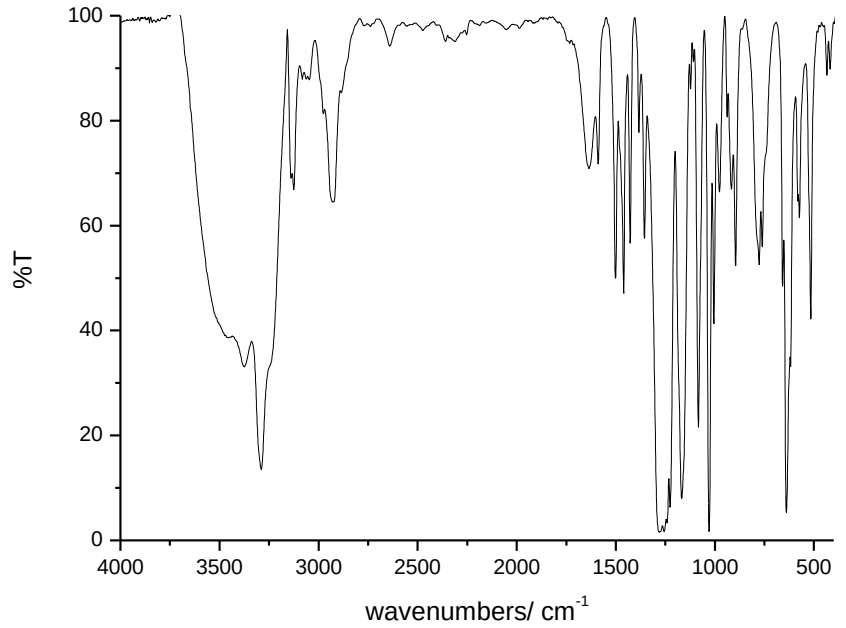

Figure S4. IR spectrum of air-dried $[Fe^{II}_2(\mathbf{I^4MTD})_2](F_3CSO_3)_4$ (**C1**).

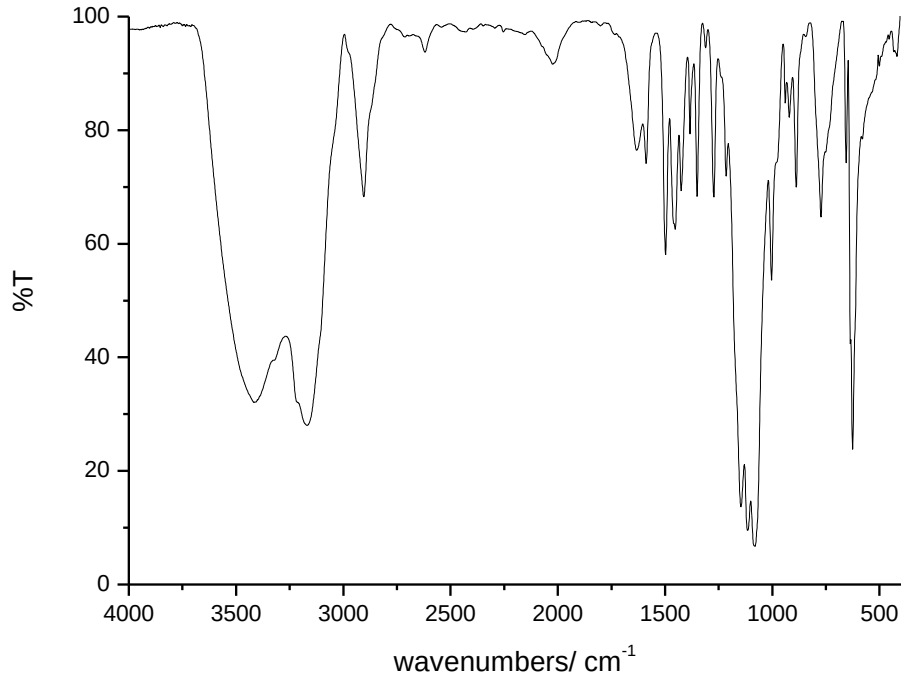

Figure S5. IR spectrum of air-dried $[Fe^{II}_2(\mathbf{I^4MTD})_2](ClO_4)_4$ (**C2**).

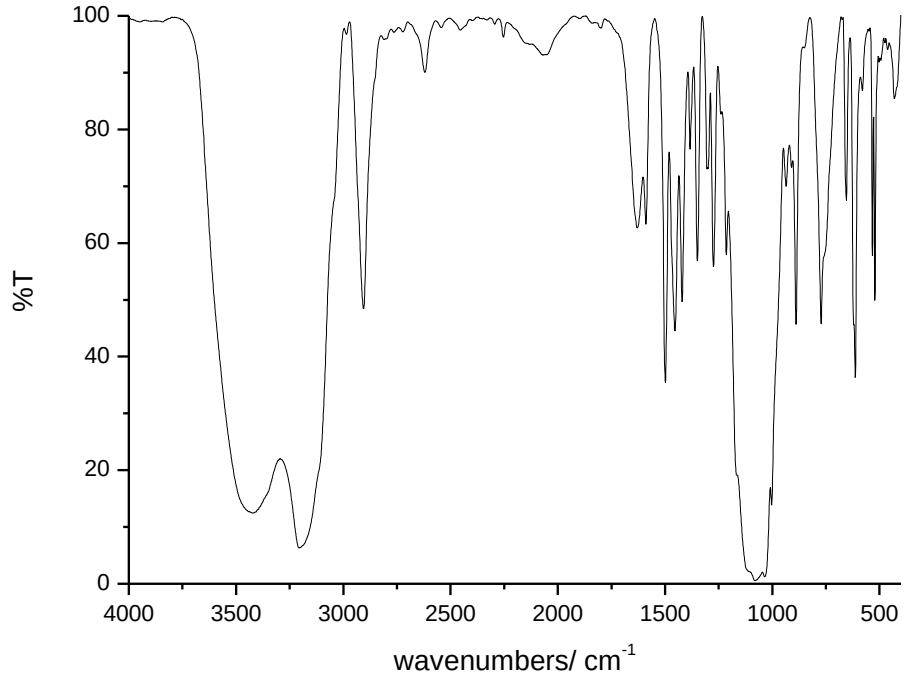

Figure S6. IR spectrum of air-dried $[Fe^{II}_2(\mathbf{I^4MTD})_2](BF_4)_4$ (**C3**).

3.7.4 X-ray Diffraction Measurements

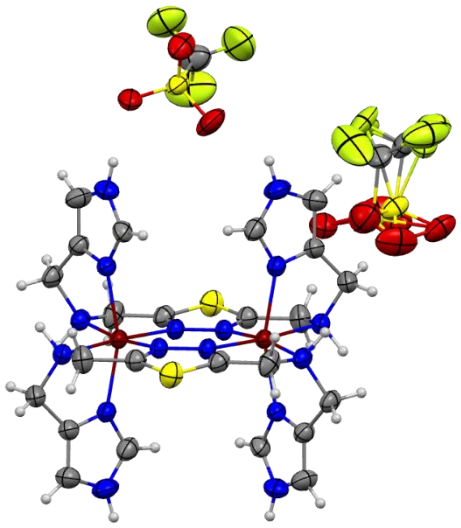

Figure S7. Molecular structure of $[Fe^{II}_2(\mathbf{I^4MTD})_2](F_3CSO_3)_4 \cdot$solvents (**C1**·solvents) with thermal ellipsoids at 173 K. Solvent molecules could not be solved. Color code: Fe is dark red, N blue, S yellow, C grey, H white, O red and F light green.

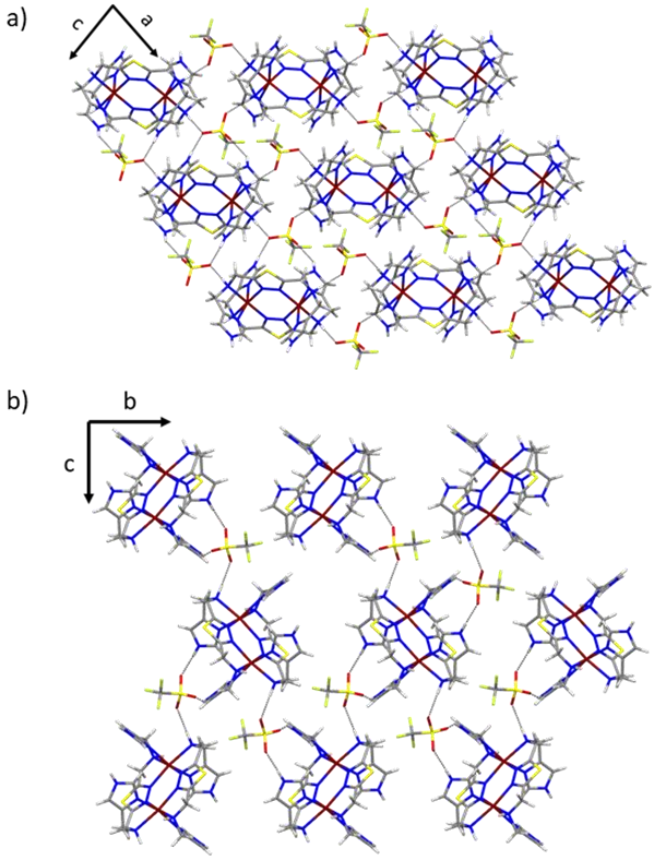

Figure S8. Crystal packing and hydrogen bonding (black dashed lines) via anions in $[Fe^{II}_2(\mathbf{I^4MTD})_2](F_3CSO_3)_4 \cdot$solvents (**C1**·solvents) at 173 K. Non-bridging counter ions have been omitted for clarity. **a)** View along crystallographic *b*-axis. **b)** View along crystallographic *a*-axis. Color code: Fe is dark red, N blue, S yellow, C grey, H white, O red and F light green.

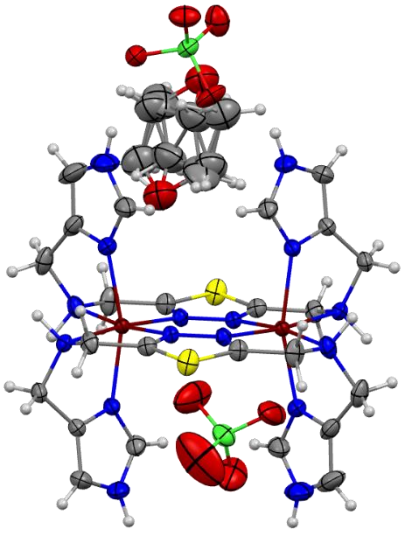

Figure S9. Molecular structure of $[Fe^{II}_2(\mathbf{I^4MTD})_2](ClO_4)_4 \cdot THF$ (**C2**·THF) with thermal ellipsoids at 173 K. Color code: Fe is dark red, N blue, S yellow, C grey, H white, O red and Cl green.

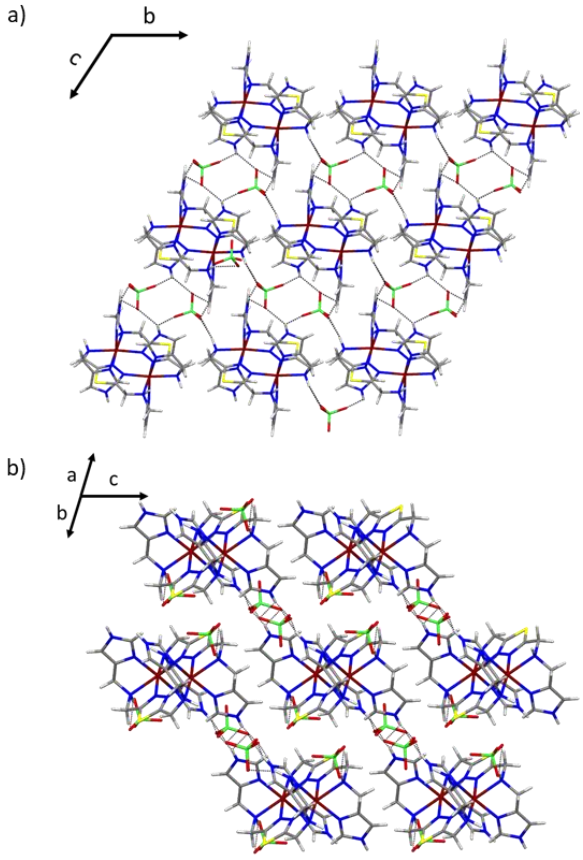

Figure S10. Crystal packing and hydrogen bonding (black dashed lines) via anions in $[Fe^{II}_2(\mathbf{I^4MTD})_2](ClO_4)_4 \cdot THF$ (**C2**·THF) at 173 K. Non-bridging counter ions and solvent molecules have been omitted for clarity. **a)** View along crystallographic *a*-axis. **b)** View along the angle bisector of the crystallographic *a*- and *b*-axis. Color code: Fe is dark red, N blue, S yellow, C grey, H white, O red and Cl green.

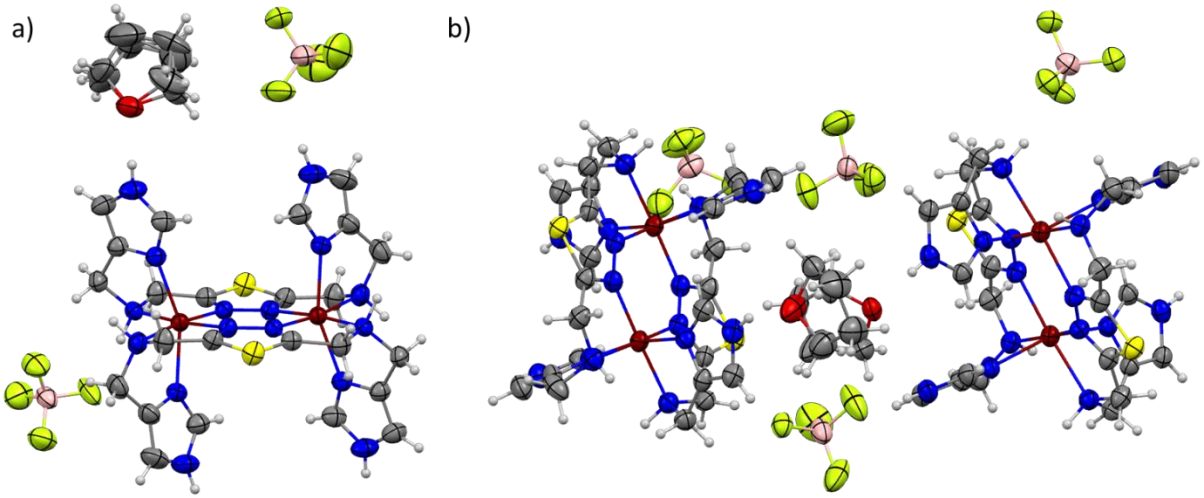

Figure S11. Molecular structure of $[Fe^{II}_2(\mathbf{I^4MTD})_2](BF_4)_4\cdot$THF(**C3**·THF) with thermal ellipsoids at **a)** 200 K and **b)** 100 K. Color code: Fe is dark red, N blue, S yellow, C grey, H white, O red, B pink and F light green.

Table S1: Crystallographic parameters for all discussed crystal structures of **C1 – C3**.

	C1·solvents (@173 K)	**C2**·THF (@173 K)	**C3**·THF (@100 K)	**C3**·THF (@200 K)
formula	C28 H32 F12 Fe2 N16 O12 S6	C28 H40 Cl4 Fe2 N16 O17 S2	C64 H96 B8 F32 Fe4 N32 O4 S4	C128 H192 B16 F64 Fe8 N64 O8 S8
molar weigth [g/mol]	1316.75	1190.38	2423.84	4847.68
crystal system	monoclinic	triclinic	monoclinic	orthorombic
space group	C2/c	P-1	$P2_1/c$	Pbca
a/Å	19.7359(6)	10.3301(9)	23.2819(9)	19.1991(3)
b/Å	12.3918(2)	11.0779(10)	18.9278(6)	10.6968(2)
c/Å	23.0394(7)	11.5540(9)	10.8273(4)	24.2411(5)
α/°	90	116.252(6)	90	90
β/°	110.176(2)	90.726(7)	93.334(3)	90
γ/°	90	107.913(7)	90	90
V/Å^3	5288.8(3)	1111.07(18)	4763.2(3)	4978.37(16)
Z	4	1	2	1
T/K	173(2)	173(2)	100(2)	200(2)
$\rho_{calcd.}$ [g/cm^3]	1.654	1.779	1.69	1.617
μ [mm^{-1}]	0.895	1.077	0.812	0.777
R(int)	0.0313	0.0177	0.0488	0.0317
S	1.058	1.057	1.053	1.082
R1 (l > 2σ (l))	0.0511	0.0455	0.1316	0.0432
wR2 (all data)	0.1438	0.124	0.3981	0.1402

3.7.5 Magnetic Data

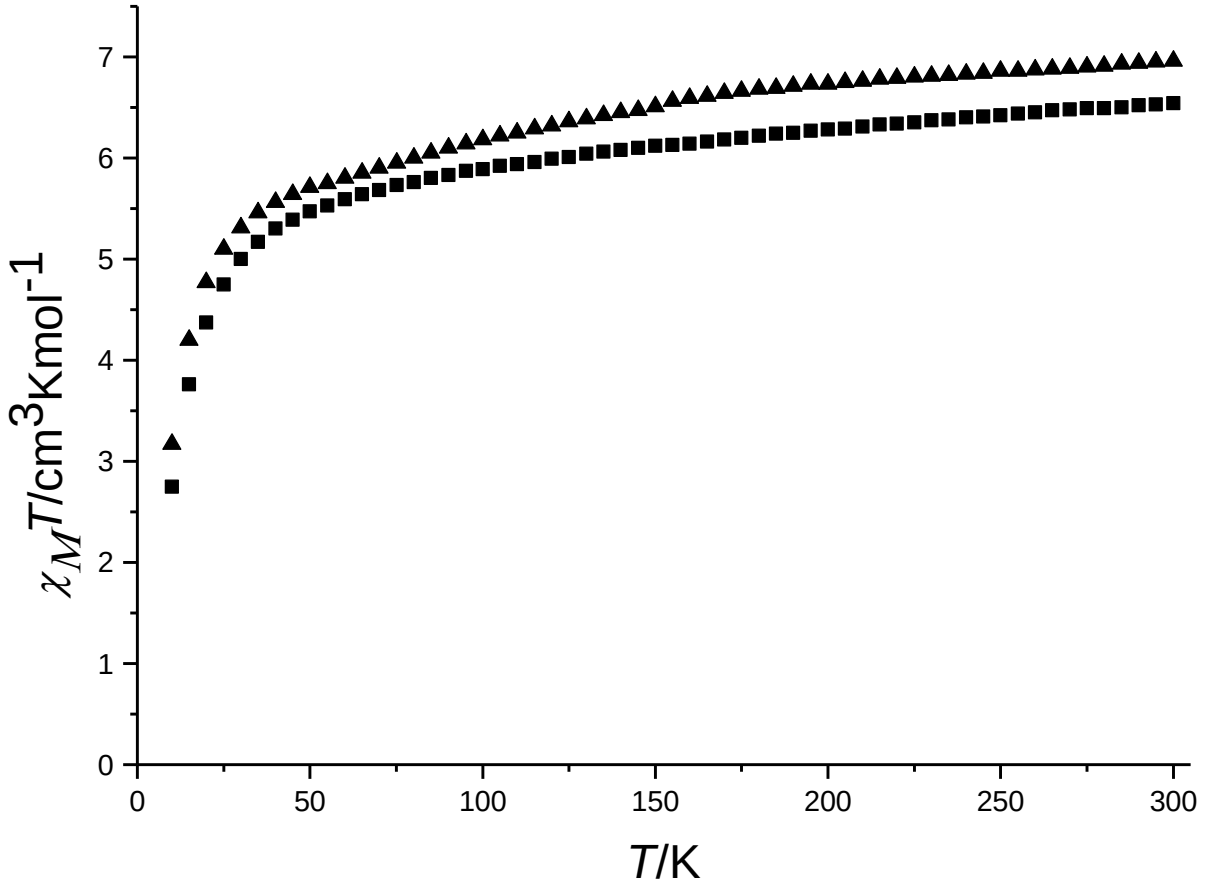

Figure S12. $\chi_M T$ vs T data for the dried compounds **C1** (squares) and **C2** (triangles). The data are given per dinuclear iron(II) molecule.

4. First Cobalt(II) Spin Crossover Compound with N_4S_2-Donorset

This chapter covers the synthesis and characterization of the novel bis-tridentate **PSTD** (2,5-bis[(2-pyridylmethyl)thio]methyl-1,3,4-thiadiazole) ligand. Although the ligand was synthesized to generate dinuclear complexes, only mononuclear complexes were obtained. While the Fe(II) complex stays in the LS over the whole measured temperature region, the Co(II) shows a gradual SCO behavior. The properties were investigated with the help of single-crystal structure analysis and magnetic susceptibility measurements. The results are presented as scientific article previously published in *Molecules*. Reprinted with the permission from:

F. Fürmeyer, D. Münzberg, L. M. Carrella, E. Rentschler, *Molecules* **2020**, *25*(4), 855.
DOI: 10.3390/molecules25040855.

Author contribution.
Fabian Fürmeyer designed the synthesis. Together with Danny Münzberg, who was supervised by him during the bachelor thesis, he synthesized and characterized the ligands and complexes. The magnetic data was gathered and analyzed by Fabian Fürmeyer. Luca M. Carrella performed the single-crystal X-ray structure measurement and refined the data. The manuscript was written by Fabian Fürmeyer and improved with the help of Luca M. Carrella and Eva Rentschler. Finally, Eva Rentschler had the overall supervision in the interpretation of the data throughout the manuscript process. All authors have read and agreed to the published version of the manuscript.

‘First Cobalt(II) Spin Crossover Compound with N_4S_2-Donorset’

Fabian Fürmeyer, Danny Münzberg, Luca M. Carrella and Eva Rentschler *

Department of Chemistry, Johannes Gutenberg University Mainz, 55128 Mainz, Germany; fuermeyer@uni-mainz.de (F.F.); dmuenzbe@students.uni-mainz.de (D.M.); carrella@uni-mainz.de (L.M.C.)
***** Correspondence: rentschler@uni-mainz.de; Tel.: +49-613-1392-5491

Received: 30 January 2020; Accepted: 11 February 2020; Published: 14 February 2020

Keywords: spin crossover; iron(II); cobalt(II); N_4S_2-donorset; 1,3,4-thiadiazole, magnetism

4.1 Graphical Abstract

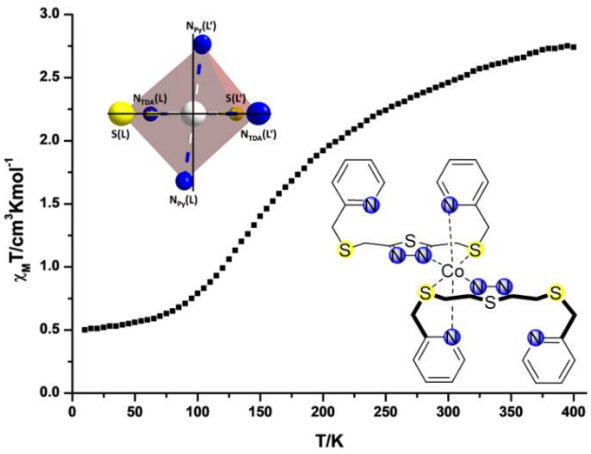

4.2 Abstract

Herein we report the synthesis and characterization of a novel bis-tridentate 1,3,4-thiadiazole ligand (**L** = 2,5-bis[(2-pyridylmethyl)thio]methyl-1,3,4-thiadiazole). Two new mononuclear complexes of the type $[M^{II}(\mathbf{L})_2](ClO_4)_2$ (with M = Fe^{II} (**C1**) and Co^{II} (**C2**)) have been synthesized, containing the new ligand (**L**). In both complexes the metal centers are coordinated by an N4S2-donorset and each of the two ligands is donating to the metal ion with just one of the tridentate pockets. The iron(II) complex (**C1**) is in the low spin [LS] state below room temperature and shows an increase in the magnetic moment only above 300 K. In contrast, the cobalt(II) complex (**C2**) shows a gradual spin crossover (SCO) with $T_{1/2}$ = 175 K. To our knowledge, this is the first cobalt(II) SCO complex with an N_4S_2-coordination.

4.3 Introduction

Switching metal complexes between two different electronic states, high spin [HS] and low spin [LS], by external stimuli such as temperature, light irradiation or pressure is known as spin crossover (SCO). Due to the molecular bistability and the associated change in the optical and magnetic properties upon switching, these compounds can possibly be used in memory storages, displays and sensors [1–8]. However, abruptness of the property changes and the occurrence of a thermal hysteresis is necessary for future applications. Both depend on the cooperative interactions between the metal centers in the solid state. 'Intermolecularly', the cooperativity can be enhanced by hydrogen bonding or π-π-stacking interactions between the complexes. 'Intramolecularly', in polynuclear complexes, the spin-bearing metal centers can be bridged via organic ligands, leading to close proximity and a stronger communication of these metal centers [5,9–13]. Although SCO coordination polymers often show large thermal hysteresis [14,15], research on discrete polynuclear, and in particular in dinuclear SCO systems recently increased because the latter have better reproducibility and easier characterization. The dimeric structural motif as the simplest and smallest model for investigating intramolecular cooperative interactions also offers potential access to three states ([HS-HS], [HS-LS] and [LS-LS]) [4,16,17]. However, the design of ligands that simultaneously act as a bridge and induce a suitable ligand field is a difficult task.

Our group recently reported on the synthesis and characterization of symmetrical dinuclear iron(II) compounds with bridging ligands based on the 1,3,4-oxadiazole as well as on the 1,3,4-thiadiazole backbone [18–20]. For the thiadiazole-based ligand 2,5-bis[(2-pyridylmethyl)amino]methyl-1,3,4-thiadiazole with pyridyl donor sidearms, the complexes are in the [LS-LS] state at low temperatures and show a gradual but incomplete spin crossover only above room temperature [19]. Inspired by the fruitful work of *S. Brooker et al.* [21], we herein report the modification of the previous reported ligand [19] by replacing the amino for thioether linkages. The longer C-S bonds compared to the C-N bonds give greater flexibility of the ligand, and thus, should enable the population of the [HS-LS] and/or the [HS-HS] state at elevated temperatures. However, rather than obtaining the dimeric $[Fe_2(\mu\text{-}\mathbf{L})_2]^{4+}$ complex cation, we exclusively isolated two new mononuclear complexes $[M^{II}(\mathbf{L})_2](ClO_4)_2$ (with M = Fe^{II} (**C1**) and Co^{II} (**C2**) and **L** = 2,5-bis[(2-pyridylmethyl)thio]methyl-1,3,4-thiadiazole). While the iron(II) complex (**C1**) remains in the [LS] state as well, the cobalt(II) complex shows a gradual SCO.

4.4 Results and Discussion

4.4.1 Synthesis

The synthesis of the ligand is presented in Scheme 1. We have previously reported the preparation of 2,5-bis(chloromethyl)-1,3,4-thiadiazole (**1**) [19]. Thioacetic acid S-pyridine-2-ylmethylester (**2**) was synthesized as described in literature [21]. Finally, the ligand (**L** = 2,5-bis[(2-pyridylmethyl)thio]methyl-1,3,4-thiadiazole) was obtained according to

[21] by treating **2** with sodium ethanolate and thereafter reacting with **1** in a nucleophilic substitution.

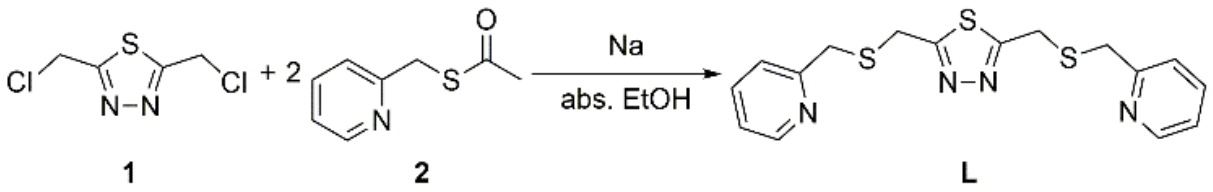

Scheme 1: Synthesis of the Ligand (**L**) starting from 2,5-bis(chloromethyl)-1,3,4-thiadiazole (**1**).

The iron(II) and cobalt(II) complexes, $[M^{II}(\mathbf{L})_2](ClO_4)_2$, have been synthesized in a stochiometric reaction of the ligand (**L**) with the corresponding perchlorate salt ($Fe(ClO_4)_2 \cdot xH_2O$ and $Co(ClO_4)_2 \cdot 6H_2O$) in methanol. The compounds were obtained as single crystals (**C1** and **C2**) suitable for X-ray diffraction experiments via slow evaporation of the complex solutions. The iron(II) complex reaction was performed under nitrogen atmosphere and by using absolute methanol. The dried complexes are stable to air, no oxidation was observed.

4.4.2 Variable Temperature Magnetic Susceptibility Measurements

Variable temperature magnetic susceptibility measurements were carried on dried samples in the temperature range of 300–400 K for **C1** and of 10–400 K for **C2** in an applied magnetic field of 1000 Oe (0.1 T) and with a scan rate of 1.5 K/min. The temperature-dependent magnetic susceptibility date of the samples **C1** and **C2** are shown in Figure 1. **C1** shows a $\chi_M T$ value of 0.15 cm^3Kmol^{-1} at 300 K accounting for a diamagnetic iron(II) ion in the [LS] state. Also, the structural data obtained by X-ray crystallography at 173 K (described below) confirms an LS state of the iron(II) indicating that no spin crossover occurs until 300 K. Raising the temperature to 400 K, the $\chi_M T$ value slightly increases to 0.36 cm^3Kmol^{-1}. Although this rise is no evidence of a spin crossover, it is at least a strong indication. The diamagnetic nature of **C1** at room temperature is further confirmed by the 1H-NMR spectra of the complex, shown along with that of the ligand in Figure S3 in the supporting information.
At low temperature, compound **C2** shows a $\chi_M T$ value of 0.47 cm^3Kmol^{-1}, which accounts for a cobalt(II) ion in the [LS] state in accordance with the single X-ray structure analysis at 120 K. With increasing temperature, the $\chi_M T$ product remains almost constant until 100 K, then raises up to 2.20 cm^3Kmol^{-1} at 250 K. This is explained by a gradual spin transition of the complex from [LS] to [HS] with a transition temperature $T_{1/2}$ of 175 K. No magnetic hysteresis is observed. In fact, when using a cooling/heating rate of 1.5 K/min, the $\chi_M T$ vs. T curves for the heating or cooling mode cannot be distinguished. The $\chi_M T$ values for [LS] and [HS] cobalt(II) are slightly higher than the calculated ones ([LS] = 0.38 cm^3Kmol^{-1} and [HS] = 1.88 cm^3Kmol^{-1}) using the spin-only formalism. This is expected because the spin-only formalism does not take into account orbit angular momentum contribution.

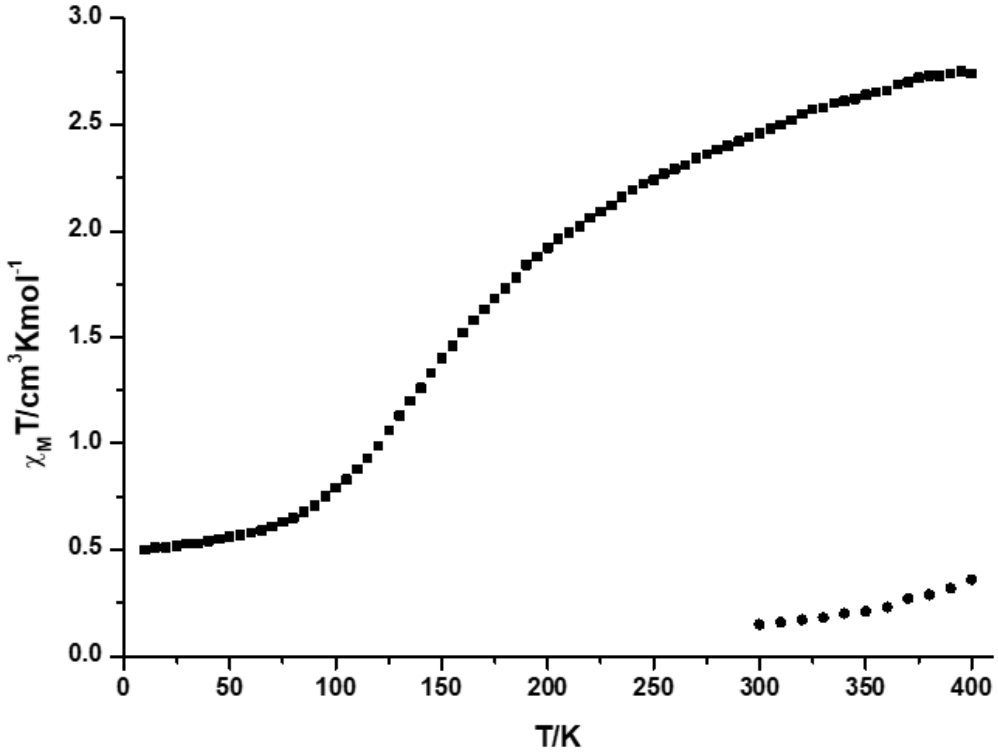

Figure 1. $\chi_M T$ vs. T data for the compounds **C1** (dots) and **C2** (squares). The Data is given per molecule.

It is known from literature that cobalt(II) complexes with N-donor ligands, which form with iron(II) only [LS] complexes, might show SCO and is well studied for terpyridine complexes [2,4,22]. However, to the best of our knowledge, the cobalt(II) complex reported here is the only one showing this phenomena with Co(II) in a N4S2 coordination.

4.4.3 Crystal Structures

The complex $[Fe^{II}(\mathbf{L})_2](ClO_4)_2$ (**C1**) crystallizes in the monoclinic space group $P2_1/c$ at 173 K. The crystal structure of complex $[Co^{II}(\mathbf{L})_2](ClO_4)_2$ (**C2**) was measured at two different temperatures (120 K and 250 K) to confirm the spin crossover phenomenon. For both temperatures, the monoclinic space group is $P2_1/c$. In all three structures, **C1** (@173 K) and **C2** (@120 K) and **C2** (@250 K) the complex cation consists of one metal ion and two ligand molecules, showing pseudo centrosymmetry as sketched in Figure 2. Each ligand contributes with one of the tridentateN_2S binding pockets to the N_4S_2 octahedral coordination sphere. The second potentially donating binding pocket is not coordinating.

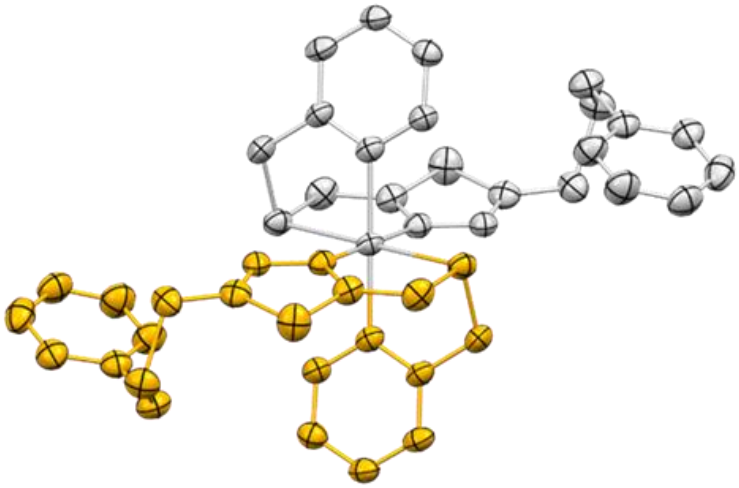

Figure 2. Sketch of the pseudo centrosymmetry of the complex cation representative for all three structures of **C1** and **C2**.

For all complex cations (**C1** and **C2** at both temperatures), the *cis*-angles within the donor atoms of one ligand (N_{TDA}(**L**,**L'**)-M-N_{Py}(**L**,**L'**), N_{TDA}(**L**,**L'**)-M-S(**L**,**L'**) and N_{Py}(**L**,**L'**)-M-S(**L**,**L'**), Figure 3) are ranging from 83° to 85°, while the *cis*-angles between the donor atoms of the different ligands (N_{TDA}(**L**)-M-N_{Py}(**L'**), N_{TDA}(**L**)-M-S(**L'**) and N_{Py}(**L**)-M-S(**L'**) and vice versa) are ranging from 95° to 97°. This results in *trans*-angles (N_{TDA}(**L**)-M-N_{TDA}(**L'**), N_{Py}(**L**)-M-N_{Py}(**L'**) and S(**L**)-M-S(**L'**)) of almost 180° and in a slightly distorted octahedral coordination for the metal centers, in which the axis N_{Py}(**L**)-M-N_{Py}(**L'**) is inclined around 5–6° from the ideal geometry (black lines) towards the ligands due to the strain within the ligand backbone.

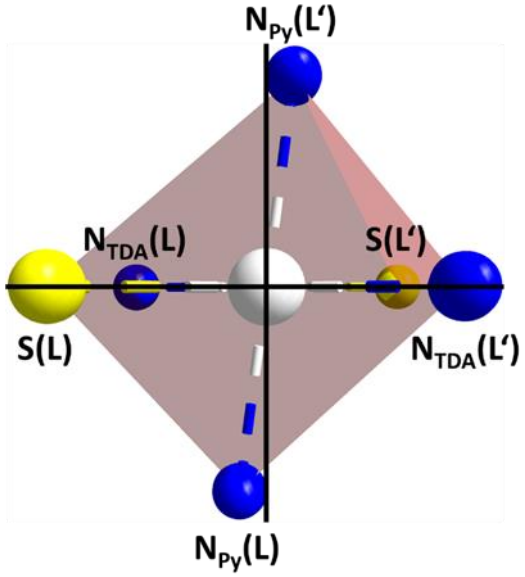

Figure 3. Coordination octahedron for the metal(II) ion of **C1** and **C2**.

The crystal structures further compromise two perchlorate anions to counterbalance the charge. All the complexes crystallize without any solvent molecules, which allows to investigate dried crystalline samples.
The average Fe-N bond length of 1.990 Å and Fe-S bond length of 2.264 Å in **C1** (@173 K) are in accordance with those reported in literature and account for an iron(II) ion in the [LS] state [23–29]. Figure S7 shows the crystal structure/asymmetric unit of **C1** (@173 K). Detailed information on bond lengths and angles for **C1** and **C2** are summarized in Table 1.

Table 1. Selected bond lengths [Å] and bond angles [°] for the compounds $[Fe^{II}(\mathbf{L})_2](ClO_4)_2$ (**C1**) and $[Co^{II}(\mathbf{L})_2](ClO_4)_2$ (**C2**).

Selected Parameters [a]	**C1** (@173 K)	**C2** (@120 K)	**C2** (@250 K)
M-N_{TDA}(**L**)	1.967(1)	1.979(4)	2.057(2)
M-N_{Py}(**L**)	2.014(1)	2.019(4)	2.075(2)
M-N_{TDA}(**L'**)	1.964(1)	1.981(4)	
M-N_{Py}(**L'**)	2.016(1)	2.027(4)	
M-S(**L**)	2.263(1)	2.472(2)	2.479(1)
M-S(**L'**)	2.264(1)	2.470(2)	
cis N_{TDA}-M-N_{Py}	84.1–95.9	84.6–95.6	85.1, 94.1
cis N_{TDA}-M-S	85.3–94.8	82.9–97.4	83.8, 96.2
cis N_{Py}-M-S	84.8–95.2	83.2–96.7	82.8, 97.2
av. *trans* X-M-X	179.8	179.6	180.0

[a] N_{TDA} = N donor atom on thiadiazole; N_{Py} = N donor atom pyridine; X = S, N_{TDA} or N_{Py} donor atom.

For **C2** (@250 K), the average Co-N bond length of 2.066 Å, as well as the average Co-S bond length of 2.479 Å indicate a [HS] cobalt(II) ion [30–36]. Cooling to 120 K results in a spin crossover from the [HS] to the [LS] state for the cobalt(II) center as shown by magnetic data. The average Co-N distance decreases to from 2.066 Å to 2.002 Å, which is in accordance with literature [37–39]. The shortening of the Co-N bond is explained by the decrease of electron density in the antibonding d-orbitals from $t_{2g}^5e_g^{*2}$in the [HS] state to $t_{2g}^6e_g^{*1}$ in the [LS] state. Notably, the average Co-S distance remains about the same (2.479 Å @250 K and 2.472 Å @120 K) upon changing the electronic state of the cobalt(II) ion. This is explained by the Jahn-Teller distortion expected for a d^7-Co(II) ion in [LS] state, with four short Co-N bonds in equatorial plane and two long 'axial' Co-S bonds. Upon cooling down the transition from [HS] to [LS] also affects the counter ion. Ordering of one of the perchlorate anions in the crystal structure results in a phase change. While at 250 K only half of the complex is in the asymmetric unit, the entire complex cation is found at 120 K. This is accompanied by a doubling of the cell volume from 1990 Å3 (@250 K) to 3874 Å3 (@120 K) (see Figure 4 and Figures S8 and S9 in ESI).

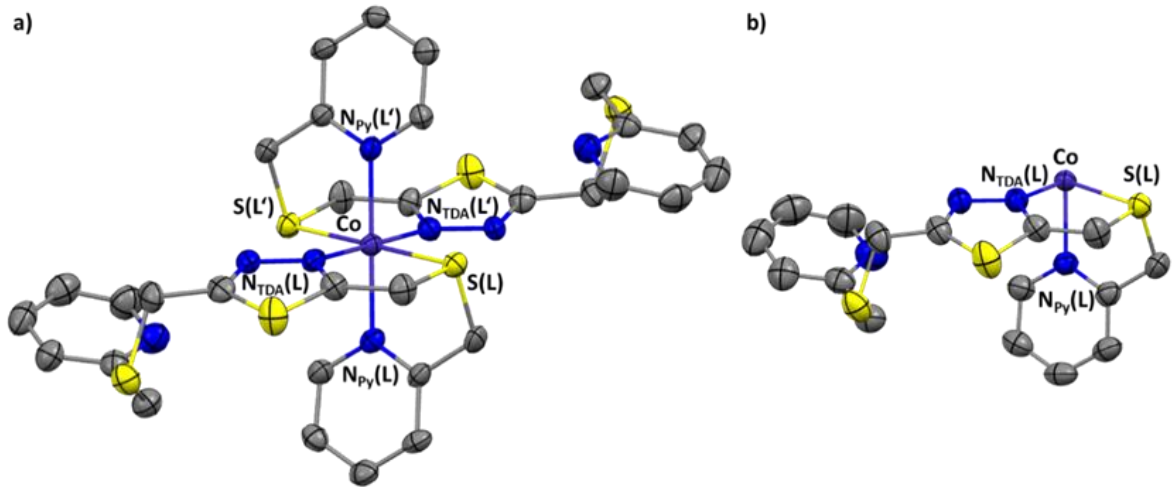

Figure 4. Crystal structures of the complex cations of **C2** (asymmetric unit) with thermal ellipsoids at (**a**) 120 K and (**b**) 250 K. Hydrogens, solvent molecules ions have been omitted for clarity. Color code: Co is dark blue, N blue, S yellow, and C grey.

When comparing our findings with the dinuclear structures obtained by *S. Brooker et al*. [21], the question arises, why the use of our new ligand (**L**) results in mononuclear complexes? In the dimeric complexes of *S. Brooker et al*. two iron(II) ions are coordinated by two ligand molecules, thus each iron(II) center has a N_4S_2 coordination sphere, and the two sulphur donor atoms are coordinating cis to each other as depicted in Figure 5a. Changing the 1,3,4-triazole to the 1,3,4-thiadiazole as the backbone in the thioether-linked ligand leads to a different strain and to closer proximity of the sulphur donor atoms in the *cis* coordination, which is highly unfavorable. Hence, we exclusively obtained mononuclear complexes in which the sulphur donor atoms are coordinating *trans* to each other (Figure 5b). Similar findings were previously reported for iron(II) complexes with 1,3,4-triazole or 1,3,4-thiadiazole bridging ligands with an amino–rather than a thioether-linker group. Here, changing from the 1,3,4-triazole to the 1,3,4-thiadiazole backbone results in a larger angle between the intraligand donor atoms and the amine donor atoms of the two facing ligands, which are in closer proximity compared to the ones in the 1,3,4-triazole [19].

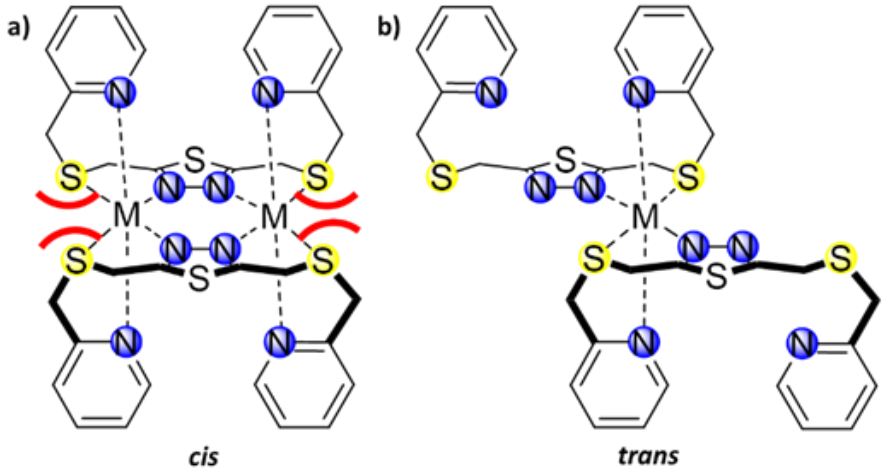

Figure 5. Schematic representation of the two coordination modes for the sulphur donor atoms. (**a**) The sulphur donor atoms are coordinating *cis* to each other, which is necessary to obtain dinuclear complexes. (**b**) The sulphur donor atoms are coordinating *trans* to each other, as described for the mononuclear complexes herein.

4.5 Materials and Methods

4.5.1 General Methods and Materials

All chemicals were purchased from Alfa Aesar, Deutero, Fisher Chemicals, TCI, Sigma-Aldrich and Acros Organics and used without further purification. Absolute solvents were dried according to known procedures and used freshly distilled [40]. The NMR spectra were recorded at room temperature with a Bruker Avance DSX 400 and analyzed with the program MestReNova [41]. Magnetic susceptibility measurements were performed on a Quantum Design SQUID magnetometer MPMSXL in a temperature range between 10–400 K with an applied field of 1 kOe. ESI and FD mass spectra as well as elemental analysis (C,H and N) were measured at the microanalytical laboratories of the Johannes Gutenberg University Mainz. X-ray diffraction data were collected at 173 K with STOE STADIVARI and at 120 K with a STOE IPDS 2T at the Johannes Gutenberg University Mainz. The structures were solved with ShelXT [42] and refined with ShelXL [43] implemented in the program Olex2 [44]. **Caution!** The prepared perchlorate complexes are potentially explosive. Even though no explosions occurred, only small amounts should be prepared and handled with care.

4.5.2 Ligand Synthesis

2,5-Bis(chloromethyl)-1,3,4-thiadiazole (**1**) and thioacetic acid S-pyridine-2-ylmethyl ester (**2**) were prepared as described in literature [19,21]. The ligand (**L** = 2,5 bis[(2-pyridylmethyl)thio]methyl-1,3,4-thiadiazole) was synthesized based on similar nucleophilic substitution to that found in literature [21].

2,5-Bis[(2-pyridylmethyl)thio]methyl-1,3,4-thiadiazole (L)

Sodium (1.17 g, 51.0 mmol, 8.5 equiv.) was dissolved in ethanol (100 mL) at 0 °C and under nitrogen atmosphere. Thioacetic acid S-pyridine-2-ylmethyl ester (**2**) (2.11 g, 12.6 mmol, 2.1 equiv.) in ethanol (25 mL) was added, and the resulting brown solution was stirred at 0 °C for 30 min. Afterwards, 2,5-bis(chloromethyl)-1,3,4-thiadiazole (**1**) (1.10 g, 6.0 mmol, 1.0 equiv.) in ethanol (25 mL) was added at room temperature and the orange suspension was stirred for 17 h. The reaction mixture was poured into water (150 mL) and ethanol was removed under reduced pressure. The resulting suspension was extracted three times with dichloromethane (50 mL). The combined organic extracts were washed with brine (30 mL) and dried over magnesium sulfate. The solvent was removed under reduced pressure and the resulting crude product was purified by column chromatography (SiO_2, dichloromethane/methanol 49:1) to give the pure product as brown oil. Yield: 1.54 g (4.28 mmol, 71.4%). ^{1}H-NMR (400 MHz, $CDCl_3$, 25 °C): δ = 8.57–8.51 (m, 2H, *H*-6, py), 7.67–7.54 (m, 2H, *H*-4, py), 7.32–7.29 (m, 2H, *H*-3, py), 7.19–7.05 (m, 2H, *H*-5, py), 4.01 (s, 4H, C*H*$_2$, tda), 3.84 (s, 4H, C*H*$_2$, py) ppm. ^{13}C-NMR (100 MHz, $CDCl_3$, 25 °C): δ = 170.7 (*C*, tda), 157.3 (*C*-1, py), 149.9 (*C*-6, py), 136.8 (*C*-4, py), 123.5 (*C*-3, py), 122.3 (*C*-5, py), 37.8 (*C*H$_2$, py), 29.5 (*C*H$_2$, tda) ppm. ESI-MS (MeOH): *m*/*z* (%) = 361.06 (96) [(M+H)$^+$], 383.04 (32) [(M+Na)$^+$], 743.10 (100) [(2M+Na)$^+$]. Elemental analysis ($C_{16}H_{16}N_4S_3$): calcd. C 53.30, H 4.47, N 15.54; found C 52.83, H 4.58, N 15.78.

4.5.3 Complex Synthesis

To a yellow solution of the ligand (**L**) (0.1 mmol) in methanol (3 mL), an almost colorless solution of the corresponding metal(II) salt [0.1 mmol, $Fe(ClO_4)_2 \cdot xH2O$ or $Co(ClO_4)_2 \cdot 6H2O$] in methanol (3 mL) was added. Slow evaporation at room temperature of the obtained orange solutions resulted in the formation of crystals suitable for X-ray diffraction after several hours. The iron(II) complex was prepared under nitrogen atmosphere and by using dried solvents.

$[Fe^{II}(L)_2](ClO_4)_2 \cdot$(C1)

$Fe(ClO_4)_2 \cdot xH_2O$ (27 mg) and 2,5-bis[(2-pyridylmethyl)thio]methyl-1,3,4-thiadiazole (**L**, 36 mg) were used to obtain **C1** (38 mg, 77.9%) as dark brown crystals suitable for X-ray diffraction. $C_{32}H_{32}Cl_2FeN_8O_8S_6$ $[Fe^{II}(\mathbf{L})_2](ClO_4)_2$ (975.76): calc. C 39.39, H 3.31, N 11.48; found (after drying in vacuo) C 38.96, H 3.03, N 11.28.

$[Co^{II}(L)_2](ClO_4)_2 \cdot$(C2)

$Co(ClO_4)_2 \cdot 6H_2O$ (36 mg) and 2,5-bis[(2-pyridylmethyl)thio]methyl-1,3,4-thiadiazole (**L**, 37 mg) were used to obtain **C2** (48 mg, 98.1%) as orange crystals suitable for X-ray diffraction. $C_{32}H_{32}Cl_2CoN_8O_8S_6$ $[Co^{II}(\mathbf{L})_2](ClO_4)_2$ (978.85): calc. C 39.27, H 3.30, N 11.45; found (after drying in vacuo) C 39.00, H 3.21, N 11.34.

4.6 Conclusion

In conclusion, using the novel bis-tridentate 1,3,4-thiadiazole ligand (**L** = 2,5-bis[(2-pyridylmethyl)thio]methyl-1,3,4-thiadiazole), we were able to synthesize and characterize two new complexes $[M^{II}(\mathbf{L})_2](ClO_4)_2$ (with M = Fe^{II} (**C1**) and Co^{II} (**C2**)). Due to the fact that mononuclear complexes were obtained, rather than the expected dinuclear ones, we assume this is due to the fact that the sulphur donor atoms of the thioether linkages are large compared to the nitrogen donor atoms of the amino linkages reported by Herold [19]. Thus, the cis-coordination of two Sulphur donor atoms is unfavorable. The magnetic data of the mononuclear compound together with the single-crystal X-ray structure analysis reveal a [LS] state for the iron(II) complex (**C1**) until 400 K. The cobalt(II) compound (**C2**) shows a gradual SCO between 100 K and 250 K from [LS] to [HS] state with a transition temperature T1/2 of 175 K. To our knowledge, this is the first cobalt(II) complex with a N_4S_2 coordination environment, showing SCO behavior, that has been reported.

Supplementary Materials: The following are available online at http://www.mdpi.com/1420-3049/25/4/855/s1, Figure S1: ^{1}H-NMR of 2,5-bis[(2-pyridylmethyl)thio]methyl-1,3,4-thiadiazole (L). Figure S2: ^{13}C-NMR of 2,5-bis[(2-pyridineylmethyl)thio]methyl-1,3,4-thiadiazole (L). Figure S3: Comparison of the ^{1}H-spectra of a) $[Fe^{II}(L)_2](ClO_4)_2$ (C1) and b) 2,5-Bis{[(pyridine-2-ylmethyl)-thio]-methyl}-1,3,4-thiadiazole (L). Figure S4: Mass spectrum of 2,5-bis[(2-pyridylmethyl)thio]methyl-1,3,4-thiadiazole (L). Figure S5: IR spectrum of dried $[Fe^{II}(L)2](ClO4)2$ (C1). Figure S6: IR spectrum of dried $[Co^{II}(L)_2](ClO_4)_2$ (C2). Figure S7: Molecular structure of $[Fe^{II}(L)_2](ClO_4)_2$ (C1) with thermal ellipsoids at 173 K. b) Asymmetric unit without hydrogens, solvent molecules and counter ions. Color code: Fe dark red, N blue, S yellow, C grey, H light grey, Cl green and O red. Figure S8: Molecular structure of $[Co^{II}(L)_2](ClO_4)_2$ (C2) with thermal ellipsoids at 120 K. Color code: Co dark blue, N blue, S yellow, C grey, H white, Cl green and O red. Figure S9: Molecular structure of $[Co^{II}(L)_2](ClO_4)_2$ (C2) with thermal ellipsoids at 250 K. Color code: Co dark blue, N blue, S yellow, C grey, H white, Cl green and O red. Table S1: Crystallographic parameters for the discussed crystal structures of C1 and C2. CCDC 1980403 for **C1** (@173 K), 1980401 for **C2** (@120 K), 1980402 for **C2** (@250 K) contain the supplementary crystallographic data for this paper. These data can be obtained free of charge from The Cambridge Crystallographic Data Centre via www.ccdc.cam.ac.uk/data_request/cif.

Author Contribution: F.F. conceived the synthesis. With the help of D.M. he synthesized and characterized the ligand and the complexes. F.F. gathered and analyzed the magnetic data. L.M.C. performed the X-ray acquisition data and analysis. E.R. supervised the project. F.F., L.M.C. and E.R. contributed to the manuscript. All authors have read and agreed to the published version of the manuscript.

Funding: This research received no external funding.

Acknowledgments: Dieter Schollmeyer is kindly acknowledged for collecting the crystal structure data of **C2** (@120 K).

Conflicts of Interest: The authors declare no conflict of interest.

4.7 References

1. Gütlich, P.; Goodwin, H.A. (Eds.) *Spin Crossover in Transition Metal Compounds I*; Topics in Current Chemistry; Springer: Berlin/Heidelberg, Germany, 2004; Volume 233, ISBN 978-3-540-40394-4.
2. Gütlich, P.; Goodwin, H.A. *Spin Crossover in Transition Metal Compounds II*; Topics in Current Chemistry; Springer: Berlin/Heidelberg, Germany, 2004; Volume 234, ISBN 978-3-540-40396-8.
3. Gütlich, P.; Goodwin, H.A. *Spin Crossover in Transition Metal Compounds III*; Topics in Current Chemistry; Springer: Berlin/Heidelberg, Germany, 2004; Volume 235, ISBN 978-3-540-40395-1.
4. Halcrow, M.A. (Ed.) *Spin-Crossover Materials*; JohnWiley & Sons Ltd.: Oxford, UK, 2013; ISBN 9781118519301.
5. Kahn, O. Spin-Transition Polymers: From Molecular Materials toward Memory Devices. *Science* **1998**, *279*, 44–48.
6. Gütlich, P.; Hauser, A.; Spiering, H. Thermisch und optisch schaltbare Eisen(II)-Komplexe. *Angew. Chem.* **1994**, *106*, 2109–2141.
7. Dhers, S.; Feltham, H.L.C.; Brooker, S. A toolbox of building blocks, linkers and crystallisation methods used to generate single-chain magnets. *Coord. Chem. Rev.* **2015**, *296*, 24–44.
8. Brooker, S. Spin crossover with thermal hysteresis: Practicalities and lessons learnt. *Chem. Soc. Rev.* **2015**, *44*, 2880–2892.
9. Barrios, L.A.; Peyrecave-Lleixà, E.; Craig, G.A.; Roubeau, O.; Teat, S.J.; Aromí, G. Unusual Crystal Packing in a Family of [Fe{2,6-bis(pyrazol-3-yl)pyridine} 2] 2+ Compounds and the Effect on the Occurrence of Spin Crossover and Its Cooperative Character. *Eur. J. Inorg. Chem.* **2014**, *2014*, 6013–6021.
10. Halcrow, M.A. Structure:function relationships in molecular spin-crossover complexes. *Chem. Soc. Rev.* **2011**, *40*, 4119–4142.
11. Gütlich, P.; Goodwin, H.A. Spin Crossover—An Overall Perspective. In *Spin Crossover in Transition Metal Compounds I*; Springer: Berlin/Heidelberg, Germany, 2004; Volume 1, pp. 1–47.
12. Roberts, T.D.; Little, M.A.; Kershaw Cook, L.J.; Halcrow, M.A. Iron(ii) complexes of 2,6-di(1H-pyrazol-3-yl)-pyridine derivatives with hydrogen bonding and sterically bulky substituents. *Dalt. Trans.* **2014**, *43*, 7577–7588.
13. Bauer, W.; Lochenie, C.; Weber, B. Synthesis and characterization of 1D iron(ii) spin crossover coordination polymers with hysteresis. *Dalt. Trans.* **2014**, *43*, 1990–1999.

14. Kahn, O.; Kröber, J.; Jay, C. Spin Transition Molecular Materials for displays and data recording. *Adv*. *Mater*. **1992**, *4*, 718–728.
15. Kröber, J.; Codjovi, E.; Kahn, O.; Grolière, F.; Jay, C. A Spin Transition System with a Thermal Hysteresis at Room Temperature. *J*. *Am*. *Chem*. *Soc*. **1993**, *115*, 9810–9811.
16. Real, J.A.; Gaspar, A.B.; Niel, V.; Muñoz, M.C. Communication between iron(II) building blocks in cooperative spin transition phenomena. *Coord*. *Chem*. *Rev*. **2003**, *236*, 121–141.
17. Real, J.A.; Gaspar, A.B.; Muñoz, M.C. Thermal, pressure and light switchable spin-crossover materials. *Dalt*. *Trans*. **2005**, 2062–2079.
18. Köhler, C.; Rentschler, E. The First 1,3,4-Oxadiazole Based Dinuclear Iron(II) Complexes Showing Spin Crossover Behavior with Hysteresis. *Eur*. *J*. *Inorg*. *Chem*. **2016**, *2016*, 1955–1960.
19. Herold, C.F.; Carrella, L.M.; Rentschler, E. A Family of Dinuclear Iron(II) SCO Compounds Based on a 1,3,4-Thiadiazole Bridging Ligand. *Eur*. *J*. *Inorg*. *Chem*. **2015**, *2015*, 3632–3636.
20. Fürmeyer, F.; Carrella, L.M.; Ksenofontov, V.; Möller, A.; Rentschler, E. Phase trapping in multistep spin crossover compound. *Inorg*. *Chem*. **2020**, in press.
21. Hogue, R.W.; Feltham, H.L.C.; Miller, R.G.; Brooker, S. Spin Crossover in Dinuclear N 4 S 2 Iron(II) Thioether–Triazole Complexes: Access to [HS-HS], [HS-LS], and [LS-LS] States. *Inorg*. *Chem*. **2016**, *55*, 4152–4165.
22. Hayami, S.; Komatsu, Y.; Shimizu, T.; Kamihata, H.; Lee, Y.H. Spin-crossover in cobalt(II) compounds containing terpyridine and its derivatives. *Coord*. *Chem*. *Rev*. **2011**, *255*, 1981–1990.
23. Grillo, A.V.; Gahan, R.L.; Hanson, R.G.; Stranger, R.; Hambley, W.T.; Murray, S.K.; Moubaraki, B.; Cashion, D.J. Iron(III) and iron(II) complexes of 1-thia-4{,}7-diazacyclononane ([9]aneN2S) and 1{,}4-dithia-7-azacyclononane ([9]aneNS2). X-Ray structural analyses{,} magnetic susceptibility{,} Mössbauer{,} EPR and electronic spectroscopy. *J*. *Chem*. *Soc*., *Dalt*. *Trans*. **1998**, 2341–2348.
24. England, J.; Gondhia, R.; Bigorra-Lopez, L.; Petersen, A.R.; White, A.J.P.; Britovsek, G.J.P. Towards robust alkane oxidation catalysts: Electronic variations in non-heme iron(ii) complexes and their effect in catalytic alkane oxidation. Dalt. Trans. **2009**, 27, 5319–5334.
25. Reus, C.; Ruth, K.; Tüllmann, S.; Bolte, M.; Lerner, H.-W.; Weber, B.; Holthausen, M.C.; Wagner, M. Synthesis, Molecular Structure, and Physical Properties of the Complexes [{PhB(pz)2(CH2SMe)}2M] (M = MnII, FeII; pz = pyrazol-1-yl) Containing a Novel [N,N,S]-Heteroscorpionate Ligand. *Eur*. *J*. *Inorg*. *Chem*. **2011**, *2011*, 1709–1718.
26. Lennartson, A.; Bond, A.D.; Piligkos, S.; McKenzie, C.J. Four-Site Cooperative Spin Crossover in a Mononuclear Fe II Complex. *Angew*. *Chem*. **2012**, *124*, 11211–11214.
27. Lennartson, A.; Southon, P.; Sciortino, N.F.; Kepert, C.J.; Frandsen, C.; Mørup, S.; Piligkos, S.; McKenzie, C.J. Reversible Guest Binding in a Non-Porous Fe II Coordination Polymer Host Toggles Spin Crossover. *Chem*.*-A Eur*. *J*. **2015**, *21*, 16066–16072.

28. Arroyave, A.; Lennartson, A.; Dragulescu-Andrasi, A.; Pedersen, K.S.; Piligkos, S.; Stoian, S.A.; Greer, S.M.; Pak, C.; Hietsoi, O.; Phan, H.; et al. Spin Crossover in Fe(II) Complexes with N4 S 2 Coordination. *Inorg*. *Chem*. **2016**, *55*, 5904–5913.
29. Yergeshbayeva, S.; Hrudka, J.J.; Lengyel, J.; Erkasov, R.; Stoian, S.A.; Dragulescu-Andrasi, A.; Shatruk, M. Heteroleptic Fe(II) Complexes with N 4 S 2 Coordination as a Platform for Designing Spin-Crossover Materials. *Inorg*. *Chem*. **2017**, *56*, 11096–11103.
30. Wei, Z.; Xie, X.; Zhao, J.; Huang, L.; Liu, X. A novel hexadentate ligand and its complexes with divalent metal ions (Zinc, Copper, and Cobalt): Synthesis, characterization, and electrochemical investigation. *Inorg*. *Chim*. *Acta* **2012**, *387*, 277–282.
31. Funkemeier, D.; Mattes, R. Synthesis and structural studies of copper(II), nickel(II) and cobalt(II) complexes of a 14-membered trans-N2S2 dibenzo macrocycle with two pendant pyridylmethyl groups. *J*. *Chem*. *Soc*. *Dalton Trans*. **1993**, 1313–1319.
32. Mohamadou, A.; Jubert, C.; Barbier, J.-P. Novel cobalt(II) complexes with pyridyl/ether or pyridyl/thioether ligands. The conversion of pyridyl/thioether cobalt(II) complex to pyridyl/sulfinato cobalt(III) compound. *Inorg*. *Chim*. *Acta* **2006**, *359*, 273–282.
33. Magwa, N.P.; Hosten, E.; Watkins, G.M.; Tshentu, Z.R. The coordination and extractive chemistry of the later 3d transition metals with bis ((1 R -benzimidazol-2-yl)methyl)sulfide. *J*. *Coord*. *Chem*. **2013**, *66*, 114–125.
34. Hogue, R.W.; Schott, O.; Hanan, G.S.; Brooker, S. A Smorgasbord of 17 Cobalt Complexes Active for Photocatalytic Hydrogen Evolution. *Chem*. *A Eur*. *J*. **2018**, *24*, 9820–9832.
35. Wu, H.; Yang, Z.; Wang, F.; Peng, H.; Zhang, H.; Wang, C.; Wang, K. V-shaped ligand 1,3-bis(1-ethylbenzimidazol-2-yl)-2-thiapropane and manganese(II), cobalt(II) and copper(II) complexes: Synthesis, crystal structure, DNA-binding properties and antioxidant activities. *J*. *Photochem*. *Photobiol*. *B Biol*. **2015**, *148*, 252–261.
36. Pandiyan, T.; Hernández, J.G.; Medina, N.T.; Bernés, S. Geometrical isomers of bis(benzimidazol-2-ylethyl)sulfide)cobalt(II) diperchlorates: Synthesis, structure, spectra and redox behavior of pink-[Co(bbes)2](ClO4)2 and blue-[Co(bbes)2](ClO4)2. *Inorg*. *Chim*. *Acta* **2004**, *357*, 2570–2578.
37. Singh, A.K.; Mukherjee, R. Cobalt(ii) and cobalt(iii) complexes of thioether-containing hexadentate pyrazine amide ligands: C–S bond cleavage and cyclometallation reaction. *J*. *Chem*. *Soc*. *Dalt*. *Trans*. **2008**, 260–270.
38. Nandi, S.; Bannerjee, D.; Datta, P.; Lu, T.H.; Slawin, A.M.Z.; Sinha, C. Cobalt-thioalkylazoimidazole complexes: Structures, spectra and redox properties. *Polyhedron* **2009**, *28*, 3519–3525.
39. Thomas, L.; Hsiung, T.; Breen, J.; Worrell, J.H. Kinetics of substitution and isomerization of nitrite ion on aqua(7-methyl-4, 10-dithia-1, 7, 13- triazatridecane)cobalt(III) and the structure of the product. *J*. *Coord*. *Chem*. **1992**, *26*, 15–34.
40. Eaborn, C. Purification of Laboratory Chemicals. *J*. *Organomet*. *Chem*. **1981**.
41. Cobas, J.C.; Sardina, F.J. Nuclear magnetic resonance data processing. MestRe-C: A software package for desktop computers. *Concepts Magn*. *Reson*. **2003**, *19A*, 80–96.
42. Sheldrick, G.M. SHELXT—Integrated space-group and crystal-structure determination. *Acta Crystallogr*. *Sect*. *A Found*. *Adv*. **2015**, *71*, 3–8.

43. Sheldrick, G.M. Crystal structure refinement with SHELXL. *Acta Crystallogr*. *Sect*. *C Struct*. *Chem*. **2015**, *71*, 3–8.
44. Dolomanov, O.V.; Bourhis, L.J.; Gildea, R.J.; Howard, J.A.K.; Puschmann, H. OLEX2: A complete structure solution, refinement and analysis program. *J*. *Appl*. *Crystallogr*. **2009**, *42*, 339–341.

Sample Availability: Not available.

4.8 Supporting Information

4.8.1 NMR Spectroscopy

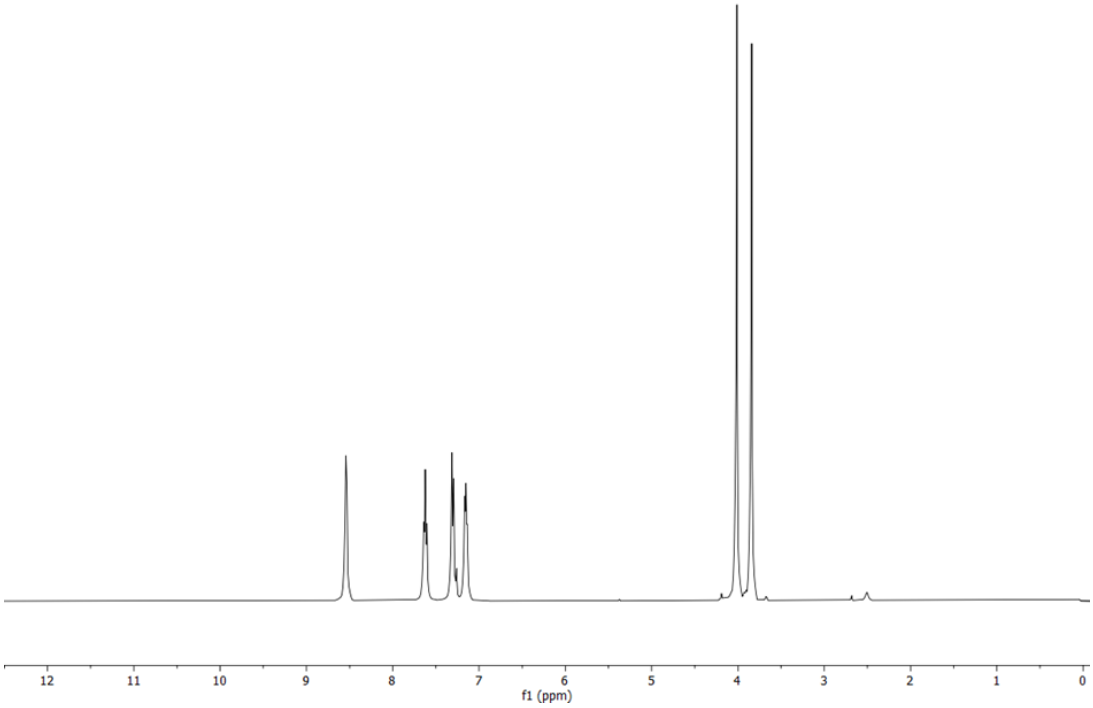

Figure S1. ^{1}H-NMR of 2,5-bis[(2-pyridylmethyl)thio]methyl-1,3,4-thiadiazole (**L**).

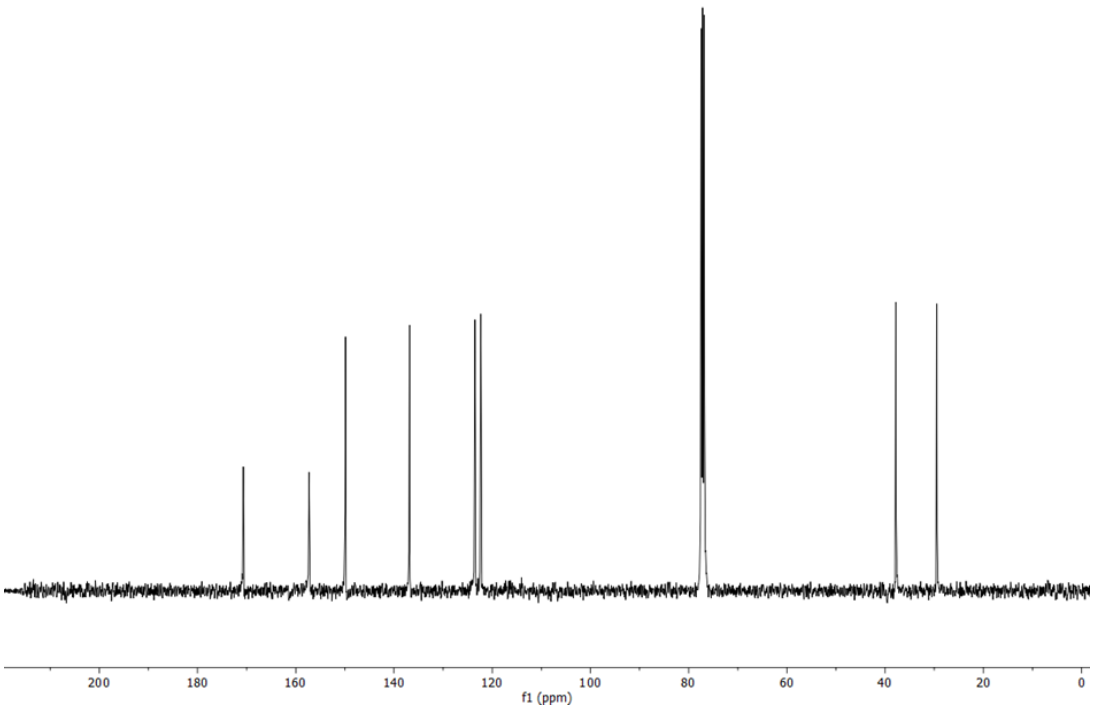

Figure S2. ^{13}C-NMR of 2,5-bis[(2-pyridylmethyl)thio]methyl-1,3,4-thiadiazole (L).

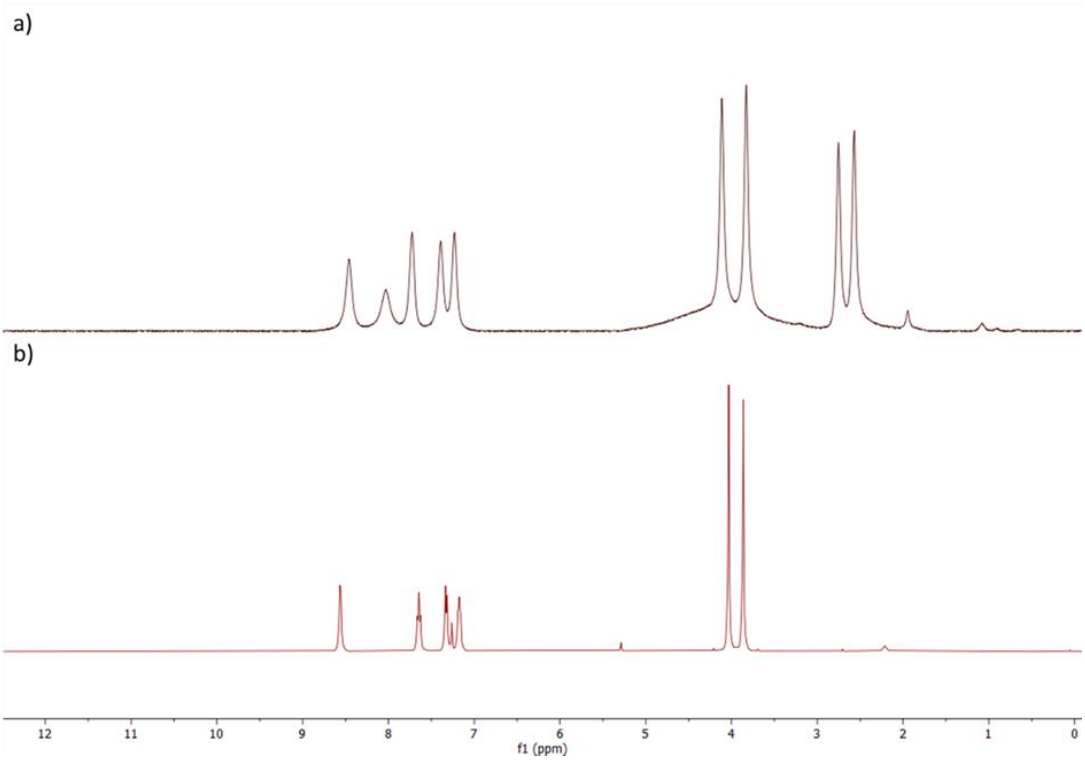

Figure S3. Comparison of the ^{1}H-NMR spectra of **a)** $[Fe^{II}(\mathbf{L})_2](ClO_4)_2$ (**C1**) in DMSO-d_6 and **b)** 2,5-bis[(2-pyridylmethyl)thio]methyl-1,3,4-thiadiazole (**L**) in $CDCl_3$.

4.8.2 Mass Spectrometry

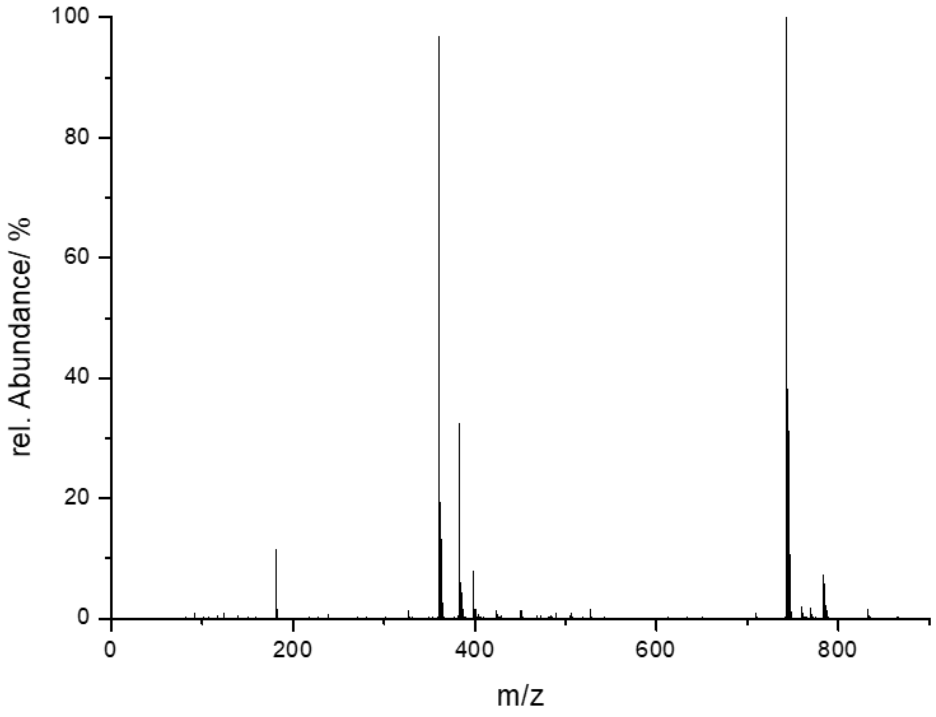

Figure S4. Mass spectrum of 2,5-bis[(2-pyridylmethyl)thio]methyl-1,3,4-thiadiazole (**L**).

4.8.3 IR Spectroscopy

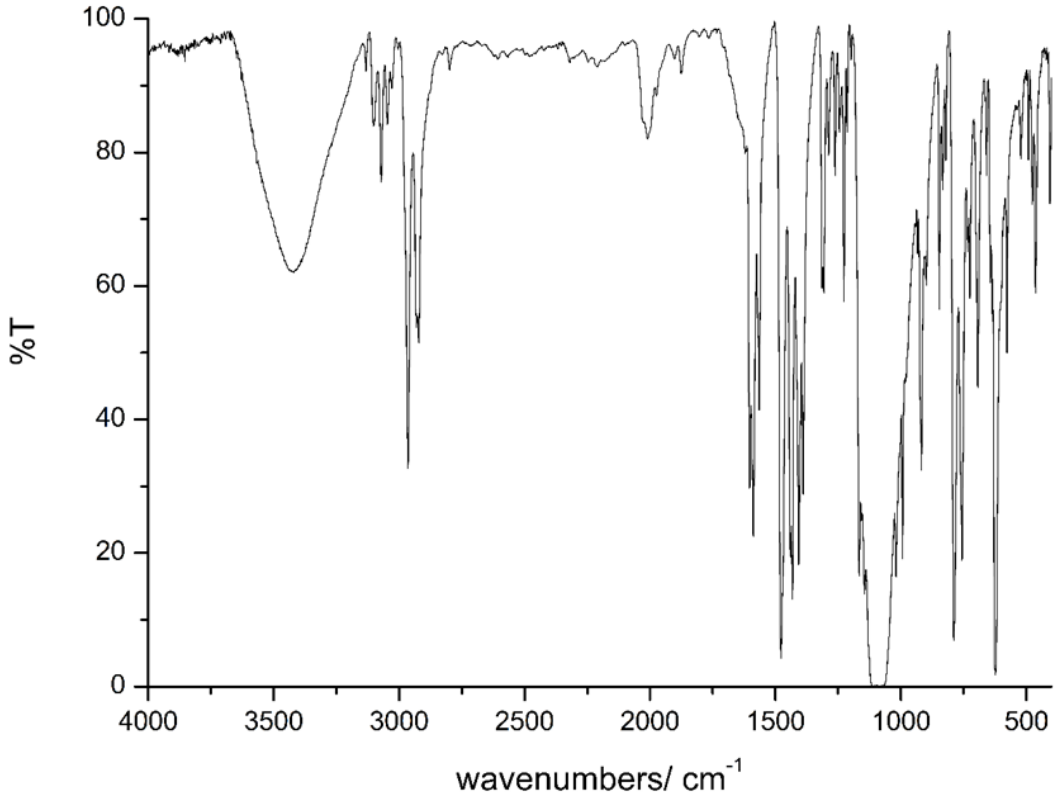

Figure S5. IR spectrum of dried $[Fe^{II}(\mathbf{L})_2](ClO_4)_2$ (**C1**).

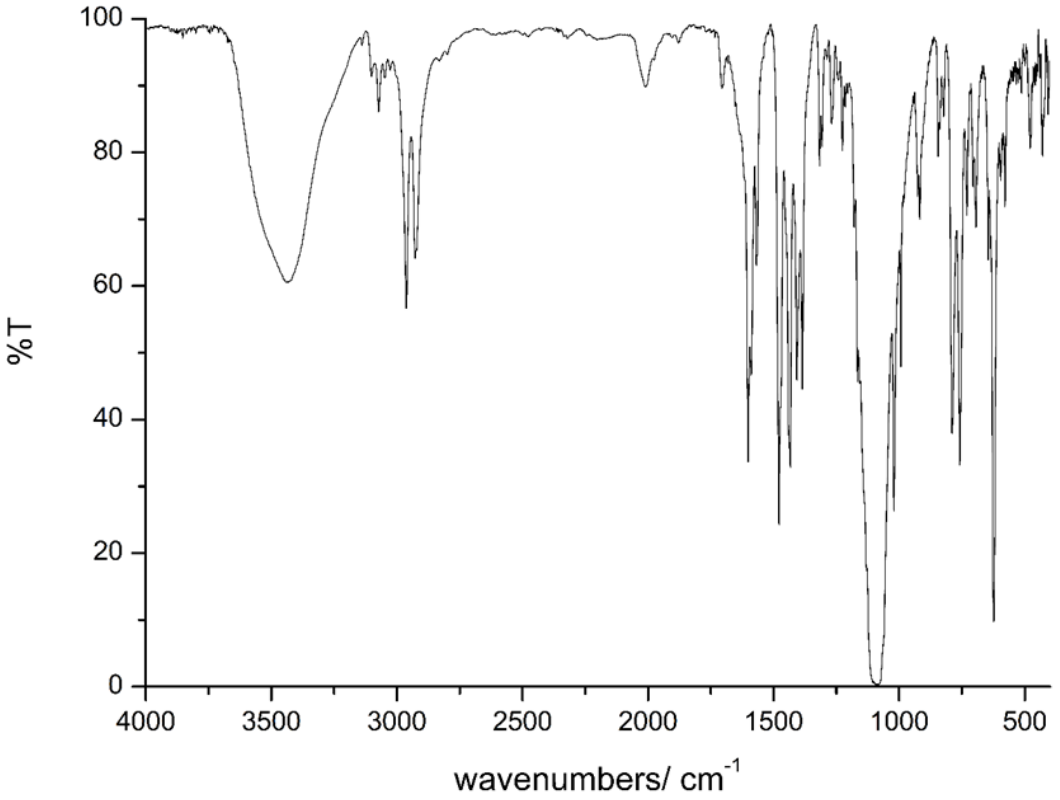

Figure S6. IR spectrum of dried $[Co^{II}(\mathbf{L})_2](ClO_4)_2$ (**C2**).

4.8.4 X-ray Diffraction Measurements

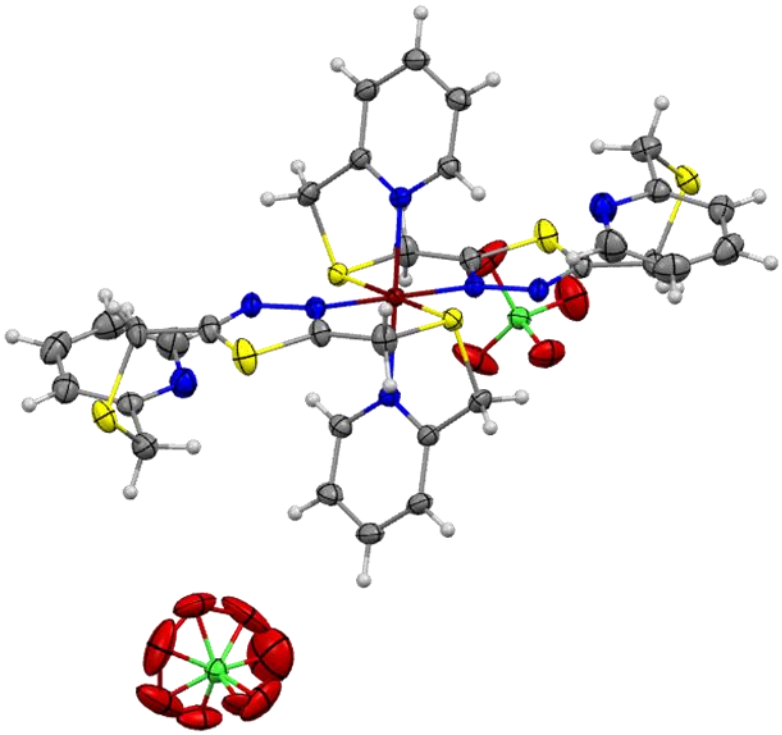

Figure S7. Molecular structure/ asymmetric unit of $[Fe^{II}(\mathbf{L})_2](ClO_4)_2$ (**C1**) with thermal ellipsoids at 173 K. Color code: Fe dark red, N blue, S yellow, C grey, H light grey, Cl green and O red.

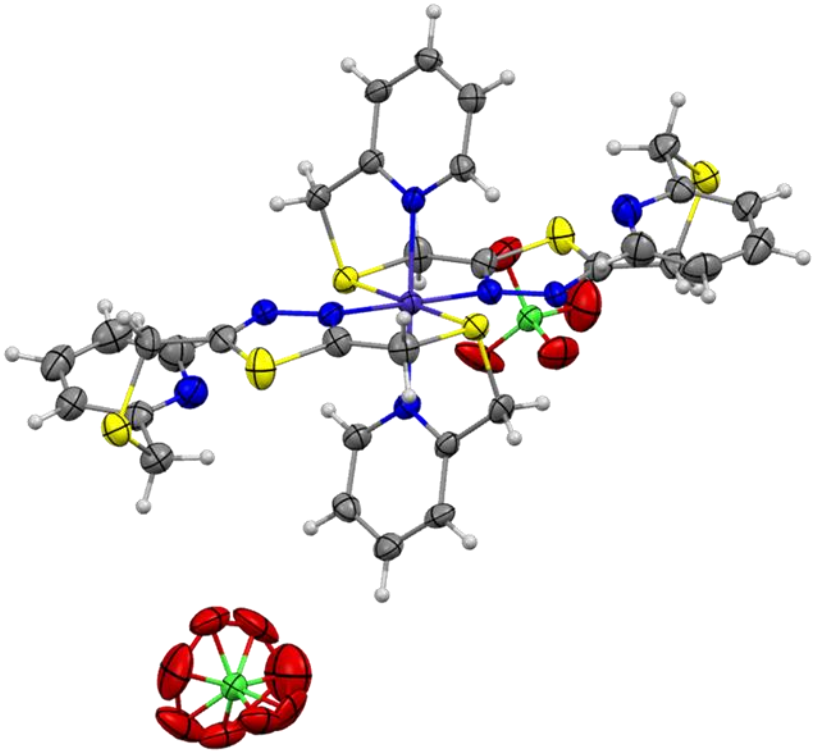

Figure S8. Molecular structure/ asymmetric unit of $[Co^{II}(\mathbf{L})_2](ClO_4)_2$ (**C2**) with thermal ellipsoids at 120 K. Color code: Co dark blue, N blue, S yellow, C grey, H white, Cl green and O red.

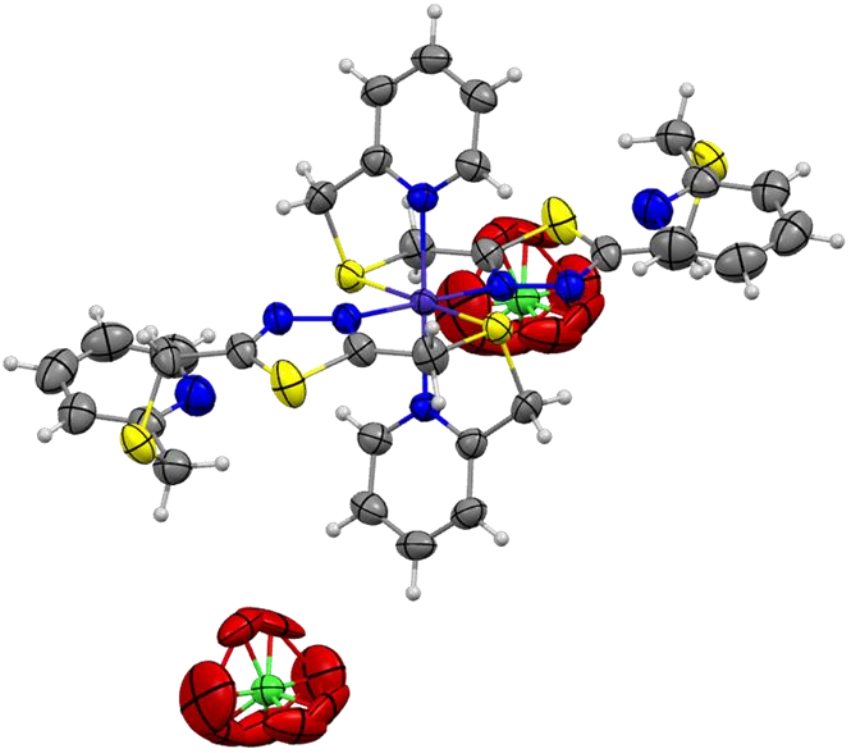

Figure S9. Molecular structure of $[Co^{II}(\mathbf{L})_2](ClO_4)_2$ (**C2**) with thermal ellipsoids at 250 K. Color code: Co dark blue, N blue, S yellow, C grey, H white, Cl green and O red.

Table S1. Crystallographic parameters for the discussed crystal structures of **C1** and **C2**.

	C1 (@173 K)	**C2** (@120 K)	**C2** (@250 K)
formula	C32 H32 Cl2 Fe N8 O8 S6	C32 H32 Cl2 Co N8 O8 S6	C32 H32 Cl2 Co N8 O8 S6
molar weigth [g/mol]	975.76	978.84	978.84
crystal system	monoclinic	monoclinic	monoclinic
space group	$P2_1/c$	$P2_1/c$	$P2_1/c$
a/Å	10.7228(2)	10.6468(8)	10.7440(13)
b/Å	18.2829(5)	18.1665(10)	18.254(2)
c/Å	20.0702(4)	20.2042(15)	10.9219(15)
α/°	90	90	90
β/°	97.117(2)	97.583(6)	111.706(10)
γ/°	90	90	90
V/Å^3	3904.3(2)	3873.6(5)	1990.24(4)
Z	4	4	2
T/K	173(2)	120(2)	250(2)
$\rho_{calcd.}$ [g/cm^3]	1.660	1.678	1.633
μ [mm^{-1}]	0.906	0.967	0.941
R(int)	0.0226	0.0487	0.0272
S	1.041	1.032	1.097
R1 (l > 2σ (l))	0.0365	0.1484	0.0944
wR2 (all data)	0.1033	0.1802	0.1148

5. Summary and Outlook

The present work aimed at the synthesis and characterization of new dinuclear Fe(II) SCO complexes using novel bis-tridentate 1,3,4-thiadiazole bridging ligands. Previous results of our group showed the potential of the 1,3,4-thiadiazol bridging motif to synthesize symmetric bimetallic Fe(II) complexes which show SCO behavior. However, the complexes based on the **PMTD** (2,5-bis[(2-pyridylmethyl)amino]methyl-1,3,4-thiadiazole) ligand are found to be in the [LS-LS] state independent of the non-coordinating anions, showing only a gradual and incomplete spin transition to the [HS-LS] state above room temperature. In this work, the **PMTD** ligand was modified with the goal to thermally access all three spin states [HS-HS], [HS-LS] and [LS-LS]. In total, four new ligands were synthesized, allowing for nine dinuclear complexes and two mononuclear complexes, which were characterized with a variety of complementary techniques including single-crystal X-ray structure analysis, temperature-dependent magnetic susceptibility measurements and Mössbauer spectroscopy. The presented complexes nicely demonstrate the various intra- and intermolecular influences that may alter the sensitive SCO properties.

One modification was the substitution of the pyridyl side arms of the **PMTD** ligand for the pentamerous N-donating heterocycles imidazole and thiazole, resulting in the two novel **I^{2}MTD** (2,5-bis[(1*H*-imidazol-2-ylmethyl)amino]methyl-1,3,4-thiadiazole) and **TMTD** (2,5-bis[(thiazol-2-ylmethyl)amino]methyl-1,3,4-thiadiazole) ligands. The five-membered rings enlarge the biting angle between the amine linkages and the heterocycle and thus form a larger coordination pocket for the metal ions, possibly stabilizing the [HS-HS] state at elevated temperatures due to the longer metal ion-donor atom bond lengths. The variation of the second heteroatom within the heteroaromatic rings in the side arms gives the possibility to subtle modify the electronic and structural properties of the ligand and thus the ligand field strength Δ_O. Both ligands were used to generate a series of three new dinuclear Fe(II) complexes $[Fe^{II}_2(\mathbf{I^2MTD}/\mathbf{TMTD})_2](X)_4\cdot$solvents (with X = BF_4^-, ClO_4^- or $F_3CSO_3^-$). The **I^{2}MTD** based complexes are in the [HS-HS] state at room temperature and remain in this state until very low temperatures independent from the different counter ions as shown by magnetic data and X-ray structure analysis. On the other hand, all three bimetallic Fe(II) compounds using the **TMTD** ligand show different SCO behavior. By means of single-crystal X-ray structure analysis, this is attributed to the different intermolecular distances between the complex cations along the formed 1D chains in the solid state, originating from the various non-coordinating anions. While $[Fe^{II}_2(\mathbf{TMTD})_2](F_3CSO_3)_4\cdot$2MeCN with the largest counter ion shows a gradual one-step spin transition from the [LS-LS] directly to the [HS-HS] state above room temperature, $[Fe^{II}_2(\mathbf{TMTD})_2](BF_4)_4\cdot$3MeCN with the smallest counter ion undergoes a rather abrupt SCO around 200 K from the [HS-LS] to the [HS-HS] as revealed by temperature-dependent magnetic susceptibility measurements. However, two-step SCO behavior was achieved for

$[Fe^{II}_2(\mathbf{TMTD})_2](ClO_4)_4 \cdot 3MeCN$ with two separate spin transition from the [LS-LS] to the [HS-LS] state at around 100 K and from the [HS-LS] to the [HS-HS] state at around 215 K. When slowly cooled, the SCO is accompanied by two phase transitions, allowing to unambiguously identify distinct [HS-LS] molecules in the [HS-LS] state crystallographically. On contrary, upon rapid cooling no phase transition is observable, resulting in the superposition of the HS and LS Fe(II) ions in the [HS-LS] state. Mössbauer studies could support the interesting finding that the cooling rate is crucial to detect the phase transition. This result will be of importance for further understanding and investigation of SCO compounds, since in the past it was not always be possible to elucidate whether the [HS-LS] state is displayed by a 1:1 mixture of [HS-HS] and [LS-LS] molecules or by discrete [HS-LS] molecules.

On the basis of the probed properties of the complexes with the **I^{2}MTD** ligand, the **I^{4}MTD** (2,5-bis[(1*H*-imidazol-2-ylmethyl)amino]methyl-1,3,4-thiadiazole) ligand was synthesized. The ligand was designed to alter the position of the protonated nitrogen atom in the imidazolyl side arm and thus to investigate the different intermolecular hydrogen bonding interaction pathways between the complex cations compared to the complexes based on the **I^{2}MTD** ligand. In fact, the variation of the side arm resulted in two to three dimensional hydrogen bonding networks between the complex cations and the different non-coordinating counter ion within the complex series $[Fe^{II}_2(\mathbf{I^4MTD})_2](X)_4 \cdot$solvents (with X = BF_4^-, ClO_4^- or $F_3CSO_3^-$). The complexes $[Fe^{II}_2(\mathbf{I^4MTD})_2](F_3CSO_3)_4$ Et_2O/2MeCN and $[Fe^{II}_2(\mathbf{I^4MTD})_2](ClO_4)_4 \cdot$THF show a temperature-independent [HS-HS] as proven by single-crystal structure analysis and magnetic susceptibility measurements. Interestingly, while magnetic data revealed an incomplete gradual spin transition from the [HS-HS] to the [HS-LS] state below 200 K for $[Fe^{II}_2(\mathbf{I^4MTD})_2](BF_4)_4 \cdot$THF, single-crystal structure analysis showed that the intermediate [HS-LS] spin state is a 1:1 mixture of localized [HS-HS] and [LS-LS] molecules. The distinct difference between the properties of the bulk material and the crystal structure is attributed to different solvent content, since the freshly prepared samples almost immediately lose the volatile solvent molecules and therefore crystallinity, when exposed to air. The different properties within the complexes of this series is explained by different crystal packing effects, since the local ligand field strength for the Fe(II) ions is the same for all three complexes. While the triflate and perchlorate complexes show a densely packed 3D hydrogen network or strongly intertwined 2D layers, respectively, the complex cations in the tetrafluoroborate compound are arranged in 2D layers, which are clearly separated by solvent molecules and anions. To compensate for the local volume change of the [LS-LS] dimers compared to the [HS-HS] ones after the spin transition, the stacking between the layers changes, resulting in alternating layers of solely [HS-HS] or [LS-LS] molecules for $[Fe^{II}_2(\mathbf{I^4MTD})_2](BF_4)_4 \cdot$THF.

The bridging ligand **PSTD** (2,5-bis[(2-pyridylmethyl)thio]methyl-1,3,4-thiadiazole) was synthesized to give the ligand system greater flexibility, since the C-S bonds are longer compared to the C-N bonds in the **PMTD** ligand. This should result in dinuclear Fe(II) complexes based on the **PSTD** ligand able to populate the [HS-LS] and/or the [HS-HS] state at higher temperatures. However, no dimeric Fe(II) complexes were obtained. Instead a mononuclear Fe(II) complex $[Fe^{II}(\mathbf{PSTD})_2](ClO_4)_2$ was synthesized and characterized by single-crystal X-ray structure analysis and magnetic susceptibility measurements, showing a

temperature-independent LS state over the whole measured temperature region. Since the ligand field was too strong for Fe(II), a mononuclear Co(II) complex $[Fe^{II}(\mathbf{PSTD})_2](ClO_4)_2$ was synthesized, which shows a gradual spin transition from the LS to the HS state. This was the first time SCO behavior was achieved for a Co(II) ion in N_4S_2 coordination environment. Only mononuclear compounds were obtained because the sulphur donor atoms of the thioether linkages are large compared to the nitrogen donor atom of the amino linkages. Hence, the necessary *cis*-coordination of the sulphur donor atoms to obtain bimetallic complexes is highly unfavorable.

In conclusion, the presented results show the great potential of 1,3,4-thiadiazole bridging ligands to synthesize SCO materials. Future work should focus on generating more complexes based on the **TMTD** ligand with different non-coordinating anions to further establish the correlation between the counter ion size and the SCO behavior. Furthermore, LIESST studies would be interesting to investigate the properties of $[Fe^{II}_2(\mathbf{TMTD})_2](ClO_4)_4 \cdot 3MeCN$ under light irradiation, as well as TIESST studies to gain a deeper insight into the temperature dependence of the SCO behavior.

Since the **TMTD** ligand provides the appropriate ligand field to observe SCO behavior, it would be interesting to combine the coordination pocket of the ligand with other fascinating properties in mononuclear complexes. Thus, by replacing one side arm of the ligand with other functionalities such as thiol or azide, it would be possible to click the SCO complexes with nanoparticles, polymers or surfaces via chemisorption. Particularly suitable in this respect would be gold surfaces or polymers as well as nanoparticles functionalized with alkyne or alkene functions. Suitable functionalized fluorophores could also be added to the complex via "click chemistry" to combine the SCO with luminescent properties. These modifications would be one step towards multifunctional materials.

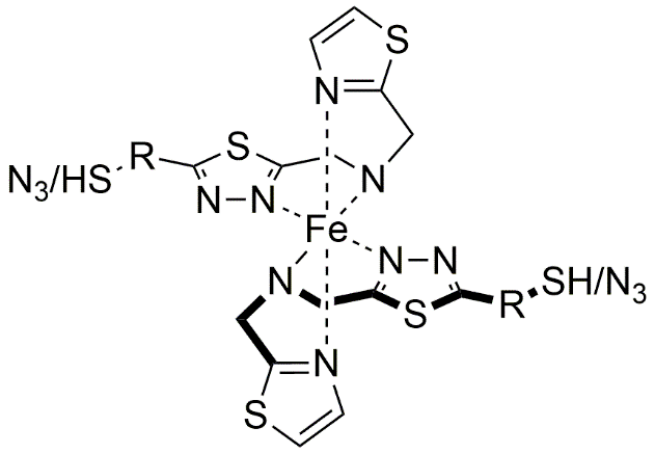

Figure 1. Sketch of a mononuclear Fe(II) complex with the coordination pocket of the **TMTD** ligand combined with further functionalities such as thiol or azide and an undefined spacer R.

Deprotonating the synthesized ligands **I^{2}MTD** and **I^{4}MTD** at the imidazolyl groups in the side arms is a perfect starting to point for new bimetallic neutral Fe(II) complexes. The deprotonation should increase the ligand field strength of the ligand, which would lead to smaller Fe-N bond length, thus stabilizing the [LS-LS] state for dimeric complexes at lower temperatures. Since there is no need for additional non-coordinating anions, hydrogen bonding are less likely to form, allowing for in depth intramolecular investigations of possible SCO properties. Additionally, neutral SCO complexes can be used to obtain thin films of switching molecules by thermal vacuum deposition, which is a key feature for future applications.

Finally, the 2,5-bis(aminomethyl)-1,3,4-thiadiazole still suits as perfect precursor for many other ligand systems, by reacting various aldehydes containing nitrogen donor heterocycles in a reductive amination reaction similar to the on described in this work. This will further establish the SCO systems based on 1,3,4-thiadiazole bridging ligands and provide a better insight of SCO properties in dinuclear complexes.

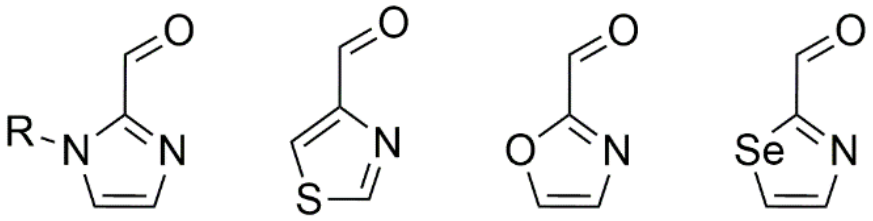

Figure 2. Possible aldehydes for new 1,3,4-thiadiazole ligand systems.

6. Experimental Section

6.1 Materials and Methods

This chapter gives more detailed information on the materials and methods that were used to synthesize and characterize the obtained compounds than the respective parts in each publication.

6.1.1 General Information

All reactions, which were carried out under exclusion of air and moisture, previously heated glassware was used. A rotary evaporator with membrane pump vacuum and a water bath with a temperature of 40 °C was used. Solids and high-boiling liquids were dried in a fine vacuum by using an oil pump.

6.1.2 Solvents and Chemicals

Unless otherwise stated, solvents with a purity level p.a., per analysi, were used for the reactions. Absolute solvents were used dried and freshly distilled according to literature methods.[1] The complex reactions with iron(II) were performed in a glovebox under nitrogen atmosphere and only dried and degassed solvents were used to prevent oxidation of iron(II) to iron(III). All other chemicals were purchased from *Alfa Aesar*, *Acros Organics*, *Fisher Chemicals*, *Sigma-Aldrich*, or *TCI Chemicals* and, unless otherwise specified, were used without further purification.

6.1.3 Chromatography

The purification with column chromatography was performed by rapid chromatography.[2] Silica gel with a particle size of 35 - 70 µm from *Acros Organics* was used as stationary phase. The reaction control was by using silica gel coated aluminium plates from *Macherey-Nagel* (Alugram SIL G/UV254). Detection was done under UV-light of the wavelength λ = 254 nm and λ = 365 nm and with the help of the following staining reagents.

- Vanillin: 1.0 g vanillin, 100 mL methanol, 12 mL acetic acid, 4 mL conc. sulfuric acid
- Ninhydrin: 0.2 g ninhydrin, 100 ml ethanol, 3 mL acetic acid

The chromatograms were immersed in the solution and then developed using a hot air blower. The mixing ratios given for the eluents refer to volume fractions.

6.1.4 NMR Spectroscopy

The samples were dissolved in deuterated solvents and the spectra were recorded at room temperature on a *Bruker* Avance DSX 400 ($\nu(^1H$ = 400.13 MHz, $\nu(^{13}C)$ = 100.61 MHz). The chemical shift (expressed in ppm) refers to the signal of the deuterated solvent used relative to tetramethylsilane as standard ($CDCl_3$ δ [ppm] = 7.26 {^{1}H}, 77.16 {^{13}C}; MeOD-d_4 δ[ppm] = 3.31 {^{1}H}, 49.00 {^{13}C}; DMSO-d_6 δ [ppm] = 2.50 {^{1}H}, 39.52 {^{13}C}).[3] The deuterated solvents were purchased from the company *Deutero*. The program MestReNova from *Mestrelab Research* was used for the evaluation.[4]

6.1.5 IR Spectroscopy

The IR spectra were measured at room temperature in the range from 4000 cm^{-1} to 400 cm^{-1} on the following instruments:

- FT/IR NICOLET 5700 from *Thermo Fisher Scientific*. The evaluation was performed with the software Omnic.
- FT/IR-4100 from *JASCO*. A small amount of the sample was homogenized with potassium bromide in a ratio of 1:10 and processed under pressure (10 t) to a pellet. The data was evaluated with the JASCO Spectra Manager software.

The diagnostic and the 8 - 12 bands with the highest intensity were given.

6.1.6 Mass Spectrometry

- FD mass spectra were recorded by the analytical department of the Institute of Inorganic Chemistry and Analytical Chemistry of the Johannes Gutenberg University in Mainz on a DFS mass spectrometer (Trace 1310) from *Thermo Fisher Scientific*.
- ESI mass spectra were recorded by the analytical department of the Institute of Organic Chemistry of the Johannes Gutenberg University in Mainz on an Agilent 6545 QTOF-MS from *Agilent*.

6.1.7 X-ray Structure Analysis

X-ray structure analysis of suitable single crystals were performed on the following instruments:

- STOE IPDS 2T, measurements executed by Dr. D[redacted] S[redacted] at the Institute of Organic Chemistry of the Johannes Gutenberg University in Mainz.
- STOE STADIVARI, measurement executed at the company [redacted] in Darmstadt.
- STOE STADIVARI, measurements executed by Dr. L[redacted] M. C[redacted] at the Institute of Inorganic Chemistry and Analytical Chemistry of the Johannes Gutenberg University in Mainz.

Further details of the measurements are given separately for each measurements in the corresponding publications or in the appendix. The crystal structures were solved with SHELXT[5] and refined with SHELXL[6] implemented in the program Olex^2.[7]

6.1.8 Magnetic Measurements

Magnetic susceptibility measurements were performed in the range of 2 to 400 K with an applied field of 1 kOe (0.1 T), unless otherwise specified, on a Quantum Design MPMSXL SQUID magnetometer. The crystalline samples were filled into a gelatine capsule and fixed inside a plastic straw. The magnetic contribution of the capsule and straw was determined experimentally and subtracted from the measured value. The molar magnetic susceptibilities χ_M were calculated using the molar masses of the compounds and taking into account the diamagnetic contribution χ_D. The diamagnetic contribution χ_D of the samples was calculated using equation 5.1. The values obtained correspond very well to the Pascal constants.[8]

$$\chi_D \sim \frac{M}{2} 10^{-6} \text{ emu mol}^{-1} \qquad (5.1)$$

6.1.9 ^{57}Mössbauer Spectroscopy

^{57}Mössbauer spectra were recorded by Dr. V[redacted] K[redacted] using a gas-flow N_2-cryostat with He-exchange gas at the Institute of Inorganic Chemistry and Analytical Chemistry of the Johannes Gutenberg University in Mainz. The Mössbauer spectrometer is operating in the velocity range from -4 to +4 mm/s (constant acceleration mode) equipped with a ^{57}Co(Rh)-source. The spectra were fitted using the Lorentzian-analysis of the program Recoil.[9]

6.1.10 Elemental Analysis

Elemental analyses (C, H, N) were performed by the analytical department of the Institute of Organic Chemistry of the Johannes Gutenberg University in Mainz using a vario EL cube element analyzer from *Elementar*.

6.2 Syntheses

This chapter contains the syntheses and characterization of precursors for the ligands reported in this work, which were not described in the publications.

6.2.1 1,2-Dichloroacetyl hydrazide

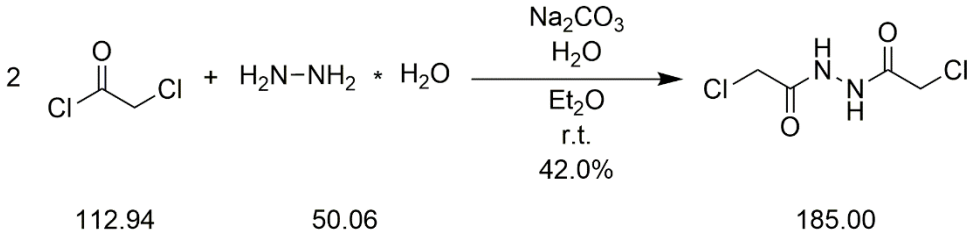

1,2-Dichloroacetyl hydrazide was synthesized by a modified procedure from literature.[10,11] Chloroacetyl chloride (31.8 mL, 0.40 mol, 1.0 equiv.) in diethyl ether (120 mL) was added dropwise to a suspension of hydrazine hydrate (20.1 g, 0.40 mol, 1.0 equiv.) in diethyl ether (60 mL), while the temperature was kept below 35 °C. The mixture was stirred for 30 minutes and afterwards water (80 mL) and sodium carbonate (42.4 g, 0.40 mol, 1.0 euqiv.) was added. After completion of the CO_2 evolution, further chloroacetyl chloride (31.8 mL, 0.40 mol, 1.0 equiv.) in diethyl ether (60 mL) was added dropwise. The suspension was stirred over night at room temperature and afterwards filtrated. The precipitate was washed with diethyl ether and recrystallized from ethyl acetate to give the product as colorless solid. Yield: 31.1 g (0.17 mol, 42.0%). ^{1}H- NMR (400 MHz, $CDCl_3$, 25 °C): δ = 10.48 (s, 2H, N*H*), 4.15 (s, 4H, CH_2) ppm. FD-MS (MeOH): *m*/*z* (%) = 183.73 (86) [M^+], 185.70 (53) [M^+].

6.2.2 2,5-Bis(chloromethyl)-1,3,4-thiadiazole

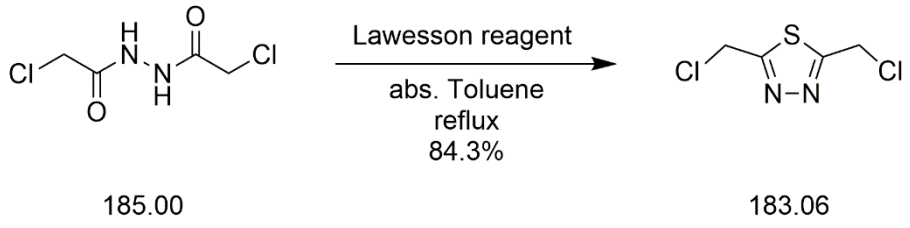

2,5-Bis(chloromethyl)-1,3,4-thiadiazole was synthesized following the procedure from literature.[11,12] 1,2-Dichloroacteyl hydrazide (6.0 g, 32.4 mmol, 1.0 equiv.) and Lawesson reagent (15.8 g, 38.9 mmol, 1.3 equiv.) was dissolved in absolute toluene and refluxed over night. The solvent was removed under reduced pressure and the yellow residue was purified by

column chromatography (SiO_2). The side products were eluated with dichloromethane and then the product was isolated as yellow oil with a solvent mixture of dichloromethane and diethyl ether (9:1). Yield: 5.0 g (27.3 mmol, 84.3%). ^{1}H- NMR (400 MHz, $CDCl_3$, 25 °C): δ = 4.96 (s, 4H, CH_2) ppm. ^{13}C NMR (100 MHz, $CDCl_3$, 25 °C): δ = 169.4 (*C*, TDA), 38.4 (*C*H_2). ESI-MS ($CHCl_3$): *m*/*z* (%) = 182.95 (100) [M+H$^+$], 184.95 (68) [M+H$^+$], 186.95 (11) [M+H$^+$].

6.2.3 Thioacetic acid S-pyridine-2-ylmethyl ester

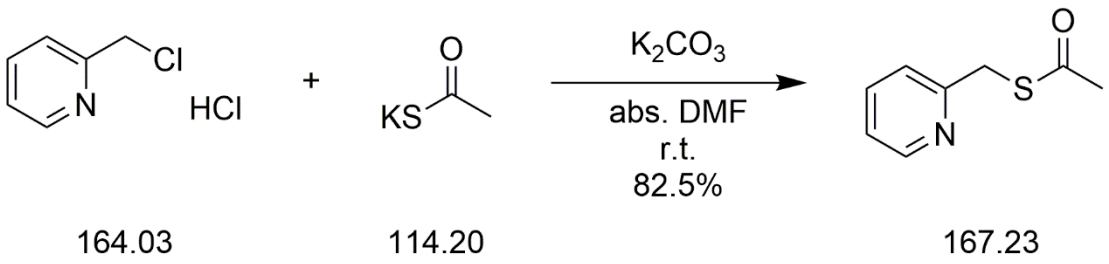

Thioacetic acid S-pyridine-2-ylmethyl ester was synthesized following the procedure from literature.[13] Potassium thioacetate (2.30 g, 20.1 mmol, 1.1 equiv.), potassium carbonate (5.06 g, 36.6 mmol, 2.0 equiv.) and 2-picolylchlorid hydrochloride (3.00 g, 18.3 mmol, 1.0 equiv.) were dissolved in absolute dimethylformamide (40 mL). The solution was stirred over night at room temperature under nitrogen atmosphere and exclusion from light. The mixture was filtered and the solvent was removed under reduced pressure. The residue was dissolved in toluene (3 x 40 mL) and the solvent was removed under reduced to remove the dimethylformamide. The resulting oil was dissolved in dichloromethane (40 mL), washed with water (2 x 40 mL) and brine (40 mL) and dried over magnesium sulfate. After removal of the solvent under reduced pressure, the pure product was obtained as brown oil. Yield: 2.53 g (15.1 mmol, 82.5%). ^{1}H- NMR (400 MHz, $CDCl_3$, 25 °C): δ = 8.52 – 8.50 (m, 1H, *H*-6, py), 7.63 – 7.57 (m, 1H, *H*-4, py), 7.36 – 7.31 (m, 1H, *H*-3, py), 7.17 – 7.10 (m, 1H, *H*-5, py), 4.23 (s, 2H, CH_2), 2.34 (s, 3H, CH_3). ESI-MS (MeOH): *m*/*z* (%) = 168.05 (100) [M+H$^+$].

6.3 References

[1] C. Eaborn, J. Organomet. Chem. 1981, 213, C62.
[2] W. C. Still, M. Kahn, A. Mitra, J. Org. Chem. 1978, 43, 2923–2925.
[3] G. R. Fulmer, A. J. M. Miller, N. H. Sherden, H. E. Gottlieb, A. Nudelman, B. M. Stoltz, J. E. Bercaw, K. I. Goldberg, Organometallics 2010, 29, 2176–2179.
[4] J. C. Cobas, F. J. Sardina, Concepts Magn. Reson. 2003, 19A, 80–96.
[5] G. M. Sheldrick, Acta Crystallogr. Sect. A Found. Adv. 2015, 71, 3–8.
[6] G. M. Sheldrick, Acta Crystallogr. Sect. C Struct. Chem. 2015, 71, 3–8.
[7] O. V. Dolomanov, L. J. Bourhis, R. J. Gildea, J. A. K. Howard, H. Puschmann, J. Appl. Crystallogr. 2009, 42, 339–341.
[8] G. A. Bain, J. F. Berry, J. Chem. Educ. 2008, 85, 532–536.
[9] K. Lagarec, D. Rancourt, Recoil User Manual -- Mossbauer Spectral Analysis Software for Windows, 1998.
[10] R. Zhang, R. Jordan, O. Nuyken, Macromol. Rapid Commun. 2003, 24, 246–250.
[11] F. Fürmeyer, 1,3,4-Thiadiazol-Brückenliganden Für Eisen(II)-Spin-Crossover-Verbindungen, Master Thesis, Johannes Gutenberg University, Mainz, 2017.
[12] C. F. Herold, L. M. Carrella, E. Rentschler, Eur. J. Inorg. Chem. 2015, 2015, 3632–3636.
[13] R. W. Hogue, H. L. C. Feltham, R. G. Miller, S. Brooker, Inorg. Chem. 2016, 55, 4152–4165.

7. Appendix

This chapter contains additional figures, which were not provided in the publications and their respective supporting information.

7.1 NMR Spectroscopy

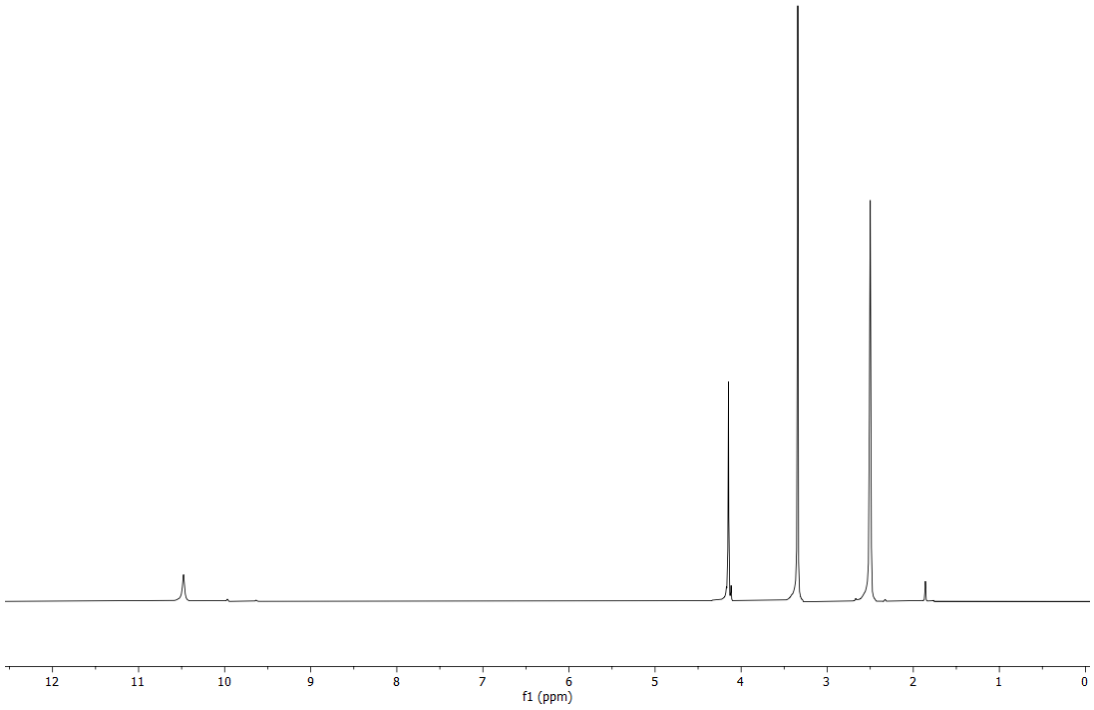

Figure A1. ^{1}H-NMR of 1,2-Dichloroacteyl hydrazide.

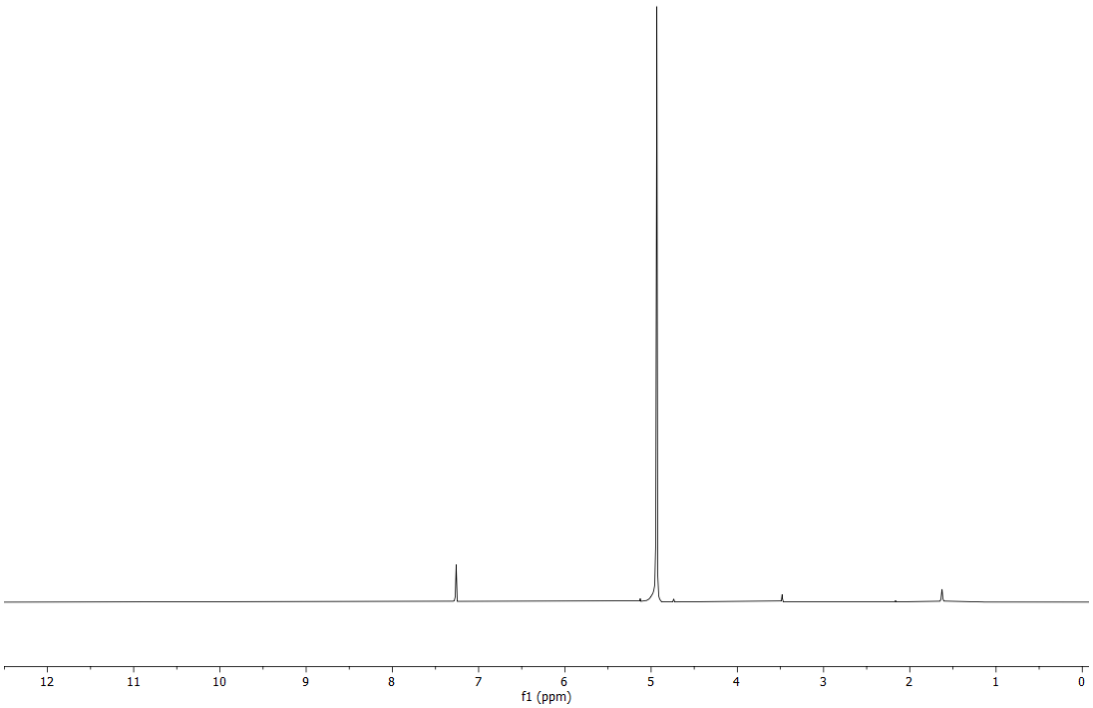

Figure A2. ^{1}H-NMR of 2,5-bis(chloromethyl)-1,3,4-thiadiazole.

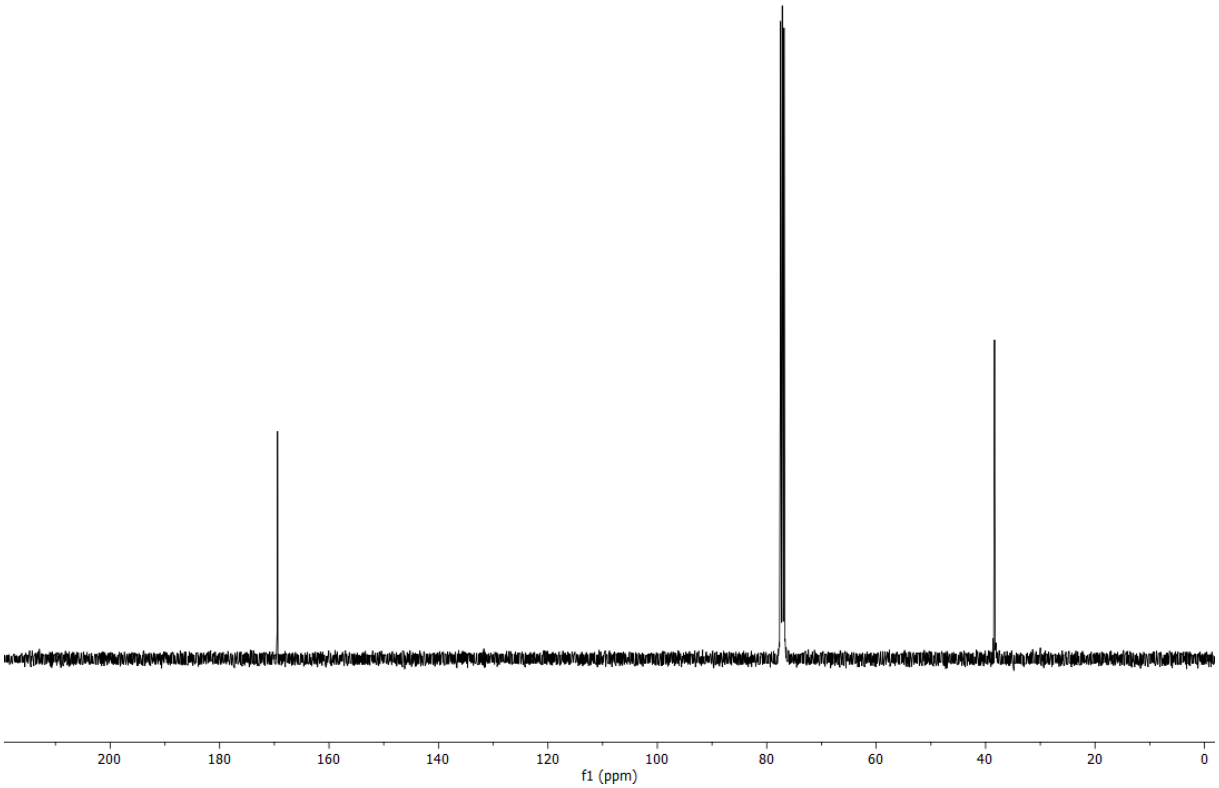

Figure A3. ^{13}C-NMR of 2,5-bis(chloromethyl)-1,3,4-thiadiazole.

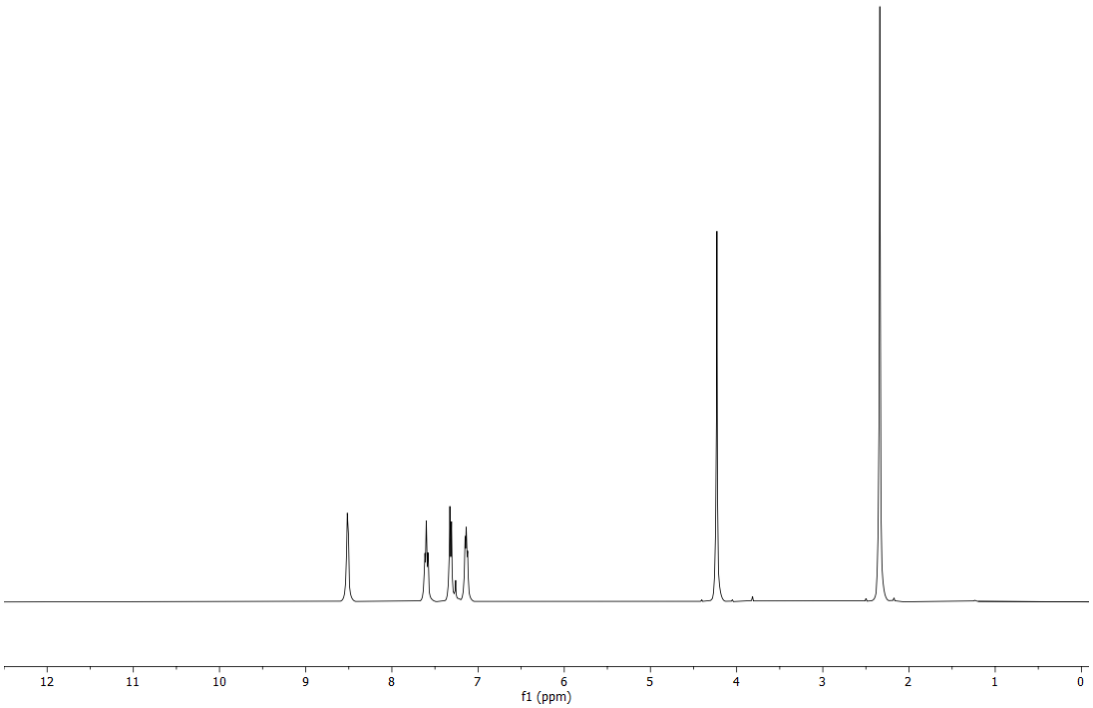

Figure A4. ^{1}H-NMR of thioacetic acid S-pyridine-2-ylmethyl ester.

7.2 IR Spectroscopy

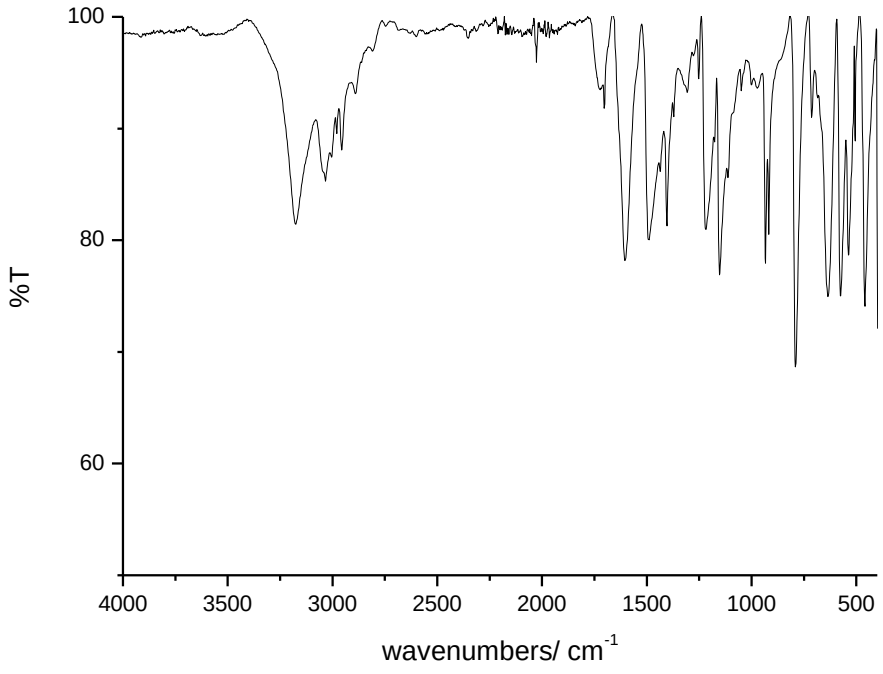

Figure A5. IR spectrum of 1,2-Dichloroacteyl hydrazide.

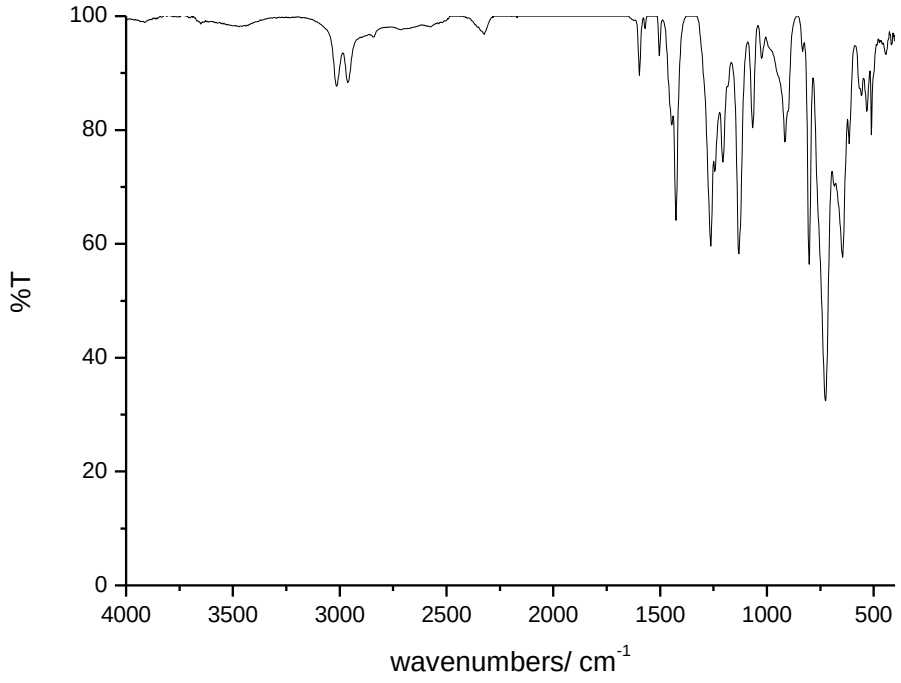

Figure A6. IR spectrum of 2,5-bis(chloromethyl)-1,3,4-thiadiazole.

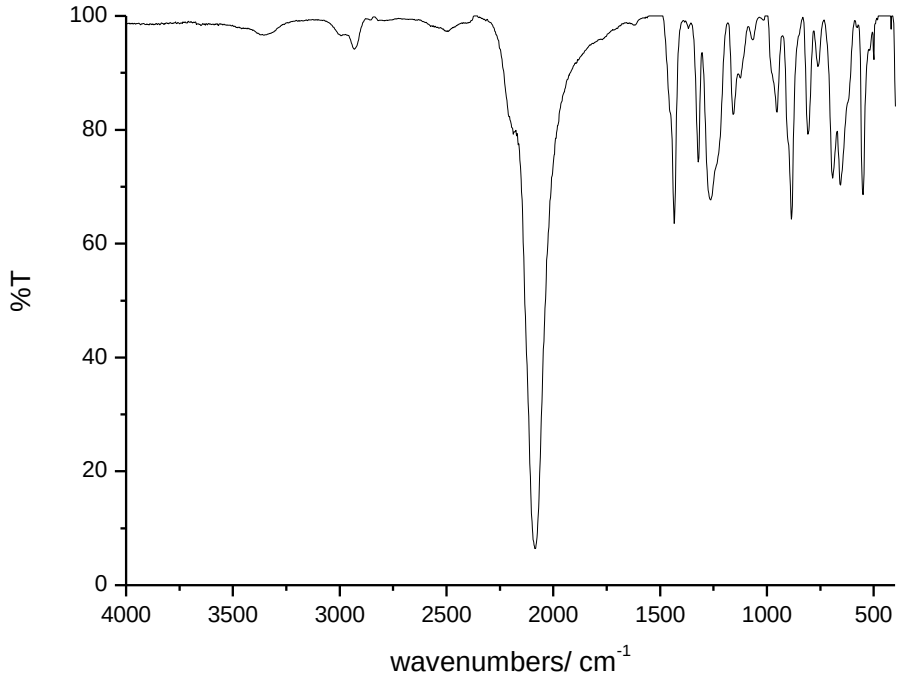

Figure A7. IR spectrum of 2,5-bis(azidomethyl)-1,3,4-thiadiazole.

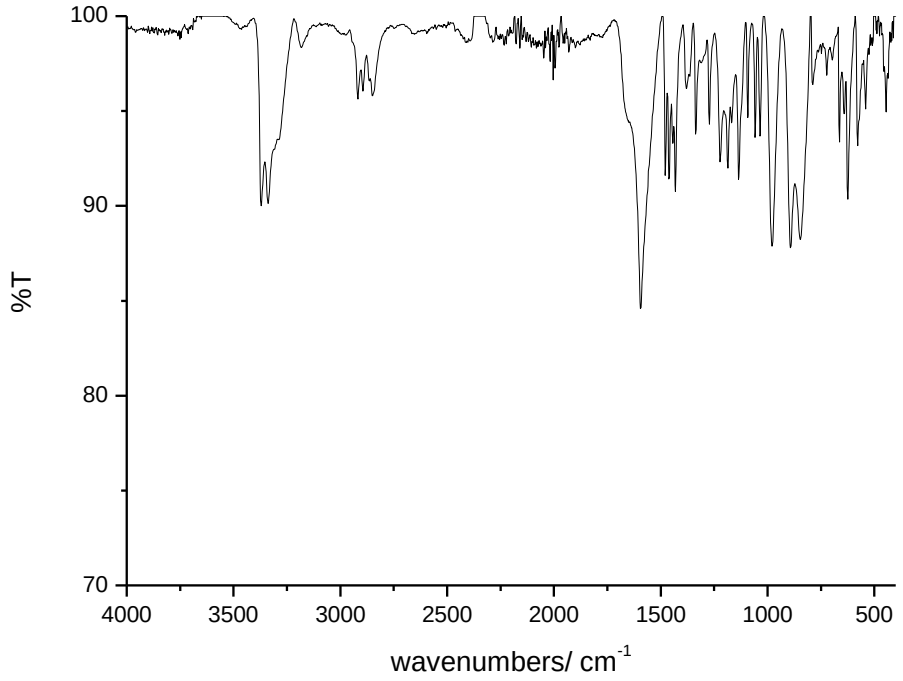

Figure A8. IR spectrum of 2,5-bis(aminomethyl)-1,3,4-thiadiazole.

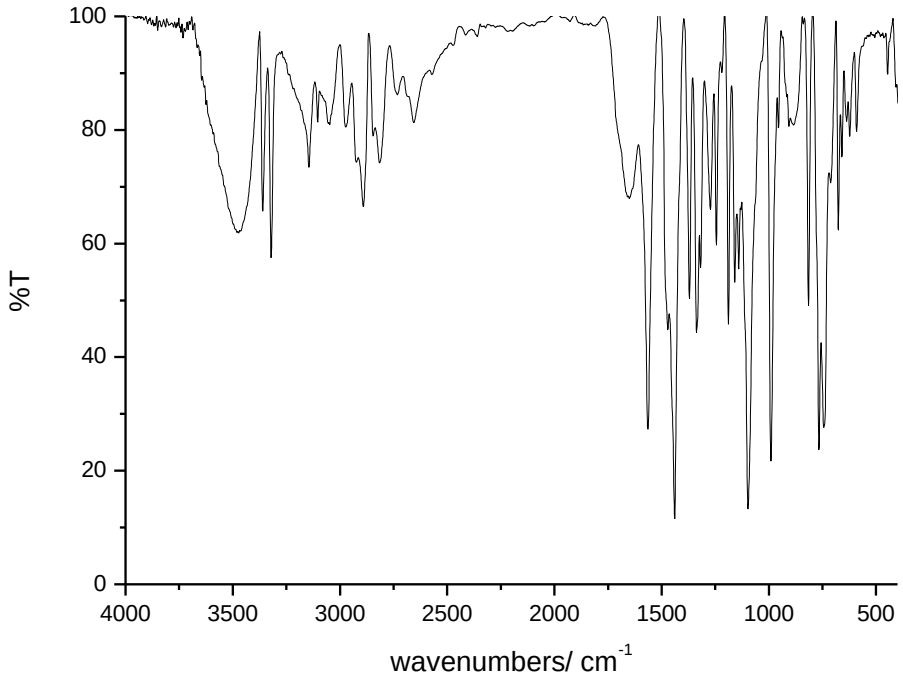

Figure A9. IR spectrum of 2,5-bis[(1*H*-imidazol-2-ylmethyl)amino]methyl-1,3,4-thiadiazole (**I^{2}MTD)**.

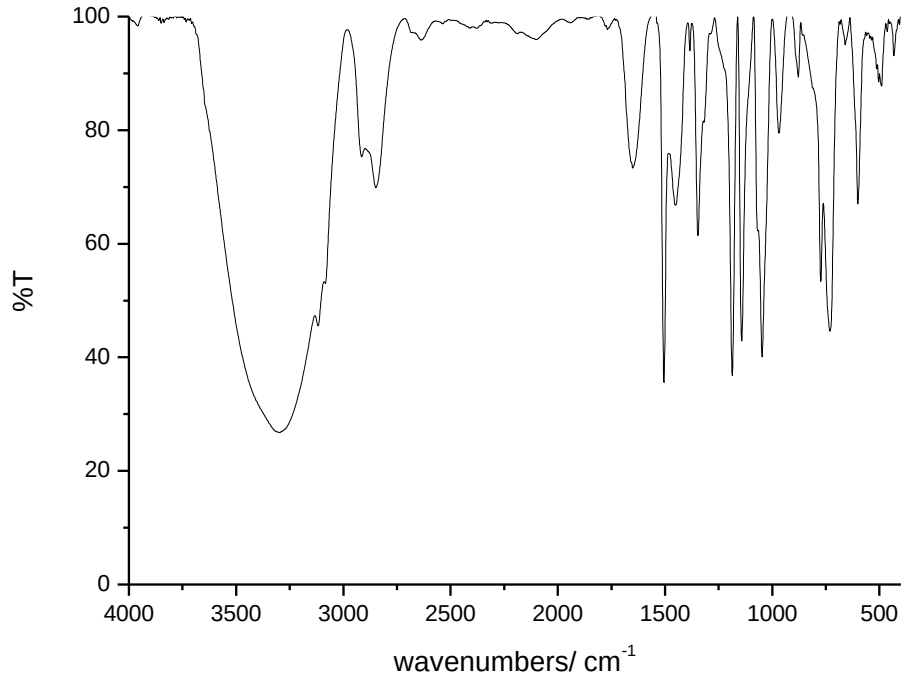

Figure A10. IR spectrum of 2,5-bis[(thiazol-2-ylmethyl)amino]methyl-1,3,4-thiadiazole (**TMTD)**.

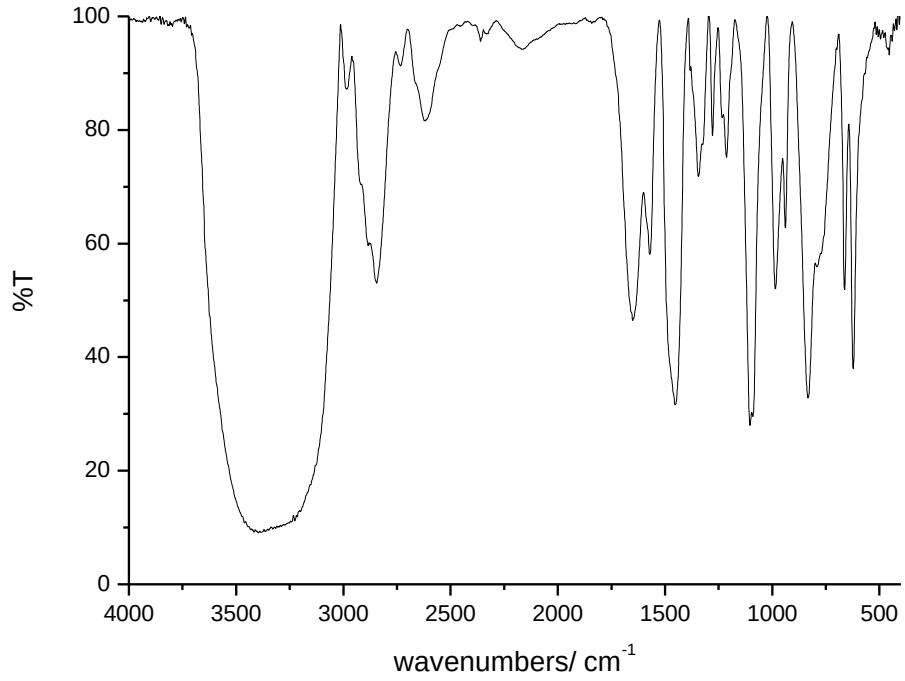

Figure A11. IR spectrum of 2,5-bis[(1*H*-imidazol-4-ylmethyl)amino]methyl-1,3,4-thiadiazole (**I^{4}MTD)**.

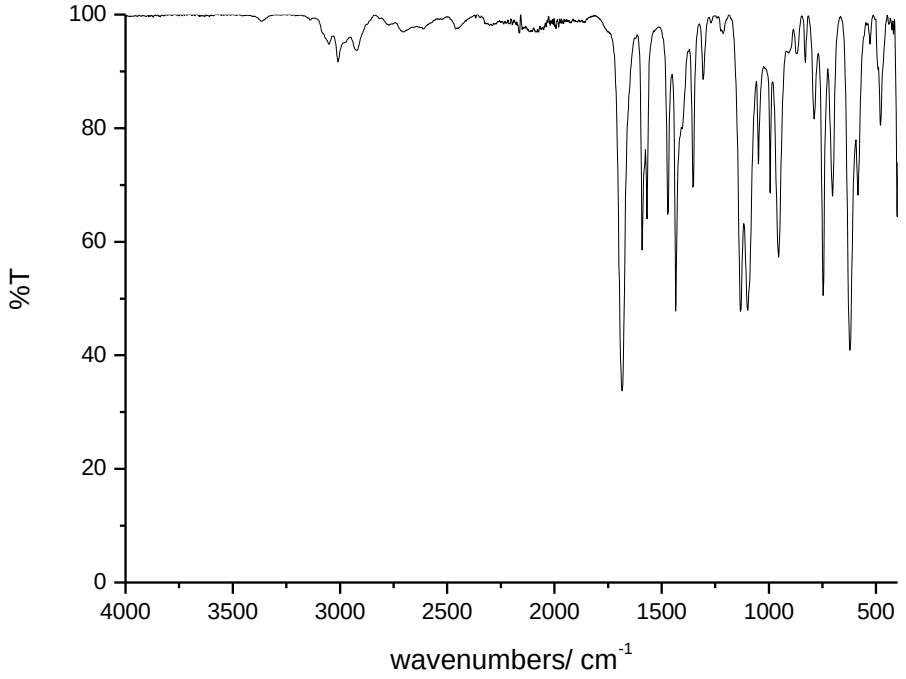

Figure A12. IR spectrum of thioacetic acid S-pyridine-2-ylmethyl ester.

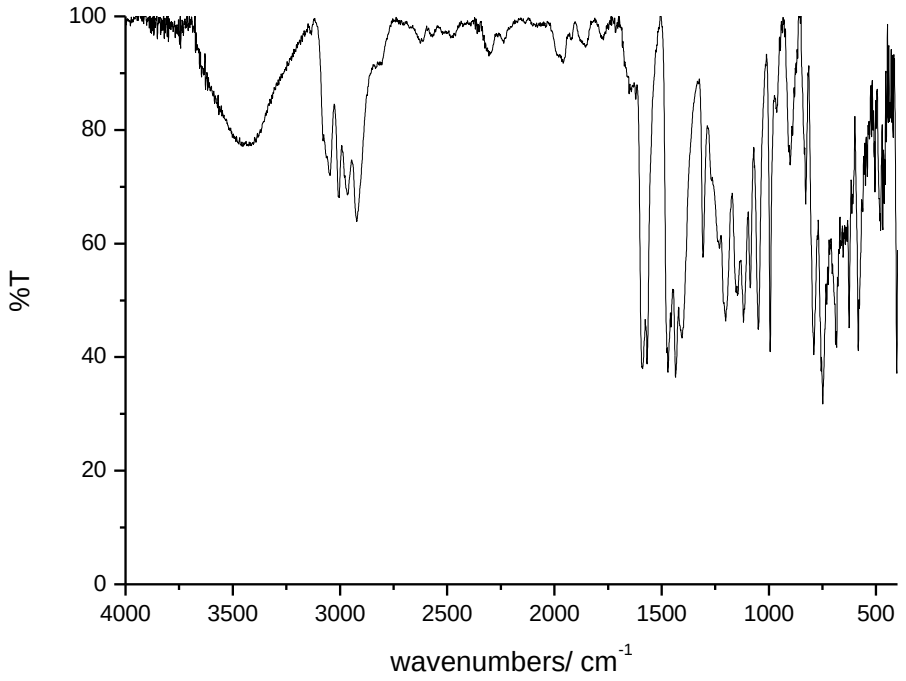

Figure A13. IR spectrum of 2,5-bis[(2-pyridylmethyl)thio]methyl-1,3,4-thiadiazole (**PSTD**).

7.3 Mass Spectrometry

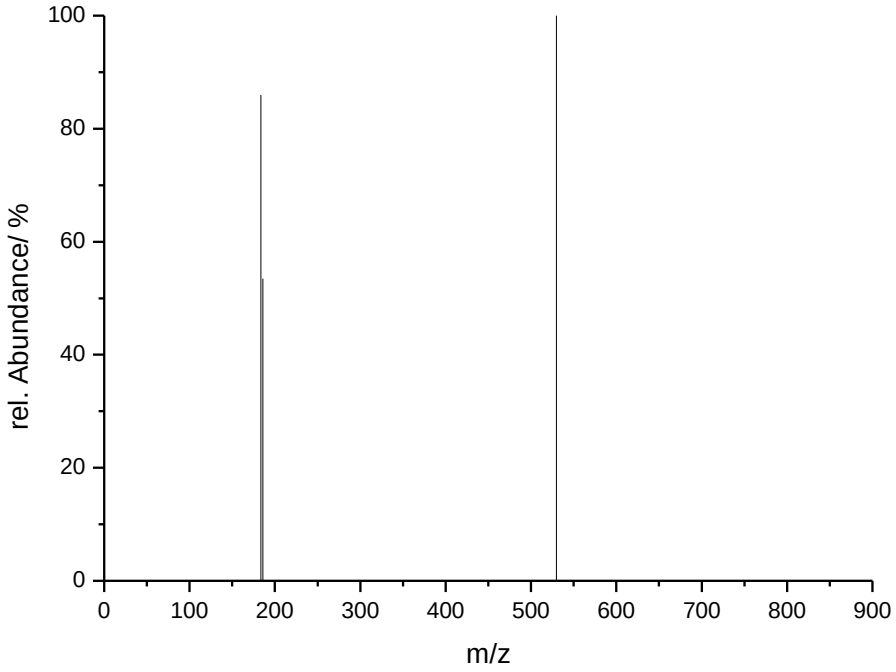

Figure A14. FD mass spectrum of 1,2-Dichloroacteyl hydrazide.

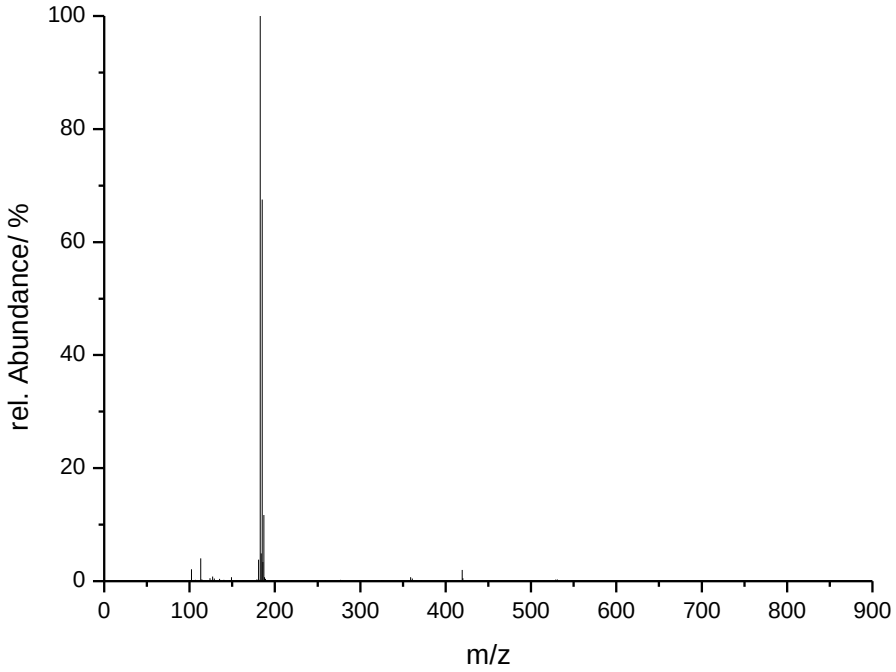

Figure A15. ESI mass spectrum of 2,5-bis(chloromethyl)-1,3,4-thiadiazole.

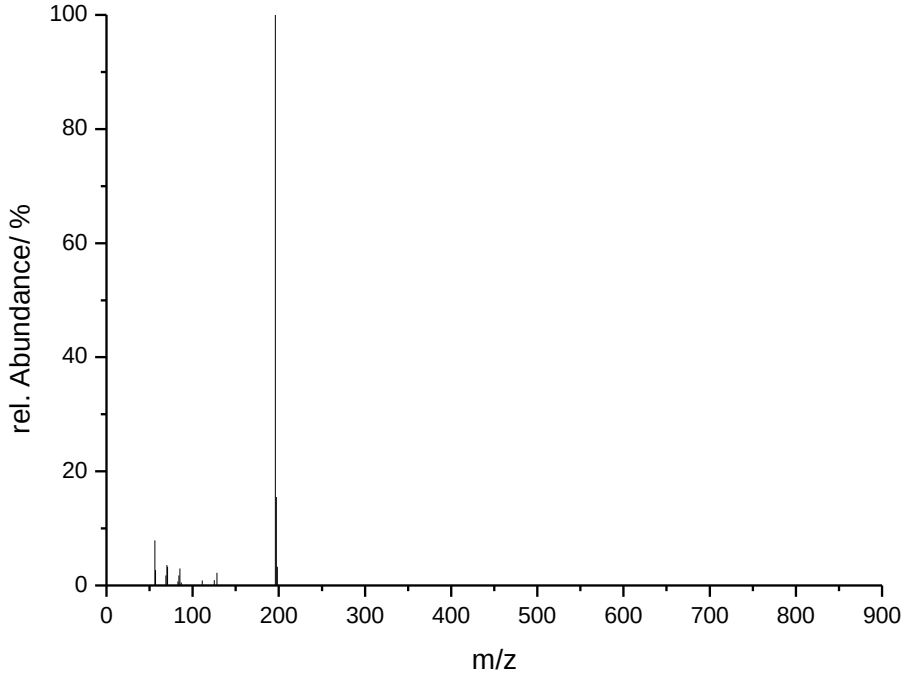

Figure A16. FD mass spectrum of 2,5-bis(azidomethyl)-1,3,4-thiadiazole.

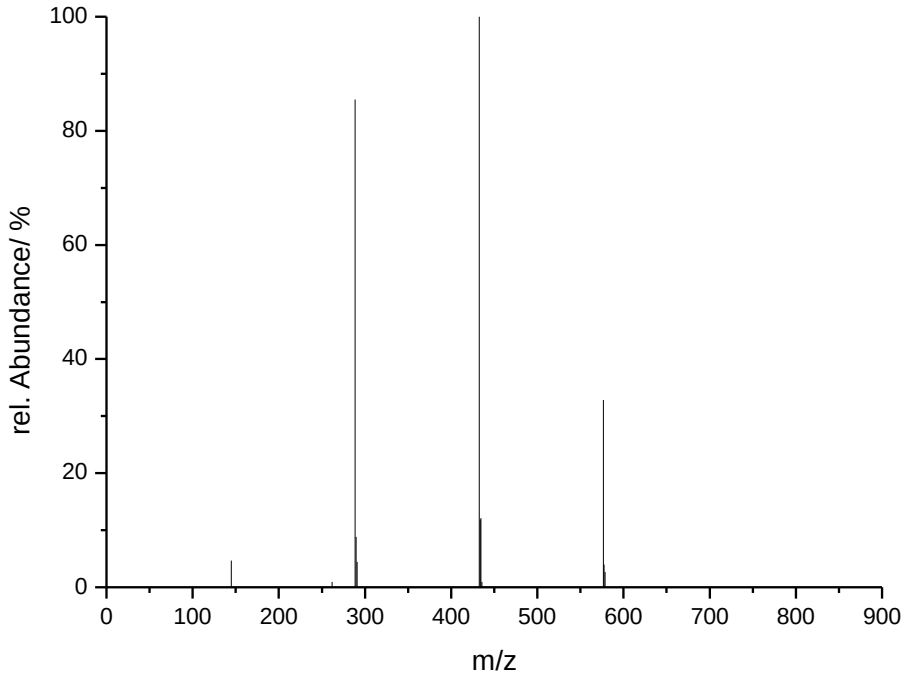

Figure A17. FD mass spectrum of 2,5-bis(aminomethyl)-1,3,4-thiadiazole.

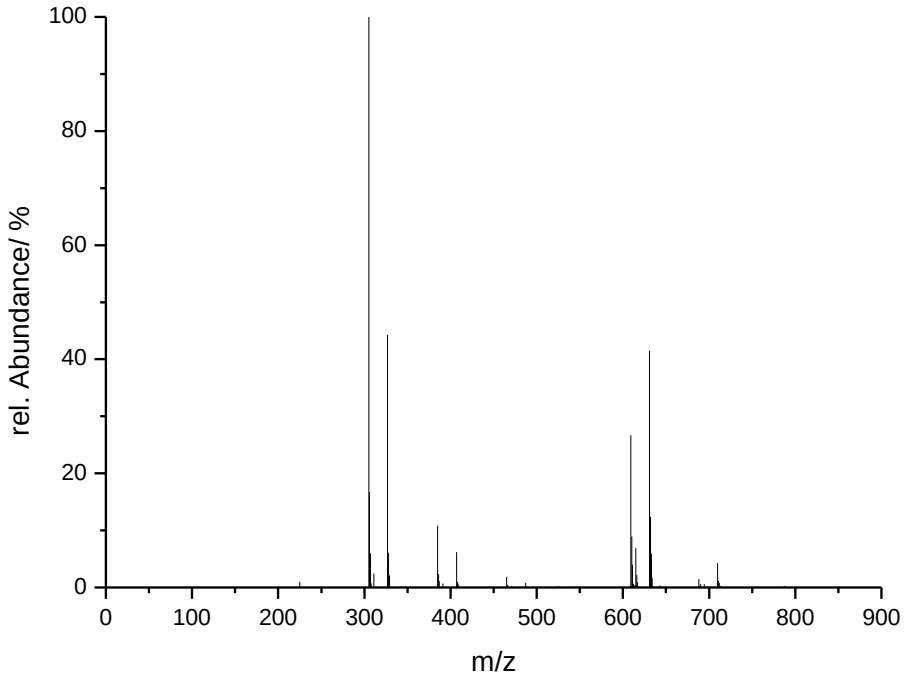

Figure A18. FD mass spectrum of 2,5-bis[(1*H*-imidazol-2-ylmethyl)amino]methyl-1,3,4-thiadiazole (**I^{2}MTD)**.

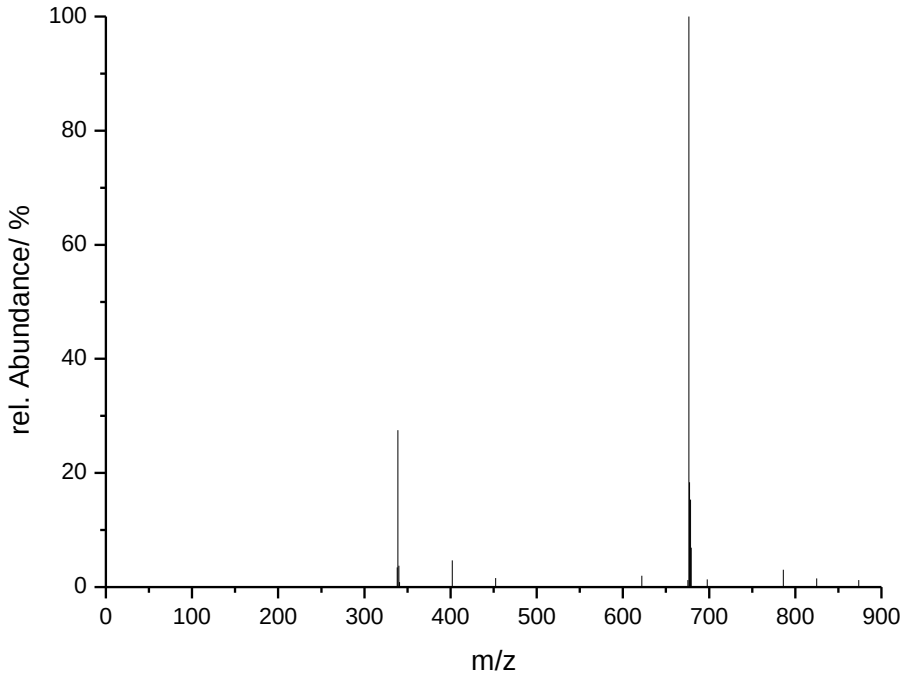

Figure A19. FD mass spectrum of 2,5-bis[(thiazol-2-ylmethyl)amino]methyl-1,3,4-thiadiazole (**TMTD)**.

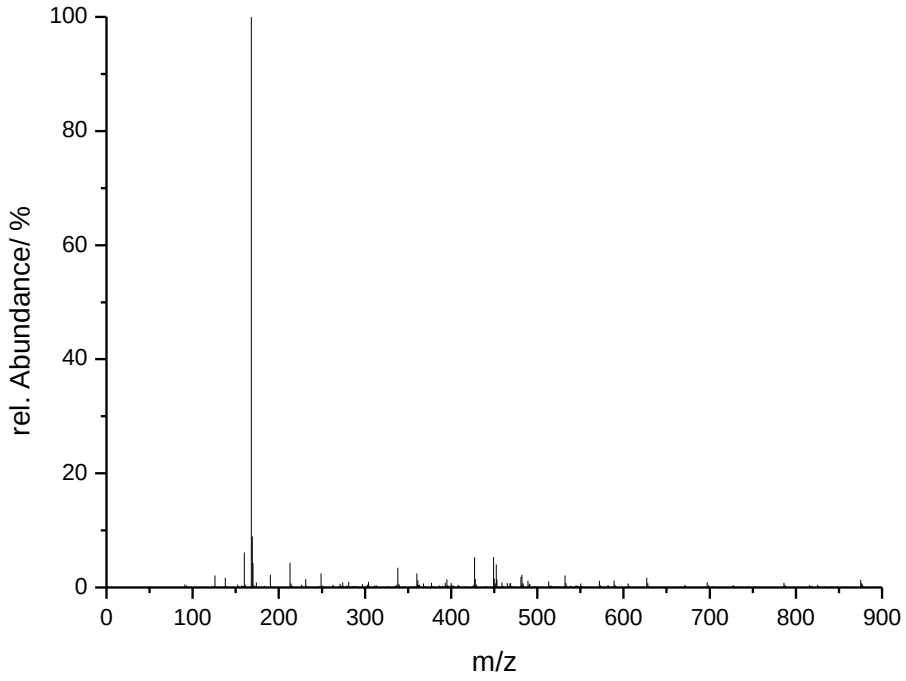

Figure A20. ESI mass spectrum of thioacetic acid S-pyridine-2-ylmethyl ester.

8. Curriculum Vitae

Fabian Fürmeyer

Schloßgasse 1, 55234 Gau-Heppenheim, Germany | phone: +49 6731 4749067 |
mobile: +49 157 76290783 | e-mail: f.fuermeyer@web.de | birth: 04.12.1991, Mainz

Education

05/2017 – present	**PhD studies in Chemistry**, Johannes Gutenberg University Mainz, Department of Chemistry, Workgroup of Prof. Dr. Eva Rentschler Subject: Fe(II) and Co(II) Spin Crossover Compounds using 1,3,4-Thiadiazole Bridging Ligands
10/2014 – 04/2017	**Master of Science Chemistry,** Johannes Gutenberg University Mainz, Department of Chemistry, Workgroup of Prof. Dr. Eva Rentschler Title of the thesis: 1,3,4-Thiadiazol-Brückenliganden für Eisen(II)-Spin-Crossover-Verbindungen Overall grade: 1.6
04/2011 – 09/2014	**Bachelor of Science Chemistry**, Johannes Gutenberg University Mainz, Department of Chemistry, Workgroup of Prof. Dr. Till Opatz Title of the thesis: Synthese von Thiophenen über α-Thionitrile Overall grade: 1.9
08/2002 – 03/2011	**Higher Education Entrance Qualification (Abitur)**, Gymnasium am Römerkastell, Alzey Overall grade: 2.2

Work Experience

05/2017 – present **Research Associate**, Johannes Gutenberg University Mainz, Department of Chemistry, Workgroup of Prof. Dr. Eva Rentschler

- Independent research (project/synthesis planning, preparative work, evaluation of the obtained data)
- Routine use of common synthesis and analytical methods (Schlenk technique, Glovebox, NMR, IR, MS, UV/Vis, SQUID, XRD)
- Publication of the results in scientific articles and presentation to international audience
- Supervision of students in the context of bachelor and master theses, research modules and interhsips

Skills

Languages	German (Native)	●●●●●
	English (Proficient)	●●●●○
	French (Beginner)	●○○○○
Software	Microsoft Office, Origin	●●●●○
	ChemDraw, MestReNova,	●●●○○
	Olex2, Mercury, Avogadro, PHI	●●○○○

Conferences & Workshops

10/2018 **Applied Project Management: Getting a Grip on your PhD**, Softskill course of the general postgraduate program (GPP) of the Johannes Gutenberg University Mainz to introduce basic project management methods

10/2018 **Molecular Spintronics**, *Summer School* of Spin+X (SFB/TRR 173), INNdependence Hotel, Mainz, Germany

07/2018 **Chemical Science Poster Price**, 4th international conference on Advanced Complexes Inorganic Nanomaterials (ACIN), Namur, Belgium

04/2018 **Gekonnt Präsentieren**, Softskill course of the general postgraduate program (GPP) of the Johannes Gutenberg University Mainz to improve rhetorical skills, body language and structured presenting

03/2018 **Poster presentation**, 14th Meeting of Coordination-Chemists (KCT), Heidelberg, Germany

01/2018 **Molecular Magnetism**, *Master Class* of Material Science in Mainz (MAINZ), Johannes Gutenberg University, Mainz

Publications

05/2020	**2D Layer Arrangement of Solely [HS-HS] or [LS-LS] Molecules in the [HS-LS] State of A Dinuclear Fe(II) Spin Crossover Complex** F. Fürmeyer, L. M. Carrella, E. Rentschler, *Crystals* **2020**, *10*(6), 448.
02/2020	**First Cobalt(II) Spin Crossover Compound with N_4S_2-Donorset** F. Fürmeyer, D. Münzberg, L. M. Carrella, E. Rentschler, *Molecules* **2020**, *25*(4), 855.
01/2020	**Phase Trapping in Multistep Spin Crossover Compound** F. Fürmeyer, L. M. Carrella, V. Ksenofontov A. Möller, E. Rentschler, *Inorg. Chem.* **2020**, *59*, 2843.

Activities

Voluntary work

2013 – 2017	Head of a ball sports group for men
2012 – 2018	Coach of a mixed volleyball team
Hobbies	Orchestral music (playing trumpet)**,** winter sports and Volleyball